



**AN INSIGHT INTO ENHANCED OIL RECOVERY PROCESS BY CHEMICAL
WATER INJECTION INTO OIL RESERVOIRS**

By

IMAN NOWROUZI

BSc. Eng. (Petroleum), MSc. Eng. (Petroleum)

**Submitted in Fulfilment of the Academic Requirements for
Master of Science in Chemical Engineering**

**School of Engineering
College of Agriculture, Engineering and Science
University of KwaZulu-Natal
Howard College Campus
Durban, South Africa**

July 2021

Supervisor: Prof Amir H. Mohammadi

Co-supervisor: Dr Abbas Khaksar Manshad

COLLEGE OF AGRICULTURE, ENGINEERING AND SCIENCE

DECLARATION 1 - PLAGIARISM

I, **Iman Nowrouzi** declare that

1. The research reported in this thesis, except where otherwise indicated, is my original research.
2. This thesis has not been submitted for any degree or examination at any other university.
3. This thesis does not contain other persons' data, pictures, graphs or other information, unless specifically acknowledged as being sourced from other persons.
4. This thesis does not contain other persons' writing, unless specifically acknowledged as being sourced from other researchers. Where other written sources have been quoted, then:
 - a. Their words have been re-written but the general information attributed to them has been referenced
 - b. Where their exact words have been used, then their writing has been placed in italics and inside quotation marks, and referenced.
5. This thesis does not contain text, graphics or tables copied and pasted from the Internet, unless specifically acknowledged, and the source being detailed in the thesis and in the References sections.

Signed:

CMC March 2021

COLLEGE OF AGRICULTURE, ENGINEERING AND SCIENCE

DECLARATION 2 - PUBLICATIONS

Publication 1:

Nowrouzi, Iman, Mohammadi, Amir H., and Manshad, Abbas Khaksar. "Utilization of methanol and acetone as mutual solvents to reduce interfacial tension (IFT) in enhanced oil recovery process by carbonated smart water injection." *Journal of Molecular Liquids* 304 (2020): 112733.

Publication 2:

Nowrouzi, Iman, Mohammadi, Amir H., and Manshad, Abbas Khaksar. "Water-oil interfacial tension (IFT) reduction and wettability alteration in surfactant flooding process using extracted saponin from *Anabasis Setifera* plant." *Journal of Petroleum Science and Engineering* 189 (2020): 106901.

Publication 3:

Nowrouzi, Iman, Mohammadi, Amir H., and Manshad, Abbas Khaksar. "Primary evaluation of a synthesized surfactant from waste chicken fat as a renewable source for chemical slug injection into carbonate oil reservoirs." *Journal of Molecular Liquids* 306 (2020): 112843.

Publication 4:

Nowrouzi, Iman, Mohammadi, Amir H., and Manshad, Abbas Khaksar. "Effect of a synthesized anionic fluorinated surfactant on wettability alteration for chemical treatment of near-wellbore zone in carbonate gas condensate reservoirs." *Journal of Petroleum Science* 17(6) (2020):1655–1668.

Publication 5:

Nowrouzi, Iman, Mohammadi, Amir H., and Manshad, Abbas Khaksar. "Effects of methanol and acetone as mutual solvents on wettability alteration of carbonate reservoir rock and imbibition of carbonated seawater." *Journal of Petroleum Science and Engineering* 195 (2020): 107609.

Publication 6:

Nowrouzi, Iman, Mohammadi, Amir H., and Manshad, Abbas Khaksar. "Characterization and evaluation of a natural surfactant extracted from Soapwort plant for alkali-surfactant-polymer (ASP) slug injection into sandstone oil reservoirs." *Journal of Molecular Liquids* 318 (2020): 114369.

Publication 7:

Nowrouzi, Iman, Mohammadi, Amir H., and Manshad, Abbas Khaksar. "Characterization and likelihood application of extracted mucilage from Hollyhocks plant as a natural polymer in enhanced oil recovery process by alkali-surfactant-polymer (ASP) slug injection into sandstone oil reservoirs." *Journal of Molecular Liquids* 320 (2020): 114445.

Publication 8:

Nowrouzi, Iman, Mohammadi, Amir H., and Manshad, Abbas Khaksar. "Effects of a ketone mutual solvent on the dynamic and equilibrium behaviors of crude oil swelling in enhanced oil recovery process by carbonated seawater flooding." *Journal of Petroleum Science and Engineering* 196 (2020): 108005.

Publication 9:

Nowrouzi, Iman, Mohammadi, Amir H., and Manshad, Abbas Khaksar. Synergic effect of dissolved carbon dioxide and a natural based surfactant on interfacial tension reduction, wettability alteration, and oil swelling during chemical water injection into carbonate oil reservoirs. *Journal of Fuel* 290 (2020):120011.

Publication 10:

Nowrouzi, Iman, Mohammadi, Amir H., and Manshad, Abbas Khaksar. Chemical enhanced oil recovery by different scenarios of slug injection into carbonate/sandstone composite oil reservoirs using an anionic surfactant derived from Rapeseed oil. *Journal of Energy & Fuels* 35, (2021): 1248–1258.

Publication 11:

Nowrouzi, Iman, Mohammadi, Amir H., and Manshad, Abbas Khaksar. Double-Chain Single-Head modification of extracted saponin from *Anabasis Setifera* plant and its effects on surfactant-alkali slug injection into carbonate oil reservoirs. *Journal of Petroleum Science and Engineering* 201, (2021): 108438.

Publication 12:

Nowrouzi, Iman, Mohammadi, Amir H., and Manshad, Abbas Khaksar. Effects of generated CO₂-foam by a plant-derived surfactant on oil recovery in secondary pre-generated foam injection in fractured carbonate oil reservoirs. Submitted for reviewing 2021.

Signed:

CMC Feb 2021

15/03/2021

Abstract

Water injection into oil reservoirs in the tertiary stage of production is one of the most common and in some reservoirs the most effective method of enhanced oil recovery (EOR). Additives to injected water are usually engineered and adjusted for better performance and improvement of parameters affecting oil production. This type of water injection is known as chemical water injection. In one division, smart water injection, carbonated water injection, injection of surfactant solutions, polymers, alkalis and mutual solvents can be considered as various methods of chemical water injection. In addition, sometimes to increase the performance of chemical water, a combination of several types of additives and foam injection is recommended according to the structure of the reservoirs. Chemical water injection is sometimes used with special chemicals such as fluorinated surfactants to treat reservoir rock around gas condensate wellbores and remove the liquid blockage in this area. In this project, the effects of different types of additives on the performance of chemical water in different types of reservoirs have been investigated. Chemical and natural additives including mineral salts, dissolved carbon dioxide, natural surfactants such as saponin extracted from *Anabasis Setifera* plant in pure and improved samples, saponin extracted from *Soapwort* plant, surfactant synthesized from natural oils and fats such as anionic surfactant synthesized from *Rapeseed* oil and anionic surfactant synthesized from waste chicken fat, mucilage extracted from *Hollyhocks* plant as a natural polymer, methanol and acetone as mutual solvents and an anionic fluorinated surfactant were investigated. Some of them were used in combination with each other or other materials such as conventional polymers and alkalis. New materials were extracted, synthesized and characterized. Various experiments such as surface and interfacial tension, wettability and contact angle, foam analysis and emulsion stability, surfactant adsorption on rock and flooding under different scenarios were performed according to the methodology of each additive. The results of this project, considering the materials used for chemical enhancement of injected water, are summarized as follows:

- Mutual solvents: Both methanol and acetone reduced water-oil interfacial tension more than diluted saline water. These solvents had a great effect on reducing the contact angle and wettability towards hydrophilicity. Besides, the addition of acetone to injected water increased oil swelling.

- Saponin extracted from *Anabasis Setifera* plant: This non-ionic surfactant had a critical micelle concentration (CMC) equivalent to 3000 ppm at 75 °C. The surfactant solution in CMC reduced the interfacial tension of water and oil to 1.066 mN/m. The interfacial tension values in the optimal salinities resulting from the dissolution of different mineral salts were again reduced. This surfactant changed the wettability of carbonate rock to hydrophilicity by recording a contact angle of 56.5° and finally, a 15.4% increase in oil recovery was achieved by surfactant flooding in CMC and optimal salinity into a carbonate

plug. Injection of pre-generated foam from the surfactant solution at the optimum concentration resulted in 66% oil recovery from a fractured carbonate plug.

- Modified saponin extracted from *Anabasis Setifera* plant: This non-ionic surfactant performed better than its prototype. A CMC of 4000 ppm at 75 °C was obtained for it. Interfacial tension of 3.6×10^{-2} mN/m and contact angle of 86.1° were obtained in CMC. Finally, an increase in oil recovery of 19.1% was achieved by injecting surfactant-alkali slug into a carbonate plug.

- The anionic surfactant synthesized from *Rapeseed* oil had a CMC of 4500 ppm at 80 °C. The interfacial tension of water-oil at this concentration was equal to 3.4×10^{-2} mN/m. The wettability of the sandstone/carbonate composite changed to hydrophilicity. An increase in oil recovery of 14.6–25.7% was achieved under different injection scenarios into sandstone/carbonate composite plugs. The combination of dissolved carbon dioxide with surfactant solution at different concentrations improved the EOR parameters such as interfacial tension, wettability and oil swelling.

- Anionic surfactant synthesized from waste chicken fat recorded a CMC equivalent to 5500 ppm at 75 °C. This surfactant reduced the interfacial tension to 4.3×10^{-2} mN/m and altered the wettability of carbonate rock to hydrophilicity. A 17.8% increase in oil recovery was achieved by injecting an alkali-surfactant-polymer (ASP) slug into a carbonate plug.

- Saponin extracted from *Soapwort* plant: This nonionic surfactant had a CMC of 2250 ppm at 80 °C. The interfacial tension at this concentration decreased to 0.834 mN/m and the sandstone wettability shifted to hydrophilicity. Finally, a 32.1% increase in oil recovery was achieved by injecting ASP-slug into a sandstone plug.

- Polymer extracted from *Hollyhocks* plant: This polymer increased the viscosity of the injected fluid to suitable values for EOR and its non-Newtonian behavior was confirmed due to changes in the polymer solution viscosity against increasing shear rate. Finally, injection of the optimal solution containing this polymer and anionic surfactant synthesized from waste chicken fat and alkali in the volume of 0.5 PV into a sandstone plug increased the oil recovery by 27.9%.

- Synthesized anionic fluorinated surfactant: This surfactant had a CMC of 3500 ppm at ambient temperature and changed the carbonate rock wettability to gasophilic proportion to the surfactant concentration.

Table of Contents

DECLARATION 1 - PLAGIARISM	2
DECLARATION 2 - PUBLICATIONS	3
Abstract	6
Table of Contents	8
Chapter 1: Introduction	13
1.1. Definition and necessity of enhanced oil recovery	13
1.2. Chemical water injection	14
1.2.1. Smart water	14
1.2.2. Carbonated water	15
1.2.3. Mutual solvents	15
1.2.4. Surfactant	15
1.2.5. Polymer	16
1.2.6. Combined methods	16
1.3. The main research question.....	16
Chapter 2: Literature review	18
2.1. Outstanding studies in the field of smart water injection.....	18
2.2. Outstanding studies in the field of Carbonated water injection	22
2.3. Outstanding studies in the field of mutual solvents injection	25
2.4. Outstanding studies in the field of Surfactants injection	26
2.5. Outstanding studies in the field of Polymeric solution injection	28
Chapter 3: Methodology	31
3.1. Materials	31
3.1.1. Crude oils and condensate.....	31
3.1.2. Brine.....	32
3.1.3. Gases	33
3.1.4. Salts and alkalis.....	33
3.1.5. Mutual solvents.....	34

3.1.6.	Commercial Polymer	34
3.1.7.	Rocks.....	35
3.1.8.	Raw materials.....	36
3.1.9.	Chemicals used in the synthesis process.....	38
3.2.	Equipment.....	39
3.2.1.	Balance.....	39
3.2.2.	Density measurement device	39
3.2.3.	Ultrasonic homogenizer and magnetic stirrer	40
3.2.4.	Conductivity and pH measurement devices.....	41
3.2.5.	Viscometer	42
3.2.6.	Rotary evaporator.....	42
3.2.7.	Cutting and coring machines.....	43
3.2.8.	Porosity and permeability devices	44
3.2.9.	IFT and contact angle devices.....	44
3.2.10.	Core flooding system.....	46
3.2.11.	HP-HT imbibition cell	47
3.2.12.	Gas-liquid imbibition.....	48
3.2.13.	Carbonated water preparation system.....	49
3.2.14.	Foam generator	49
3.3.	Methods.....	50
3.3.1.	Effects of mutual solvents on smart carbonated water.....	50
3.3.2.	Surfactant, polymer and alkali	54
3.3.2.2.	Modified saponin of <i>Anabasis Setifera</i> plant.....	58
3.3.2.3.	Extracted saponin from <i>Soapwort</i> plant.....	61
3.3.2.4.	Synthesized surfactant from <i>Rapeseed oil</i>	61
3.3.2.5.	Synergic effect of dissolved carbon dioxide and the <i>Rapeseed oil</i> surfactant	63
3.3.2.6.	Synthesized surfactant from waste chicken fat	64

3.3.2.7.	Synthesized fluorinated anionic surfactant	64
3.3.2.8.	Extracted mucilage from <i>Hollyhocks</i> plant as a natural polymer.....	67
Chapter 4:	Findings and analyses.....	69
4.1.	Effects of mutual solvents on smart carbonated water.....	69
4.1.1.	Density and IFT experiments results.....	69
4.1.2.	Contact angle result.....	78
4.1.3.	Imbibition results	88
4.1.4.	Effect of acetone on dynamic behavior of crude oil swelling.....	91
4.2.	Extracted saponin from <i>Anabasis Setifera</i> plant	103
4.2.1	FTIR, ¹ H NMR and TGA analyses results.....	103
4.2.2.	Surface tension and interfacial tension results	105
4.2.3.	Contact angle results	109
4.2.4.	Oil recovery by surfactant flooding	112
4.2.5.	CO ₂ -foam characterization.....	112
4.2.6.	Oil recovery by secondary CO ₂ -foam flooding in a carbonate fractured plug.....	118
4.3.	Modified saponin of <i>Anabasis Setifera</i> plant.....	120
4.3.1.	FTIR, ¹ HNMR and TGA analyses	120
4.3.2.	Surface tension.....	122
4.3.3.	Water-oil interfacial tension results	123
4.3.4.	Contact angle experiments results.....	126
4.3.5.	Oil recovery by Surfactant-alkali injection	128
4.4.	Extracted saponin from <i>Soapwort</i> plant.....	130
4.4.1.	Surfactant characterization.....	130
4.4.2.	Surface tension and foaming behaviors of the surfactant	132
4.4.3.	Water-oil IFT	134
4.4.4.	Sandstone wettability alteration	137
4.4.5.	Oil recovery	139
4.5.	Synthesized surfactant from <i>Rapeseed</i> oil	141

4.5.1.	FTIR, ¹ H NMR and TGA analyses	141
4.5.2.	Surface tension and water-oil interfacial tension	144
4.5.3.	Contact angle	146
4.5.4.	Foamability	147
4.5.5.	Emulsion stability	149
4.5.6.	Surfactant adsorption	149
4.5.7.	Oil recover by ASP injection	151
4.6.	Synergic effect of dissolved carbon dioxide and the <i>Rapeseed</i> oil surfactant	154
4.7.	Synthesized surfactant from waste chicken fat	163
4.7.1.	FTIR and TGA analyses	163
4.7.2.	Surface tension and water-oil interfacial tension	165
4.7.3.	Contact angle	167
4.7.4.	Nitrogen-foam characterization	168
4.7.5.	Compatibility and emulsion stability	171
4.7.6.	Oil recovery by ASP injection	173
4.8.	Synthesized fluorinated surfactant	174
4.8.1.	FTIR and TGA analyses	174
4.8.2.	Surface tension and contact angle results.....	175
4.8.3.	Surfactant adsorption in carbonate porous media	179
4.8.4.	Foam stability.....	181
4.8.5.	Imbibition tests results	181
3.1.	Extracted mucilage from Hollyhocks plant as a natural polymer	182
3.1.1.	Characterization	182
3.1.2.	Viscous behavior.....	184
3.1.3.	Oil recovery	192
Chapter 5: Conclusion and recommendations		193
5.1.	Effects of mutual solvents on smart carbonated water.....	193
5.1.1.	Interfacial tension.....	193

.5.1.2	Wettability and imbibition	193
5.1.3.	Oil swelling.....	194
5.2.	Extracted saponin from <i>Anabasis Setifera</i> plant	195
5.2.1.	CO ₂ -foam characterization.....	196
5.3.	Modified saponin of <i>Anabasis Setifera</i> plant.....	196
5.4.	Extracted saponin from <i>Soapwort</i> plant.....	197
5.5.	Synthesized surfactant from <i>Rapeseed</i> oil	197
5.6.	Synergic effect of dissolved carbon dioxide and the <i>Rapeseed</i> oil surfactant	198
5.7.	Synthesized surfactant from waste chicken fat	199
5.8.	Synthesized fluorinated surfactant	199
5.9.	Extracted mucilage from <i>Hollyhocks</i> plant as a natural polymer.....	200
References	202

Chapter 1: Introduction

In this chapter, while dividing oil production from reservoirs and defining various methods of oil production, the necessity of research on issues related to EOR is explained. Also, the types of chemical water injection methods as the main approach of this project are defined and the mechanisms of each are described. The meaning of oil reservoirs in this project is conventional underground reservoirs that are mainly accumulated in formations of carbonate, sandstone and a combination of the two. Finally, the problem of the research is explained.

1.1. Definition and necessity of enhanced oil recovery

Much of the energy needed by communities comes from fossil fuels, and oil reservoirs are one of its largest sources. However, the production of these resources has many challenges and it is not possible to produce most of the original oil-in-place (OOIP) with the primary methods. In other words, most of the primary oil remains in the reservoir after natural production. This residual oil is mentioned in some sources from 50 to 65% of the OOIP depending on the type of reservoirs and production mechanism [1- 3]. In addition, many reasons justify the use of artificial production methods from available and conventional reservoirs. Some of these reasons are as follows [4]:

- Current industry developments cannot guarantee discoveries.
- Discoveries are likely to be difficult in coastal, deep-sea, or hard-to-reach areas.
- Production from unconventional sources is more expensive than production from conventional sources.
- Production from unconventional surface resources has irreparable environmental consequences.

Oil reservoirs have different production rates at different stages of exploitation. Following the reduction of production over time, the production process is divided into three parts of primary, secondary and tertiary. In the primary stage, production is done by the natural force of the reservoir. The natural force of the reservoir can be supplied by mechanisms such as the solution gas drive, active aquifer and gas cap drive. After natural production with the force caused by the initial pressure of the reservoir, usually, water and immiscible gas injection are done according to the economic and technical issues of the reservoir to provide pressure and increase the sweep efficiency. In the third stage, other methods are also used to improve specific parameters affecting oil production. The methods used in tertiary oil production are known as “enhanced oil recovery”. These methods generally include thermal methods and injection of gases such as

hydrocarbons, nitrogen, air, carbon dioxide, and factory gases and chemical solutions. Chemical water injection is one of the most common and effective methods of EOR in which by engineering the type and concentration of additives according to the reservoir conditions such as temperature, pressure and salinity, the parameters affecting the reduction of capillary pressure are reached to the desired values. Figure 1-1 shows one of the most common divisions of the chemical water injection method. In the following, each type of chemical water is defined and described.

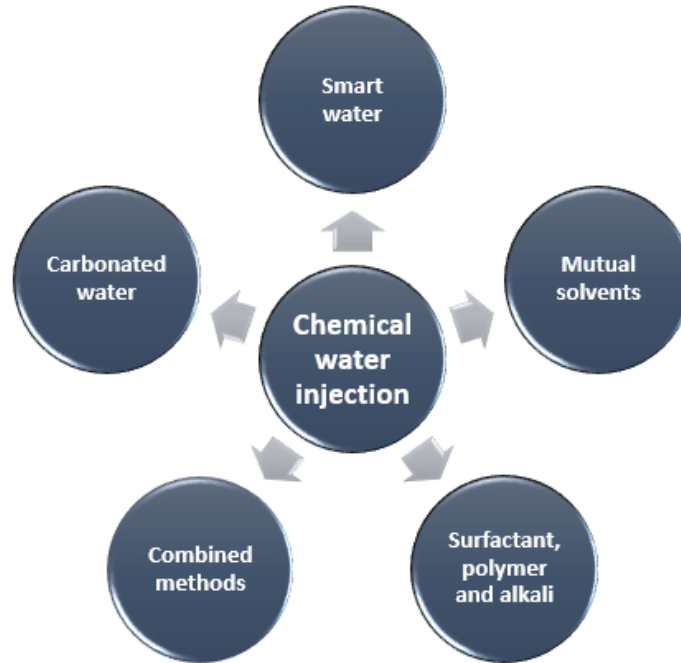


Figure 1-1: Types of chemical water injections in the EOR stage.

1.2. Chemical water injection

1.2.1. Smart water

Changes in injectable water chemistry through the regulation of soluble ions are known as smart water, engineered water, advanced ion management, and low-salinity water. There are two types of ion regulation in this method: first, changing the ion concentration means increasing the useful ions in the EOR process and reducing the concentration of adverse ions in it, and second, dilute or purify saline water samples to reduce total salinity [5, 6]. Smart water increases oil recovery by mechanisms such as fine migration [7], mineral dissolution [7], limited release of mixed-wet particles [7], increased pH effect and reduced interfacial tension [8], emulsification/snap-off [8], saponification [8], surfactant-like behavior [8], multi-component ion exchange [9], double-layer Effect [10], particle-stabilized interfaces/lamella [11], salt-in effects [11], osmotic pressure [11], Salinity shock [11], wettability alteration [11]. However, its main

mechanism is the wettability alteration of reservoir rock from petrophilicity to moderate and hydrophilicity. At the same time, smart water in low concentrations can reduce the interfacial tension of water and oil to some extent. Seawater is a simple example of naturally engineered water that contains a set of different ions, but diluted seawater samples perform better in these mechanisms [12- 14]. The cheapness and availability of resources for smart water injection operations, along with its efficiency, has attracted the attention of many researchers, so that in recent years, a large number of published articles in the field of EOR has been allocated.

1.2.2. Carbonated water

Carbonated water injection is a type of chemical water injection that is obtained by dissolving carbon dioxide in injected water. Mechanisms of carbonated water in EOR include crude oil swelling through the transfer of carbon dioxide mass from the aqueous phase to the oil, wettability alteration and dissolution of reservoir rock, especially carbonate rock, and the formation of a side acidizing [15]. However, crude oil swelling is mentioned as the main mechanism of this method. In addition to EOR, carbonated water is also used for carbon dioxide capturing in underground reservoirs, and research on both uses is well developed. The mechanisms of carbonated water, regardless of the composition of the base fluid, depending on the degree of dissolution of carbon dioxide in the water. Besides, when this method is used to carbon dioxide capture as a greenhouse gas, the greater solubility of carbon dioxide in saline water is more desirable.

1.2.3. Mutual solvents

Mutual solvents are a type of additive to water that are soluble in both water and oil. This dissolution may be partial, general, or miscible. This feature allows the additive to be transferred from the injected phase to the trapped oil, through the interface, and change its properties. Reducing the viscosity and swelling of crude oil are the main mechanisms of this method. However, there is a possibility of reducing the interfacial tension and wettability of the reservoir rock, taking into account the nature of the solvent.

1.2.4. Surfactant

It can be said that after soluble ions, surfactants are the most common additives to water for injections. Surfactants are amphiphilic molecules that have two parts, hydrophobic and hydrophilic. This feature allows them to dissolve in both the aqueous and oil phases and causes them to act at the fluid surface. Surface activity forms a thin film at the water-oil interface and changes interfacial tension. The most common classification of surfactants is based on the ionic charge of their hydrophilic heads. Accordingly, surfactants are in non-ionic, anionic, cationic and amphoteric types, which have been used extensively in EOR studies and field operations. The main mechanism of surfactants is to reduce interfacial tension.

However, they are also capable of modifying the reservoir rock wettability and forming emulsions and foams. Surfactants are used in different scenarios as a single component or combination with various alkalis and polymers. Surfactants are extracted and synthesized from various chemical and natural sources.

1.2.5. Polymer

It is common to inject polymers individually or with surfactants and alkalis into reservoirs to increase oil recovery. Also, polymers are injected into reservoirs to prevent excessive water production [16]. Polymers swell by absorbing water in their structure and give it a gel-like property. As a result, the viscosity of water increases. Increasing the injection phase viscosity compared to the oil viscosity reduces the water/oil mobility ratio and causes the injection front to move pistonically and regularly [4, 17, 18]. Polymers have also been used to stabilize injection foam and water-oil emulsions [19, 20]. The piston-like movement in the injection front prevents the fingering and the premature production of injected water and increases the sweeping efficiency. When polymer solutions are injected as slugs with surfactants and alkalis, in addition to increasing the viscosity of the injection phase, the interfacial tension also decreases and consequently the capillary pressure in the porous medium also decreases [21]. ASP slugs in small volumes usually have a large impact because the interface on the injection front is the most important part of water-oil interactions and a small volume slug easily covers this part. This saves on additives, which are usually expensive materials.

1.2.6. Combined methods

Combined EOR methods are designed to take advantage of the mechanisms of two or more methods in an operation. In chemical water injections, combining methods can mean using two or more additives in one program. The use of polymers and alkalis with surfactants is the most common type of chemical water engineering. Besides, the composition of other additives is done creatively and according to the mechanisms of each additive and the type of reservoir. So far, many additives have been studied in combination with chemical water injection in the laboratory and field. Soluble carbon dioxide and ions, soluble ions and polymers, soluble ions and alkalis, surfactants and soluble carbon dioxide, nanoparticles and soluble carbon dioxide are among these compounds. In the composition of additives, it should be noted that the synergistic effects do not cause incompatibility with reservoir fluids and reactions leading to the formation of sediments.

1.3. The main research question

As mentioned, water injection is one of the most powerful methods of EOR. Chemical water injection is an improved example of water injection in which the type of chemical additive is of particular importance.

Additives are used to control EOR mechanisms in the water injection program. Additives in this method can be simply soluble ions or the complexity of targeted synthesized materials to reduce interfacial tension. These additives with new sources are tested in two ways: single component and in combination with other additives. New sources are identified based on the need to optimize mechanisms and are used to extract and synthesize additives. Different types of the reservoir and different scenarios of chemical water injection cause work to be done on the discovery and production of new additives. Accordingly, any new additive claiming to be useful in a chemical water injection program must be subjected to various tests related to EOR. In this project, new additives such as surfactants and polymers have been tested from various sources. In addition, they are tested in combination with some simple, traditional and common additives such as soluble salts and carbon dioxide. The main research question is how these additives work, individually and in combination, in different chemical water injection processes and scenarios. In a more detailed look and considering the additives used, the following questions are answered in this research:

- 1) What is the active ingredient in surfactants extracted from plant extracts and what parameters does it affect?
- 2) What are the effects of salinity of injected fluid on the performance of surfactants extracted from plants?
- 3) What effect does modifying the structure of surfactants extracted from plants on the parameters compared to the base surfactant?
- 4) What are the temperature stability of natural polymer and its performance in increasing the injection phase viscosity?
- 5) What does the combination of methods (surfactant, polymer, smart water, carbonated water and mutual solvents) help to increase oil recovery? How?
- 6) How does the F-chemical treat condensate reservoir rock?

Chapter 2: Literature review

This chapter reviews past studies of research into chemical water injections, including smart water, carbonated water, mutual solvents, surfactants, and polymers.

2.1. Outstanding studies in the field of smart water injection

Low salinity water is the first type of smart water used in the field. Yousef et al. published the report in 2012. According to the results of two single-well chemical tracer tests (SWCTT) in an Upper Jurassic carbonate reservoir, flooding of diluted seawater in this operation resulted in a reduction of about 7 saturation units in the remaining oil compared to the use of ordinary water [22]. This is while the laboratory study on the mechanisms of engineered water was carried out before that. It can be said that researchers first realized 70 years ago that the efficiency of saline water injection is better than fresh water and saline-free water injection has no advantage over saline water [23]. In 1997, Tang and Morrow also examined the effect of injectable water salinity on the rate of oil recovery in spontaneous water imbibition and concluded that low salinity would ultimately result in more recycling [24]. In recent years, advanced problems and mechanisms of this method have been developed, and changes in interfacial tension and wettability and production under spontaneous water imbibition and their relationship have been well expressed. For example, Zhang et al. performed smart water imbibition experiments in chalk with Mg^{2+} , Ca^{2+} , and SO_4^{2-} ions and reported an oil recovery rate of over 60%, citing wettability alteration as the main cause [25]. Webb et al. performed smart water imbibition experiments in carbonate cores. They used seawater as smart water and reported a 40% increase in production compared to imbibition by primary saline under the same conditions [26]. Saudi Aramco also reported a 16 to 18 percent increase in oil recycling in flooding of low-salt water in carbonate rock samples, citing wettability alteration as the main reason [27]. Aghaeifar et al. explored different strategies of this technique in a high-temperature offshore to achieve an optimal propagation program using modified seawater as smart water. They finally concluded that smart water has a greater effect on oil recovery by secondary injection than tertiary injection [28]. Shabaninejad et al. investigated the ability of low-salt smart water to recycle oil using imbibition experiments in high-clay sandstone cores using micro-CT analysis techniques. They observed that oil recycling was proportional to the intensity of the change in wettability [29]. Sharma et al. investigated geochemical reactions between saline water and carbonate rock during smart water flooding [30]. Xie et al. investigated the effect of low-salt smart water injection at high sandstone reservoir temperature using three combined saline water samples and contact angle and zeta-potential tests. According to them, the management and modification of ions at high temperatures is more important [31]. Wang et al. investigated the mechanisms of wettability alteration and interfacial tension affecting capillary pressure in the smart waterflooding process at high and

low salinities. They showed that the values of interfacial tension at low salinity due to dilution are lower than these values due to the high salinity of water [32]. Amirian et al. investigated the injection of low-salt smart water into the pore dimensions using flooding in a glass micro-model. They stated that the possibility of snap-off could be reduced by increasing the number of capillaries, reducing interfacial tension and changing wettability [33]. Ameri et al. investigated the injection of smart water at low and medium salinities resulting from the dissolution of $MgSO_4$, $MgCl_2$, Na_2SO_4 , $CaCl_2$, $NaCl$ and KCl salts on asphaltene deposition and interfacial tension between water and oil. Their results show a decreasing and then increasing trend relative to the salt concentration, in both interfacial tension and asphaltene deposition [34]. Larki et al. investigated the effect of oil acid number on increasing oil recovery by smart water injection in the presence of silica nanoparticles and found that the used injected fluid was more capable of recycling oil with a lower acid number [35]. Kakati et al. investigated the use of smart water injection into light paraffinic oil reservoirs. In the interfacial tension tests, they achieved an initial value of 17.73 mN/m resulting from a total salinity of 34000 ppm to 11.69 mN/m as a result of 50% dilution of smart water [36]. Kakati and Sangwai investigated the effect of $NaCl$, $MgCl_2$ and $CaCl_2$ salts in a wide range of salinity on the interfacial tension of smart water and five samples of pure hydrocarbons at ambient temperature and atmospheric pressure. They observed lower levels of interfacial tension at lower salt concentrations [37]. Lashkarbolooki and Ayatollahi calculated the interfacial tension of 15000 ppm solutions of each of the $NaCl$, KCl , $MgCl_2$, and $CaCl_2$ salts and crude oil by pendant drop experiments. They observed that with increasing temperature, the effect of the type of ion decreases and the difference in the equilibrium interfacial tension values of different solutions and crude oil decreases [38]. Moustafa and Shedid investigated the effect of magnesium and potassium sulfate by considering the salinity of sodium chloride on EOR by smart water injection. They found that higher concentrations of magnesium and potassium sulfate in injected water, as well as higher concentrations of magnesium sulfate along with lower concentrations of sodium chloride, further increase oil recovery [39]. Direct observations of Mahzari et al. from the injection of low-salt smart water into micro-models and the use of different oils conforms that oil recycling mainly depends on two factors: pore wettability and the tendency of oil to form micro-dispersions [40]. Manshad et al. investigated the effect of different concentrations of $NaCl$, KCl , $MgCl_2$, Na_2SO_4 , $MgSO_4$, KI and K_2SO_4 salts on the interfacial tension of smart water and oil. According to the results, K_2SO_4 salt has a greater ability to reduce interfacial tension. Also, there is an optimal concentration for each salt in which interfacial tension is minimized [41]. Manshad et al. Further investigated the effects of these salts on the wettability of carbonate rocks. The methodology they used was optimizing smart water based on contact angle experiments and then performing imbibition experiments under optimum fluid. They introduced a solution containing K_2SO_4 salt at a concentration of 2000 ppm as the optimal fluid. Also, they designed an observational wettability experiment in which the oil-wet rock section remains in the optimal solution and changes in the oil spot

surface are reported by imaging. They performed and compared this experiment for optimal fluid and distilled water. Figures 2-1 and 2-2 show the results of this experiment for the distilled water and the optimal solution, respectively. Finally, more than 40% of oil recycling was achieved by optimal fluid imbibition [5].

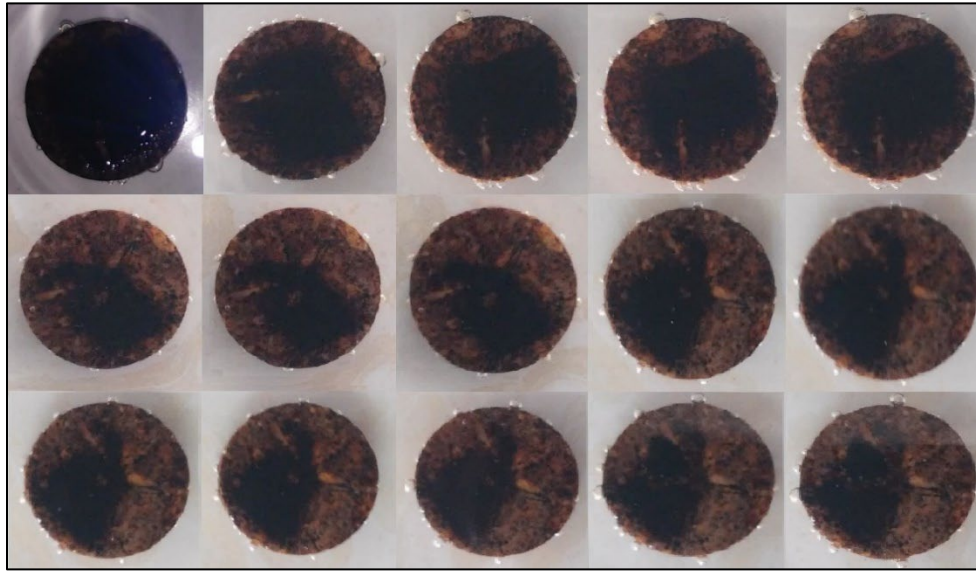


Figure 2-1: The results of wettability observatory test of distilled water in given periods [5].

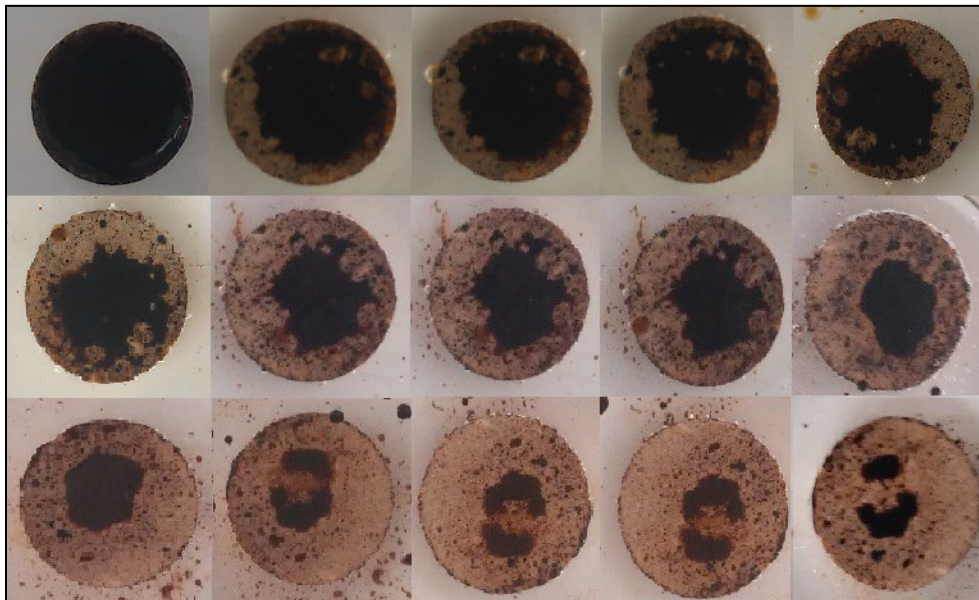


Figure 2-2: The results of wettability observatory test of smart solution (2000 ppm solution using K_2SO_4 salt) [5].

Nowrouzi et al. used NaCl, KCl, MgCl₂, CaCl₂, Na₂SO₄, MgSO₄, KI and K₂SO₄ salts as a two-component combination to prepare smart water at concentrations of 1000 + 1000, 2000 + 2000, 5000 + 5000 and 10000 + 10000 ppm, and investigated the dissolution effects of these salts on the interfacial tension and contact angle. They then investigated and reported the effects of seawater ions in 10 dilution stages on the interfacial tension of water and oil and the wettability of carbonate rock. Thus, they obtained the lowest amount of interfacial tension by the combination of MgCl₂ + K₂SO₄ at 6.731 mN/m, which according to the initial amount of fresh water and oil (24.145 mN/m), showed a decrease of 72%. The minimum contact angle for the combination of KCl + MgSO₄ with a concentration of 2000 + 2000 ppm was recorded at 39.80°. The interfacial tension of seawater at initial concentration with crude oil was 27.671 mN/m. In addition to these trends, the reduction of the contact angle value in the aged sections in solution with each dilution step indicates better use of managed seawater than conventional seawater [42]. Further studies on smart water are given in Table 2-1.

Table 2-1: Summary of recent researches on smart water.

Year	Authors	Material	Experiments	Mechanisms	Results
2018	AlHammadi et al. [43]	Diluted formation brine, carbonate	Flooding and pH	micro-dispersion formation	Rock-brine interactions would not have any impact on the release of oil from rock surface and at <10,000 ppm, these processes may be a by-product of LSWI instead of the mainstream event.
2018	Alhuraishawy et al. [44]	NaCl-brine, Sandstone	Imbibition and flooding tests	Mineral dissolution, fine migration	The oil recovery factor increases as injected water salinity decreases.
2017	Chen et al. [45]	Diluted brines, calcite	Contact angles and IFT	Mineral dissolution, IFT reduction and wettability alteration	Mechanisms are enhanced by diluting the saline water.
2018	Chen et al. [46]	SO ₄ ²⁻ -free brine, carbonate	Contact angle	Wettability alteration	Formation brine caused a strongly water-wet system
2016	Lashkarbolooki et al. [47]	NaCl, KCl, CaCl ₂ and MgCl ₂ solutions, carbonate	Contact angle	Wettability alteration	The monovalent cation bonded to the chloride anion showed better performance.
2017	Mahani et al. [48]	Synthetic brines by NaCl, MgCl ₂ .6H ₂ O, CaCl ₂ .2H ₂ O, KCl, SrCl ₂ .6H ₂ O, Na ₂ SO ₄ , NaHCO ₃ , carbonate	Contact angle, IFT	Wettability alteration	Temperatures enhance adsorption of the potential determining ions which then modifies wettability to a less-oil-wetting state.
2017	Moustafa and Shedid [39]	Modified seawater with Magnesium and Potassium sulfates, sandstone	Flooding	Wettability alteration and lowering interfacial tension	The increase of magnesium and potassium sulfate in actual sea waters injected increases the oil recovery
2018	Pooryousefy et al. [49]	CaCl ₂ with various concentrations, sandstone minerals	Contact angle, zeta potential	Wettability alteration	Contact angle on the muscovite surface decreased with increasing salinity of CaCl ₂

2.2. Outstanding studies in the field of Carbonated water injection

The first laboratory research on carbonated water injection was performed in 1940 [50]. The K&S project, the first operational plan for carbonated water injection, began in 1958 and was completed in 1960 [51]. Despite the antiquity of this method, the information available about its various aspects remained limited for many years. Therefore, in recent years, researchers have conducted many studies on this method to better understand its mechanisms. In a comprehensive review of the carbonated water injection method, Esene et al. emphasized that in this method, the mass transfer of dissolved carbon dioxide reduces the viscosity of the oil, thereby increasing oil mobility and sweep efficiency [52]. Ahmadi et al. investigated the effects of operational parameters on the efficiency of carbonated water injection. They found that the rate of oil recovery directly depends on the flow rate and concentration of carbon dioxide in carbonated water. Also, they considered the wettability alteration of carbonate rock from oil-wet to neutral, reduction of viscosity and swelling of oil as effective mechanisms to increase oil recovery in the carbonated water injection process [53]. In a similar study, Esene et al. examined the effects of injection rate and rock dissolution on oil recycling in the carbonated water injection process based on computational dynamic modeling and showed that oil recycling increases with increasing injection rate. However, there is an optimal injection rate above which there is not much increase in oil recovery. Besides, increasing the pressure causes the rock to dissolve more and this can change the permeability in the field [54]. In another study, Esene et al. stated that based on sensitivity analysis, pressure and temperature are the most influential and least effective parameters on carbonated water performance in increasing oil recovery, respectively. They stressed the need to carry out carbonated water injection in optimal technical, economic, and environmental prospects [55]. In another study by these researchers, the existence of an optimal injection rate at which the most efficient carbon dioxide mass transfer occurs between phases was reported [56]. The mutual effects of carbonate rock and fluid in the carbonated water imbibition process were investigated by Manshad et al. and Nowrouzi et al. [5, 15]. Based on the results, significant oil recovery under the imbibition process was obtained and porosity and permeability of carbonate rock were increased. Also, wettability altered from strong oil-wet to strong water-wet. They considered the dissolution of carbonate rock surface minerals by carbonic acid composed of carbon dioxide and saline water as the reason for the change in wettability and increase in the porosity and permeability of carbonate rock. Mahzari et al., using a large-scale carbonated water injection model, showed that the dissolution of minerals occurs mostly in areas close to the injection wellbore. Also, their simulation results showed that short-cycle injection of carbonate water followed by ordinary water reduces dissolution, while significant oil recovery is achieved [57]. The effect of salinity, temperature and pressure on increasing oil recycling under carbonated water imbibition was investigated in another study by Nowrouzi et al. They observed that the recovery of oil under imbibition

decreases with increasing temperature and increases with increasing pressure. Besides, adjusting the salinity of the base fluid showed that an optimal salinity value results in the highest oil recycling rate under carbonated water imbibition. However, they attributed the better performance of carbonated water at optimum salinity to the mechanism of soluble ions rather than carbonated water mechanisms [6]. Carbonated water in combination with other additives has also been studied by researchers. Manshad et al. showed the effect of combining smart water and carbonated water on the interfacial tension of water and oil by pendant drop experiments. The results showed that the combination of different ions of smart water have different effects on interfacial tension and among them, ions obtained from K_2SO_4 dissolution have the greatest effect on interfacial tension [41]. In a similar study, Hamouda and Bagalkot investigated the effect of $MgCl_2$ and Na_2SO_4 salts in carbonated water on the interfacial tension and mass transfer of carbon dioxide in the water and n-decane system. Their findings confirmed the increase in interfacial tension and mass transfer of carbon dioxide by Na_2SO_4 and their decrease by dissolved $MgCl_2$ in carbonated water [58]. Lashkarbolooki et al. showed the role of carbon dioxide and soluble ions in the interfacial tension changes of water and acidic oil. They found that dissolved carbon dioxide increased the interfacial tension of water and acidic oil, while soluble ions decreased the interfacial tension [59]. In another study, the researchers examined the swelling behavior of crude oil during the injection of carbonated water containing chloride anion. According to the findings, the solubility of carbon dioxide in the aqueous phase is not the only parameter affecting the swelling behavior of crude oil and the type of crude oil and ion as well as temperature have a significant effect on the mobility of carbon dioxide molecules and their division from the aqueous phase to the oil phase [60]. Lashkarbolooki et al., after examining the dynamic interfacial tension in the carbonated water injection process, stated that dissolved carbon dioxide increases the ionization of natural alkaline surfactants in non-acidic crude oils such as asphaltene and resin by lowering the pH of the aqueous solution and as a result the interfacial tension decreases [61]. Chaturvedi et al. investigated the combination of carbonated water and polyacrylamide polymer to control the mobility of carbon dioxide. They considered the use of polymer to be effective in increasing the viscosity of carbonated water and the absorption of carbon dioxide in water and ultimately increasing oil recycling [62]. Bagalkot et al. investigated the effect of Silica Nanofluid on the mass transfer of carbon dioxide in a carbonated water-hydrocarbon system. They found that the combination of Silica Nanofluid and carbonated water increased the mass transfer of carbon dioxide to the system and reduced the density and viscosity of hydrocarbons [63]. Other information from some carbonated water studies is given in Table 2-2.

Table 2-2: Summary of recent researches on carbonated water injection.

Year	Authors	Material	Experiments	Parameters	Mechanisms	Results
2017	Ruidiaz et al.[64]	Crude oil with API of 28, Dolomite and limestone rocks	Amott–Harvey, core-flooding	Rock type, brine concentration and pressure	Wettability alteration	Oil recovery can be directly associated with wettability alteration and it is dependent on the parameters examined
2015	Seyyedi et al.[65]	Crude oil with API of 26.16, Quartz, Mica, and Calcite	Contact angle	Rock type Pressure	Wettability alteration	Contact angle dependence to pressure but no specific relationship
2018	Seyyedi et al.[66]	Crude oil with an API of 20.87	Micromodel and PVT rigs	Oil compositional variations	CO ₂ transfer	The remaining oil after the injection of CO ₂ is heavier than the primary oil, while the remaining oil in the carbonated water injection has a lower viscosity
2017	Seyyedi et al. [67]	Crude oil with API of 20.8, sea-water, sandstone	Core Flood	Secondary and tertiary recovery factor	CO ₂ transfer	High efficiencies occur in both secondary and tertiary carbonated water injections.
2018	Zaker et al. [68]	Crude oil with API° of 21.49, Brin containing MgSO ₄ · 7H ₂ O	Pendant drop IFT	Brine composition, concentration, pressure, temperature	IFT reduction	As the temperature increases, the measured dynamic IFT values getting more close to each other.
2018	Foroozesh, and Jamiolahmady [69]	n-decane, Sandstone	Coreflood	Rate of injection	CO ₂ transfer	If the Equilibrium Number, Ne= L MTC A/qinj, is higher than 0.2 the system can achieve the equilibrium state during CWI.
2016	Riazi and Golkari [70]	Crude oil with API of 24.46	Pendant drop IFT	Pressure and temperature	IFT reduction	IFT reduction depends on pressure, temperature and time.
2018	Bakhshi et al. [71]	2types of crude oil with API of 33.8 and 22.2, sandstone and carbonate	Coreflood	Wettability condition, salinity and crude oil and rock types	CO ₂ diffusion and transfer	CWF proved to be a competent method of EOR in both secondary and tertiary modes while showing more effectiveness in secondary mode than in tertiary.
2018	Adiputra et al. [72]	Crude oil with API of 42.25, 2type of sandstone	imbibition	Soaking time and pressure	CO ₂ -water-rock reactions	0–37% oil recovery.
2017	Honarvar et al. [73]	Crude oil with API of 31.56, carbonate rock	Pendant drop IFT and coreflood	Salinity and composition of brines	IFT	maximum oil recovery of 21.75%, 61.63%, and 52.58% was achieved with conventional WF, SCWI, and TCWI, respectively
2018	Mahzari et al. [74]	Live-oil, Carbonate rock	Coreflood	Reservoir condition	CO ₂ -water-rock reactions	26% higher in carbonated water injection as a secondary injection than seawater injection
2018	Lashkarbolooki et al. [75]	Crude oil with API of 21.5	Pendant drop	Pressure, temperature and time	Oil swelling	As the pressure increases, the oil swelling rate increases but there is no clear trend with temperature changes
2018	Lashkarbolooki et al. [76]	2types of crude oil with API of 20.5 and 35,	Pendant drop IFT	Oil type, Pressure, temperature and time	IFT reduction	IFT of crude oil/CW and solubility of CO ₂ in the aqueous phase as functions of temperature and pressure
2018	Hamouda and Bagalkot [77]	n-decane	Pendant drop IFT	Pressure, temperature and time	IFT reduction	The IFT at 35 °C was smaller than at 45 °C, and beyond this pressure, the IFT at 35 °C was bigger than at 45 °C, up to a certain pressure

2.3. Outstanding studies in the field of mutual solvents injection

Injection of mutual solvents as chemical additives to EOR has long been proposed. However, compared to other chemical water injection methods, it has not been extensively researched. In the first study, Holm et al. (1962) used alcohol as mutual solvents. They demonstrated the high efficiency of these solvents when injected slug by flooding experiments [78]. Dehaghani and Badizad used solvents of heptane, methanol, toluene, and gas condensate to dilute and reduce the viscosity of heavy oil. They observed a decrease in the viscosity of heavy oil with toluene and heptane, but at higher concentrations of the solvent, this effect was reduced. In the case of methanol, the viscosity increased due to the formation of hydrogen bonds. However, gas condensate showed a better performance in viscosity reduction than all solvents [79]. Chernestsky et al. introduced water- Dimethyl Ether solvent injection as a new method of EOR and showed by flooding experiments that significant efficiency could be achieved using this method [80, 81]. Chahardowli et al. investigated the injection of an aqueous solution containing Dimethyl Ether and a polymer. They increased oil recycling by adding solvent to injected water, citing a decrease in oil viscosity and an increase in oil volume through the transfer of solvent mass to oil [82]. Ratnakar et al. simulated the phase behavior of Dimethyl Ether solvent in reservoir conditions, using experiments and the PVT model, and reported similar results in decreasing viscosity and increasing oil volume [83- 85]. Mahdizadeh et al. proposed a model to investigate the EOR in heterogeneous chalk reservoirs with Dimethyl Ether. After validating the model against the flooding test, they reported an increase in the final amount of oil recycling for when the slug size increased from 0.2-1.8 PV at a concentration of 10% solvent [86]. AlZayer et al. investigated the effect of two solvents of dissolved carbon dioxide and Diethyl Ether, in the injection phase. Carbon dioxide solvent was studied as carbonated water which showed a good increase in oil recycling in a carbonate plug. A similar result was reported for Diethyl Ether. Their preferred mechanism for both of these solvents was the mass transfer from the aqueous phase to the oil phase, followed by a decrease in viscosity and oil swelling [87]. Lu et al. investigated the effect of 1-Pentanol solvent at low concentrations in saline water on reservoir rock wettability. They observed a change in wettability from hydrophobic to hydrophilic and a change in the contact angle of 80° at a concentration of 0.1 M of this solvent. They considered the transfer of solvent mass from the water phase to the water-rock-oil interface as the reason for the strengthening of the thin film formed on the rock surface and its wettability alteration. Also, they showed that the solvent performed better with increasing high salinity. Figure 2-3 shows the mechanism of change of wettability of carbonate rock by this solvent without and in the presence of salinity [88].

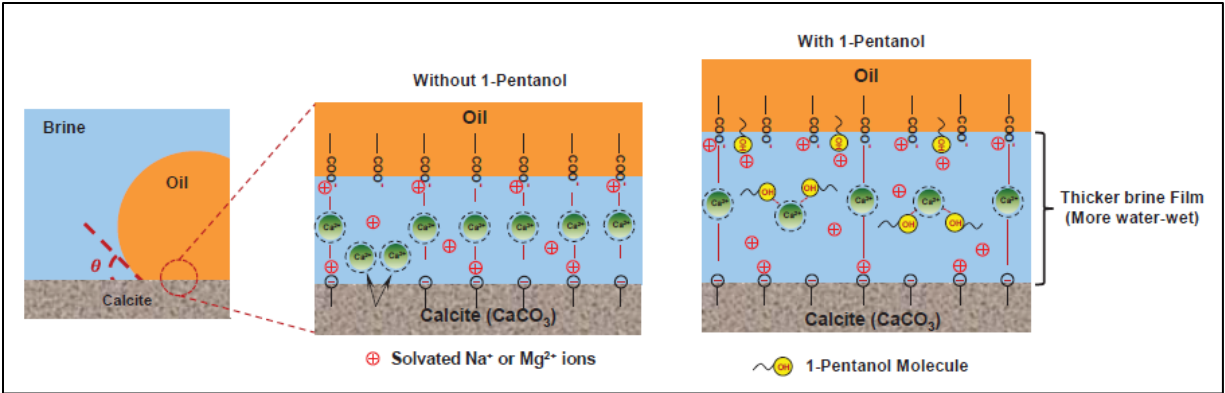


Figure 2-3: Schematic illustration of the influence of 1-pentanol on the wettability of Petroleum fluid-Brine-Calcite [88].

2.4. Outstanding studies in the field of Surfactants injection

Different types of surfactants are added to injected water with the main purpose of reducing the interfacial tension of oil and water. These additives have various functions in reducing interfacial tension and improving other EOR mechanisms. In recent years, research into new sources and the synthesis of new and engineered surfactants has been developed to minimize interfacial tension. Saxena et al. investigated a synthetic surfactant based on *Madhuca longifolia* (Mahua) oil in EOR processes. They obtained ultra-low IFT in the range of 10^{-2} mN/m, change in wettability from hydrophobic to hydrophilic, and a 20% increase in oil recovery factor in the surfactant-polymer slug injection into sandstone plugs [89]. They also obtained an optimal interfacial tension of about 2.123×10^{-2} mN/m at CMC and 2.037×10^{-3} mN/m at optimal salinity using a soap-nut surfactant. The wettability of sandstone was changed to hydrophilicity and a 30% increase in oil recovery was achieved by injecting a small pore volume of surfactant-slug augmented with polymer slug into a sandstone plug [90]. Kiani et al. synthesized a new series of anionic surfactants (iC18S (FO-180)) and studied them in EOR processes at different salinities. Significant reduction in interfacial tension and contact angle of surfactant droplets on glass and final oil recovery factor equal to 72% in surfactant flooding process in glass micro-models were their results [91]. Company et al. investigated Internal Ketone Sulfonates (IKS) as a new surfactant in the seawater injection process. Reduction of interfacial tension in optimal salinity up to 3.5×10^{-4} mN/m and very high recovery factor was achieved in water injection [92]. Ganie et al. investigated an engineered combination of different ratios of lignin-based surfactants as low-cost additives. In addition to reducing interfacial tension to 0.7-0.8 mN/m and increasing the recovery factor by 19%, they reported hexamethylenetetramine as the amine, lignin, and sodium dodecylbenzenesulfonate at 2% total active concentration as the best combination [93]. Najimi et al. used ionic liquids [C8Py][Cl] and [C18Py][Cl] as surfactants. Using the Taguchi experimental design method, they reported a 70% reduction in interfacial tension at high salinity of NaCl, with only 1000 ppm ionic liquids [94]. Manshad et

al. Investigated ionic liquids [C18Py][Cl], [C8Py][Cl], [C18mim][Cl] and [C12mim][Cl] as surfactants in EOR processes. By screening, they selected [C18mim][Cl] solutions as a more effective additive and recorded a 13% increase in oil recycling by flooding in a carbonate plug [95]. Kumar and Mandal synthesized a family of zwitterionic surfactants and studied them in EOR. Synthetic surfactants were based on carboxybetaine and had hydrophobic tails with 12, 14, 16 and 18 carbon. Their results confirm further reduction of interfacial tension by increasing the number of carbon atoms in the hydrophobic tail. Flooding of a small slug of surfactants, polymers and alkalis also resulted in a 30% increase in oil recycling [96]. Madani et al. synthesized and used a non-toxic, environmentally friendly amino acid-based surfactant. The reduction of interfacial tension in their studies did not reach ultra-low values, but the change in wettability in both sandstone and carbonate samples and the final oil recovery of 57.26% in the total secondary and tertiary flooding were achieved [97]. Pal et al. reduced the amount of interfacial tension to 10^{-2} - 10^{-3} mN/m by synthesizing Gemini surfactant based on sunflower oil and examining its effects on EOR processes. Besides, emulsion and fumigation experiments showed that the synthesized surfactants were suitable for EOR [98]. Pal et al. synthesized another coconut oil-based surfactant and reported its use in EOR. In addition to obtaining ultra-low IFT and changing the wettability of quartz to hydrophilic, they increased the oil recovery factor by 20.05% using surfactant flooding in a sand pack [99]. Pal et al. investigated the use of synthesized Gemini cationic surfactants in EOR. The values of interfacial tension in their experiments reached the range of 10^{-2} - 10^{-3} mN/m and the wettability of the rock changed to intermediate. Also, an increase in oil recycling in surfactant floods in sand packs was reported from 29 to 34% [100]. Pillai et al. used imidazolium-based ionic liquids as surfactants in EOR experiments. Their results confirmed the use of ionic liquids used in high temperature and salinity conditions of the reservoir so that the efficiency of 32% in flooding of a chemical slug containing ionic liquid, polymer and alkaline in a sand pack was achieved [101]. Hashemi et al. examined a Lysine Derivative Surfactant for use in EOR. The surfactant reduced the interfacial tension of the water-kerosene system by more than 40% and also changed the wettability of the carbonate rock hydrophilic. Finally, a 12% increase in oil recovery factor was achieved by surfactant flooding in a carbonate plug [102]. Yan et al. used a new series of Double-Chain Single-Head Sulfobetaine surfactants to reduce interfacial tension in the water-oil System. They were able to bring the interfacial tension to ultralow values of 10^{-2} mN/m [103]. Hussain et al. synthesized a new series of quaternary ammonium Gemini surfactants and tested their application in EOR. Their results, in addition to the temperature stability of the synthesized surfactants and their good solubility in saline water, show that with increasing spacer length in the structure of Gemini surfactants, CMC and surface tension decrease [104]. The use of plant extracts as surfactants in EOR has also been studied. Recent studies in this field indicate the diverse plant sources of these surfactants. For example, Chhetri et al. investigated the effects of Soapnut extract at different concentrations on reducing interfacial tension and found it to be effective in

EOR processes [105]. Deymeh et al. used *Seidlitzia Rosmarinus* as a surfactant and calculated the interfacial tension of the surfactant solution with Kerosene as the oil phase by the pendant drop method and were able to reduce the interfacial tension from 32 to 8.9 mN/m [106]. Pordel Shahri et al. calculated the interfacial tension values of *Zizyphus Spina-Christi* Leaves extract and Kerosene oil phase. The amount of interfacial tension reduced from 48 to 9 mN/m at different concentrations of surfactant [107]. Zendejboudi et al. investigated the interfacial tension of crude oil and solutions containing *Zizyphus Spina-Christi* powder by reported its values from 32 to 11 mN/m [108]. In addition to these reports, Mulberry Tree leaves extract, Henna extract, Olive, Spistan and *Prosopis* Leaf extracts, *Matricaria Chamomilla* extract, *Trigoonella Foenum-Graceum* extract were used as surfactants in reducing the interfacial tension of water and oil phase [109- 113]. The common denominator of all plant extracts used to reduce interfacial tension is the presence of surfactants such as saponins in their composition.

2.5. Outstanding studies in the field of Polymeric solution injection

Polymeric solutions can contain polymers, polymeric surfactants and co-polymers. In recent years, much research has been done on the injection of polymer solutions. Babu et al. synthesized and characterized a Castor Oil-based polymeric surfactant. They observed that the viscosity of the polymeric solution increased with increasing polymeric surfactant concentration. The polymeric surfactant, unlike conventional polymers, showed Newtonian behavior with a shear rate of up to 50 s^{-1} and then showed non-Newtonian pseudoplastic behavior [114]. Zhong et al. Synthesized and characterized a new water-soluble polymer called hydrophobically acrylamide-modified terpolymer (PAAN) using micellar copolymerization. Using viscosity tests, they showed the ability to use synthesized polymers in EOR. Their results showed the stability of the polymer at high reservoir temperatures and shear rates. Also, the viscosity of the aqueous solution reached suitable values for EOR [115]. Fakher et al. used hydrolyzed polyacrylamide-Fly ash reinforced polymer in EOR. They observed that at concentrations below 0.1 % wt, fly ash did not remain stable in solution, and at concentrations above 2 %wt, fly ash blocked the injection tube. Finally, they determined the best polymer and fly ash concentrations in the range of 0.5-1 %wt. They also showed that the mean injection pressure was not strongly affected by the fly ash concentration [116]. Qi et al. synthesized a novel AM-co-AMPS Polymer and used it to enhanced oil recovery. The viscosity of the polymeric solution increased significantly with increasing concentration. The polymer increased the viscosity of the solution well even at low concentrations. However, increasing salinity slightly reduced the viscosity of the solution [117]. Sarsenbekuly et al. investigated the application of a novel thermo-viscosifying functional polymer in EOR. This type of polymer was used to eliminate challenges such as instability and reduced viscosity at high temperatures and salinities. Their results showed that in most concentrations of polymers, viscosity increases with increasing temperature, unlike conventional polymers.

Their tested polymer at a total salinity of 9583.74 mg/L still showed this behavior [118]. Wang et al. examined the steady and dynamic rheological behaviors of a novel thermoviscosifying water-soluble polymer for use in EOR. The polymer used increased the viscosity of the solution with increasing temperature and salinity. They stated that based on the intelligent behavior, the resulting polymer solution has the potential to increase the sweep efficiency and adjust the mobility ratio [119]. Wang et al. synthesized and characterized a graft-modified copolymer using Welan Gum to increase oil recovery. The synthesized polymer with increasing salinity showed a good performance in increasing viscosity and increased oil recycling at a concentration of 1000 mg/L, 14.18% more than conventional HPAM polymer [120]. Nowrouzi et al. used Tragacanth Gum as a natural polymeric surfactant. The temperature stability of natural polymer was demonstrated using TGA. The viscosity of the polymeric solutions reached appropriate values to control the mobility ratio and its non-Newtonian behavior was confirmed by changes in viscosity against shear rate. Finally, a 21.4% increase in oil recovery was achieved by injecting a small volume of the polymeric surfactant-alkaline slug into a carbonate plug [121].

Despite extensive development and studies on the above topics, there are still many shortcomings in the literature and many cases are missing based on studies conducted on these topics. The following are some of the literature gaps that are filled in this project based on topic breakdown:

- The effect of added solvents in injected water on the IFT and wettability is a topic that has not been well-addressed in the literature and most studies focus on mechanisms of reducing viscosity and oil swelling.
- The plant extracts always have impurities that may weaken the performance of the surfactants. For example, most plant tissues contain some natural coagulants, such as tannins. Tannins are a series of polyphenolic biomolecules that bind and precipitate proteins and other organic molecules such as alkaloids and amino acids. Tannins and other natural coagulants cause their inactivation and deposition by adsorbing surfactant molecules. This prevents the adsorption of surfactant molecules in the water-oil interface. In addition, impurities reduce the amount of effective material in reducing interfacial tension. This means that by decreasing the purity of the effective substance, it decreases in a given unit of mass. However, in most of these cases in the literature, IFT has not reached the ideal value for EOR and the naturals have a weaker performance compared to chemical and engineered surfactants. One solution to this weakness is to purify the extract to increase the purity of saponin in it.
- Items such as cheapness, affordability and environmental friendliness of surfactants are also among the general issues that should be considered in the use of surfactants in any way.

- Surfactants have different performances at different conditions. Very high salinity and temperatures normally reduce their efficiencies. On the other hand, their adsorption on the porous medium of reservoir rock wastes them. Adsorption causes the surfactant to be injected at a concentration higher than CMC into the reservoir. However, in laboratory studies, little attention is paid to this important issue. It can be said that this is the main gap in the literature. Also, surfactants are often expensive, which contradicts the objectives of the EOR projects and they are sometimes toxic, which can cause environmental issues. Therefore, the latter factors should be taken into account when designing and synthesizing surfactants. Other factors, such as the use of injection fluid at optimal concentrations of salinity and alkali should be considered too.
- Some issues such as the desired performance in reducing IFT and stability in reservoir conditions should be considered.
- A limited number of fluorinated surfactants have been used to change the wettability of near-wellbore zone in gas condensate reservoirs. Accordingly, the identification and study of new chemicals for this purpose remains essential.
- Reduction of IFT, as the main mechanism of surfactants, is not considered in the carbonated water injection. On the other hand, the mechanism of oil swelling in the injection of surfactant solution is not very significant. Although many studies have been performed on combined methods including carbonated water, the combination of using surfactant(s) and carbonated water has rarely been studied, the effect of the presence of surfactants on carbonated water performance is not well known and there is very limited information in the literature.

Chapter 3: Methodology

This chapter includes three sections: Materials, Laboratory Equipment, and Theory of Laboratory Methods. Also, the procedure of each method is described and displayed as a graphical flowchart.

3.1. Materials

3.1.1. Crude oils and condensate

Three samples of crude oil extracted from Gachsaran, Karanj and Sarvestan reservoirs with the specifications of Tables 3-1, 3-2 and 3-3 and a sample of condensate gas extracted from South Pars gas field with the specifications of Table 3-4 as the reservoir fluids were used. Gachsaran and Karanj reservoirs are located in southwestern Iran and Sarvestan reservoir is located in central Iran. The South Pars gas field is located in southern Iran and northern Qatar.

Table 3-1: Analysis of Gachsaran crude oil.

Component	C ₁	C ₂	C ₃	iC ₄	nC ₄	iC ₅	nC ₅	C ₆	C ₇	C ₈	C ₉	C ₁₀	C ₁₁	C ₁₂ ⁺	Total
Molar Percent	0.00	0.08	0.73	0.72	2.22	1.10	1.10	8.66	9.32	6.60	7.14	5.36	5.01	51.96	100.00
Molecular weight = 247															
Molecular weight of C ₁₂ ⁺ = 380															
Specific gravity of C ₁₂ ⁺ @ 15.55 °C = 0.9369															
Saturation pressure of reservoir fluid @ 60.6 °C = 14.04 MPa															

Table 3-2: Analysis of Karanj crude oil.

Component	C ₁	C ₂	C ₃	iC ₄	nC ₄	iC ₅	nC ₅	C ₆	C ₇	C ₈	C ₉	C ₁₀	C ₁₁	C ₁₂ ⁺	Total
Molar Percent	0.00	0.77	2.16	0.76	.244	0.84	0.80	9.26	9.35	7.87	8.52	7.23	5.39	44.61	100.00
Molecular weight = 232															
Molecular weight of C ₁₂ ⁺ = 392															
Specific gravity of C ₁₂ ⁺ @ 15.55 °C = 0.9669															
Saturation pressure of reservoir fluid @ 60.6 °C = 18.58 MPa															

Table 3-3: Analysis of Sarvestan crude oil.

Hydrocarbons	
Propane	-
i-butane	-
n-butane	4.59
i-pentane	11.66
n-pentane	18.92
2-methyl pentane	16.28
3-methyl pentane	7.45
n-hexane	19.47
Methyl cyclo pentane	8.12
Benzene	5.18
Cyclo pentane	1.46
1,1-dimethyl cyclo pentane	5.06
Other isomers	1.81
Total	100.00

Table 3-4: Analysis of South Pars gas condensate.

Component	C ₄	C ₅	C ₆	C ₇	C ₈	C ₉	C ₁₀	C ₁₁	C ₁₂	Total
Molar Percent	8.76	10.34	11.55	15.89	18.97	13.67	9.96	6.42	4.44	100.00
Molecular weight = 124										
Specific gravity @ 15.55 °C = 0.7384										
Saturate (Paraffin + Naphthene) = 88.9 vol. %										
Olefins = 0.8 %vol.										
Aromatics = 10.03 %vol.										

3.1.2. Brine

Three samples of saline water extracted from Gachsaran, Karanj reservoirs and the Persian Gulf were used for different experiments.

Table 3-5: Analysis of saline water samples.

Component	Concentration in (ppm)		
	Sea Water	Gachsaran-f _w	Karanj-f _w
Cl ⁻	11500	39050	48570
SO ₄ ²⁻	6860	220	160
HCO ₃ ⁻	180	210	420
Mg ²⁺	930	1700	620
Ca ²⁺	1920	3500	9120
Na ⁺	7330	25300	46200
Fe ²⁺	Negligible	30	70
Sr ²⁺	Negligible	Negligible	90
K ⁺	90	180	110
PH	7.67	7.50	7.23
TDS	33194	74000	105000

3.1.3. Gases

Hydrocarbon gas with analysis of Table 3-6, carbon dioxide and nitrogen purchased from Abughaddareh Industrial Gases Co. Iran with a purity of 99.99 mole% was used.

Table 3-6: The hydrocarbon-gas components.

Component	Molar Percent
Methane	87.7
Ethane	4.7
Propane	1.74
Iso-butane	0.37
n-butane	0.42
Iso-pentane	0.13
n-pentane	0.10
Hexane	0.08
Nitrogen	4.7
Carbon dioxide	0.06
Total	100.00

3.1.4. Salts and alkalis

NaCl, KCl, CaCl₂, MgCl₂, FeSO₄, K₂SO₄ and NaHCO₃ salts and Na₂CO₃ and NaOH alkalis purchased from MP-Biomedicals Netherlands with the properties listed in Table 3-7 were used in various experiments.

Table 3-7: Properties of the used salts and alkalis.

Salt	Assay [%]	Molecular Weight [g/gmol]	Density [g/cm ³]	Water Solubility [g/l]
NaCl	>99	58.44	2.16	359
KCl	>99	74.55	1.98	281–567
MgCl ₂	>99	95.21	2.32	530–730
CaCl ₂	>96	110.98	2.15	600–1524
FeSO ₄	>99	151.908	2.84	150- 510
K ₂ SO ₄	>99	174.25	2.66	111–240
NaHCO ₃	>99	84.0066	2.20	69-236
Na ₂ CO ₃	>99	105.9888	2.54	160.4
NaOH	>99	39.99	2.13	1000

3.1.5. Mutual solvents

Methanol and acetone as mutual solvents with a purity of 99.9% were purchased from the MP-Biomedicals. Acetone with the chemical formula C₃H₆O and methanol with the chemical formula CH₃OH have a density of 0.784 and 0.792 g/cm³ at 25 °C and both are miscible in water. Figure 3-1 shows the molecular structure of acetone and methanol.

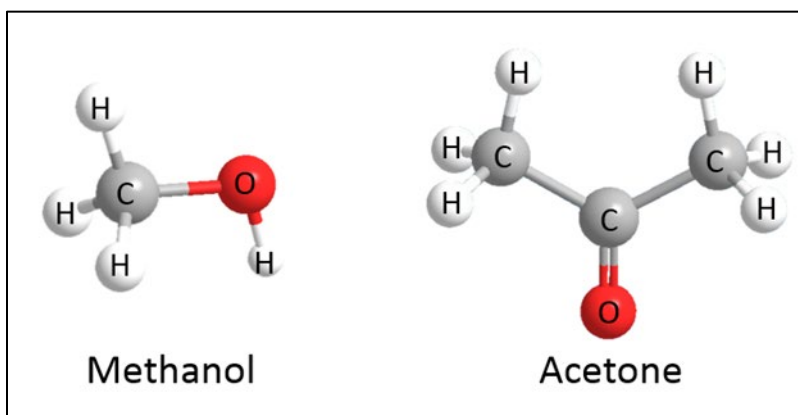


Figure 3-1: Molecular structure of acetone and methanol.

3.1.6. Commercial Polymer

Partially hydrolyzed polyacrylamide (PHPA) was purchased from the German company Merck and used as a chemical polymer.

3.1.7. Rocks

Three samples of carbonate rock, sandstone and carbonate-sandstone composite were used in the experiments. Carbonate rocks from the outcrop of Asmari Formation and sandstone from the outcrop of Aghajari Formation and composite rock from the Asmari Formation located in southwestern Iran were sampled and used. Figure 3-2 shows the XRD and SEM analyses of the carbonate rock. This rock contained 61% dolomite and 39% calcite. Figure 3.3 shows the XRD and FESEM analyses for sandstone and Figure 3-4 shows the XRD and SEM analyses for the composite. The used sandstone contained 53% quartz, 15% feldspar and 29% iron oxide and the composite rock contained 58.4% calcite, 28.7% dolomite and 14.9% quartz.

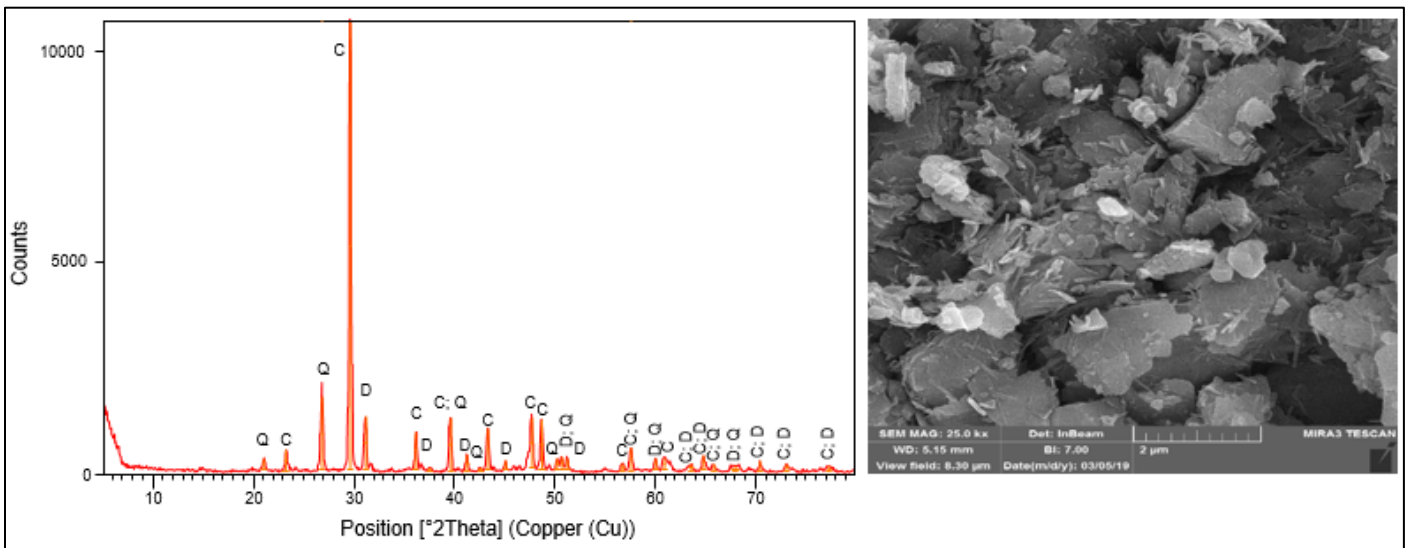


Figure 3-2: XRD (left) and SEM (right) analyses of the Carbonate/Sandstone Composite rock samples.

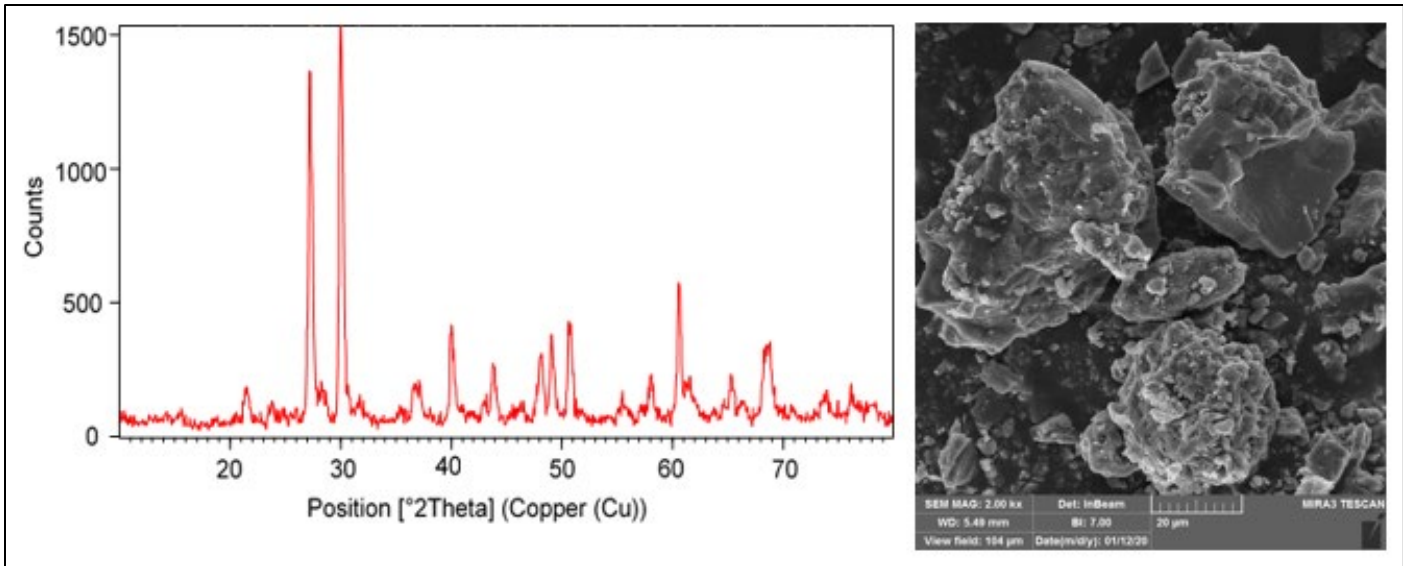


Figure 3-3: XRD (left) and SEM (right) analyses of the Sandstone rock samples.

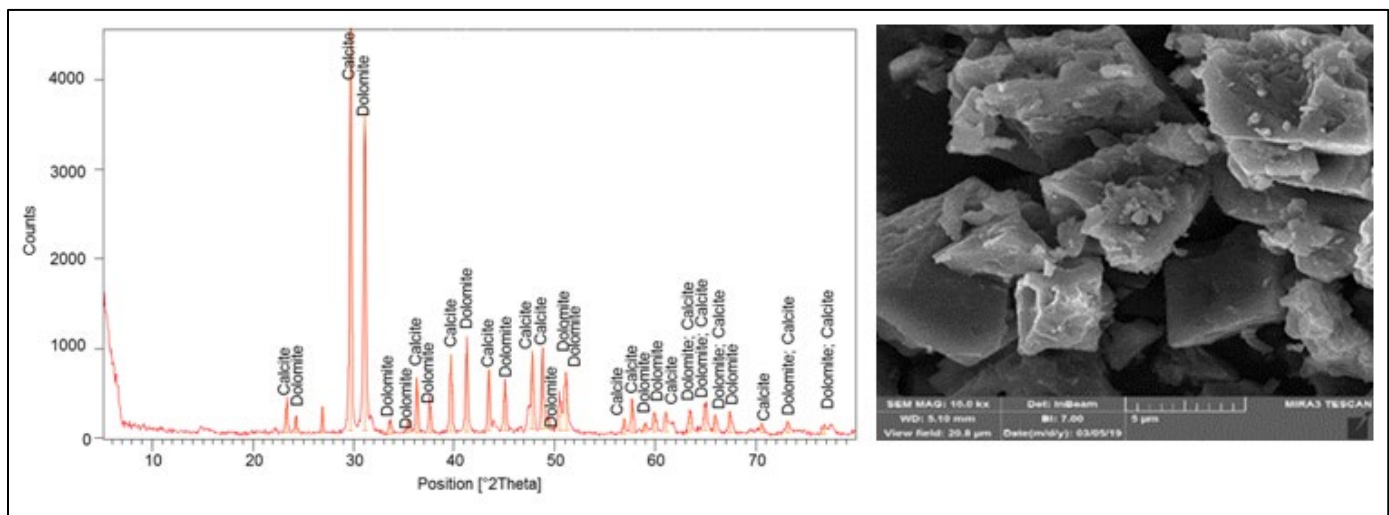


Figure 3-4: XRD (left) and SEM (right) analyses of the carbonate rock samples.

3.1.8. Raw materials

These materials include plant tissues and natural oils that were used as raw materials in the preparation of surfactants and polymer.

Anabasis Setifera plant was obtained from the greenhouse of the School of Agriculture of Shiraz University and used as a source of surfactant. Figure 3-5 shows the image of this plant.

Rapeseed oil was purchased from a local store. The characteristics of the used *Rapeseed* oil included: a density of 0.940 g/cm^3 , a viscosity of 80.68 cp , an acidity of 16.2 mg KOH/g and a free fatty acid of 0.98% . Figure 3-6 shows the oilseeds and flowers of *Rapeseed* plant.

Chicken skin fat was purchased from a local store. This fat is extracted by grinding chicken skin and heating it. Usually, 30 grams of pure fat per 100 grams of primary tissue is produced in this way, and it is traditionally used to prepare soaps and poultices to prevent dry skin. The characteristics of the used fat included: a density of 0.962 g/cm^3 , a viscosity 87.68 cp at $75 \text{ }^\circ\text{C}$, an acidity of 16.8 mg KOH/g and a free fatty acid of 0.58% .

The dried root of the *Soapwort* plant was purchased from a local herbal medicine store and used as a source of surfactant extraction. The root of this plant has traditionally been used for washing clothes. Also, its tea is used to treat coughs.

Hollyhocks plant seeds were purchased from a local herbal medicine store as one of the richest sources of mucilage in plant tissues. The seeds' tea is traditionally used to treat cough. Figure 3-7 shows the image of the plant.



Figure 3-5: Anabasis plant image [122].



Figure 3-6: The flower and seeds of the *Rapeseed* plant.



Figure 3-7: Image of Hollyhocks plant.

3.1.9. Chemicals used in the synthesis process

N, N-Dimethylformamide, anhydrous with a purity of 99.8%, fatty acid acyl chloride with a purity of 99.8%, potassium carbonate with a purity of 99.00%, ethanol 80%, ethyl acetate with a purity of 99.8%, n-hexane with a purity of 96.00%, AB-8 macroporous resin, HCl 1mol/L, polyethylene glycol 400, potassium hydroxide, diethyl ether, sodium bicarbonate, chlorosulphonic acid, pyridine, sodium carbonate, n-butanol, phenol with a purity of 99.00%, perfluorononane with a purity of 97.00%, sulfur trioxide with a purity of 99.00%, sodium sulfate with a purity of 99.99%, 1, 2-Dichloroethane with a purity of 99.80%, sodium

hydroxide with a purity of 99.90%, sodium sulfate with a purity of 99.00% and petroleum ether with a purity of 90.00% were purchased from the German company Merck.

3.2. Equipment

3.2.1. Balance

AND Scale (HR-120, Japan) with an uncertainty of 0.0001 g for weighing any materials was used. Figure 3-8 shows the image.

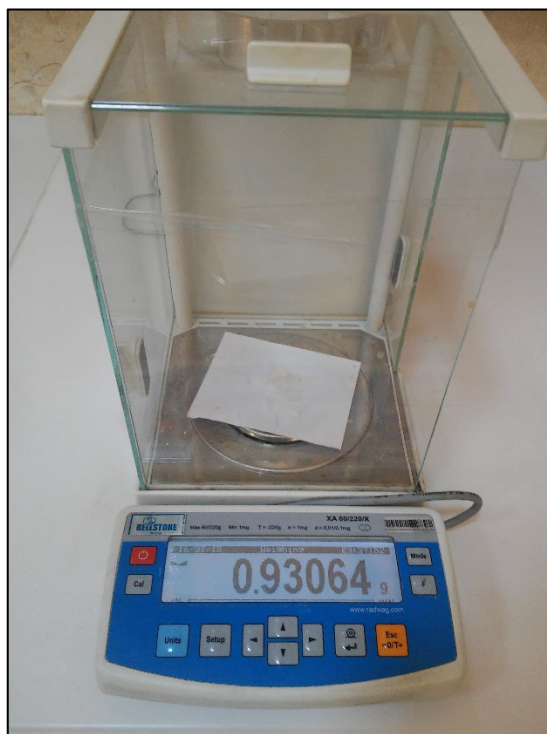


Figure 3-8: Image of AND scale, model HR-120, Japan.

3.2.2. Density measurement device

The high-pressure and high-temperature DMA HPM density meter made by the Austrian company of Anton Paar was used to calculate the density of fluids in this research. The basis of this device is a U-shaped tube oscillation, which must be thoroughly washed with water and acetone and dried with nitrogen gas before use. The calculated cell volume is 2 cm³. The raw data measured from the DMA HPM is transferred to the mPDS 2000 V3 evaluation unit and the density is estimated. The pressure range of the device is 0-140 MPa and its operating temperature range is from -10 °C to +200 °C. This device can calculate the density in the range of 0-3 g/cm³ with uncertainty ± 0.0001 g/cm³. Figure 3-9 shows the DMA HPM density meter.



Figure 3-9: DMA HPM density meter.

3.2.3. Ultrasonic homogenizer and magnetic stirrer

The UP200H ultrasonic stirrer made by the German company of Hielscher was used. The basis of this device is the conversion of electric excitation to ultrasound and its transfer to liquids through various sonotrodes. The output power of this device is 400 W. This device has a very wide range of applications. The possibility of use for a uniform combination of liquids in each other, as well as the possibility of application in the field of nanotechnology and the combination of nanomaterials in basic fluids, is one of the important applications of this type of stirrer. The efficiency of the device is over 90% and its frequency range is 24 kHz with a controlled rate of ± 1 kHz.

A magnetic stirrer of MS7-H550-S made by DLAB Company was used for the solution. This stirrer has a magnetic-thermal plate and allows dissolution at different temperatures. Figure 3-10 shows the images of the Ultrasonic homogenizer and magnetic stirrer.



Figure 3-10: Ultrasonic homogenizer (left) and magnetic stirrer (right) images.

3.2.4. Conductivity and pH measurement devices

The pH measuring device made by METTLER TOLEDO and the conductivity measuring of Cond7310 made by Inolab were used. Figure 3-11 shows images of these devices.



Figure 3-11: Images of pH measuring (left) and conductivity (right) devices.

3.2.5. Viscometer

The DV2T Touch Screen Viscometer (Brookfield, USA) according to Figure 3-12 was used to measure the viscosity of the solutions.



Figure 3-12: Viscometer.

3.2.6. Rotary evaporator

A rotary evaporator of RE100-Pro made by DLAB Company was used to concentrate the solutions. Figure 3-13 shows the image of this device.



Figure 3-13: RE100-Pro rotary evaporator.

3.2.7. Cutting and coring machines

Coring and cutting machines made by Fars EOR Technologies Company of Iran were used to prepare rock cores with a diameter of 1.5 in and thin sections. Figure 3-14 shows the images of these devices.



Figure 3-14: Cutting and coring machines.

3.2.8. Porosity and permeability devices

The porosity measuring device with the brand name of He Porosity-90-102 and the permeability measuring device of Gasperm-90-101 made by Fars EOR Technologies Co. of Iran were used to measure the porosity and permeability of the core samples. The porosity device calculates the porosity using helium gas flow according to Boyle's law, and the permeability measuring device calculates the absolute permeability of core samples by considering the Darcy equation and the passage of helium gas through the porous medium. Figure 3-15 shows images of these devices.



Figure 3-15: Images of He-Porosity-90-102 (left) and Gasperm-90-101 (right).

3.2.9. IFT and contact angle devices

3.2.9.1. Pendant drop IFT and contact angle device

The IFT400 was used to measure interfacial tension above 3 mN/m and gas-liquid surface tension tests. The device is worked based on the pendant drop method. IFT400 has two manually syringe pistons, the cell with two against glass windows and a thermal cover, a metal needle, light source, camera and Lens for imaging and a computer with image processing software. During the tests of water-oil IFT, the needle is closed in the cell bottom and an oil drop is floated in an aqueous solution. The camera snapshot momentarily from the oil drop and the software calculates water-oil IFT using Equation 3-1. The temperature of the cell is adjusted by a temperature regulator and thermal cover. The IFT400 device was also used for contact angle experiments. For this purpose, an intracellular holder is inserted to hold a section at the top of the cell in an aqueous solution with a slight distance from the tip of the needle. The device software is capable of plotting the tangent lines on both sides of the droplet by inserting a user-defined baseline and specifying

the boundary between the surface of the rock and the droplet, and displaying the angles on both sides of the droplet and the average angle as output. Figure 3-16 shows the image and schematic of the device.

$$\gamma = \frac{\Delta\rho g D^2}{H} \quad (3-1)$$

where $\Delta\rho$ is the density difference of droplet and bulk in g/cm^3 , g is the gravity acceleration in cm/sec^2 , D is the large droplet diameter in cm and H is a function of drop shape coefficient $S = d/D$ and d is the horizontal diameter at a distance D above the droplet.

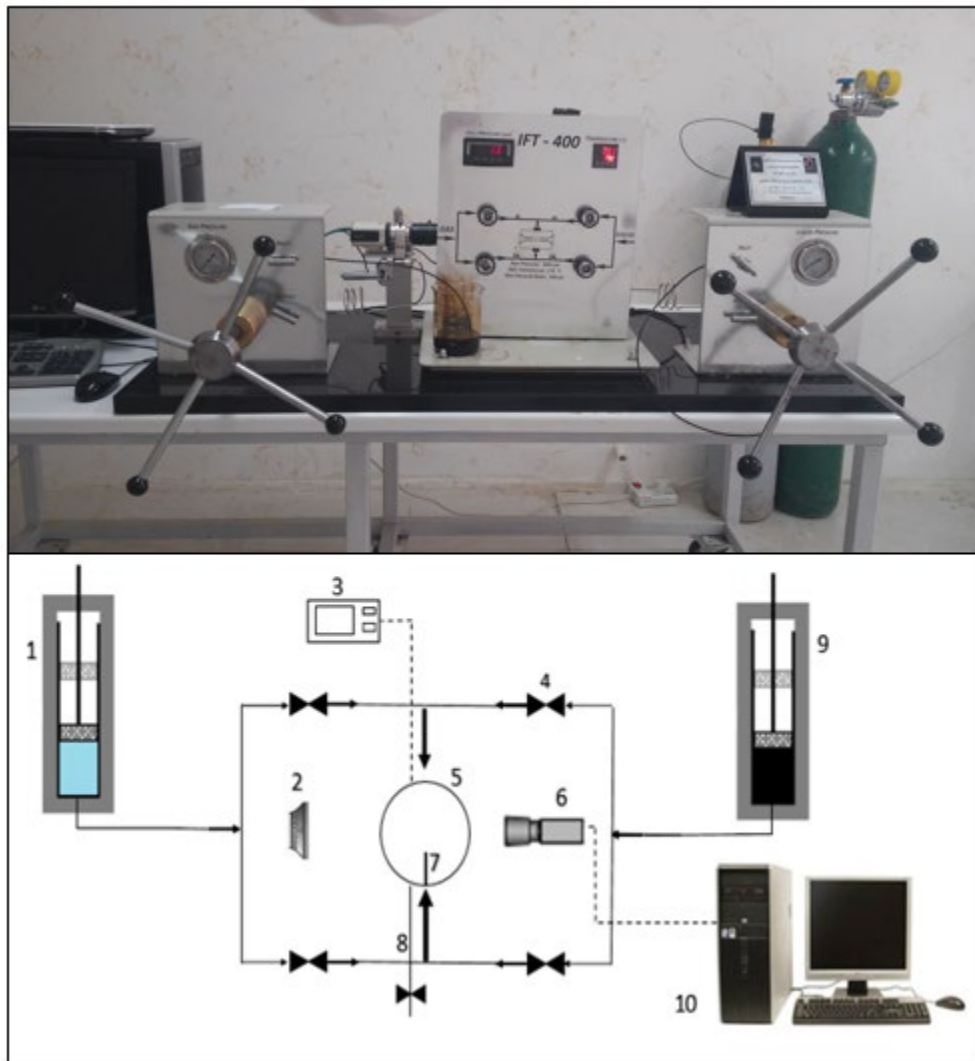


Figure 3-16: IFT400 image and schematic. 1: Bulk flow pump. 2: Light source. 3: Indicator and regulator of temperature and pressure. 4: High-pressure valve. 5: Cell. 6: Camera. 7: Metallic needle. 8: Discharge line. 9: Drop fluid pump. 10: Computer equipped with device software.

3.2.9.2. Spinning drop IFT device

An interfacial tension measuring was used to measure water-oil interfacial tension in the range of less than 3 mN/m. The ability to measure interfacial tension in the range of 0.0001-50 mN/m, and temperature change up to 100 °C, are features of this device. A drop of oil is placed by a syringe in a horizontal column filled with an aqueous solution and then rotation begins. A camera reports the status of the drop to the device software at any time. The basis of this device is in calculating interfacial tension by the spinning drop method based on Equation 3-2. Figure 3-17 shows the device image.

$$\gamma = 0.521 \left(\frac{D^3}{P^2} \right) \Delta\rho \quad (3-2)$$

Where D is the diameter of the droplet, P is the number of revolutions of the droplet, and $\Delta\rho$ is the difference between the density of the oil phase and the aqueous phase.



Figure 3-17: Spinning drop IFT device.

3.2.10. Core flooding system

The core flooding device according to the image and schematic of Figure 3-18 made by Fars EOR Co. was used for flooding tests. The hydraulic fluid is pumped automatically to the rear of the pistons of 3 cylinders, each cylinders containing a particular fluid. The required fluid is injected into the plug with the flow rate or input-pressure adjusted by the operator. The core-holder has two flow distributor spices on both sides and special rubber to block the flow around the plug. Cylinders containing, saline water, surfactant solution and oil and the core-holder are located inside an oven to apply the temperature. The water and oil produced are extracted by the outlet line and collected in a graded container.

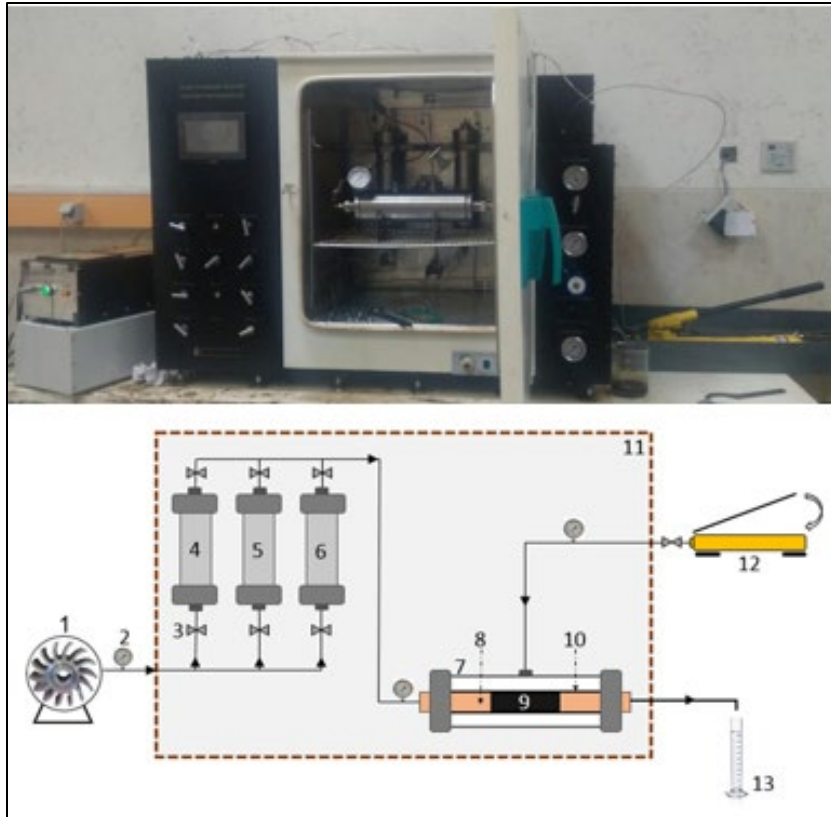


Figure 3-18: Image and schematic of core-flooding device. 1: HPLC pump, 2: Barometer, 3: Valve, 4: Cylinder containing crude oil, 5: Cylinder containing brine, 6: Cylinder containing surfactant solution, 7: Core holder, 8: Fluid flow distributor, 9: plug, 10: Rubber blocker, 11: Oven, 12: Manual hydraulic pump, 13: Container collecting outlet fluid.

3.2.11. HP-HT imbibition cell

For high pressure and temperature imbibition tests, an imbibition container was designed and made using stainless steel. The upper narrow chamber is calibrated in this container and the produced oil can be calculated from the groove created in the body and sealed with sturdy glass. Another similar groove is created against the graduated groove to facilitate viewing and reading of the collected oil volume using a light. There are inlet and outlet at the top and bottom of the container for connecting to the high-pressure line to carbonated water injection. This container is capable of withstanding pressures up to 2000 psi and temperatures up to 180 °C and according to its grading, it has an uncertainty of $\pm 0.1 \text{ cm}^3$. The imbibition container is shown in Figure 3-19.



Figure 3-19. High-pressure and high-temperature imbibition cell.

3.2.12. Gas-liquid imbibition

The schematic of the liquid-gas imbibition device is shown in Figure 3-20. The basis of this system is to float a gas saturated plug in a liquid container. The plug is connected to the hook of a forcegauge with rope, which is held by an adjustable stand and the forcegauge indicates the weight of the floating plug with an uncertainty of 0.001 kgf, instantaneously. It is necessary to achieve a completely stagnant state and balance of floating plug during the experiment.

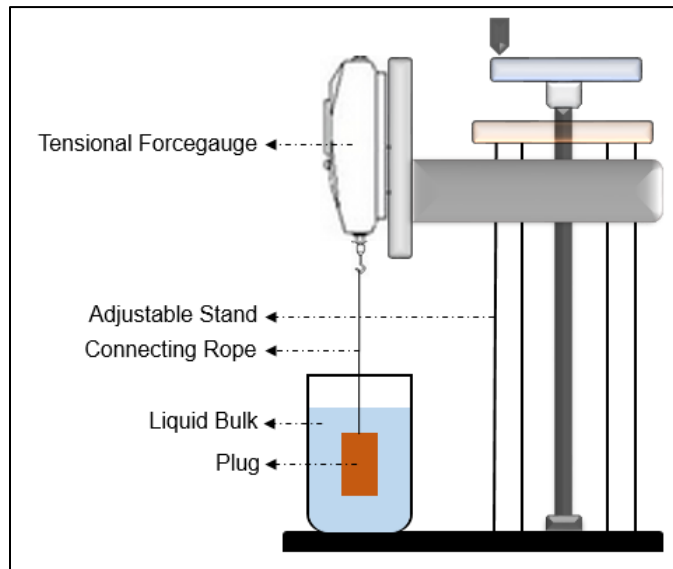


Figure 3-20: Schematic of the liquid-gas imbibition system.

3.2.13. Carbonated water preparation system

To provide carbonated water, a system consisting of a cylinder and a piston connected by a high-pressure line to the oil-hydraulic pump and the gas capsule was designed. The system is housed in an oven with an accuracy of 0.1 °C for applying temperature. A valve is located in the high-pressure line connected to the gas cylinder. The base fluid is poured into the cylinder and after closing the top cap, CO₂ gas is added. After the addition of CO₂, the gas inlet valve is closed and after adjusting the temperature, the system pressure is supplied by raising the piston. The schematic and image of the carbonated water supply system at different pressures and temperatures are shown in Figure 3-21.

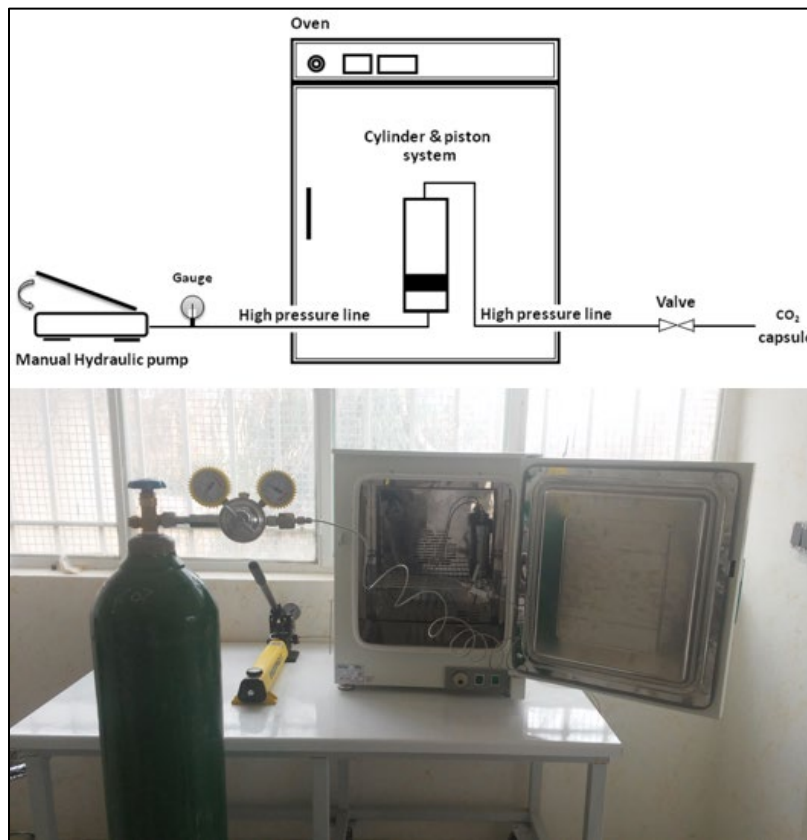


Figure 3-21: Schematic and image of carbonate water supply system.

3.2.14. Foam generator

Figure 3-22 shows a schematic of the foam preparation system. It has a 100 cm height glass foam chamber with a diameter of 2 cm. A mesh metal for better distribution of gas flow is placed at the bottom of the

chamber and joined to a gas capsule. An outlet valve is closed above the chamber and a gas flow-meter is placed in the gas inlet valve. The foam column temperature is supplied by circulating hot water around it.

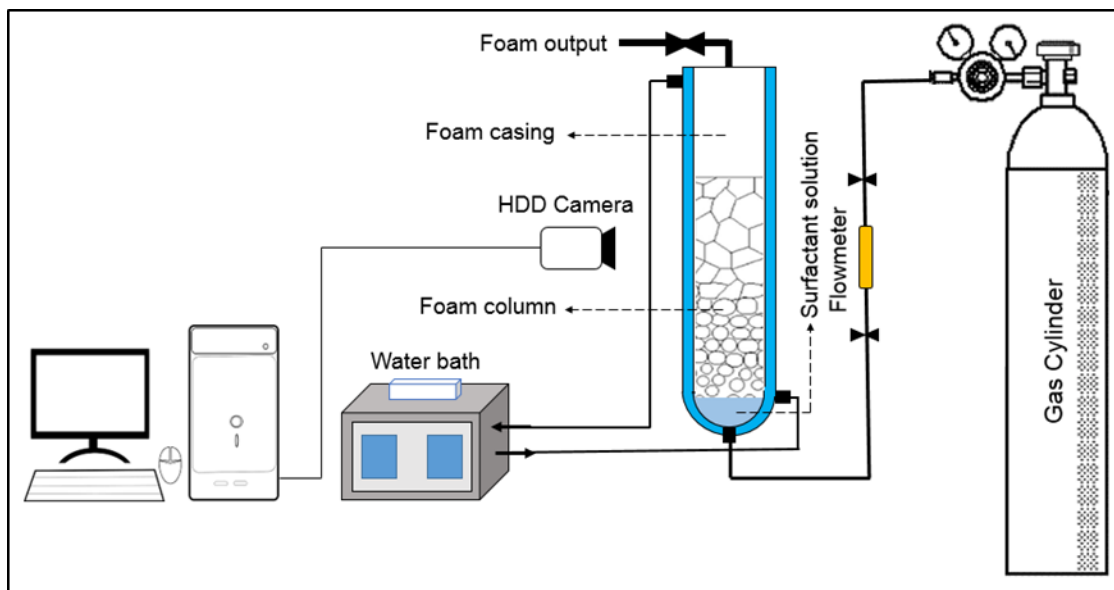


Figure 3-22: Foam generator.

3.3. Methods

3.3.1. Effects of mutual solvents on smart carbonated water

The low-salinity type of smart water was investigated in this study. Then its combination with soluble carbon dioxide and methanol and acetone as mutual solvents was investigated in a new combined method. The novelty of this part of the research is the introduction of a new hybrid method including mutual solvents and smart carbonated water. Laboratory steps include dilution of seawater as smart water, preparation of solvent-containing binary solutions, the addition of carbon dioxide, measurement of the solution densities, and finally, performing the interfacial tension, oil swelling, contact angle and imbibition experiments. Seawater was brought to concentrations of 22000, 16500, 13200 and 11000 ppm by adding distilled water. Diluted seawater was used as the base fluid in later stages. Then, acetone and methanol solvents were mixed separately with base fluids in volume ratios of 5%, 10% and 15%. The density of the solutions was measured by DMA HPM at 75 °C and pressures of 14.7, 500, 1000 and 1500 psi. Before measuring the density of carbonated fluids, to add carbon dioxide to the system, the described carbonated water preparation device was used and then carbonated solutions were introduced into the density measuring device under the desired conditions. In the next step, the interfacial tension of fluids without the presence of carbon dioxide was measured at 75 °C and pressures of 14.7, 500, 1000 and 1500 psi by IFT400. In the next part, to measure

the interfacial tension of carbonated solutions and crude oil, carbonation of the solutions was performed by the IFT400 device. For this purpose, after injecting the solutions in the droplet cell, the carbon dioxide capsule is connected to the fluid inlet of the device and the carbon dioxide gas enters the system exactly like the transfer of the solutions to the cell, and then the system pressure is brought to the desired values. At this stage, a turbid fluid is visible in the cell, which is due to incomplete dissolution and the presence of small bubbles of carbon dioxide in the bulk. Therefore, the waiting time is necessary to achieve complete dissolution and obtain a clear fluid at this stage. The temperature of the device was adjusted and fixed before the pressure to prevent pressure fluctuations after the temperature change. A noteworthy point in the preparation of binary solutions due to the nature of solvents, ie volatility and the ability to dissolve some containers in itself, is that only glass containers with lids were used to prevent them from evaporating in the environment. Narrow sections were cut and polished to perform contact angle tests and to check for a change in wettability. Using high-pressure nitrogen gas, the particles obtained from cutting and polishing were removed from the surfaces of the thin sections. The sections were then placed in toluene to remove fatty acids from hand contact for 1 day. The washed and dried sections were aged for 1 month in the tested crude oil at 75 °C to obtain hydrophobicity. The stages of preparation of sections, which are shown in Figure 3-23, are common to all parts of this project and were done according to the same method. Contact angle experiments were performed after the aging of each section in the desired solutions. Contact angle tests were performed exactly following IFT tests. That is, these experiments were performed for all solutions taking into account the same temperature and pressure conditions. Aging time was considered 1 day in each experiment. Optimal fluids were then selected for testing production under imbibition. The basis of this choice was less interfacial tension and more hydrophilic wettability. Carbonate plugs were cut accordingly. Preliminary information of the plugs such as porosity and permeability were recorded with the described devices and then saturated with crude oil and placed in a high-pressure and high-temperature imbibition cell as previously described in a system such as that shown in Figure 3-24. For each optimal fluid, one-dimensional imbibition, one-dimensional co-current spontaneous imbibition (COCSI), one-dimensional counter-current spontaneous imbibition (COUCSI) and multi-dimensional COUCSI and imbibition in a fractured plug were performed. Figure 3-25 shows examples of plugs prepared for imbibition experiments. To measure crude oil swelling, the pendant drop tests were performed following the interfacial tension tests. The software converts pixels into millimeters using a scale it receives from the user and reports droplet volume in cubic millimeters. This scale is given to the software by entering and specifying the needle diameter in millimeters. The software calculates the droplet volume assuming the droplets are symmetrical from two-dimensional images. A 1.48 mm metal needle was used in the interfacial tension and oil swelling tests. The percentage of oil swelling at any time relative to the previous moment is calculated by Equation 3-3. Due to the proximity of droplet volume values at very short intervals, data were recorded at 0.5 min

intervals. Figure 3-26 summarizes the related dynamic oil swelling test with images of the volume of oil droplets changing in the aqueous medium over time. At the beginning of the oil swelling test, it should be noted that the association of the cell with sources of the aqueous solution, carbon dioxide, or temperature and pressure changes that lead to droplet volume changes can cause a serious error in the test. Therefore, sufficient time was spent to maintain the temperature and pressure before the oil droplet floated, and the temperature was adjusted before the pressure to eliminate the interaction of temperature with the cell pressure. Also, for added security, after the oil drop floated, the cell was disconnected from the syringe pumps by valves installed in the connected lines.

$$\text{Oil swelling (\%)} = \frac{|V_t - V_i|}{V_i} \times 100 \quad (3-3)$$

Where V_i is the initial volume of the oil drop and V_t is equal to the volume of the oil drop at time t .



Figure 3-23: The process of preparing thin sections of rock for contact angle experiments.

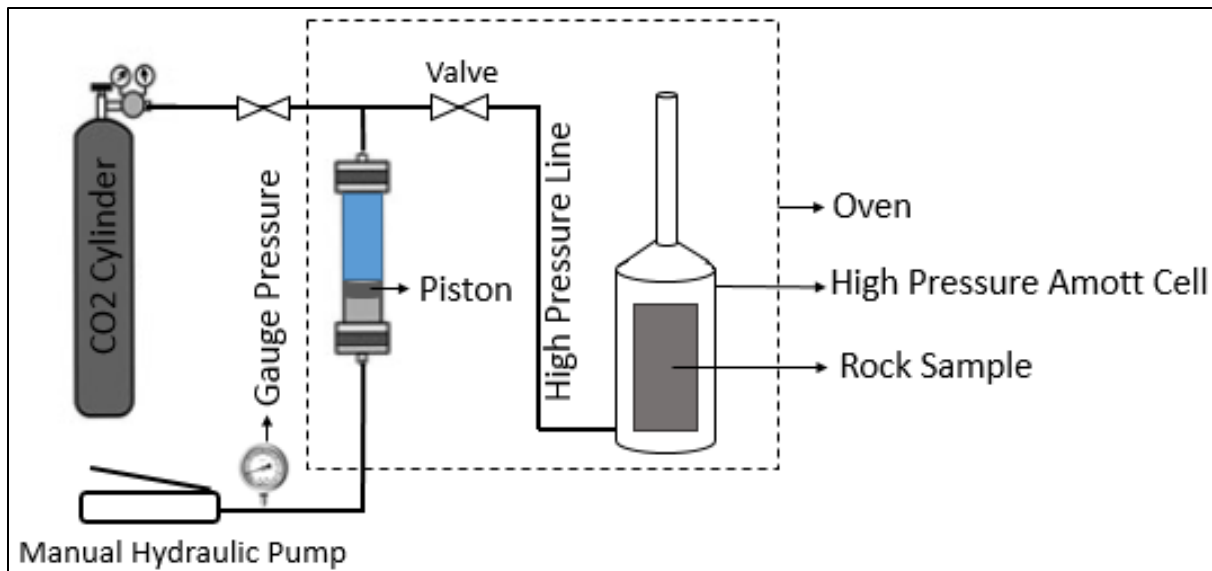


Figure 3-24: Schematic of pressure and temperature application system in carbonated water imbibition tests.

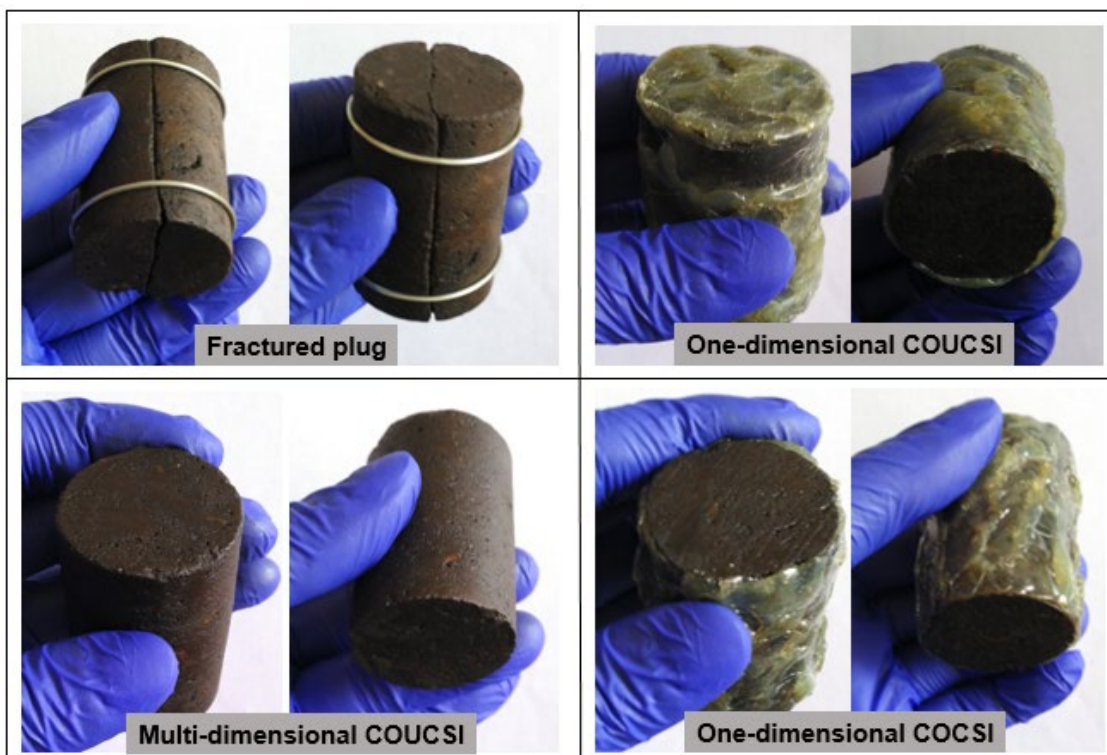


Figure 3-25: Examples of plugs prepared for imbibition tests.

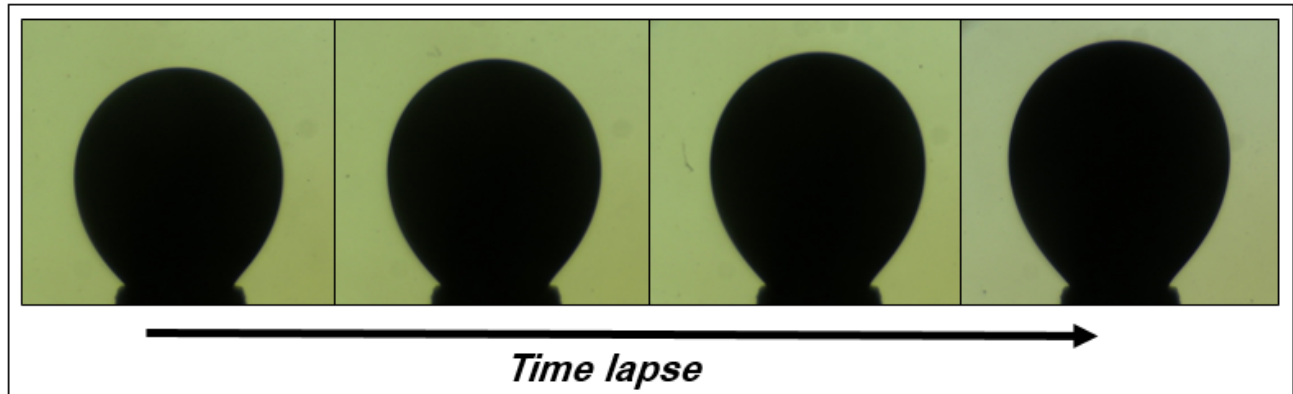


Figure 3-26: Summary of dynamic oil swelling test; increasing the volume of the oil droplet floating in the aquatic environment against time.

3.3.2. Surfactant, polymer and alkali

In this part of this chapter, the study of chemical water injection containing surfactants, polymers and alkalis in different scenarios is described. Used surfactants include natural and newly synthesized surfactants. Therefore, each surfactant after preparation (extraction and purification) and synthesis was characterized by related analyses. These materials include saponin extracted from *Anabasis Setifera* and its improved specimen, saponin extracted from *Soapwort* plant, surfactant synthesized from *Rapeseed* oil and surfactant synthesized from waste chicken fat. The polymers and alkalis used were not new and were only used to investigate various slug injection scenarios. Therefore, the innovation of this part of the research is the introduction, characterization and use of new surfactants to EOR by chemical water injection method. As mentioned in previous chapters, fluorinated surfactants are also sometimes injected into hydrocarbon reservoirs for various purposes. Their main application is to treat the area around the well-bore by changing the wettability to gas-wetting to remove condensate formed in these areas. In addition to the aforementioned surfactants, a fluorinated surfactant was synthesized and its effects on the treatment of reservoir rock were investigated. In the following, the laboratory method of examining each of these materials is described.

3.3.2.1. Extracted saponin from *Anabasis Setifera* plant

3.3.2.1.1. General study

In this part of the laboratory study of surfactant extracted from the *Anabasis Setifera* plant, a general method was followed. This process is shown in Figure 3-27. The steps are described in detail below. The tested oil extracted from the Gachsaran reservoir and the used rock were carbonate samples.



Figure 3-27: Graphical flow chart of a general study of the use of a surfactant in EOR. 1: synthesis or preparation of surfactants, 2: characterization and determination of functional groups, 3: temperature stability measurements, 4: surface tension measurement of surfactant solution and estimation of CMC, 5: measurement of IFT of surfactant solutions and oil and optimum salinity, 6: wettability tests, 7: flooding and calculation of recovery factor.

3.3.2.1.1.1. Extraction and preparation of surfactant solutions

Extraction was done by the maceration method. This involves soaking the tissues of the plant (powdered or coarse) in a suitable container mixed with a liquid as a solvent and aging for at least three days at ambient temperature with shaking. Then, the upper liquid is concentrated by heating and filtration the mixture [123]. In this work, 400 g leaves and plant stems were dried in the shade and at ambient temperature after cleaning. The crushed plant and 80%-alcohol solvent were poured into the flask. The flask was shaken every one hour by an orbital shaker for one hour to completely mix the contents into the solvent phase and get the extract well. After the necessary time, the supernatant liquid was filtered and concentrated by a distillation device at 50 °C. For complete drying, the sample was immersed in a vacuum pump for 24 hours in a desiccator. For complete drying of the solution, the sample was distilled for 24 hours in a desiccator with a vacuum pump. Purification of saponin was done by the optimization method of Massiot et al. [124]. For this purpose, the raw extract of saponin was dissolved in 50 ml distilled water and transferred to the

separator funnel. For every 6g of the original plant, 2.5 ml of saturated butanol was added to the water and stirred well. The funnel was placed on the stand so that after a few minutes, two layers were formed, and the lower layer consisted mostly of water and an upper layer containing butanol. The lower juice layer was again mixed with the same initial amount of butanol and again, the butanol layer was separated and stored. The separation was carried out three times, and the three butanol phases were mixed and then evaporated in a vacuum at a temperature of 55 °C and pure saponin was prepared. The sediment was dissolved in a minimum of 100% methanol volume and collected in the manner described.

3.3.2.1.1.2. FTIR, ¹H NMR, and TGA analyses

To identify the functional groups of the surfactant by FTIR analysis, a bit of surfactant in combination with KBr was used. IR spectra were recorded on the Tensor 27 FT-IR Bruker spectroscopy. The spectroscopy has a spectrum of 370-7500 cm⁻¹ and is equipped with an MIR-acle-attenuated total reflectance accessory that helps analyze liquid and solid samples.

The ¹H NMR spectrum of surfactant was recorded on a Bruker 500 MHz NMR spectrometer at 25 °C. The sample was solved in DMSO-d₆. Processing and interpreting the signal was done with Topspin 1.4 software and MestRe Nova.

Thermogravimetric calculations for 15mg of the Surfactant sample extracted from the *Anabasis Setifera* was done in a Netzsch TG209 F1 analyzer. The analysis was done in a pure nitrogen ambient. The sample was heated at a flow rate of 30 ml/min and a rate of 10 °C/min, from 20 to 300 °C.

3.3.2.1.1.3. Surface tension, water-oil IFT, and contact angle experiments

Surface tension and water-oil IFT tests for solutions containing surfactant at concentrations of 500, 1000, 2000, 3000, 4000, 5000, 6000ppm were carried out at 75 °C and pressure of 14.7 psi with a distilled water base and CMC was determined. Then, to estimate optimum salinity, IFT tests with a solution of surfactant at CMC and salts of NaCl, KCl, CaCl₂, MgCl₂, FeSO₄, K₂SO₄ and NaHCO₃ and formation water in different concentrations and a temperature of 75 °C and the pressure of 14.7 psi were performed. Formation water was achieved to diluted concentrations by adding distilled water in certain ratios. Finally, the contact angle was tested in the presence of a solution of surfactant at CMC and the contact angle was measured at different times. The effect of various salinity of MgCl₂, CaCl₂, KCl, NaCl, FeSO₄, K₂SO₄, and NaHCO₃ salts and formation water in different concentrations at 75 °C and 14.7 psi were investigated and recorded by repeating the contact angle tests. The device of IFT400 described in the previous sections, allows surface and interfacial tension and contact angle tests.

3.3.2.1.1.4. Surfactant flooding

The surfactant solution at CMC and optimum salinity of formation water were selected for surfactant injection and measuring the recovery based on the IFT and contact angle tests. Flooding was performed with a constant flow rate of 0.2 ml/min and temperature of 75 °C in both brine and surfactant injection.

3.3.2.1.2. CO₂-foaming behavior

In this section, the laboratory method for investigating the foaming behavior of surfactant extracted from *Anabasis Setifera* plant in the CO₂-foam injection process in fractured carbonate reservoirs is described.

3.3.2.1.2.1. CO₂-surfactant solutions surface tension

CO₂-surfactant solutions surface tension tests were performed by IFT400 device at the surfactant concentrations of 500, 1000, 2000, 3000, 4000, 5000, 6000 ppm at 75 °C and 14.7 psi with a distilled water base and the CMC value was determined.

3.3.2.1.2.2. Preparation and characterization of CO₂-foam

CO₂-foam was prepared by blowing CO₂ in a surfactant solution in CMC at a temperature of 75 °C in a Ross-Miles foam generator with the ability to adjust the temperature of the foam chamber. To prepare CO₂-foam, 40 ml of surfactant solution in CMC was poured into a foam chamber and carbon dioxide gas was blown at different flow rates. The foam prepared by the Ross-Miles foam generator was used to determine its properties

3.3.2.1.2.3. Secondary CO₂-foam flooding in fractured plug

CO₂-foam produced from surfactant solution in CMC and at optimum salinity was selected and for secondary injection as described above. Flooding with a constant flow rate of 0.5 cc/min and temperature of 75 °C was performed in both stages of saline water and foam injection. The flooding device described in the previous sections was used. To prepare the injection foam, a flooding cylinder was used as a foam production chamber and salinity and optimal flow rate were applied in it. In such a way that similar conditions with a Ross-Miles foam generator by connecting the carbon dioxide gas line to the lower inlet of the cylinder and removing its piston, the foam was prepared in it and to connect the cylinder in the flooding device after preparing the foam, the piston was placed in it. A fractured carbonate plug was used. For this purpose, a carbonate plug was divided into six equal parts by a horizontal cut and two vertical cuts.

The cut pieces were placed next to each other and screwed with Teflon. In addition to setting the matrixes together, this helps to block the area around the plug. Figure 3-28 shows the steps for preparing CO₂-foam, preparing the fractured plug, and finally setting up the flooding system.



Figure 3-28: CO₂-foam preparation and flooding process in a fractured carbonate plug.

3.3.2.2. Modified saponin of *Anabasis Setifera* plant

In this part, the molecular structure of saponin extracted from the *Anabasis Setifera* plant was modified as Double-Chain Single-Head through the Esterification process, and after characterization of the modified surfactant, EOR experiments were performed. Figure 3-29 shows the flowchart of laboratory steps. The experiments are described in detail below. Characterization of the modified surfactant was performed by ¹H NMR, FTIR and TGA analyses as previously described. The tested oil extracted from the Gachsaran reservoir and the rock used were carbonate samples.

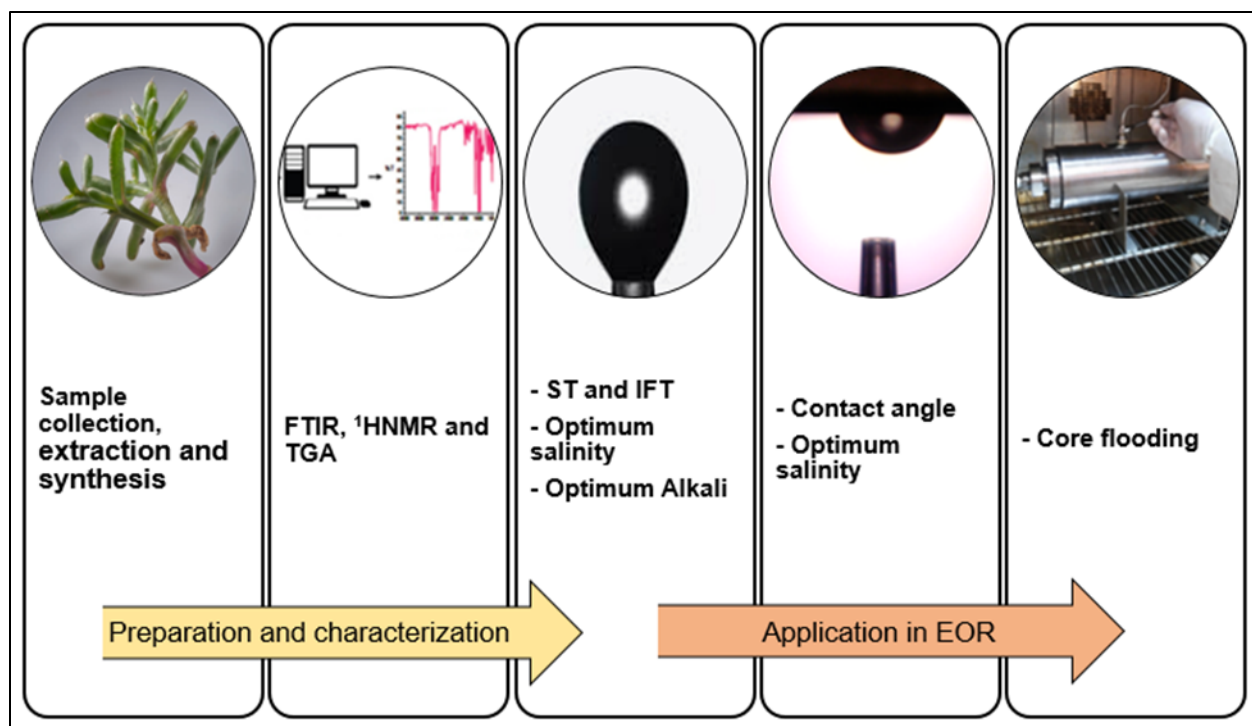


Figure 3-29: Graphical flow-chart of laboratory stages.

3.3.2.2.1. Surfactant modification

The process of esterification was used to modify the surfactant structure as Double-Chain Single-Head (Figure 3-30). To this end, 360 mg of the extracted saponin from *Anabasis Setifera* plant was dissolved in 10 cm³ of N, N-dimethylformamide, and anhydrous in the 50 cm³ round bottom flask. Acyl chloride saturated fatty acid (C12) was added to a proportion of 1:1 ratio with saponin and two times more fatty acid and potassium carbonate were added to the resulting solution. Subsequently, the mixture was stirred for 4 hours at ambient temperature and the progression of the reaction was checked with thin-layer chromatography until the end. Afterward, the combination was mixed with 10 cm³ of water and 30 g of AB-8 macroporous resin. Following one-hour standby, the resin was collected by pressure reduction filtration and washed with water several times. The product was eluted on the resin after being washed several times with ethanol. The solution was evacuated and its pH was adjusted to 4 with HCl. The watery phase was washed several times with a mixture of hexane and ethyl acetate to remove non-polar impurities; it was then dried. The product obtained at this stage was mixed with ethanol, and then the ethanol-base phase was evaporated with heat. The solid product was ultimately obtained with a very light brown color.

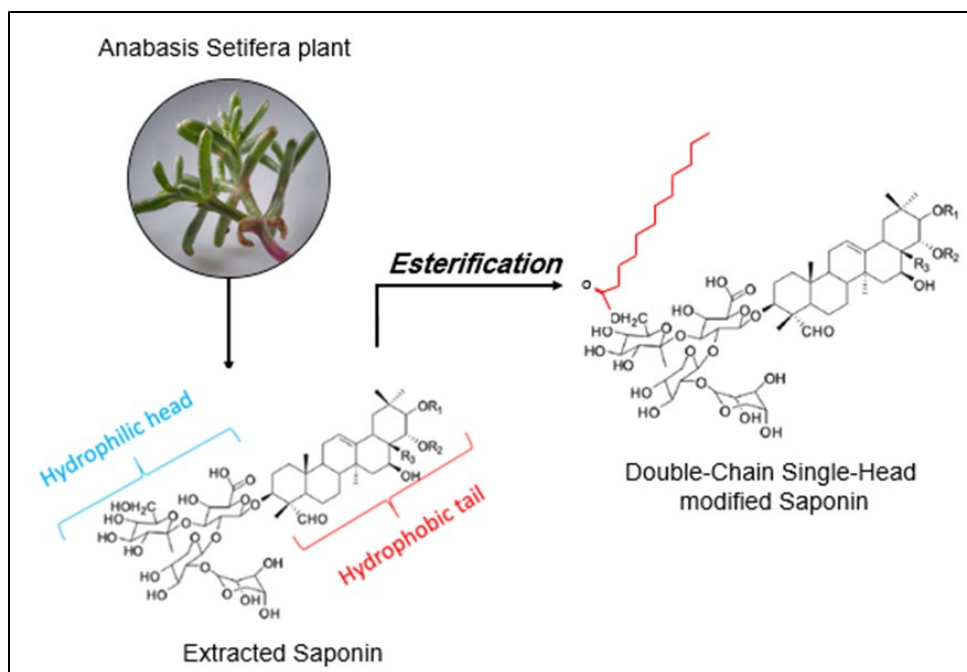


Figure 3-30: Modification of the structure of saponins extracted from *Anabasis Setifera* plant through Esterification.

3.3.2.2.2. Surface tension, interfacial tension and contact angle experiments

Surface and interfacial tension and contact angle tests were performed by the IFT400 device exactly as described in the previous step for surfactant extracted from *Anabasis Setifera* plant. Also, the effect of Na_2CO_3 alkaline on the interfacial tension of surfactant solution in CMC and crude oil was investigated. An observational experiment was also carried out to better display the wettability alteration with the surfactant solution at CMC. This test was performed on a thin section with a 5 mm thickness. One side of the section was soaked with oil, that a layer of it becomes oil-wet. Afterward, the section was placed in the desired solution at the above-mentioned reservoir temperature and photographed at the start of the test and intervals. This way, the change in the surface and distribution of oil on the section was seen and compared over time [5]. This test was carried out for a solution of surfactant in an optimum concentration.

3.3.2.2.3. Alkali-Surfactant slug injection

The optimum chemical solution containing surfactant at CMC and salinity and alkali at optimum concentrations was selected for tertiary injection and measuring the recovery. The optimum solution of injectable surfactant-alkali contained the modified surfactant at CMC of 3000 ppm, the optimum salinity of the formation water at 10000 ppm, and the optimum Na_2CO_3 alkali at 2000 ppm. Chemical-slug injection was performed according to SY/T 6424-2000 Chinese standard [125]. The flooding stages included core

saturation with the formation water, oil injection to achieve primary oil saturation, saline water flooding up to 98% water cut, ASP-slug injection of 0.5 PV volume, and eventually, re-injection of saline water up to 99% water cut.

3.3.2.3. Extracted saponin from *Soapwort* plant

Laboratory steps include preparation and characterization of surfactant from *Soapwort* plant, surface tension test and CMC estimation, water-oil interfacial tension, evaluation of different salinity and alkaline effects, contact angle tests and ASP-slug injection. The surfactant was prepared in two stages of extraction and purification of saponin extracted from the crude extract of the *Soapwort* plant. Extraction was performed using ultrasonic waves and 80% methanol solvent. In this method, ultrasonic waves with a frequency of 70 kHz at a temperature of 25 °C for one hour were used [126]. 300 g of dried and powdered roots of the plant as the richest source of saponin among its tissues, was placed along with methanol solvent in a beaker. The mixture was exposed to ultrasound for one hour. The clear supernatant was then concentrated by a rotary evaporator. The saponin purification step was performed by Massiot et al.'s method (Described in the previous sections) [124]. The surfactant characterization was performed using FTIR and TGA analyses as previously described. Surface tension tests were performed to determine CMC at 80 °C by the pendant drop method. For this purpose, surfactant solutions were prepared in different concentrations and after calculating the density, surface tension tests were performed. Water-oil Interfacial tension tests were performed for solutions containing surfactant at different concentrations and 80 °C. Then, to estimate the optimal salinity, the interfacial tension tests with surfactant solutions containing a surfactant in CMC and NaCl, MgCl₂ salts and formation water at different concentrations were performed at 80 °C. The effects of NaHCO₃, Na₂CO₃ and NaOH as weak, medium and strong alkalis on the interfacial tension of surfactant solution and crude oil were also investigated. Finally, the oil droplet contact angle tests were performed in the presence of surfactant solution in CMC and the contact angle was measured at different times. ASP injection was performed according to SY/T 6424-2000 standard of Chinese as mentioned earlier [125]. An ASP-slug containing surfactant solution in CMC, optimum salinity and alkalinity and 1000 ppm polymer with a volume of 0.5 PV was injected.

3.3.2.4. Synthesized surfactant from *Rapeseed oil*

In this part, an anionic surfactant synthesized from *Rapeseed* oil was examined. The surfactant was synthesized by Esterification and Sulphonation processes. The following is a detailed description of the test steps for surfactant synthesized from *Rapeseed* oil. The oil used in this part of the study was supplied from the Sarvestan oil reservoir and the rock used was carbonate/sandstone composite (CSC).

3.3.2.4.1. Surfactant synthesis

For the synthesis of surfactant from *Rapeseed* oil, first, the esterification process was performed. The esterification process improves the physicochemical properties of the oil by displacing the fatty acid bases in the triglyceride molecule. At this stage, 0.5 wt% of the potassium hydroxide catalyst was used in combination with the oil and polyethylene glycol 400. The temperature of the mixture was raised to 70 °C and stirred for 30 min. Purification and separation of the catalyst and excess polyethylene glycol in a separation funnel was performed by collecting ethyl ester in the top layer. The residual fatty acid was also washed with sodium bicarbonate and diethyl ether and then the product was dried by a distillation apparatus. To complete the process, the sulphonation was performed on the product of the esterification step, which was a very light brown viscous liquid. 5.40 g of chlorosulfuric acid in combination with 30 mL of pyridine was stirred at 60 °C to give a dilute solution. The dilute solution was quenched with concentrated sodium bicarbonate and sodium carbonate in a separating funnel. Removal of non-reactive organic matter was performed using an n-butanol solvent. Separation of water and pyridine from the aqueous layer was performed using the evaporation method at 120 °C. Organic impurities were also removed with petroleum ether solvent. The product was finally evaporated to give a light yellow powder which was the final anionic surfactant sodium ethyl ester sulfonate.

FTIR, ¹H NMR and TGA analyses were used to determine surfactant properties.

3.3.2.4.2. Surface tension, interfacial tension and contact angle experiments

Surface tension tests of surfactant solutions at different concentrations with distilled water base were performed by the pendant drop method at 80 °C and the CMC value was determined. The IFT400 was used to measure surface tension.

Interfacial tension tests of the surfactant solutions at different concentrations and crude oil at 80 °C were performed by the spinning drop method with the device described in the previous sections.

The contact angle and observational wettability tests were performed as described in the previous sections.

3.3.2.4.3. Foamability and emulsion stability tests

To test the properties of surfactant foam, 5 mL of each surfactant solution was poured into a test tube. The tubes were shaken for 5 seconds by a Vortex Mixer and placed at rest and the foam volume was measured over time [127].

The stability of the surfactant-crude oil emulsion was determined in CMC. A UP400 ultrasonic agitator was used to stabilize the emulsion. The surfactant solution and crude oil were exposed in an equal volume by ultrasonic waves for 30 min at 400 W. The emulsion was then poured into a falcon tube at 80 °C to observe the phase separation.

3.3.2.4.4. Surfactant adsorption in the CSC plug

First, the surfactant solution conductivity was measured by a Model-3540 device manufactured by Jenway, UK. The adsorption rate of the surfactant in the porous medium was measured by flooding its solution in CMC with a rate of 0.2 mL/min in a CSC plug with an absolute permeability of 80.36 mD, an effective porosity of 24 %, a length of 7 cm and a diameter 3.8 cm. The flooding was performed at 80 °C. The plug was dried for a day at 60 °C after washing. The unknown concentration of the surfactant at the output was measured from the conductivity calibration curve using its conductivity value. The reduction of the concentration at the outlet per injected PV was recorded as the adsorption rate. The flooding device described in previous sections was used in this experiment.

3.3.2.4.5. Oil recovery by ASP flooding

Flooding experiments were performed to obtain oil recovery of CSC plugs with the device described in the previous sections. The injection into the rock plugs was performed according to the Chinese standard of SY/T 6424-2000 [125]. Integrated injection of the surfactant solution at CMC and optimal salinity, injection of 0.50 PV of the surfactant solution at CMC and optimal salinity and NaOH alkalinity (SA), injection of 0.50 PV of the surfactant solution at CMC and optimal salinity and 1000 ppm of PHPA polymer (SP), injection of 0.25 PV of the surfactant solution at CMC and optimal salinity and NaOH alkalinity and 1000 ppm of PHPA polymer (ASP) and injection of 0.50 PV of the surfactant solution at CMC and optimal salinity and NaOH alkalinity and 1000 ppm of PHPA polymer (ASP) were performed.

3.3.2.5. Synergic effect of dissolved carbon dioxide and the *Rapeseed oil* surfactant

In this section, the effects of the combination of carbon dioxide and anionic surfactant synthesized from *Rapeseed* oil in the previous section on interfacial tension, carbonate rock wettability and crude oil swelling were investigated. For interfacial tension and oil swelling tests, surfactant solutions were prepared at concentrations of 3500, 4500 and 5500 ppm as concentrations below CMC, CMC and above CMC, respectively. Carbon dioxide was dissolved in surfactant solutions at pressures of 1000 and 2000 psi and temperatures of 30 and 80 °C. Finally, to investigate the effect of salinity of the injected fluid, IFT, oil swelling and contact angle experiments were repeated for carbonated fluids containing the surfactant in CMC at a constant pressure and temperature of 2000 psi and 80 °C. The salinity of the base fluid was

provided by dissolving NaCl at concentrations of 5000, 10000, 20000, 40000, 80000 and 120000 ppm. Carbonated water preparation and interfacial tension, contact angle and oil swelling tests were performed as previously described.

3.3.2.6. Synthesized surfactant from waste chicken fat

In this part of the research, waste chicken fat was used as a raw material for the synthesis of an anionic surfactant. The surfactant was synthesized by Esterification and Sulphonation processes and its characterization and temperature stability were measured by FTIR and TGA analyses. Experiments of pendant drop surface tension, spinning drop water-oil interfacial tension, contact angle, and chemical ASPslug injection at optimum salinity and alkalinity with polymer were performed to measure the application of the surfactant in EOR. Also, the surfactant's ability to produce nitrogen-foam was investigated by generating foam in a temperature-adjustable Ross-Miles foam generator (described earlier). The stability of the emulsion formed by the surfactant was also tested by observational experiments. The details of all the experiments performed in this part of the research in the previous stages are described.

3.3.2.7. Synthesized fluorinated anionic surfactant

This section describes a laboratory method for investigating the use of an anionic fluorinated surfactant to treat the area around the wellbore in condensate gas reservoirs through wettability alteration to gas-wetting. Laboratory steps according to Figure 3-31 include synthesis and characterization of surfactant, surface tension tests to calculate CMC, contact angle tests, compatibility and foamability, adsorption in porous media, and finally gas-liquid imbibition tests in non-treated and treated plugs in surfactant solution at optimal aging conditions in terms of maximum contact angle (more gas-wetness), each of which is described in detail below.

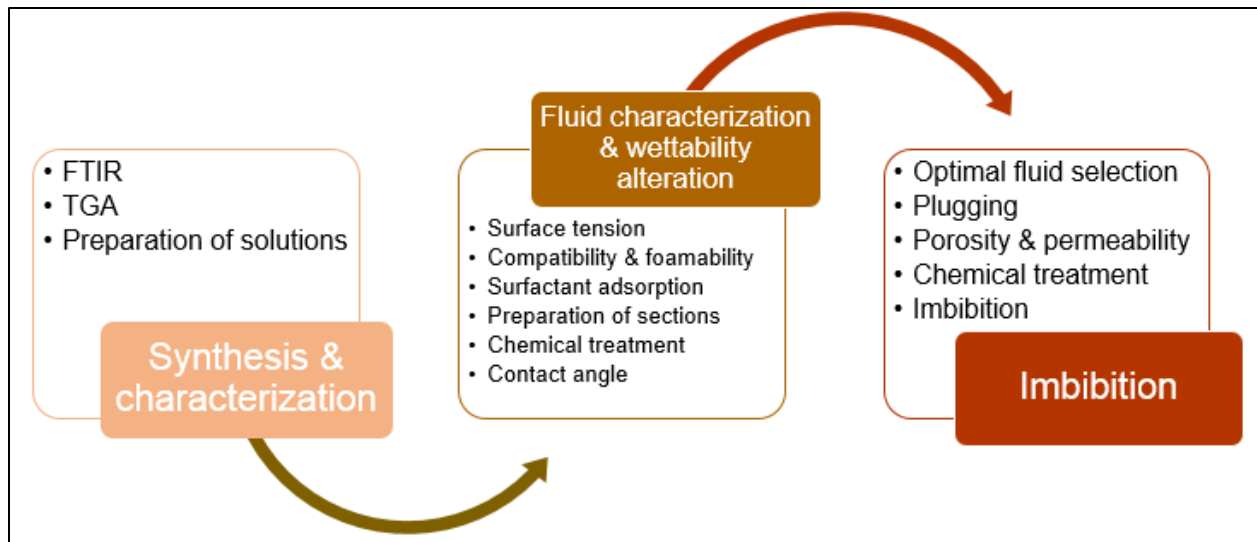


Figure 3-31: Laboratory steps of the study of fluorinated anionic surfactant for the treatment of condensate reservoir rock.

3.3.2.7.1. Surfactant synthesis

Chen et al.'s method [128] was used for the preparation of anionic fluorinated surfactant. This method follows the schematic process of **Figure 3-32**. The procedure involves two steps of preparing p-perfluorononyl phenyl ether and then preparing sodium p-perfluorononyloxy benzene sulfonate fluorinated surfactant. In the first step, phenol and perfluorononene were thoroughly mixed and stirred in a 1:1.3 molar ratio. Sulfolane was then added to the mixture and stirred for 5 min. Triethylamine with a 0.5:1 molar ratio with perfluorononene was slowly added to the mixture for 45 min and the mixture temperature was brought to 348 K. The reaction was complete after 3.5 h of triethylamine addition to the mixture. The resulting mixture was purified by distillation. Thereafter, the oily product was washed with a 5% NaOH solution and distilled water. The final product of the first stage, which was liquid, was dried with Na₂SO₄. In the second step, namely the synthesis of sodium p-perfluorononyloxy benzene sulfonate through the sulfonation of p-perfluorononyl phenyl ether obtained from the first step, 1,2-dichloroethane was added to a three-necked flask and stirred for 5 min. Sulfur trioxide was then gently added to the mixture at 298 K for 20 min with a molar ratio of 1.20:1 with p-perfluorononyl phenyl ether. After 1 h, the mixture was purified by distillation. The mixture was then recrystallized with petroleum ether and neutralized with NaOH solution. Finally, by vacuum distillation, sodium p-perfluorononyloxy benzene sulfonate white viscous liquid was obtained as the final product.

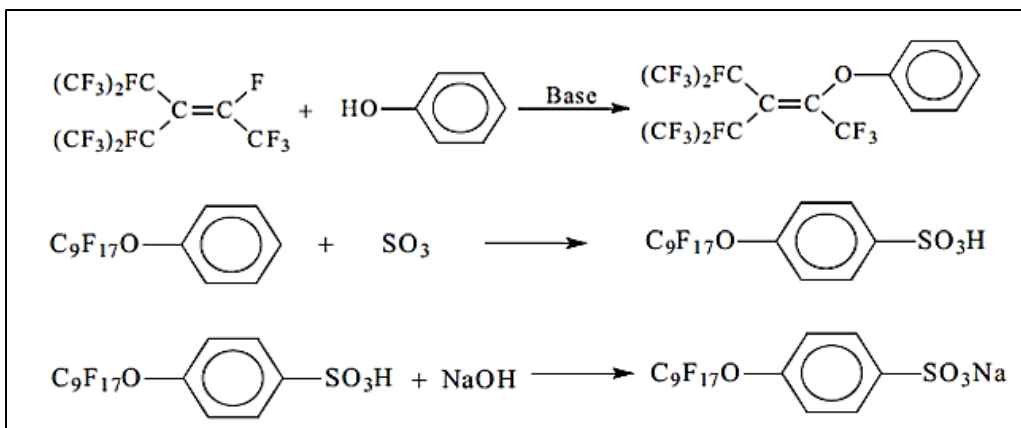


Figure 3-32: The reactions of synthesizing the anionic F-surfactant based on Chen et al.'s method [128].

3.3.2.7.2. Surface tension and contact angle

Surface tension tests of surfactant solutions at different concentrations with distilled water base were performed by the pendant drop method at 298 K and the CMC value was determined. The IFT400 was used to measure surface tension. For contact angle tests, thin sections of carbonate were prepared in the manner described earlier, but here, the washed and dried sections were aged for one month in the gas condensate at 373 K for hydrophobicity. After that, each section was aged in surfactant solutions at different concentrations and each at a certain temperature. All three parameters of surfactant concentration, temperature and aging time were examined in these experiments. For this purpose, surfactant concentrations of 500, 1500, 2500, 3500, 4500, 5500 and 6500 ppm and test temperatures of 313, 343 and 373 K and aging times of 30, 60, 120 and 240 hours were considered. With this interpretation, 84 contact angle tests were performed. The IFT400 device was also used to perform the contact angle test.

3.3.2.7.3. Foamability

For foamability tests, nitrogen-foam was prepared by blowing nitrogen in a surfactant solution at CMC and 373 K in a Ross-Miles foam generator capable of adjusting the temperature of the foam chamber (as mentioned earlier).

3.3.2.7.4. Surfactant adsorption in carbonate porous media

The adsorption test in a porous medium, as described in the previous sections, was performed for optimal fluid.

3.3.2.7.5. Imbibition tests

Gas-liquid imbibition tests in carbonate plugs were performed to show the gas-wetting properties of the plug treated by the chemical solution. The plug connects to a forcegauge and floats in the gas condensate. Then, the weight changes caused by the gas condensate imbibition are recorded. At this stage, the carbonate plug was saturated from the gas condensate and aged for a month in the gas condensate at 373 K to obtain hydrophobicity. Then, the desired plug was treated in the selected chemical solution from the previous stage and the imbibition test was performed. The optimum fluid of choice was fluid in terms of surfactant concentration and duration of treatment based on contact angle tests. However, the chemical treatment temperature was considered to be the highest test temperature of 373 K. The used device was described in the previous sections.

3.3.2.8. Extracted mucilage from *Hollyhocks* plant as a natural polymer

The laboratory method used in this part of the research includes extraction of natural polymer from *Hollyhocks* seeds, characterization and estimation of its temperature stability using FTIR and TGA, investigation of viscosity behavior and finally injection of ASP slug.

Mucilage extraction was performed by the ultrasonic method. This method is one of the most effective methods of extracting plant tissues due to the mechanical effects of ultrasonic waves and the formation of micro-channels in plant tissue as a result of the cavitation phenomenon near the solid surface [129, 130]. 300 g of *Hollyhocks* seeds were first hydrated in distilled water in a 1:20 ratio for a day at 80 °C. The hydrated seeds were exposed to direct ultrasonic waves at a frequency of 24 kHz and a power of 400 watts for 30 min. To prevent a sudden temperature rise, the beaker containing the sample was placed in an insulated container with ice and the temperature was monitored every minute. After ultrasonic application, the seeds were separated from the solution using a multilayer cheesecloth and Büchner funnel connected to the vacuum pump. The separated mucilage was mixed with three times the volume of 90% ethanol as an anti-solvent for precipitation of the polymer. The resulting colloidal mixture was then dried by an oven at 50 °C and powdered by a mill. The resulting powder was passed through a mesh 18 sieve and kept in a sealed container for later use. Using this method, 27 g of dried and powdered mucilage was obtained from every 300 g of primary seeds.

Characterization and temperature stability determination of the polymer extracted from the *Hollyhocks* plant were performed with FTIR and TGA analyses.

To investigate the viscosity, polymeric solutions with distilled water base were first prepared. The solution was mixed using a magnetic stirrer. Mucilage normally increases viscosity well at low concentrations, so solutions were prepared at 500, 1000, 2000, and 3000 ppm. To investigate fluid behavior against shear rate changes, variable shear rates were applied in viscosity tests. Due to the water absorption properties of the polymer and the time-consuming nature of the process, polymeric solutions have different rheological behaviors at different times. Therefore, it was necessary to measure the viscosity of the solutions at different times. The viscosity of the solutions was measured at 6, 12 and 24 hours of hydration. In examining the effect of hydration time, the temperature in the experiments was fixed at 30 °C. Temperature is an important and very influential parameter on viscosity. This parameter is doubly important due to the reservoir temperatures. Therefore, after estimating the appropriate time for maturation of polymeric solutions, the viscosity of the solutions at 30, 50 and 80 °C was also measured. Salinity is another parameter that affects the performance of polymers in increasing viscosity. To investigate the salinity effect, diluted samples of FW were considered as the base fluid. For this purpose, FW was used in the main concentration and 5 and 10 times diluted samples. At each dilution step, 100 mL of distilled water was added to the FW. The viscosity of saline-based polymeric solutions was measured after the optimal hydration time obtained from the previous stage and at 80 °C at different polymer concentrations and different shear rates.

In the next step, ASP slug injection was performed to calculate the oil recovery rate. Chemical flooding was performed according to the SY/T 6424-2000 standard of Chinese [125]. The ASP-slug included the anionic surfactant synthesized from waste chicken fat at CMC, an optimal NaOH alkalinity, and a suitable concentration of natural polymer according to the results of viscosity tests.

Chapter 4: Findings and analyses

In this chapter, the results obtained from the experiments have been presented in the form of tables and graphs based on the tested methods. Also, the existing mechanisms have been interpreted based on the results obtained.

4.1. Effects of mutual solvents on smart carbonated water

4.1.1. Density and IFT experiments results

Density is a term affecting IFT. Table 4-1 shows the density values for binary solutions of diluted seawater and methanol and acetone solvents at 75 °C and 0.101, 3.447, 6.894 and 10.342 MPa pressures and Table 4-2 shows the densities of these solutions when CO₂ is added to the system at 75 °C and pressures of 3.447, 6.894 and 10.342 MPa. Table 4-1 shows that the densities of binary solutions decrease with increasing concentrations of methanol and acetone, which have lower densities than seawater. As system pressure increases, density increases, but this increase is negligible and when CO₂ is added to the system (Table 4-2), the density values decrease with increasing pressure. Increasing the pressure in the carbonated water system will increase the dissolved carbon dioxide. By increasing dissolved carbon dioxide as a lighter component, the density decreases. However, it should be noted that there is a carbon dioxide source for further dissolution, such as the process of producing carbonated water in this study. Otherwise, the increase in pressure will compress the carbonated fluid and increase the density.

Table 4-1: Density values for binary solutions of diluted seawater and methanol/acetone at various pressures and a temperature of 75 °C.

Pressure [MPa]	Density [g/cm ³]																				
	Base fluid	Seawater				Diluted seawater at a concentration of 22000 ppm				Diluted seawater at a concentration of 16500 ppm				Diluted seawater at a concentration of 13200 ppm				Diluted seawater at a concentration of 11000 ppm			
		Solvent percent	0	5	10	15	0	5	10	15	0	5	10	15	0	5	10	15	0	5	10
0.101	Methanol		1.021	1.009	0.997		1.010	0.999	0.987		1.005	0.999	0.982		1.002	0.991	0.980		1.000	0.989	0.978
	Acetone	1.033	1.020	1.008	0.996	1.022	1.010	0.998	0.986	1.016	1.004	0.993	0.981	1.013	1.001	0.990	0.978	1.011	0.999	0.988	0.977
3.447	Methanol		1.023	1.010	0.999		1.012	1.000	0.990		1.005	0.996	0.983		1.003	0.994	0.981		1.003	0.991	0.981
	Acetone	1.033	1.022	1.009	0.998	1.023	1.010	0.999	0.989	1.016	1.005	0.993	0.983	1.013	1.001	0.991	0.980	1.012	1.001	0.990	0.978
6.894	Methanol		1.024	1.010	1.000		1.012	1.000	0.992		1.007	0.996	0.985		1.004	0.995	0.983		1.003	0.991	0.982
	Acetone	1.034	1.022	1.010	0.999	1.023	1.011	1.000	0.990	1.016	1.006	0.994	0.983	1.014	1.002	0.993	0.980	1.012	1.002	0.991	0.978
10.342	Methanol		1.025	1.011	1.000		1.013	1.002	0.992		1.008	0.998	0.986		1.004	0.995	0.984		1.005	0.993	0.983
	Acetone	1.034	1.022	1.010	1.000	1.024	1.012	1.001	0.992	1.017	1.006	0.995	0.984	1.015	1.003	0.994	0.981	1.013	1.003	0.992	0.980

Table 4-2: Density values for carbonated binary solutions of diluted seawater and methanol/acetone at various pressures and a temperature of 75 °C.

Pressure [MPa]	Density [g/cm ³]																				
	Base fluid	Seawater				Diluted seawater at a concentration of 22000 ppm				Diluted seawater at a concentration of 16500 ppm				Diluted seawater at a concentration of 13200 ppm				Diluted seawater at a concentration of 11000 ppm			
	Solvent percent	0	5	10	15	0	5	10	15	0	5	10	15	0	5	10	15	0	5	10	15
3.447	Methanol	1.027	1.018	1.005	0.991	1.016	1.008	0.994	0.981	1.010	1.001	0.989	0.973	1.003	1.001	0.989	0.975	1.009	1.000	0.986	0.973
	Acetone		1.016	1.001	0.991		1.004	0.990	0.979		1.000	0.984	0.971		0.998	0.982	0.970		0.995	0.987	0.972
6.894	Methanol	1.024	1.012	1.003	0.986	1.014	1.001	0.989	0.975	1.007	0.998	0.983	0.970	1.000	0.997	0.988	0.971	1.004	0.997	0.981	0.965
	Acetone		1.010	1.000	0.982		1.000	0.987	0.972		0.996	0.981	0.969		0.996	0.980	0.964		0.990	0.982	0.961
10.342	Methanol	1.022	1.006	1.001	0.983	1.010	0.998	0.987	0.970	1.002	0.993	0.981	0.968	0.999	0.991	0.981	0.965	1.002	0.991	0.973	0.960
	Acetone		1.003	0.999	0.979		0.992	0.983	0.968		0.991	0.980	0.967		0.990	0.976	0.959		0.988	0.977	0.956

Table 4-3 shows the IFT values of the binary solutions including seawater with initial and 22000, 16500, 13200 and 11000 ppm concentrations against the solvents concentrations at 75 °C and pressures of 0.101, 3.447, 6.894 and 10.342 MPa and Figs. 4-1 to 4-4 show the data of Table 5 as graphs. The overview of Figs. 4-1 – 4-4 shows that there is no particular trend in the IFT against the pressure of the system when methanol or acetone is present in different volumetric proportions. However, IFT reduction is confirmed for constant seawater concentration and increasing the concentration of both methanol and acetone solvents. By diluting the seawater and reducing its salinity, in the presence and absence of solvent, the IFT also decreases. This trend is characterized by comparing Figs. 4-1 – 4-4. However, as the salinity increases, this trend becomes slighter. To understand the reduction of IFT by increasing the ratio of methanol and acetone, the structure of the solvents and their behavior in the interface should be studied. Methanol is a co-surfactant and its structure has a polar hydrophilic section (OH) and a non-polar hydrophobic portion (CH₃) [131]. This structure adsorbs it in the interface and forms a lower IFT layer. On the other hand, methanol, like water, also has hydrogen bonds. When methanol is dissolved in water, methanol-water hydrogen bonding is placed between the water-water hydrogen bond and weakens it. The weakening of the bond will reduce the surface tension in the interface [132]. Reducing IFT by increasing methanol concentration is justified by this mechanism. Acetone also has a similar structure that is, it has both polar and nonpolar sections in its molecular structure and can act as a co-surfactant in aqueous solutions [133]. Another noteworthy point in the IFT reduction mechanism is the density of binary solutions. Both methanol and acetone have densities less than water and when dissolved in water with various volumes, proportional to the same ratios, the density of the solution decreases relative to the water density. This decrease in density causes the density of the aqueous solution to be close to the crude oil density and a lower density difference that is proportional to the volume ratio of the solvent. The density is directly related to the amount of water-oil IFT. As shown in Figs. 4-1 – 4-9, at constant concentrations of solvents, the IFT values of water-acetone solutions are

slightly less than the IFT of water-methanol solutions and crude oil. This issue can also be explained by the lower density of acetone than methanol, as well as its binary solutions with water relative to water-methanol binary solutions. When solvents are absorbed in the water-oil interface, they create a layer that can absorb more ions and enhance the layer so that the thickness of the oil-solvent-ion layer becomes greater than the thickness of the previous layer of the oil-ion. This is shown schematically in Fig. 4-10. As mentioned earlier, IFT also increases with increasing salinity in the presence of solvents. Another mechanism related to the presence of solvents and soluble ions could explain this behavior. As the salinity increases, the solubility of the solvents in the aqueous solution decreases. This results in increased solvent mass transfer from the aqueous phase to the oil phase [134]. In this way, the solvent molecules move to the oil phase instead of being absorbed in the interface, and instead of reducing the IFT, will cause oil swelling.

Table 4-4 and Figs 4-5 to 4-9 show the IFT values for seawater with initial and 22000, 16500, 13200 and 11000 ppm concentrations against concentrations of methanol and acetone in the presence of dissolved CO₂ at 75 °C and pressures of 3.447, 6.894 and 10.342 MPa. When CO₂ is added to the system, IFT reduction continues and this reduction is proportional to the increase in pressure, the base fluid salinity and the percentage volume of solvent (Figs. 4-8 – 4-9). The IFT reduction mechanisms in this study for carbonated smart water containing methanol and acetone solvents are controlled by soluble ions, methanol and acetone solvents, dissolved CO₂ and synergistic effects of ions/carbonated water with solvents. The impacts of ions and carbonated water on the IFT have been discussed in our previous studies (see references [135 - 137]). The synergistic effects of ions/carbonated water with solvents play an important role in IFT reduction. When the methanol or acetone solvent is present in the system, the CO₂ solubility increases [138, 139]. In the case of IFT, due to the reaction of carbonic acid and the nitrogenous alkalis of crude oil and the production of in-situ soap, increased CO₂ solubility in water can increase the volume of carbonic acid as one of the reaction raw materials and subsequently the reaction product in the water-oil interface. Therefore, the IFT decreases more. In other words, the solvents do not directly increase carbonic acid, but by increasing the solubility of CO₂ in water, they cause more carbon dioxide in the system. Increased solubility of carbon dioxide in water by increasing solvents fraction is due to greater solubility of carbon dioxide in solvents. For example, the solubility of carbon dioxide in methanol is about 3.5 times higher than in water at the same condition [140]. Carbonic acid is formed according to Eq. 4-1 by the reaction of dissolved carbon dioxide and water:



However, this effect is limited by the number of nitrogenous components in the oil. Considering that the reduction of IFT by carbonated water depends on the amount of dissolved CO₂, it can be said that this is one of the reasons for the intensification of IFT reduction of the carbonated solution containing solvents.

As mentioned earlier, dead crude oil was used in this study. Dead oil has lost its gas and has less light composition than live-oil at reservoir conditions. Oil components are very effective in IFT but most impacts are on heavy and polar oil components such as asphaltene and resin, which remain when gas is extracted from the oil. The use of live-oil in IFT tests is not common according to the environmental conditions of the laboratory. Normally, dead oil, synthetic oil and even Kerosene as oil phases are used. The mechanism for the reduction of IFT by carbonated water, as mentioned earlier, relates to the reaction between carbonic acid and nitrogenous alkalis of crude oil and in-situ soap production, which also remains when the gas is extracted from live-oil. However, the conditions for carbonated water injection into the reservoir and the presence of live-oil are not entirely consistent. When carbonated water is placed in the vicinity of oil, CO₂ dissolves in the oil but the components of crude oil cannot be dissolved in carbonated water. Therefore, the CO₂ transfer into live-oil within the reservoir creates a competition between dissolved hydrocarbon gas and transmitted CO₂, creating a new gas phase. The growth of this new phase can recover oil by a mechanism of oil swelling [71].

Table 4-3: Water-oil IFT values for binary solutions of diluted seawater and methanol/acetone at various pressures and a temperature of 75 °C.

		IFT [mN/m]																			
Pressure [MPa]	Base fluid	Seawater				Diluted seawater at a concentration of 22000 ppm				Diluted seawater at a concentration of 16500 ppm				Diluted seawater at a concentration of 13200 ppm				Diluted seawater at a concentration of 11000 ppm			
		Solvent percent	0	5	10	15	0	5	10	15	0	5	10	15	0	5	10	15	0	5	10
0.101	Methanol	27.341	22.761	19.124	16.248	23.184	18.673	16.212	13.441	18.323	14.170	11.913	10.944	15.231	12.560	9.918	7.996	15.422	12.087	8.903	7.407
	Acetone		20.537	14.265	13.917		18.149	14.470	11.209		12.025	10.822	10.375		11.423	8.762	7.169		10.765	8.169	6.854
3.447	Methanol	22.139	21.394	19.921	16.948	20.451	20.757	16.015	16.075	19.101	18.071	14.997	13.236	18.671	17.812	15.719	12.558	16.736	14.502	10.797	7.125
	Acetone		19.473	18.533	16.167		19.691	17.875	13.147		16.112	13.675	10.655		16.986	13.003	9.450		11.783	8.618	6.440
6.894	Methanol	28.479	22.194	19.886	17.141	24.526	17.344	15.246	13.650	16.450	14.740	10.149	8.064	15.156	12.752	10.331	9.585	14.197	12.637	9.665	8.929
	Acetone		19.255	15.891	13.096		20.085	13.892	11.475		12.641	9.713	8.417		11.968	8.567	7.412		11.159	7.438	7.182
10.342	Methanol	25.140	23.174	20.773	18.322	23.060	20.759	14.508	12.696	17.091	14.545	11.920	8.819	15.249	12.257	10.959	8.336	14.891	13.760	10.568	6.465
	Acetone		20.362	16.090	14.676		19.946	13.100	12.015		11.523	9.649	7.006		10.911	8.273	7.925		9.112	6.373	5.232

Table 4-4: Water-oil IFT values for carbonated binary solutions of diluted seawater and methanol/acetone at various pressures and a temperature of 75 °C.

Pressure [MPa]	Base fluid	IFT [mN/m]																			
		Seawater				Diluted seawater at a concentration of 22000 ppm				Diluted seawater at a concentration of 16500 ppm				Diluted seawater at a concentration of 13200 ppm				Diluted seawater at a concentration of 11000 ppm			
		0	5	10	15	0	5	10	15	0	5	10	15	0	5	10	15	0	5	10	15
3.447	Methanol		21.955	19.673	15.737	24.273	18.220	17.591	14.547	18.947	16.159	11.950	10.254	14.786	13.266	10.453	8.502	15.936	12.719	8.005	7.230
	Acetone	26.019	18.025	13.949	11.651	19.199	16.346	13.010	12.923	9.901	9.821	11.237	12.080	9.014	9.450	10.947	10.419	7.834	5.060		
6.894	Methanol		17.641	15.967	13.429	17.556	17.044	16.541	13.126	15.070	14.215	12.430	11.956	11.037	9.524	8.795	10.947	9.825	7.452	4.736	
	Acetone	18.241	16.925	15.124	12.565	14.183	13.619	10.765	13.396	11.490	9.471	11.237	10.141	7.031	6.928	10.947	8.156	5.021	3.421		
10.342	Methanol		10.752	9.415	6.824	10.724	9.201	7.422	5.012	9.151	9.065	6.729	4.653	7.648	6.156	5.012	3.923	6.511	6.012	4.116	3.315
	Acetone	12.760	9.336	8.679	6.167	7.063	5.813	4.924	6.744	5.167	3.250	7.648	5.492	4.654	3.086	6.511	5.391	3.504	2.037		

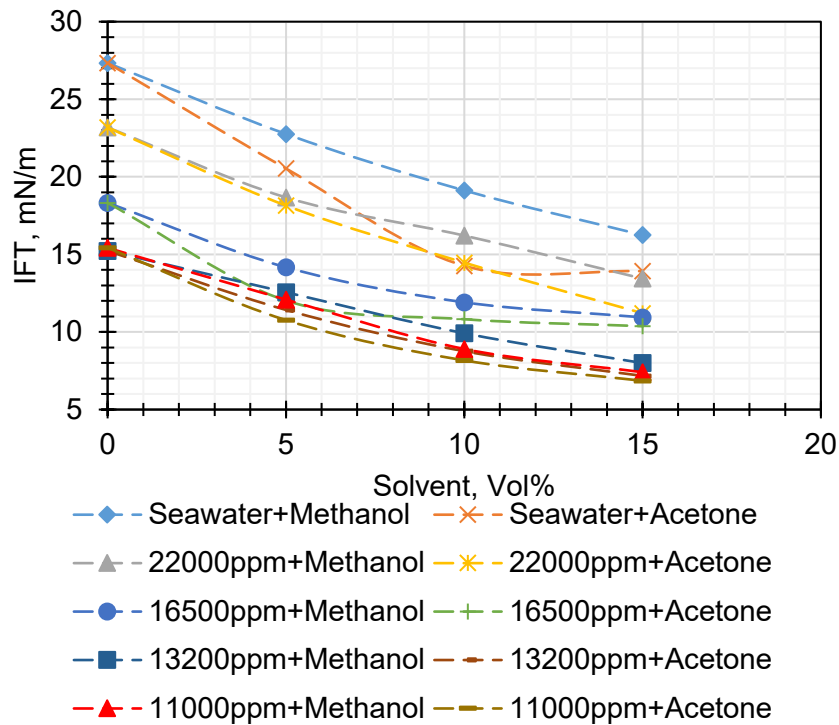


Figure 4-1: IFT graphs for binary solutions of seawater at different salinities and acetone/methanol at a pressure of 0.101 MPa and a temperature of 75 °C.

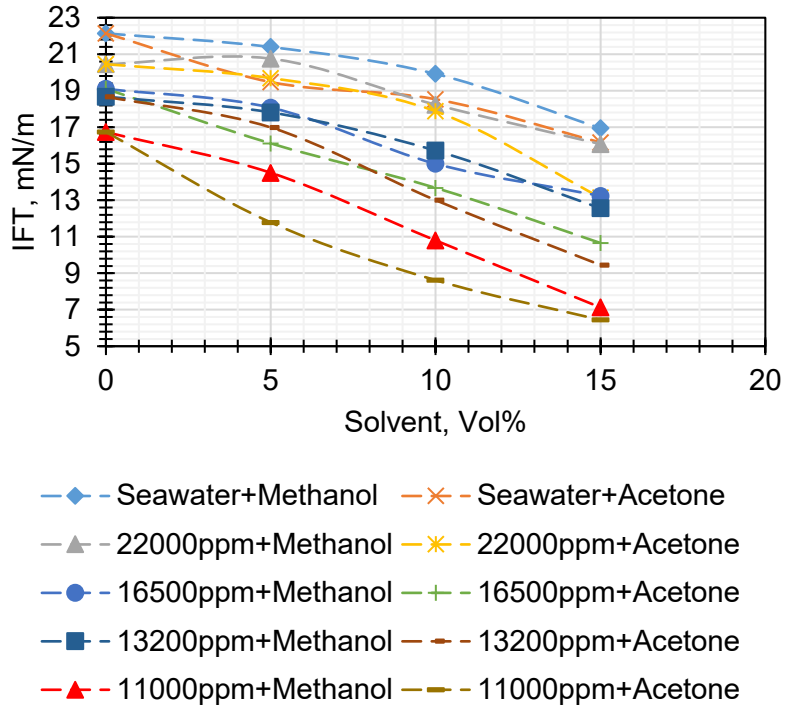


Figure 4-2: IFT graphs for binary solutions of seawater at different salinities and acetone/methanol at a pressure of 3.447 MPa and a temperature of 75 °C.

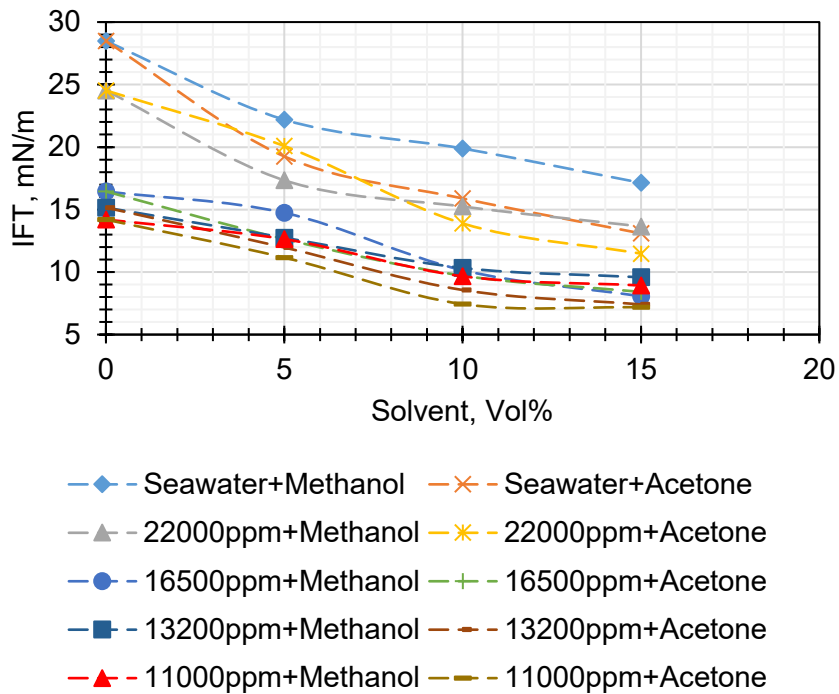


Figure 4-3: IFT graphs for binary solutions of seawater at different salinities and acetone/methanol at a pressure of 6.894 MPa and a temperature of 75 °C.

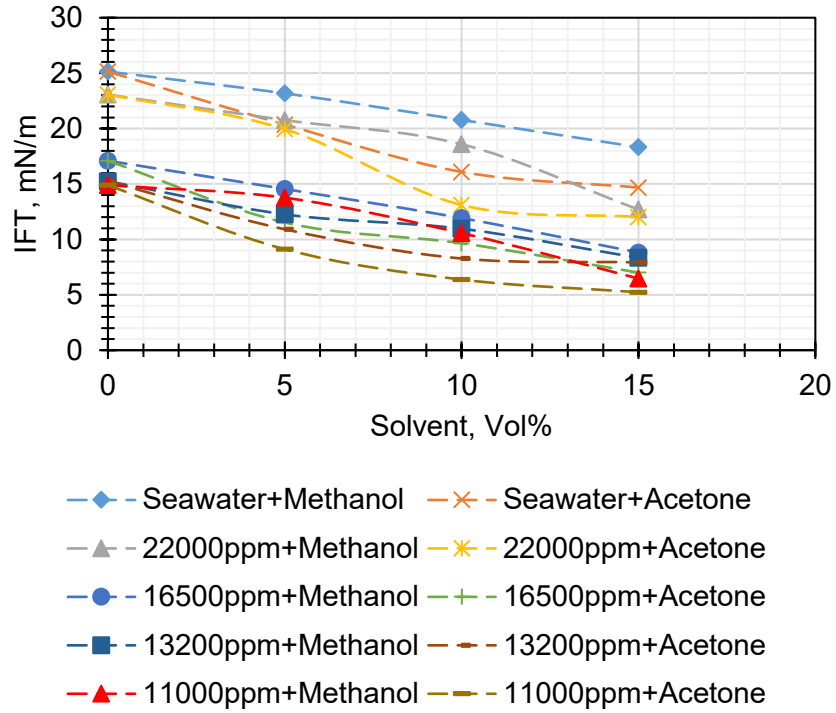


Figure 4-4: IFT graphs for binary solutions of seawater at different salinities and acetone/methanol at a pressure of 10.342 MPa and a temperature of 75 °C.

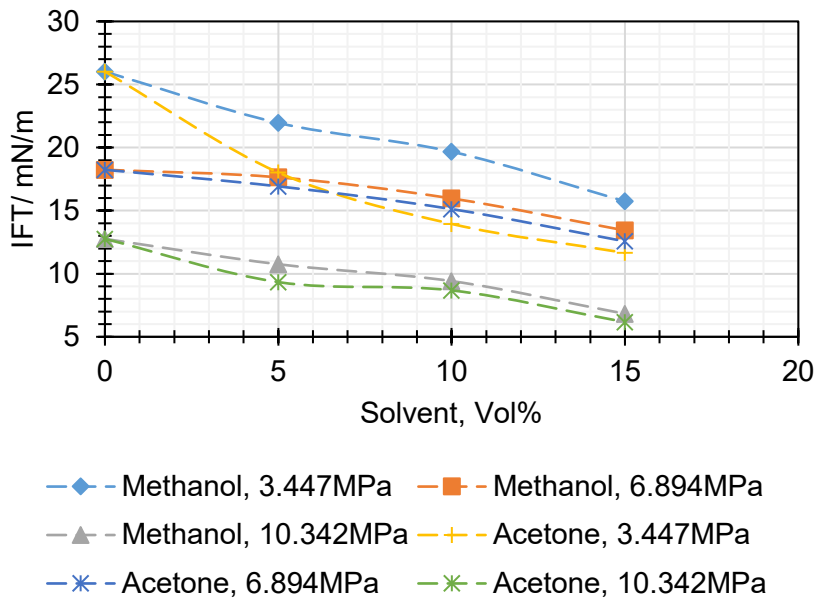


Figure 4-5: IFT graphs for carbonated binary solutions of seawater and acetone/methanol at various pressures and a temperature of 75 °C.

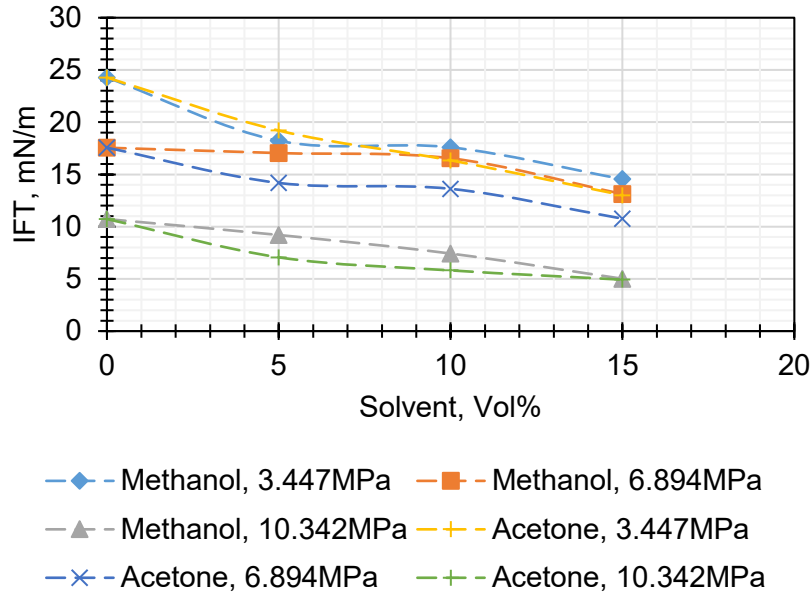


Figure 4-6: IFT graphs for carbonated binary solutions of diluted seawater at a concentration of 22000 ppm and acetone/methanol at various pressures and a temperature of 75 °C.

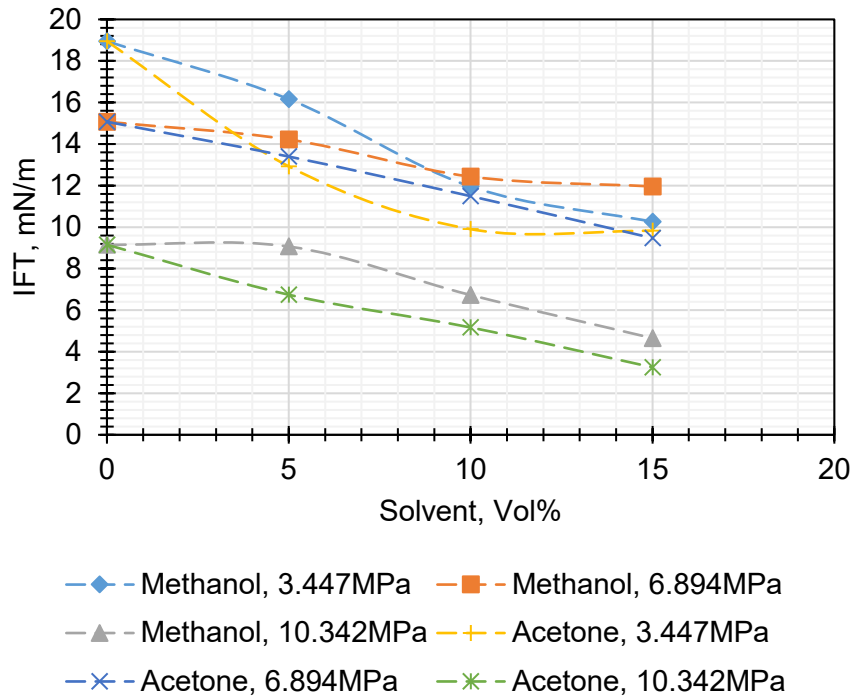


Figure 4-7: IFT graphs for carbonated binary solutions of diluted seawater at a concentration of 16500 ppm and acetone/methanol at various pressures and a temperature of 75 °C.

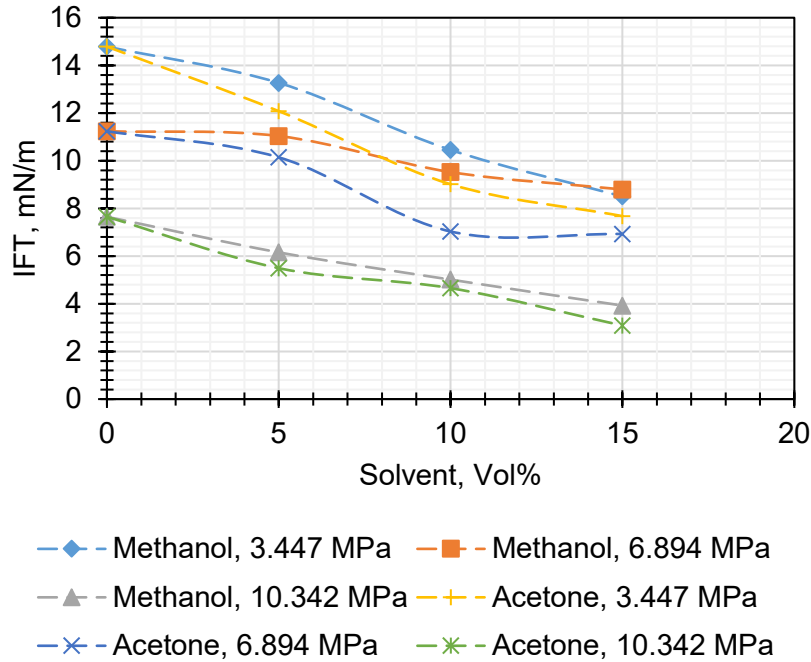


Figure 4-8: IFT graphs for carbonated binary solutions of diluted seawater at a concentration of 13200 ppm and acetone/methanol at various pressures and a temperature of 75 °C.

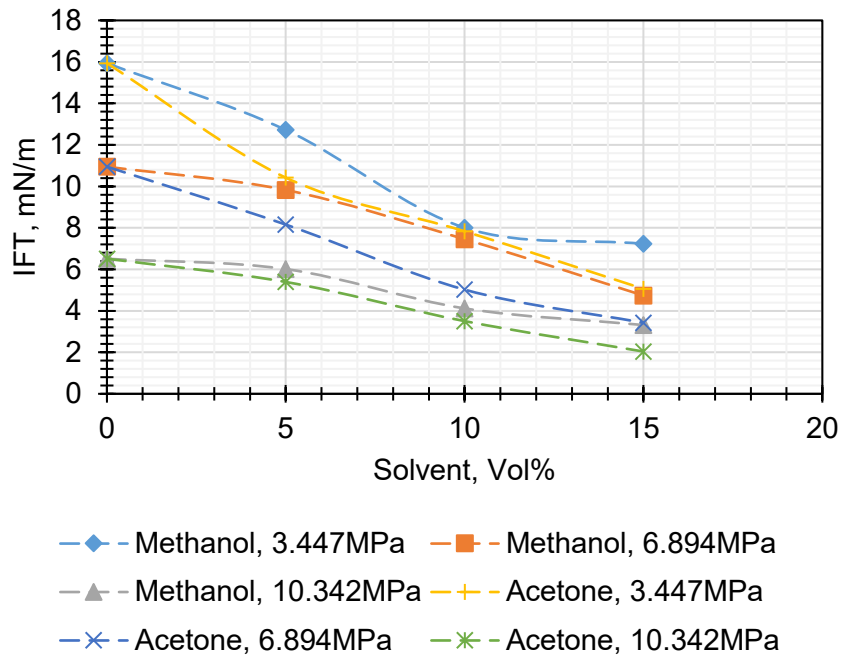


Figure 4-9: IFT graphs for carbonated binary solutions of diluted seawater at a concentration of 11000 ppm and acetone/methanol at various pressures and a temperature of 75 °C.

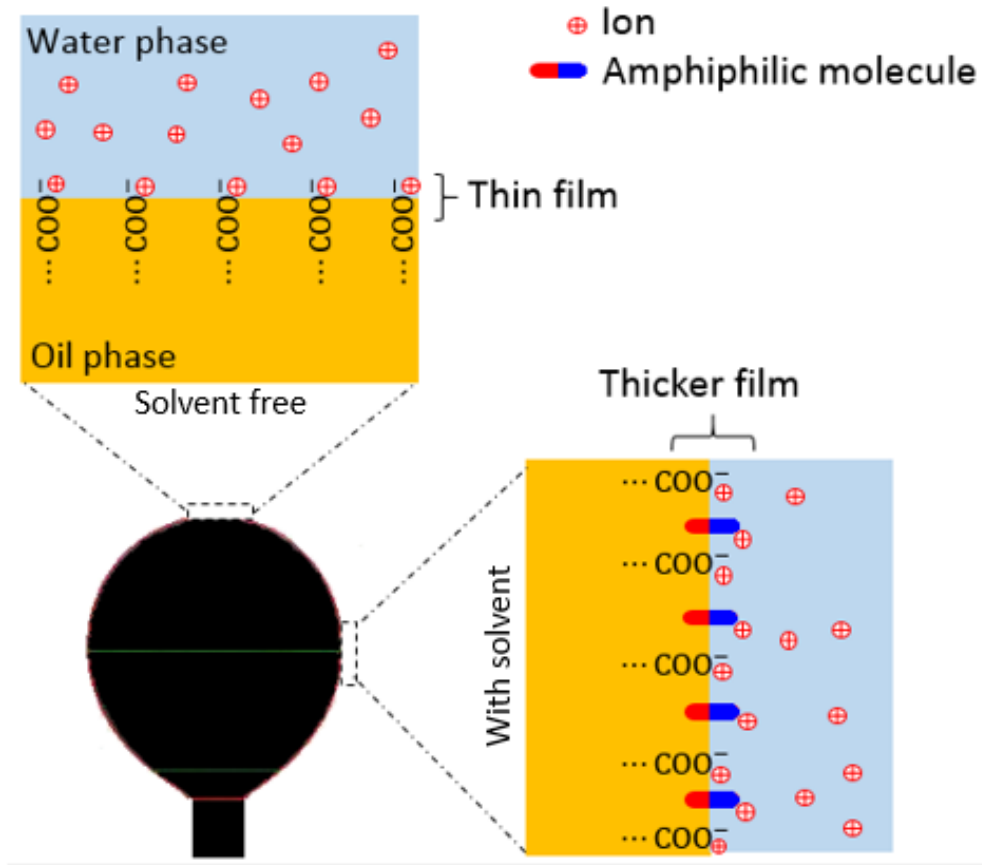


Figure 4-10: Schematic of the performances of ions and amphiphilic molecules in the formation of the thin layer at the interface and reducing the IFT.

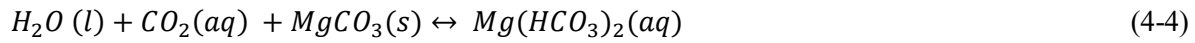
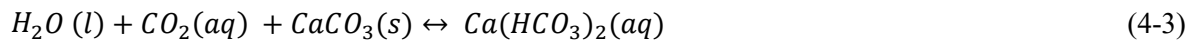
4.1.2. Contact angle result

Table 4-5 and Figures 4-11 to 4-15 show the contact angle results for seawater in diluted samples and their combination with methanol and acetone solvents at various pressures and 75 °C. The contact angle decreases with the dilution of seawater when the solvents are not present in the system. For example, at a pressure of 0.101 MPa, the contact angles for seawater at initial concentration, 5-times diluted, 10-times diluted, 15-times diluted, and 20-times diluted were obtained in the order of 107.63°, 100.24°, 96.16°, 93.40° and 90.34°. The most important mechanism for altering the wettability of carbonate rocks at high salinity is the ion-exchange, but at low salinity, the two mechanisms of salting-in effect and carbonate rock dissolution that occurs with the reaction of Equation 4-2 play major roles. The mechanisms of carbonate rock wettability alteration at lower salinity are more robust than high salinity mechanism, hence, less contact angle and more hydrophilicity at lower salinity are justified [47, 141].



It should be noted that the solubility of calcium carbonate in water is very low at ambient temperature, but at the temperature of the reservoir, this dissolution is intensified. The trend of contact angle values is irregular with increasing pressure at high salinities but with decreasing salinity, a certain trend appears that the contact angle values decrease with increasing pressure at lower salinities. Considering the dissolution mechanism according to Equation 1, the current trend is justified as increasing the pressure improves the dissolution process. Wettability alteration of carbonate rocks by low and high salinity and carbonated water has been described in our previous studies in detail [6, 42, 136, 142]. In the presence of methanol and acetone solvents, the contact angle shows a significant decrease, and with increasing concentration of solvents in the system a further decrease in contact angle size is observed. This means that both solvents are effective in wettability alteration. At 0.101 MPa pressure and the same salinity of the system, for example, 20-times diluted, the contact angle values for 5, 10 and 15 %Vol methanol were 88.71°, 84.91° and 82.14° and for the same volumes of acetone were 83.56°, 80.42° and 78.20°, respectively. The mechanism of wettability alteration by solvents is explained through their molecular structure. Methanol as alcohol is a co-surfactant and its structure has a polar and hydrophilic (OH) part and a hydrophobic non-polar part (CH₃) [131]. Therefore, it is expected to act as a surfactant in the rock-oil-solvent system. With this structure, it adsorbs on the surface of the oil-wet rock in such a way that its hydrophobic part is adsorbed on the rock and its hydrophilic part is in the opposite direction. As the adsorbed molecules increase in a uniform and appropriate direction, a thin layer is formed on the surface that is opposite to the initial wettability. Increasing the solvent concentration strengthens the formed layer. Solvents additionally by dissolving petroleum components from the surface somehow remove hydrophobic agents from the rock surface. Acetone also has a similar structure, meaning there are both polar and non-polar parts in its molecular structure and it can act as a co-surfactant in aqueous solutions [133]. But solvent and salinity mechanisms are not enough for this system separately. When both solvent and soluble ions are present in the system, there is a synergistic effect on the wettability alteration. As stated earlier, in the absence of solvents, the contact angles at lower salinities are lower and there is a trend that decreases with decreasing salinity. But according to Table 4-5 and Figures 4-11 – 4-15, in the presence of solvents, the contact angle decreases with increasing salinity, i.e. dilution of seawater in the presence of solvents increases the contact angle, which is exactly the opposite of the previous trend. When solvents are absorbed in the water-oil interface, they form a film that can absorb more ions and strengthen the film so that the thickness of the oil-solvent-ion film is greater than the thickness of the previous oil-ion film. Considering petroleum components on the rock surface as oil-wetting agents, it can be said that the presence of ions and solvents in the system strengthens the film formed on the rock surface. Furthermore, in the presence of salinity, the solubility of the solvents in water decreases and more amphiphilic molecules can join the thin film in the interface [134]. The pressure parameter in the presence of solvents in both high and low salinities affects

the contact angle as the pressure increases, the contact angle values decrease. In addition to the mechanism described for dissolution and its relation to the pressure, in the presence of solvents, the pressure causes more mass transfer of the solvents from the aqueous phase to the interface and the thin film, so the orderly process is consistent with these interpretations. With the addition of dissolved CO₂ to the system, it is expected that the mechanisms of wettability alteration will be enhanced and the contact angle generally reduced further. The dissolution of CO₂ in water causes the production of carbonic acid. The resulting carbonic acid can dissolve calcite and dolomite, thus along with the dissolution of the surface minerals, hydrophobic agents at the surface disappear. Surface dissolution of carbonate rock containing dolomite and calcite is performed according to Equations 4-3 – 4-5 [143, 144]:



In this case, the interaction of carbonate rock containing 39% calcite and 61% dolomite with carbonated water, the reaction of acidic water with dolomite is more important. Table 4-6 and Figures 4-16 – 4-20 show the results of contact angle tests for the carbonated solutions. According to the results, the contact angle decreases with decreasing base fluid salinity without methanol and acetone solvents. For example, the contact angles at 3.447 MPa pressure, for initial seawater sample, 5-times diluted, 10-times diluted, 15-times diluted and 20-times diluted were 100.30°, 95.97°, 88.14°, 86.21° and 83.61°, respectively. As salinity increases, the solubility of CO₂ in water decreases and subsequently the amount of carbonic acid produced and the surface dissolution decrease. The pressure parameter imposes a regular trend in the contact angle for carbonated solutions at both high and low salinities. With increasing pressure and subsequently increasing CO₂ solubility in water, the contact angle decreases. Further reduction of the contact angle with the addition of solvents is proportional to their volume percentage. But the contact angle sizes for binary solvent + carbonated saline water solutions are smaller without solvents and dissolved CO₂. In addition to the single-component mechanisms of salinity, dissolved CO₂ and solvents, the synergistic effect of dissolved CO₂ and solvents on the system seems to be imposed here. Many studies report the solubility of CO₂ in binary mixtures of methanol + water and acetone + water and compared them with the solubility of CO₂ in water [138, 139]. These reports indicate that the solubility of CO₂ in these binary mixtures is higher than that of CO₂ in water. Under this assumption, as the solubility of CO₂ in water increases, the volume of carbonic acid also increases and the mechanism of surface dissolution is strengthened and as a result, the contact angle is reduced. The contact angle measurements each express a concept of wettability. Based on

the most general contact angle segmentation, the values above 90° show hydrophobicity, and the values below 90° indicate hydrophilic state and the contact angle of 90° is a neutral wettability. The intensity of oil-wetting increases with the increase in the contact angle and the smaller it approaches the stronger water-wetting. According to this interpretation, and given the results, 20-times diluted seawater at 0.101 MPa produced almost neutral wettability but at higher pressures poor hydrophilic wettability was achieved by reaching the contact angle of 81.56 ° at 10.342 MPa. The solvents also produced hydrophilicity at the lowest volume ratio, which is more consistent with said trends and is in line with other parameters. Hydrophilicity was obtained much easier for carbonated solutions. For example, carbonated seawater recorded an angle of 88.14° at a pressure of 0.101 MPa only with a dilution of 10-times. Contact angle sizes are generally lower for solutions containing acetone than for solutions containing methanol. This may be because the solubility of CO₂ in binary water + acetone mixtures is higher than that of binary water + methanol mixtures [138, 139]. Besides, another cause could be greater solubility of oil in acetone than oil solubility in methanol. With greater solubility, the solvent can better eliminate petroleum-based agents at the surface of the rock, making wet wetting easier to hydrophilic and decreasing the contact angle further. As a result, wettability shifts to hydrophilicity more easily and the contact angle decreases further. The lowest contact angles for methanol and acetone solvents were 36.31° and 32.92°, respectively at 15 %Vol, 10.342 MPa CO₂ pressure, and 20-times dilution of seawater as base fluid. These fluids were selected for the continuation of the method, namely imbibition tests, with the related conditions. The results are described in the next section.

Table 4-5: Contact angle values for the oil drop on the rock thin section in the presence of diluted seawater + acetone/methanol binary mixture at 75 °C and different pressures.

Pressure, MPa	Base fluid	Contact angle [Degree]																			
		Seawater				5-times diluted				10-times diluted				15-times diluted				20-times diluted			
		Solvent percent	0	5	10	15	0	5	10	15	0	5	10	15	0	5	10	15	0	5	10
0.101	Methanol	107.63	74.43	70.98	70.10	100.24	76.89	73.27	71.18	96.16	79.12	77.06	73.29	93.40	80.38	78.02	75.35	90.34	88.71	84.91	82.14
	Acetone		71.26	69.44	68.13		74.65	70.54	69.77		78.19	75.04	70.63		75.30	70.50	69.93		83.56	80.42	78.20
3.447	Methanol	102.45	71.30	70.57	68.49	100.14	74.71	70.93	70.02	93.31	75.22	73.17	70.96	90.35	78.22	77.65	72.94	88.56	85.13	82.67	81.04
	Acetone		68.75	66.05	65.50		71.18	67.54	65.93		71.96	69.24	68.49		72.65	70.03	69.12		80.30	79.46	77.29
6.849	Methanol	102.27	67.39	65.21	62.17	100.50	71.85	67.73	63.44	90.46	74.91	70.41	67.38	86.60	75.05	71.96	70.35	85.93	81.07	79.29	76.50
	Acetone		65.30	62.45	61.07		67.52	66.12	62.03		67.83	67.00	65.14		68.55	67.06	66.93		75.16	74.79	71.37
10.342	Methanol	105.06	63.57	62.40	60.95	100.63	65.20	63.04	61.00	91.17	70.61	69.39	67.26	84.04	72.15	70.73	68.06	81.56	75.50	71.26	70.93
	Acetone		62.01	60.31	58.43		64.13	62.90	61.65		67.50	66.15	63.70		67.90	66.81	65.11		74.48	73.17	70.39

Table 4-6: Contact angle values for the oil drop on the rock thin section in the presence of diluted carbonated seawater + acetone/methanol binary mixture at 75 °C and different pressures.

Pressure, MPa	Base fluid	Contact angle [Degree]																			
		Seawater				5-times diluted				10-times diluted				15-times diluted				20-times diluted			
		Solvent percent	0	5	10	15	0	5	10	15	0	5	10	15	0	5	10	15	0	5	10
3.447	Methanol	100.30	70.65	68.04	63.15	95.97	69.25	65.70	61.33	88.14	68.49	64.19	60.21	86.21	65.83	61.09	59.80	83.61	61.38	58.51	57.97
	Acetone	100.30	70.05	67.93	62.30	95.97	65.41	62.50	60.80	88.14	64.91	63.56	59.62	86.21	61.97	60.81	59.02	83.61	60.11	57.49	56.70
6.894	Methanol	91.64	65.28	63.17	60.96	87.84	64.56	61.78	58.29	85.12	61.70	58.69	57.09	81.73	59.91	56.34	55.75	79.50	58.13	56.01	55.10
	Acetone	91.64	65.06	61.16	59.78	87.84	63.91	60.24	58.20	85.12	60.38	58.12	55.84	81.73	57.29	56.11	54.90	79.50	57.00	55.75	53.46
10.342	Methanol	86.22	59.17	56.07	54.12	84.07	54.96	50.29	47.15	81.75	50.62	46.65	42.84	77.84	47.20	43.98	41.51	75.37	43.02	39.64	36.31
	Acetone	86.22	57.90	55.75	52.09	84.07	53.11	43.50	41.32	81.75	47.55	42.50	41.60	77.84	42.26	42.01	40.10	75.37	41.79	35.29	32.92

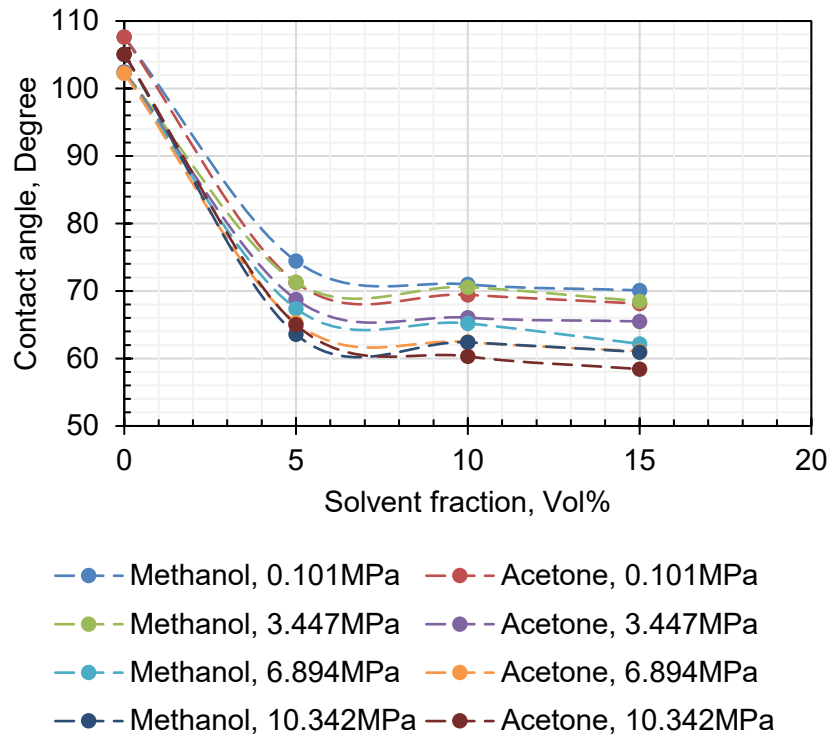


Figure 4-11: The curves of contact angle for the oil drop on the rock thin section in the presence of seawater + acetone/methanol binary mixture at 75 °C and different pressures.

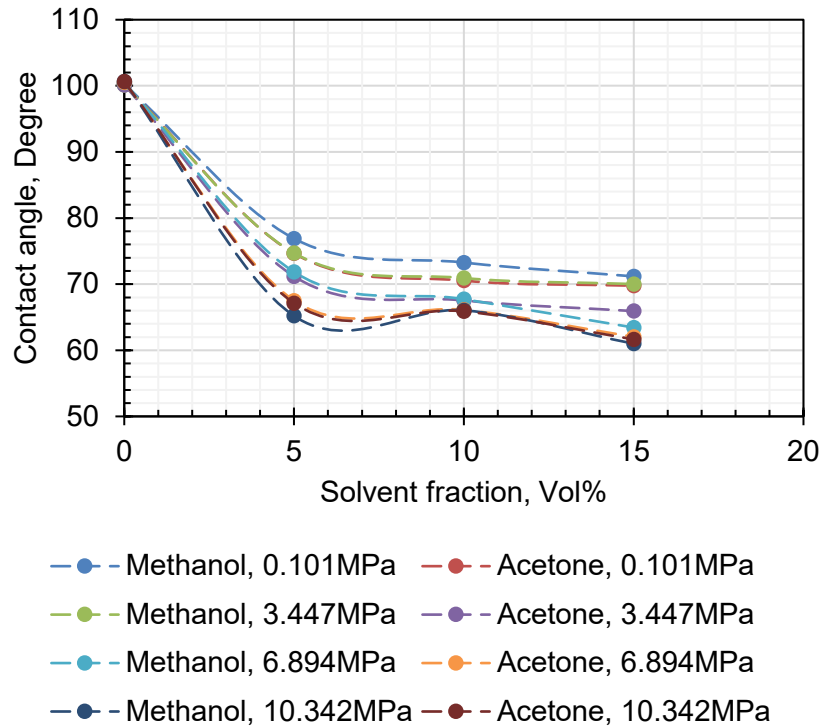


Figure 4-12: The curves of contact angle for the oil drop on the rock thin section in the presence of 5-times diluted seawater + acetone/methanol binary mixture at 75 °C and different pressures.

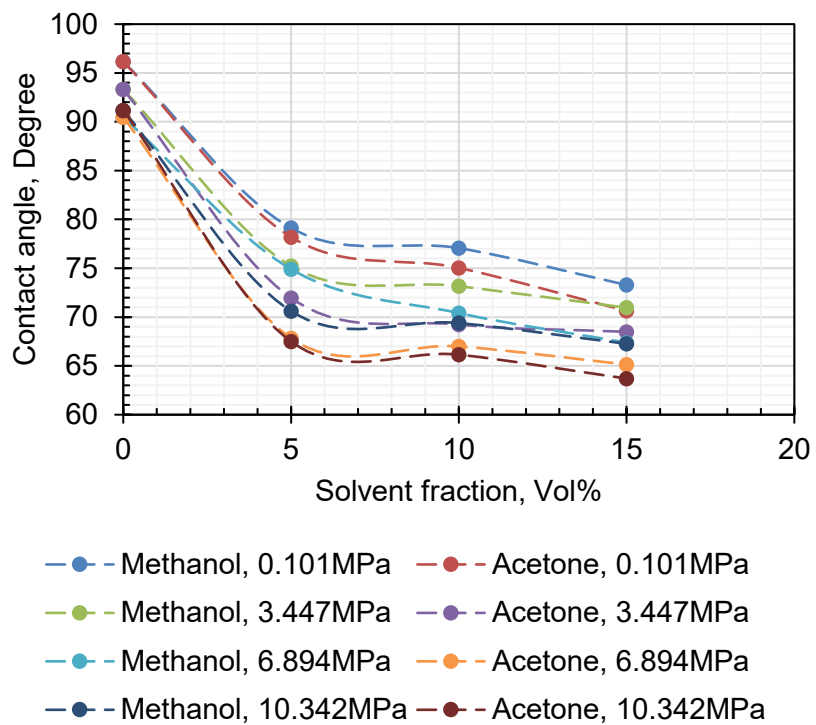


Figure 4-13: The curves of contact angle for the oil drop on the rock thin section in the presence of 10-times diluted seawater + acetone/methanol binary mixture at 75 °C and different pressures.

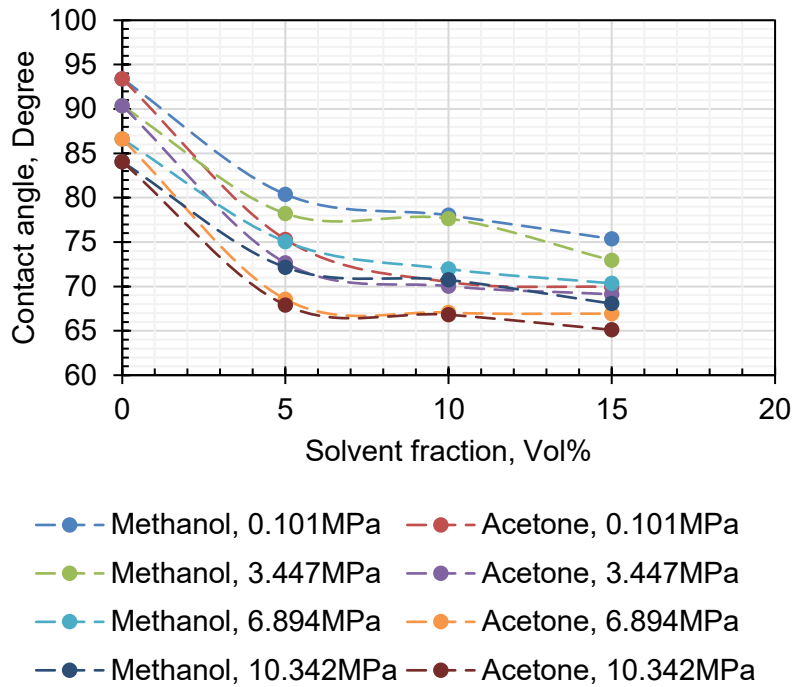


Figure 4-14: The curves of contact angle for the oil drop on the rock thin section in the presence of 15-times diluted seawater + acetone/methanol binary mixture at 75 °C and different pressures.

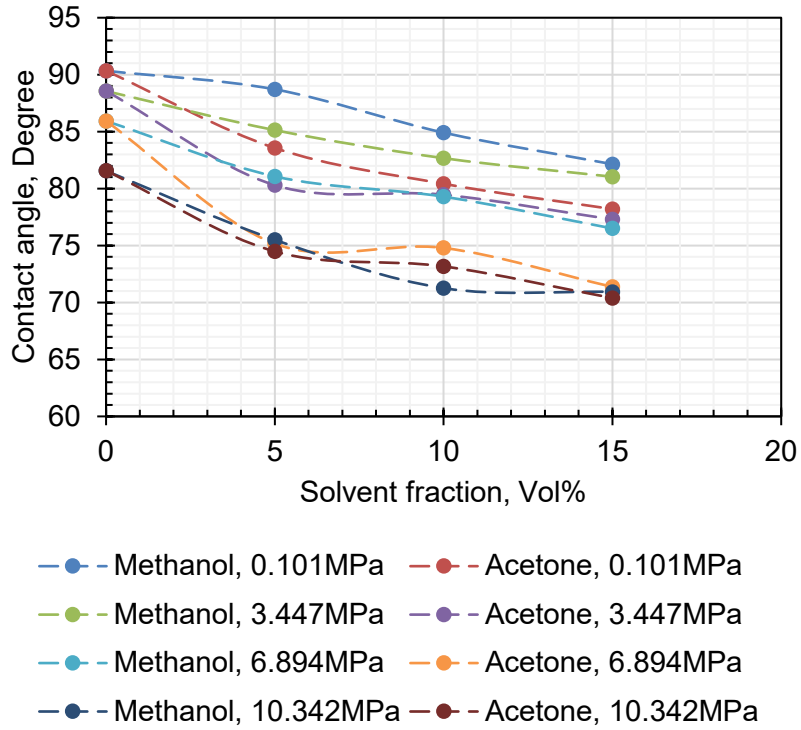


Figure 4-15: The curves of contact angle for the oil drop on the rock thin section in the presence of 20-times diluted seawater + acetone/methanol binary mixture at 75 °C and different pressures.

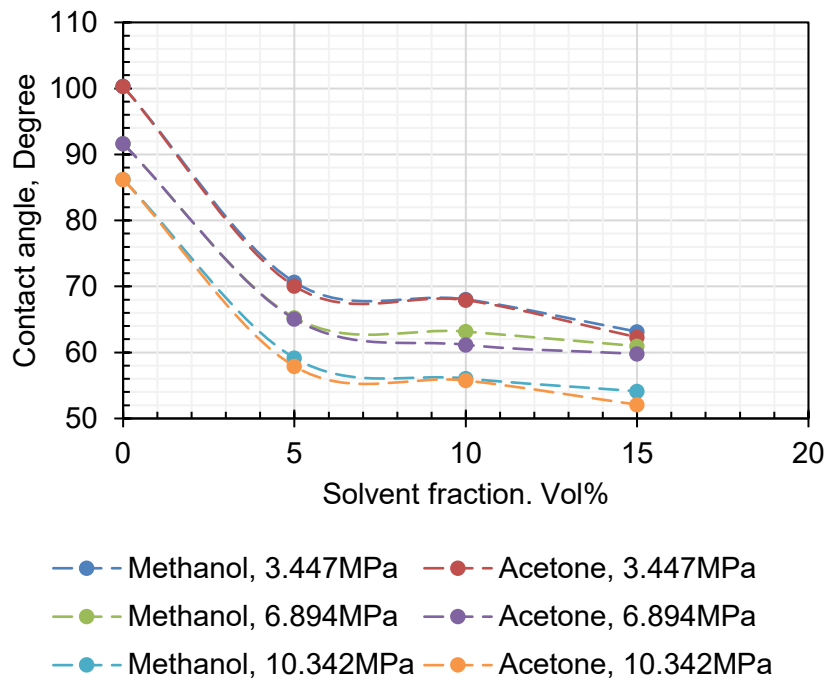


Figure 4-16: The curves of contact angle for the oil drop on the rock thin section in the presence of carbonated seawater + acetone/methanol binary mixture at 75 °C and different pressures.

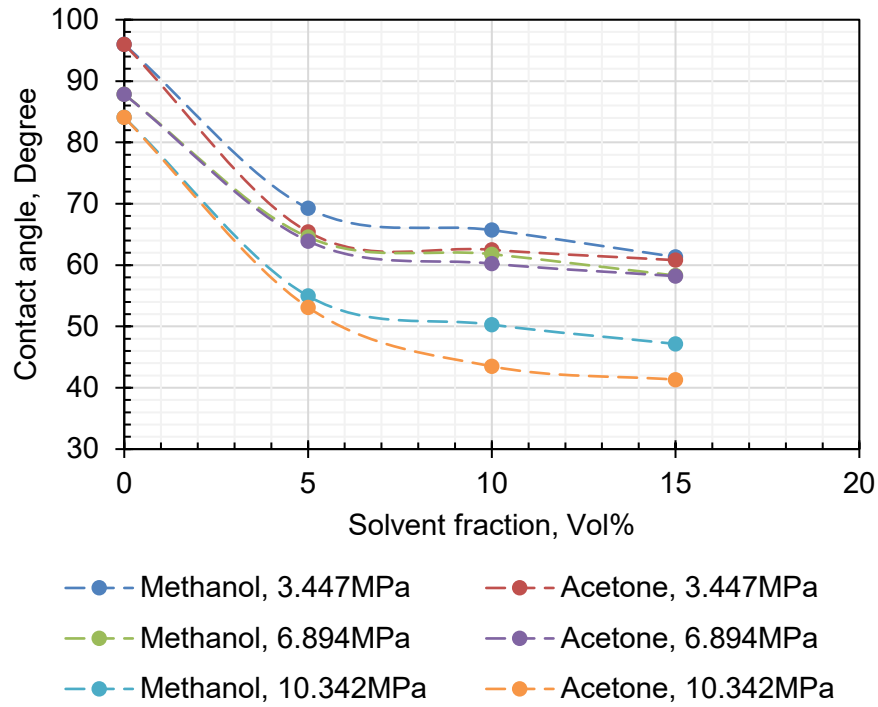


Figure 4-17: The curves of contact angle for the oil drop on the rock thin section in the presence of carbonated 5-times diluted seawater + acetone/methanol binary mixture at 75 °C and different pressures.

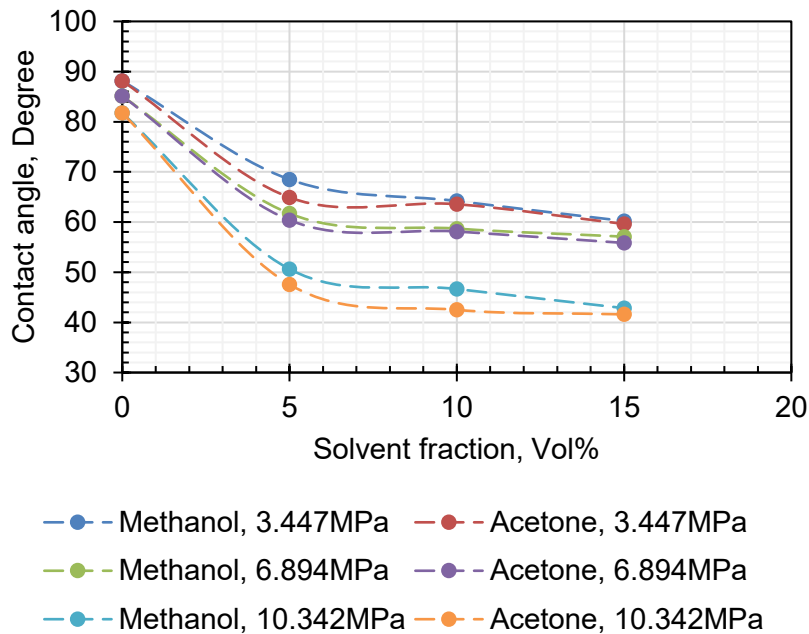


Figure 4-18: The curves of contact angle for the oil drop on the rock thin section in the presence of carbonated 10-times diluted seawater + acetone/methanol binary mixture at 75 °C and different pressures.

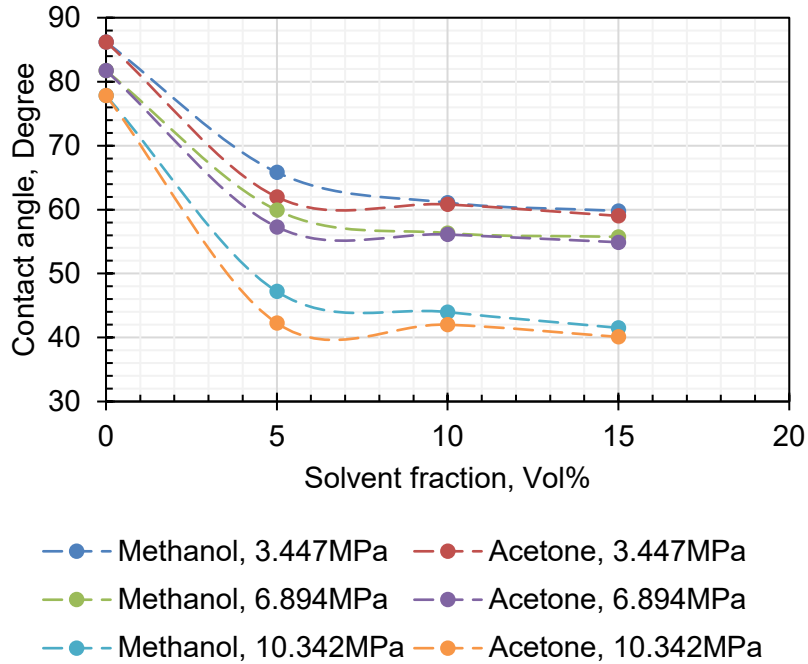


Figure 4-19: The curves of contact angle for the oil drop on the rock thin section in the presence of carbonated 15-times diluted seawater + acetone/methanol binary mixture at 75 °C and different pressures.

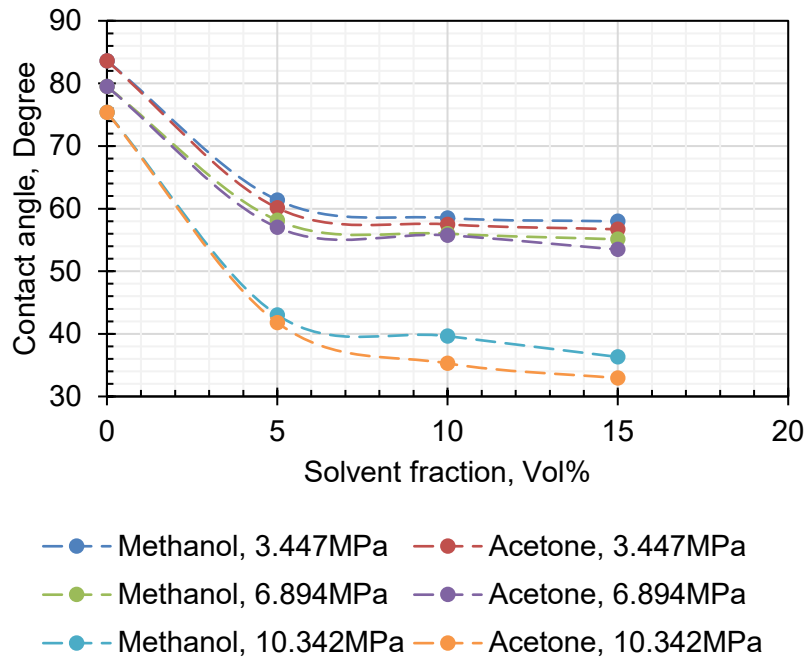


Figure 4-20: The curves of contact angle for the oil drop on the rock thin section in the presence of carbonated 20-times diluted seawater + acetone/methanol binary mixture at 75 °C and different pressures.

4.1.3. Imbibition results

Imbibition tests are normally performed for two purposes, one to measure the wettability of the porous medium and the other to measure oil production under this process. Oil production under imbibition is more important in the fractured reservoirs because it is one of the main EOR mechanisms in these types of reservoirs. Table 4-7 shows the specifications of the used plugs. Table 4-8 shows the oil production values in the imbibition experiments over time and Figure 4-21 shows the results of the oil recovery factors. Matrices in the reservoir do not always imbibe and drain across their boundaries. The curves of plugs 1, 2, 3 and 4, which were related to the imbibition of carbonated solutions containing 15 %Vol of methanol at 10.342 MPa, show the final oil production of 66.29, 28.44, 85.42, and 91.38% of primary oil saturation, respectively. The curves corresponding to plugs 5, 6, 7 and 8 used for experiments with carbonated water containing 15 %Vol acetone at 10.342 MPa also produced 70.32, 32.10, 90.60 and 94.09% of primary oil saturation. Imbibition tests in these plugs were performed as one-dimensional COCSI, one-dimensional COUCSI, multi-dimensional COUCSI and imbibition in the fractured plug, respectively. Oil production in these experiments was influenced by factors such as injectable fluid strength considering the additives involved in wettability alteration, the interfacial tension between injectable fluid and oil, oil swelling due to CO₂ mass transfer and mutual solvents from the aqueous phase to the oil phase, the dissolution of the rock, oil viscosity and ultimately the boundary conditions and fracture of the plugs. The results show that the amount of oil produced in the imbibition tests is consistent with the results of the contact angle. That is the injection fluid that has the lowest contact angle produces more oil.. It can be said that in equal conditions in terms of engineered injection fluid type and plug boundary, the oil recovery is proportional to the size of contact angle and interfacial tension so that the lower contact angle and interfacial tension yield more output. As for the mechanism of oil swelling, given that we have not done any direct test, we can only say that this effect exists and given that the imbibition cell isolated for a long time, this oil swelling affects the amount of oil measured and shows it to be slightly higher than the actual amount. The produced oil contains some dissolved CO₂ and acetone or methanol. The dissolution of the rock by carbonic acid as a result of the reaction of water and CO₂ can, in addition to increasing the permeability of the matrix, cause the rock to be damaged, such that the channels can be opened for trapped oil flow in the porous medium, and produce it [15]. Boundary conditions and the presence of the fracture in the reservoir rock are important factors in the amount of final oil recovery and the timing of the completion of the imbibition process. The amount of oil recovery under imbibition increases with the increasing area-to-volume ratio of the reservoir rock [145]. In a nutshell, it can be said that plugs with a higher surface area of contact with the environment are more productive so that the highest amount of production is in the fractured plugs and the least amount of production is in One-dimensional COUCSI. When there is a fracture in the system, the two factors of contact

area between water and matrix and capillary pressure affect the amount of production. Increasing the effective contact surface due to the fracture depends on the rise of the water level in the fracture [146]. According to the results of the imbibition experiment in the fractured plug (plug 8), oil production has risen sharply in the early times. This means that the ascent of water is completed early and the effective contact surface has increased significantly, so oil recovery at this time has been almost the highest. Besides, capillary pressure is higher at lower water saturation. Water saturation increases over time, resulting in reduced capillary pressure. As the capillary pressure decreases, oil production also declines at each time. With these interpretations, an increase in oil production occurs early which its intensity decreases after the reduction of capillary pressure. This trend is seen in all imbibition curves of Figure 4-21, although there is more intensity in the case of imbibition in the fractured system.

Table 4-7: Specifications of the used plugs and imbibition tests.

Plug No.	Permeability [md]	Porosity [%]	Pore volume [cm ³]	Mass of dry plugs [g]	Mass of oil-saturated plugs [g]	S _{oi} [%]	Original oil-in-place [cm ³]	Imbibition fluid	Imbibition type
1	12.52	15.04	9.42	143.7377	151.5690	96.11	9.05	Carbonated 20-times diluted seawater+15%Vol methanol	One-dimensional COCSI
2	13.05	15.33	9.60	141.7546	149.6638	95.27	9.14	Carbonated 20-times diluted seawater+15%Vol methanol	One-dimensional COUCSI
3	12.70	14.91	9.34	145.4193	153.0169	94.08	8.78	Carbonated 20-times diluted seawater+15%Vol methanol	Multi-dimensional COUCSI
4	12.64 [•]	15.70 [•]	9.84 [•]	140.3679	148.6059	96.76	9.52	Carbonated 20-times diluted seawater+15%Vol methanol	In fractured plug
5	13.10	15.39	9.64	141.2175	149.0920	94.49	9.10	Carbonated 20-times diluted seawater+15%Vol acetone	One-dimensional COCSI
6	12.65	14.37	9.00	145.4237	152.7011	93.53	8.41	Carbonated 20-times diluted seawater+15%Vol acetone	One-dimensional COUCSI
7	12.92	15.10	9.46	142.9130	150.7443	95.70	9.05	Carbonated 20-times diluted seawater+15%Vol acetone	Multi-dimensional COUCSI
8	12.50 [•]	15.46 [•]	9.69 [•]	141.4768	149.3859	94.31	9.14	Carbonated 20-times diluted seawater+15%Vol acetone	In fractured plug

The length of all plugs is 5.5cm.

• Before the fracture.

Table 4-8: Oil production values in the imbibition experiments.

Time [h]	Oil production in periods [cm ³]							
	Plug1	Plug2	Plug3	Plug4	Plug5	Plug6	Plug7	Plug8
0	0	0	0	0	0	0	0	0
6	0.1	0.0	0.1	0.2	0.1	0.0	0.1	0.3
12	0.3	0.0	0.4	0.6	0.5	0.1	0.4	0.7
24	0.7	0.0	0.9	1.2	0.9	0.2	0.6	1.4
48	1.1	0.1	1.0	2.4	1.4	0.3	0.8	2.6
72	1.8	0.2	1.7	3.0	1.9	0.5	1.0	3.2
96	2.2	0.4	2.4	3.4	2.5	0.8	1.5	3.7
120	2.4	0.6	2.7	3.9	3.2	1.0	2.0	4.1
144	2.6	0.8	3.0	4.5	4.0	1.2	2.7	4.7
168	2.8	1.0	3.5	4.8	4.5	1.5	3.3	5.1
192	3.0	1.2	4.2	5.3	4.7	1.8	4.1	5.8
216	3.2	1.6	4.8	6.0	5.1	2.0	4.9	6.3
240	3.7	1.7	5.4	6.5	5.4	2.2	5.6	7.0
264	4.0	2.1	6.0	7.0	5.5	2.3	6.3	7.5
288	4.6	2.2	6.6	7.8	5.6	2.4	6.9	8.1
312	5.0	2.3	7.0	8.2	5.7	2.5	7.3	8.4
336	5.4	2.3	7.2	8.4	5.8	2.5	7.7	8.5
360	5.7	2.4	7.4	8.5	5.9	2.5	8.0	8.6
408	5.9	2.5	7.5	8.7	6.0	2.6	8.1	8.6
480	6.0	2.5	7.5	8.7	6.3	2.6	8.2	8.6
600	6.0	2.5	7.5	8.7	6.4	2.7	8.2	8.6
720	6.0	2.6	7.5	8.7	6.4	2.7	8.2	-
890	-	2.6	-	8.7	6.4	2.7	-	-
960	-	2.6	-	-	6.4	2.7	-	-

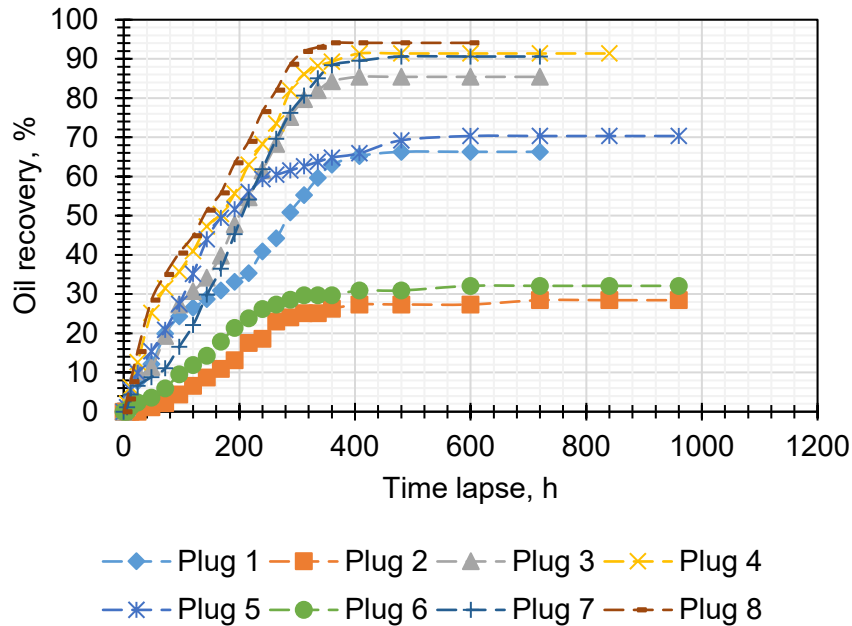


Figure 4-21: Oil recovery curves for various optimum fluids imbibition tests at 10.342 MPa and 75 °C .

4.1.4. Effect of acetone on dynamic behavior of crude oil swelling

As mentioned earlier, the volume changes of floating oil drops in the carbonated solution environment containing different acetone ratios over time became the basis for oil swelling. The curves of the percentage of oil swelling over time in the presence of carbonated water with a salinity of 11000 ppm at 3.447, 6.894 and 10.342 MPa are shown in Figures 4-22, 4-23 and 4-24, respectively. Each curve in the figures is specific to a volume ratio of acetone. Due to the oil swelling curves over time, there is an upward trend up to a certain time for each volumetric ratio of acetone and then the curve becomes horizontal. Each curve can be divided into three zones of early-times, meso-equilibrium and equilibrium. In the early-times zone, the slope of the curve changes irregularly. In the meso-equilibrium region, the oil swelling curve continues to increase over time with an almost constant slope. Finally, in the equilibrium region, the oil swelling over time reaches a constant value or with very small changes. Considering the pressure constant, it can be seen that the crude oil swelling curve for acetone-free carbonated fluid rises more sharply in the early-times and then reaches equilibrium. This means that the meso-equilibrium region in these curves is less long. With the addition of acetone to the system, the dynamic curve of the oil swelling initially shows lower values than the curve related to the acetone-free carbonated fluid, but the oil swelling values increase with a gentle slope in the meso-equilibrium region and finally in the equilibrium region, it is higher for acetone-free carbonated water. This trend is commensurate with the acetone volume ratio. In other words, the equilibrium values of oil swelling related to carbonated water containing acetone in proportion to the volumetric ratio

of acetone are greater than the equilibrium oil swelling associated with acetone-free carbonated water. Exactly proportional to the percentage of solvent volume, the distance of the curves from the oil swelling curve in the presence of acetone-free carbonated water increases in the meso-equilibrium region. Similarly, the distance between the curves from the oil swelling curve in the presence of acetone-free carbonated water in the equilibrium region increases in the opposite direction. Simply put, as the amount of acetone in the system increases, the rate of mass transfer decreases in shorter times, while in longer periods, the rate of mass transfer in the presence of acetone is higher. So that the final amount of oil swelling is higher in the presence of acetone. These trends can be seen in any amount of pressure. Figures 4-25, 4-26, and 4-27 illustrate the percentages of oil swelling versus time in the presence of carbonated water with a salinity of 16500 ppm, and Figures 4-28, 4-29, and 4-30 show the percentages of oil swelling versus time in the presence of carbonated seawater at pressures of 3.447, 6.894 and 10.342 MPa, respectively. The interpretations mentioned for Figures 4-22 – 4-24 also apply to Figures 4-27 – 4-30 and the only difference is in the value of crude oil swelling. Comparing the curves related to oil swelling in different salinity of the base fluid at each pressure and each volume ratio of acetone shows that with increasing salinity of the base fluid, oil swelling changes over time are higher than oil swelling in the presence of carbonated water with less salinity. It is generally accepted that oil swelling in interaction with carbonated water due to the transfer of CO₂ mass to oil [60, 142]. The transfer of mutual solvent mass is also a reason for oil swelling in this method [82, 84, 87]. Mechanisms affecting the rate of oil swelling over time in this particular state, that is, the combination of carbonated water and solvent at a constant temperature, depend on the presence of three additives: dissolved CO₂, the presence of acetone in the system, salinity and pressure. The solubility of CO₂ and acetone in water and oil are the most important factors influencing oil swelling, while salinity is one of the factors that affect the solubility of CO₂ and acetone. In other words, the solubility of CO₂ and acetone directly and salinity indirectly affect oil swelling. Pressure affects both the CO₂ water/oil solubility and the mass transfer rate. The CO₂ oil solubility is greater than its water solubility, which makes it easy to transfer to the oil. The system of carbonated water-oil has a one-sided phase behavior [147, 148]. This can be the reason for the steady increase in oil swelling in the curves. When acetone is added to carbonated water as a lighter solvent than water, it increases the CO₂ water solubility [139]. As a result, the CO₂ mass transfer rate over time is slower. But in the end, due to the greater volume of CO₂ in the water and the addition of a mutual solvent mass transfer mechanism, the equilibrium amount of oil swelling will be higher in the presence of acetone. The salinity is another factor in the solubility of CO₂ and acetone in water, followed by oil swelling. As the base fluid salinity increases, the CO₂ water solubility decreases [149]. As a result, CO₂ tends to move to the oil. With this interpretation, the higher oil swelling in higher salinity is justified. Besides, salinity reduces the solubility of acetone in water. With this reduction in solubility, the transfer of mutual solvent mass to oil also increases [88]. As a result, oil swelling rises. Another effective parameter is

pressure. Pressure increases the mass transfer of both additives to water, ie CO₂ and mutual solvent. So it makes sense to increase oil swelling by increasing pressure. To better understand, the values of equilibrium oil swelling are given in Table 4-9. Figures 4-31 – 4-33 show the data as curves. Considering the pressure of 3.447 MPa, the equilibrium oil swelling in the salinity of seawater and the volumetric ratios of acetone equal to 0, 5, 10 and 15% were 5.63, 6.85, 9.07 and 11.95 %, respectively. These values were equal to 3.48, 5.72, 8.22, and 9.61% for the salinity of 16500 ppm and the salinity of 11000 ppm were equal to 2.79, 4.23, 6.89 and 7.44%, respectively (Figure 4-31). At a pressure of 6.894 MPa, equilibrium oil swelling at seawater salinity and acetone volume ratios of 0, 5, 10, and 15% were 8.83, 9.48, 12.18, and 14.02%, respectively. These values were equal to 4.96, 8.02, 10.19 and 11.26% for salinity equal to 16500 ppm and at a salinity of 11000 ppm were equal to 3.01, 5.67, 7.86 and 8.24%, respectively (Figure 4-32). Finally, at a pressure of 10.342 MPa, equilibrium oil swelling in seawater salinity and acetone volume ratios of 0, 5, 10 and 15% were 9.70, 12.50, 13.64 and 16.53%, respectively. These values were equal to 6.75, 9.51, 10.89, and 12.90% for base fluid salinity of 16500 ppm, and for a salinity of 11000 ppm were equal to 4.30, 7.16, 10.07 and 12.45%, respectively (Figure 4-33). The role of salinity in oil swelling when constant pressure is considered is also shown in Figure 4-34 at 10.342 MPa. As can be seen, oil swelling decreases with decreasing salinity. Soluble ions are often adsorbed at the interface and, by pairing with polar compounds of oil, affect surface phenomena such as interfacial tension and contact angle [150 - 152]. Therefore, the ions do not directly affect oil swelling in a water-oil system. But when acetone and/or carbon dioxide are present in the system, the soluble ions change the oil swelling by changing the solubility of the transportable additives. The solubility of acetone and carbon dioxide in brine containing different ions is not the same. Therefore, their impact on oil swelling is expected to depend on their nature. The solubility of carbon dioxide in saline solutions and the capacity of ions do not follow a regular relationship, but it can be said that with increasing ionic strength, the solubility of carbon dioxide decreases and oil swelling decreases [153].

As mentioned, the presence of acetone in carbonated water, the salinity and the pressure affect the mass transfer and subsequently affect oil swelling, and it can be seen that time plays an important role in the amount of equilibrium oil swelling so that the amount of oil swelling in the presence of acetone in the early and sometimes intermediate times is less than the oil swelling associated with acetone-free carbonated water, while in equilibrium times an opposite result was seen. Reviewing the curves of Figures 4-22 – 4-30 and examining the time to balance oil swelling shows that there is a unique time for each fluid that is at a constant temperature, influenced by the volumetric ratio of acetone, salinity and pressure. Table 4-10 shows the equilibrium time for each experiment at 75 °C and different pressures. Figures 4-35, 4-36 and 4-37 show the data in this table at 3.447, 6.894 and 10.342 MPa, respectively. Comparison of Figures 4-35, 4-36 and 4-37 shows that the equilibrium time decreases with increasing pressure. Also, the results show that the equilibrium time increases with increasing the acetone component in carbonated water and decreases with

increasing salinity. These results are consistent with the effect of these parameters on the CO₂ solubility and acetone in water and their mass transfer according to what has been mentioned earlier. An increasing slope is evident in the equilibrium time-oil swelling curves with increasing acetone concentration from 10% to 15%. To justify this change in slope, it must be borne in mind that acetone acts like a co-surfactant due to its molecular structure. This feature causes its molecules to be first adsorbed in the interface and then transferred to the oil phase. Molecules adsorbed at the interface are more easily transported to the oil phase than molecules that are completely dissolved in the aqueous phase. It is possible that the entire interface surface is occupied at one concentration and then at higher concentrations, the molecules dissolved in the water remain in the aqueous phase for a longer period. From a quantitative point of view, at a pressure of 3.447 MPa, the equilibrium time of oil swelling in salinity of seawater and acetone volume ratios of 0, 5, 10 and 15% were 19.5, 22.5, 23.5 and 26.5 min, respectively. These values were 10.5, 23.5, 27.5 and 34.5 min for salinity equal to 16500 ppm and 24.5, 28.5, 37.0 and 41.5 min for a salinity of 11000 ppm, respectively (Figure 4-35). At a pressure of 6.894 MPa, the equilibrium time of oil swelling in seawater salinity and acetone volume ratios of 0, 5, 10 and 15% were 15.5, 18.0, 18.5 and 22.5 min, respectively. These values were 10.5, 21.5, 24.5, 24.5 and 31.5 min for salinity equal to 16500 ppm and 23.5, 26.0, 27.5 and 37.5 min for a salinity of 11000 ppm, respectively (Figure 4-36). At 10.342 MPa, the equilibrium time of oil swelling in the salinity of the seawater and the acetone volumetric ratios of 0, 5, 10 and 15% were 11.5, 13.5, 15.5 and 20.5 min, respectively. These values were equal to 15.5, 17.5, 22.0 and 27.5 min for the salinity of the base fluid equal to 16500 ppm and the salinity of 11000 ppm were equal to 22.5, 24.5, 26.0 and 32.5 min, respectively (Figure 4-37).

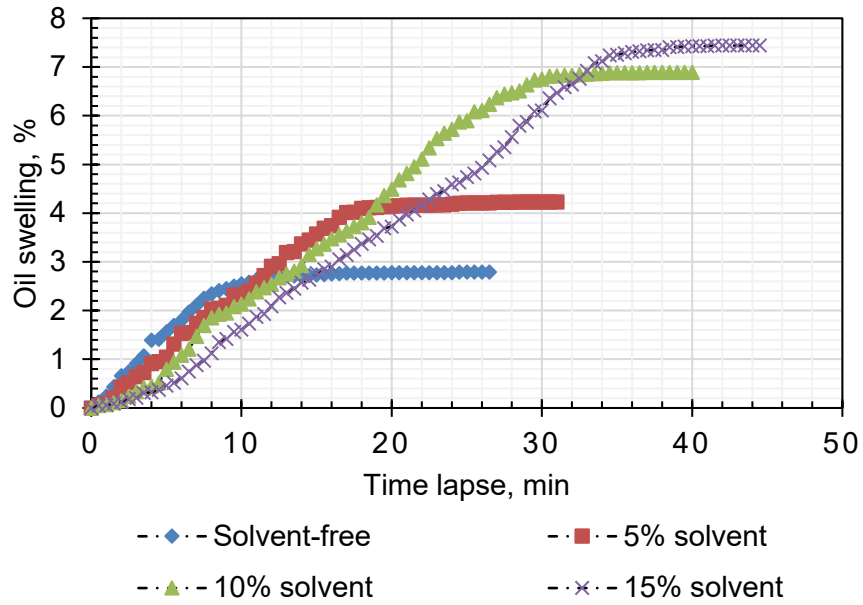


Figure 4-22: Dynamic oil swelling curves in the presence of carbonated seawater with a salinity of 11000 ppm containing acetone at different volume ratios at 75 °C and 3.447 MPa pressure.

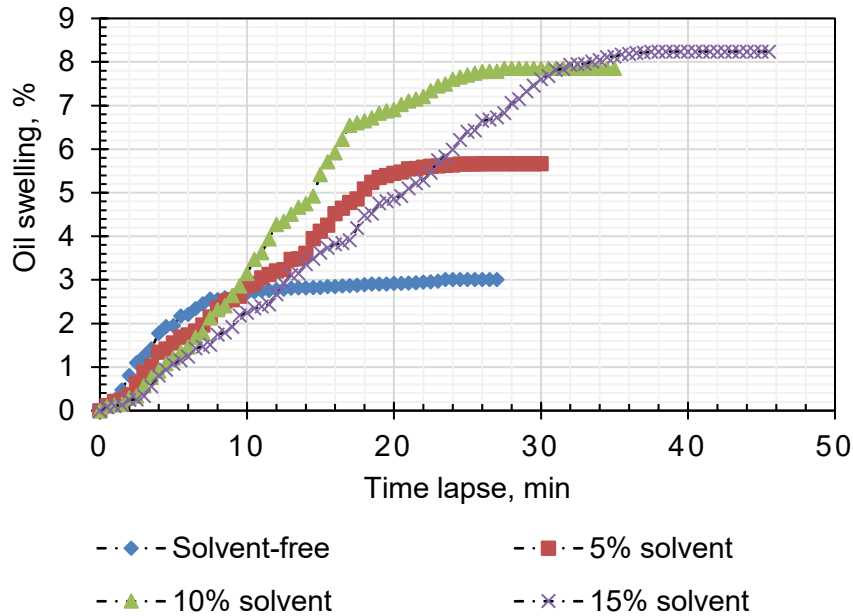


Figure 4-23: Dynamic oil swelling curves in the presence of carbonated seawater with a salinity of 11000 ppm containing acetone at different volume ratios at 75 °C and 6.894 MPa pressure.

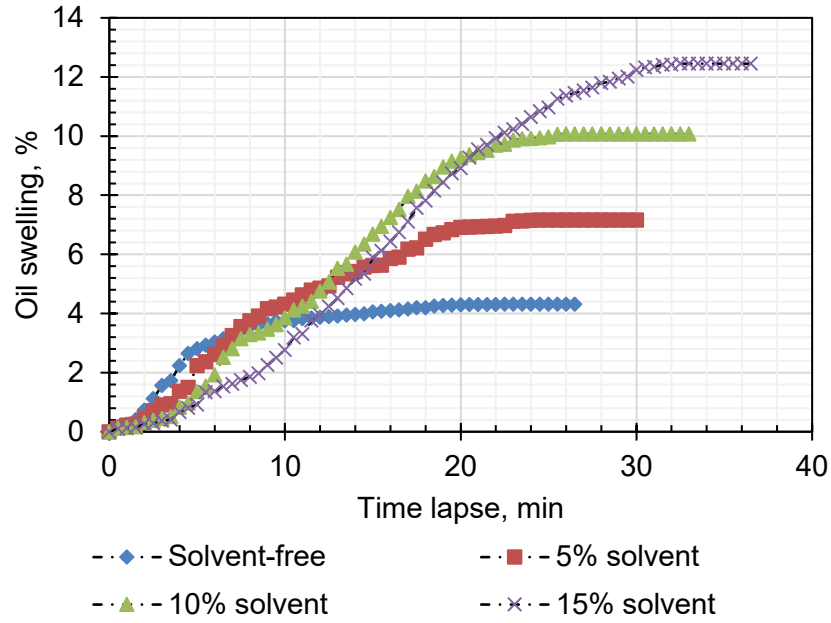


Figure 4-24: Dynamic oil swelling curves in the presence of carbonated seawater with a salinity of 11000 ppm containing acetone at different volume ratios at 75 °C and 10.342 MPa pressure.

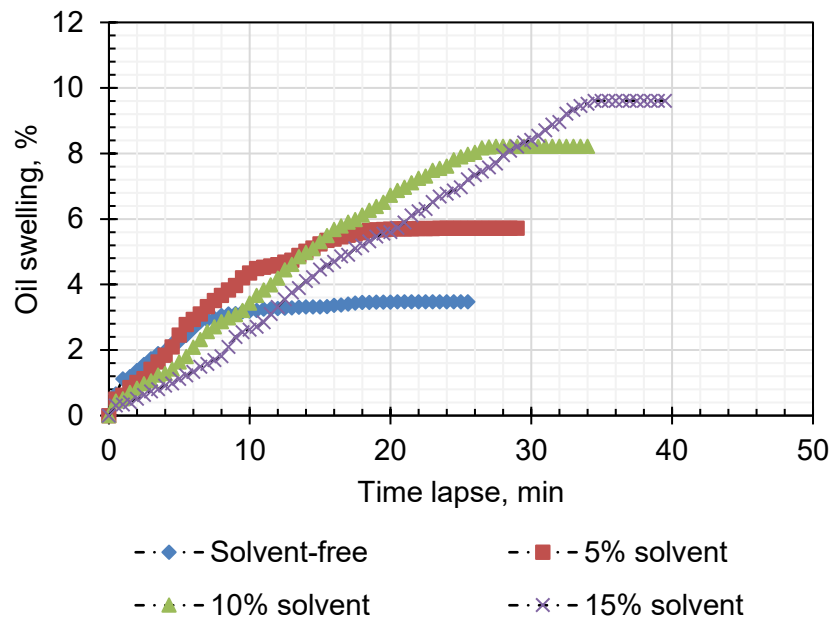


Figure 4-25: Dynamic oil swelling curves in the presence of carbonated seawater with a salinity of 16500 ppm containing acetone at different volume ratios at 75 °C and 3.447 MPa pressure.

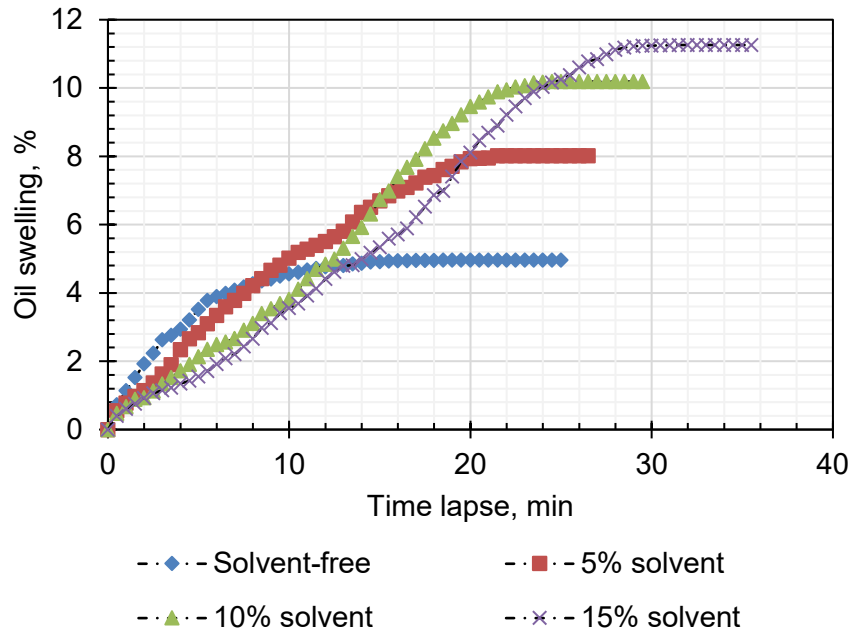


Figure 4-26: Dynamic oil swelling curves in the presence of carbonated seawater with a salinity of 16500 ppm containing acetone at different volume ratios at 75 °C and 6.894 MPa pressure.

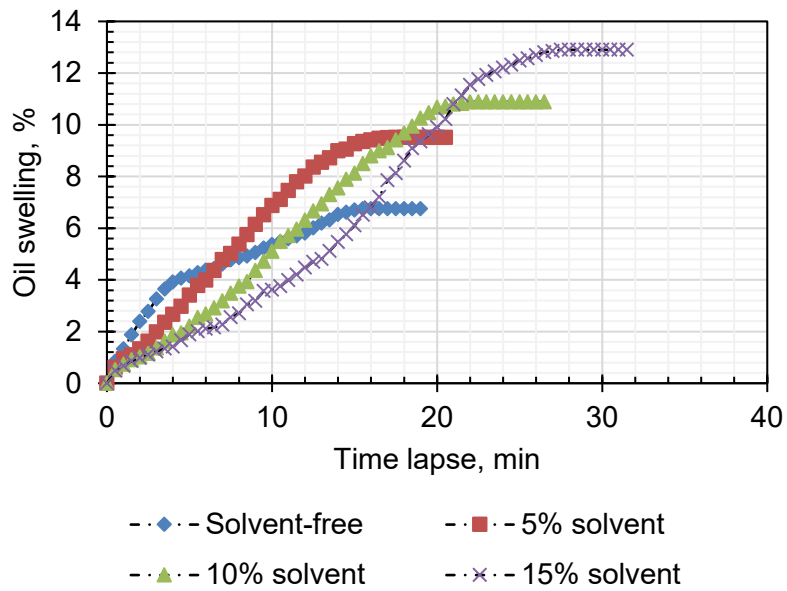


Figure 4-27: Dynamic oil swelling curves in the presence of carbonated seawater with a salinity of 16500 ppm containing acetone at different volume ratios at 75 °C and 10.342 MPa pressure.

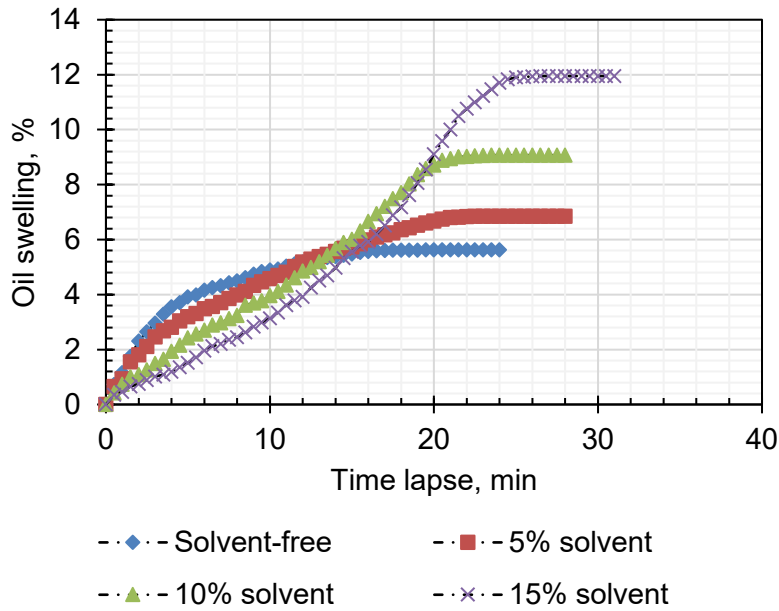


Figure 4-28: Dynamic oil swelling curves in the presence of carbonated seawater containing acetone at different volume ratios at 75 °C and 3.447 MPa pressure.

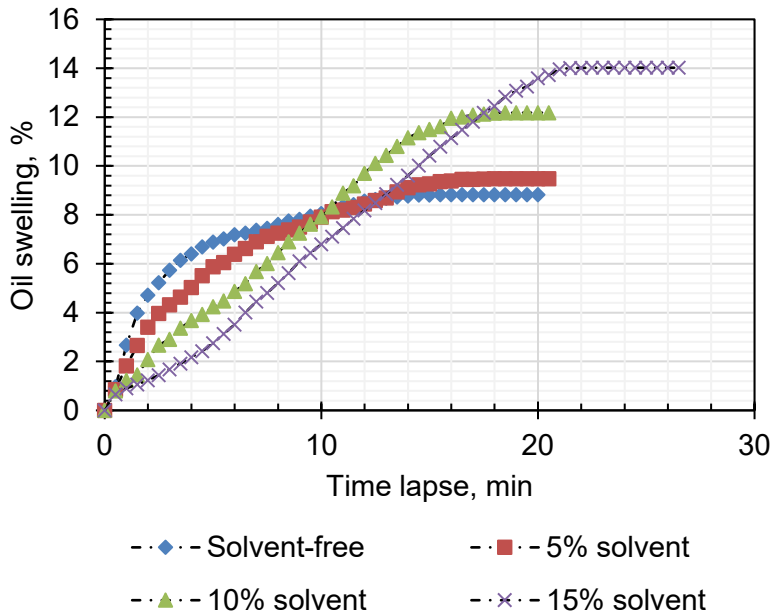


Figure 4-29: Dynamic oil swelling curves in the presence of carbonated seawater containing acetone at different volume ratios at 75 °C and 6.894 MPa pressure.

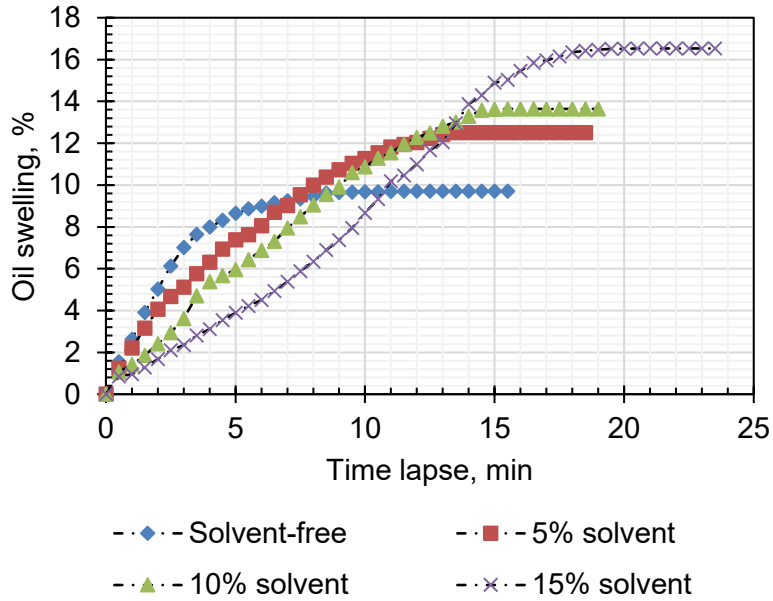


Figure 4-30: Dynamic oil swelling curves in the presence of carbonated seawater containing acetone at different volume ratios at 75 °C and 10.342 MPa pressure.

Table 4-9: Equilibrium oil swelling values in the presence of carbonated seawater containing acetone at different volume ratios and different pressures at 75 °C.

Base fluid		Equilibrium oil swelling, %											
		Seawater				16500 ppm				11000 ppm			
Solvent percent		0	5	10	15	0	5	10	15	0	5	10	15
Pressure, MPa	3.447	5.63	6.85	9.07	11.95	3.48	5.72	8.22	9.61	2.79	4.23	6.89	7.44
	6.894	8.83	9.48	12.18	14.02	4.96	8.02	10.19	11.26	3.01	5.67	7.86	8.24
	10.342	9.70	12.50	13.64	16.53	6.75	9.51	10.89	12.90	4.30	7.16	10.07	12.45

Table 4-10: Equilibrium time of oil swelling in the presence of carbonated seawater containing acetone at different volume ratios and different pressures at 75 °C.

Base fluid		Equilibrium time of oil swelling, min											
		Seawater				16500 ppm				11000 ppm			
Solvent percent		0	5	10	15	0	5	10	15	0	5	10	15
Pressure, MPa	3.447	19.5	22.5	23.5	26.5	20.5	23.5	27.5	34.5	24.5	28.5	37.0	41.5
	6.894	15.5	18.0	18.5	22.5	18.5	21.5	24.5	31.5	23.5	26.0	27.5	37.5
	10.342	11.5	13.5	15.5	20.5	15.0	17.5	22.0	27.5	22.5	24.5	26.0	32.5

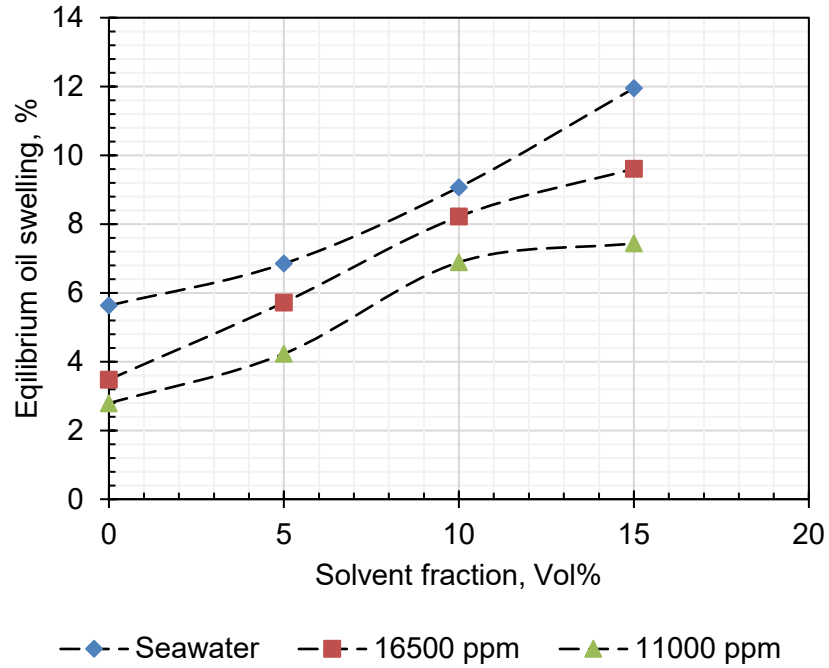


Figure 4-31: Equilibrium oil swelling curves in the presence of carbonated seawater containing acetone at different volume ratios at 3.447 MPa and 75 °C.

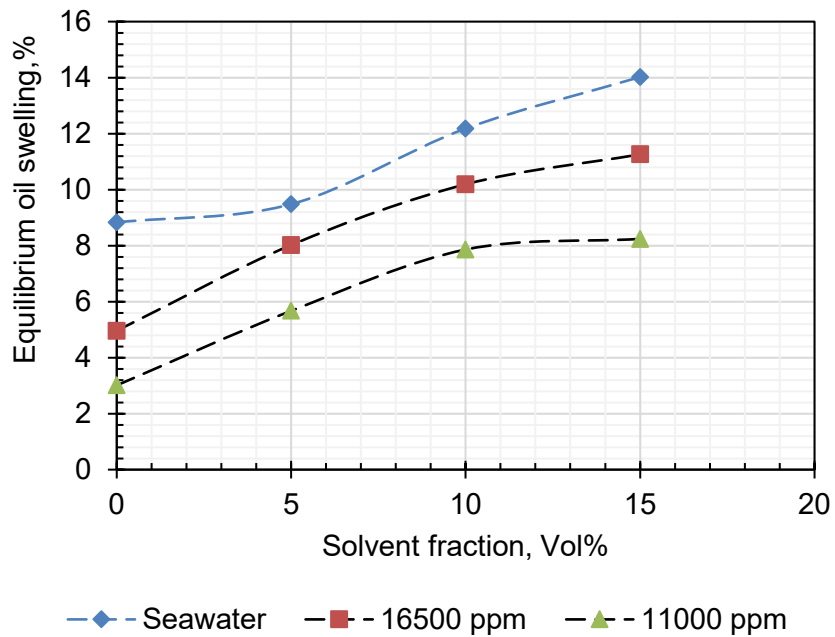


Figure 4-32: Equilibrium oil swelling curves in the presence of carbonated seawater containing acetone at different volume ratios at 6.894 MPa and 75 °C.

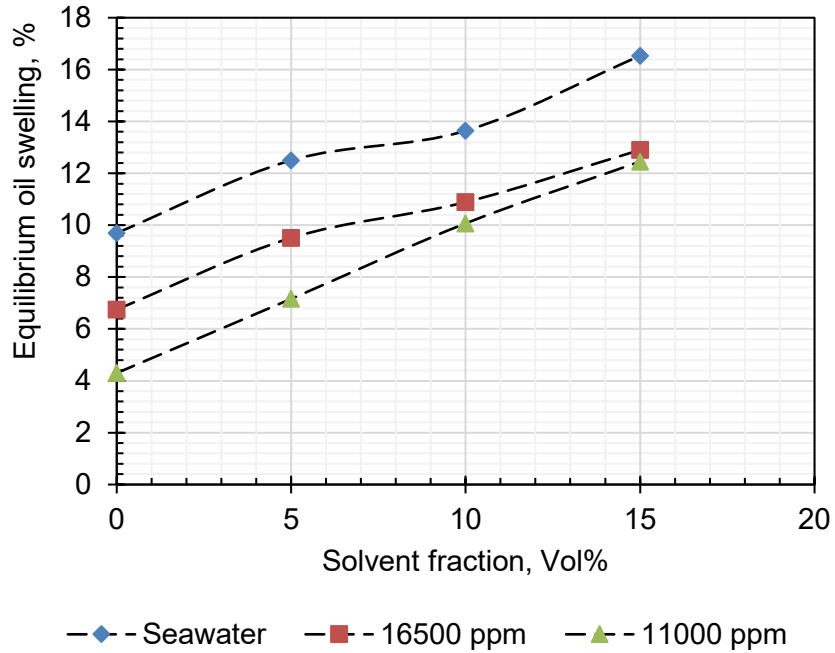


Figure 4-33: Equilibrium oil swelling curves in the presence of carbonated seawater containing acetone at different volume ratios at 10.342 MPa and 75 °C.

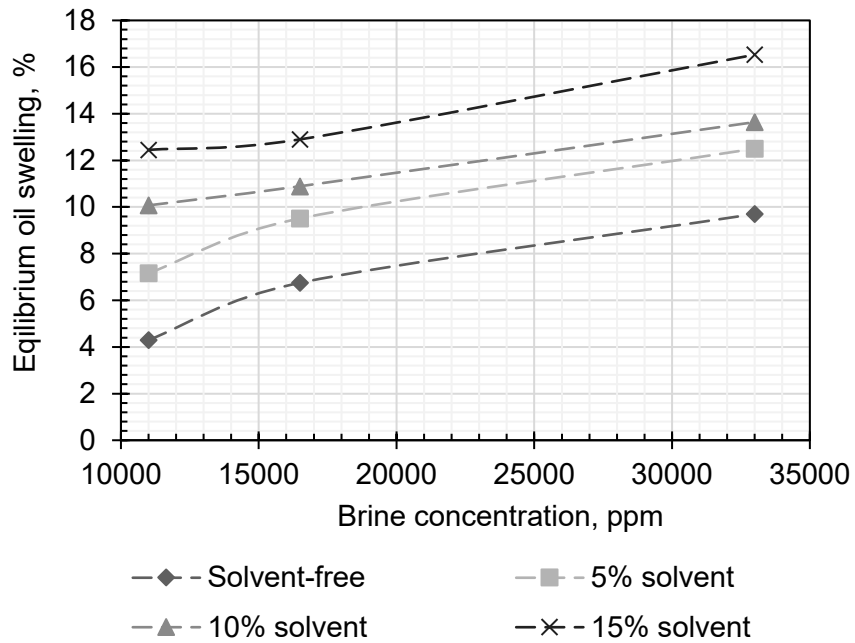


Figure 4-34: Equilibrium oil swelling curves in the presence of carbonated seawater at different concentration of the base-fluid containing acetone at different volume ratios at 10.342 MPa and 75 °C.

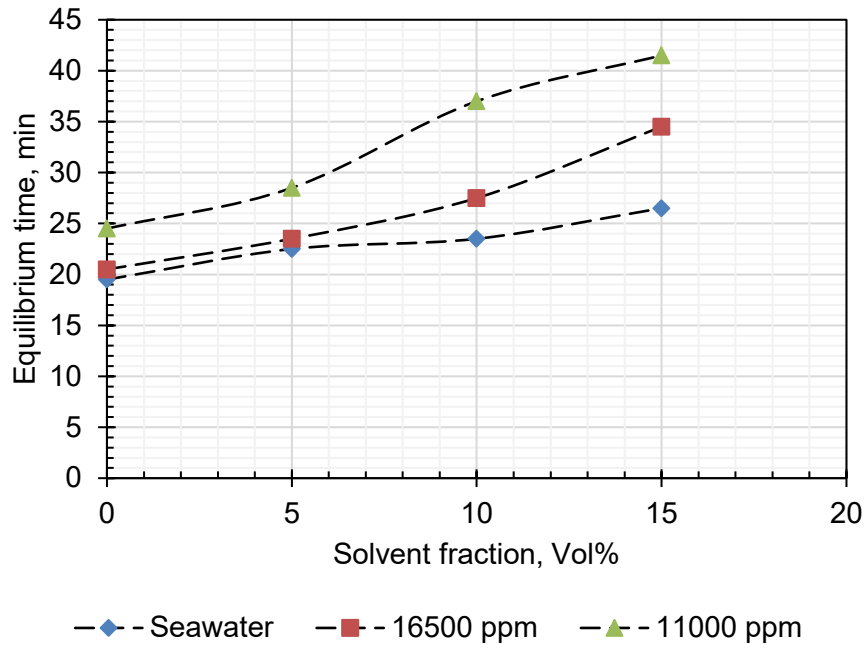


Figure 4-35: Equilibrium time of oil swelling curves in the presence of carbonated seawater containing acetone at different volume ratios at 3.447 MPa and 75 °C.

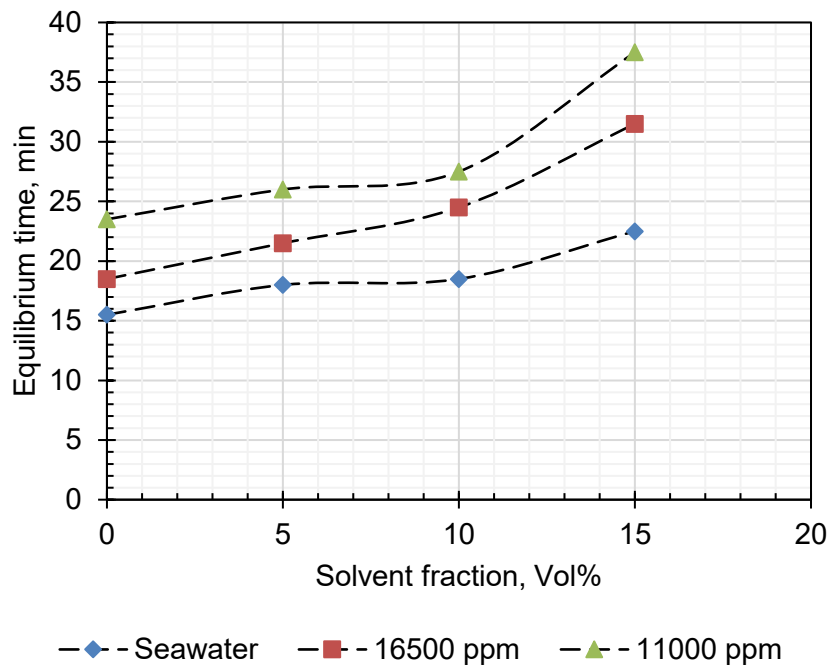


Figure 4-36: Equilibrium time of oil swelling curves in the presence of carbonated seawater containing acetone at different volume ratios at 6.894 MPa and 75 °C.

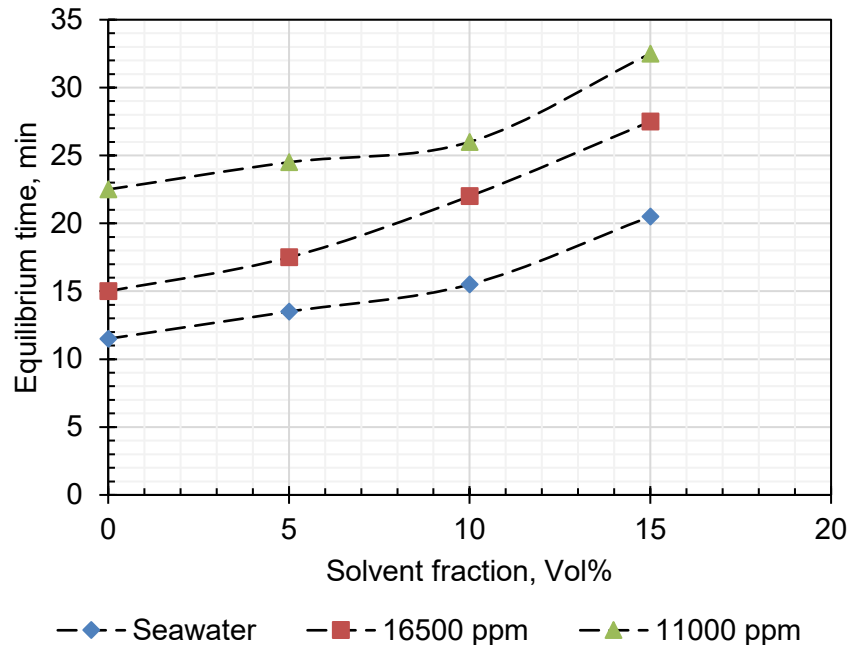


Figure 4-37: Equilibrium time of oil swelling curves in the presence of carbonated seawater containing acetone at different volume ratios at 10.342 MPa and 75 °C.

4.2. Extracted saponin from *Anabasis Setifera* plant

4.2.1. FTIR, ¹H NMR and TGA analyses results

Fig. 4-38 shows an analysis of FTIR and functional groups of surfactants extracted from the *Anabasis Setifera* plant. A peak at 3363 cm⁻¹ represents the stretching vibration of multiple hydroxyls in the side chain of oligosaccharide of saponin. The peak at 2970 cm⁻¹ associated with the C-H aliphatic sapogenin saponin graft and the weaker peak at 1605 cm⁻¹ is showed the C=C bond in sapogenin. The peak of 1384 cm⁻¹ shows the bond of -OH and finally, the peak at 1073 cm⁻¹ is coupled to the C-O stretching vibration [154].

Fig. 4-39 shows the ¹H NMR analysis. The chemical shifts in 2.68-5.27 ppm show the majority of protons in the saponin oligosaccharide while chemical changes in 0.70-2.34 ppm are mainly related to protons in the agilcone section of saponin [155].

Fig. 4-40 shows the TGA analysis. According to the data, this initial weight loss occurs at a temperature of 86 °C and reaches about 32% at 150 °C. Due to the loss of sample moisture and low weight loss after this temperature peak, it can be concluded that the stability of the surfactant is appropriate for reservoir temperatures.

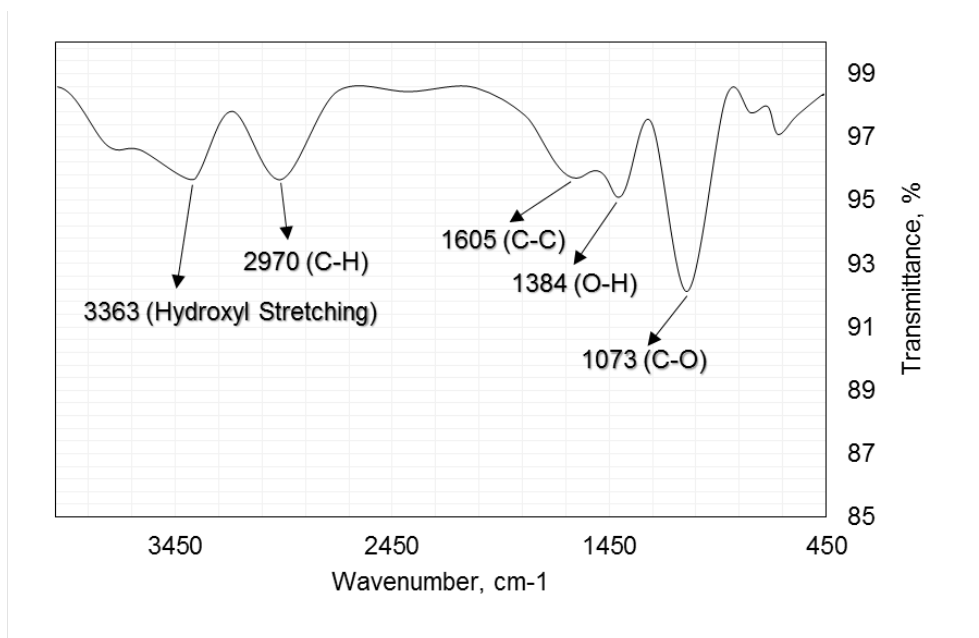


Figure 4-38: FTIR analysis chart and determination of surfactant functional groups.

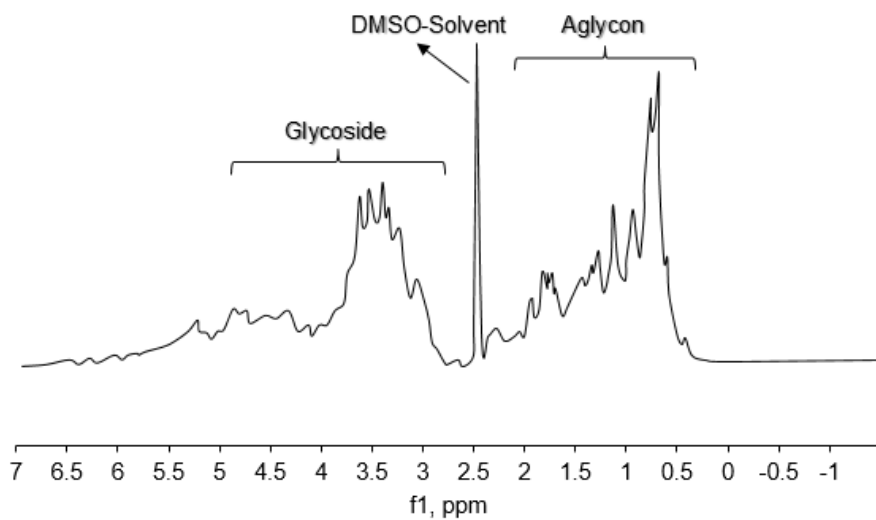


Figure 4-39: ¹H NMR analysis for saponin extracted from *Anabasis Setifera* plant.

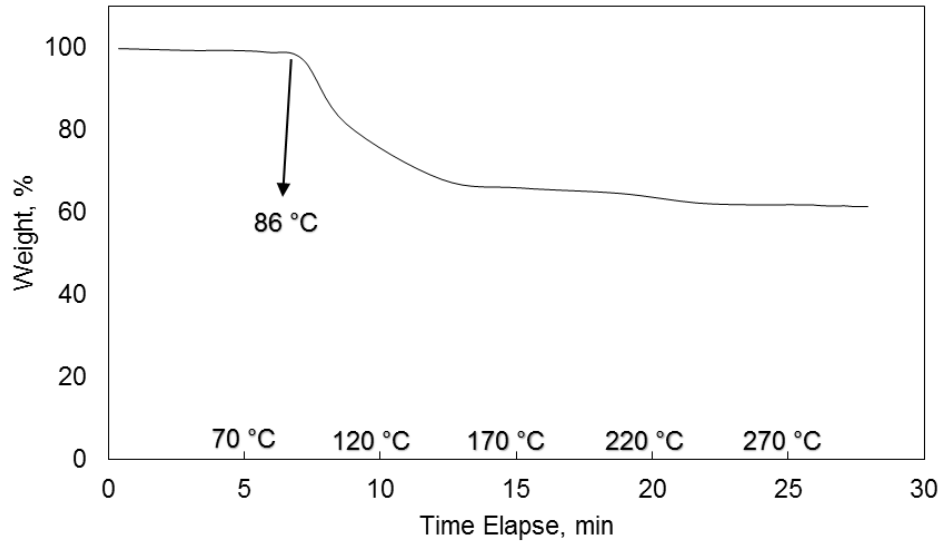


Figure 4-40: TGA analysis curve and temperature stability of the surfactant.

4.2.2. Surface tension and interfacial tension results

Fig. 4-41 shows the curve of the surfactant solutions surface tension with various concentrations. According to Fig. 4-41 and the initial value of air-water surface tension, it is evident that surface tension at 75 °C decreases with increasing surfactant concentration but this drop is higher to reach a concentration of 3000ppm and then the rate decreases and even slightly increases. The drop in the rate of surface tension reduction vs. concentration in a particular concentration is known as the critical micelle concentration. In general, the strongest concentration of the surfactant in the parameters of EOR occurs at this [121]. A physical change in the solution, which leads to a new arrangement of surfactant molecules, causes this change in the surface tension trend. Surfactant molecules are arranged at the liquid surface due to the hydrophobic-hydrophilic dual structure so that the water-wet section is dissolved in water solution and the oil-wet section avoids it. By increasing the concentration of surfactants and occupying the interface chapters by molecules, aggregations of surfactants result from the adsorption of the same parts of each other which is called the micelle. The formation of the micelle weakens the function of the surfactant molecules by limiting its release [156, 157]. Fig. 4-42 shows the process of IFT changes of surfactant solutions with various concentrations and crude oil over time and a constant temperature of 75 °C. Fig. 4-43 shows the values of equilibrium IFT after sufficient time to get the equilibrium of the system of an oil droplet in the aqueous environment. Fig. 4-44 shows the effect of different salinity of formation water and different salts. A similar trend with surface tension variations (Fig. 4-41) is also found in Fig. 4-43 for the IFT of surfactant solutions and crude oil. At a temperature of 75 °C, the IFT has an inverse relationship with the surfactant concentration and a rapid drop in IFT to a specific concentration, or CMC occurs. The IFT for

concentrations of 500, 1000, 2000, 3000, 4000, 5000 and 6000ppm was obtained at 5.797, 3.627, 2.964, 1.066, 1.082, 1.134 and 1.145mN/m, respectively. However, the initial IFT of water and oil was achieved at 25.608 mN/m. Different salinity also affects the IFT of surfactant solution at CMC and crude oil, but there is an optimal concentration proportional to the type of salinity and soluble ions. Fig. 4-44 shows the IFT values of surfactant at CMC and optimum salinity of each brine are as follows: FW, at concentration of 10000ppm equal to 0.973mN/m, NaCl at concentration of 15000ppm equal to 1.021mN/m, KCl at concentration of 10000ppm equal to 1.034mN/m, CaCl₂ at concentration of 10000ppm equal to 0.955mN/m, MgCl₂ at concentration of 10000ppm equal to 0.949mN/m, FeSO₄ at concentration of 10000ppm equal to 0.890mN/m, K₂SO₄ at concentration of 10000ppm equal to 0.838mN/m and NaHCO₃ at concentration of 20000ppm equal to 0.947mN/m. The reason for the change in IFT in the presence of ions depends on the adsorption of ions in the interface due to the presence of some polar compounds in oil such as asphaltene. The difference of IFTs between different salts is very small because the saponin is a nonionic surfactant that is insensitive to salinity. The ions resulting from the dissolution of salts behave differently in interfacial tension. This behavior depends on the nature and type of ions. Besides, the nature of ions in the face of oil compounds causes different behavior in interfacial tension. For example, the affinity of Mg²⁺ for resin molecules is higher than Ca²⁺, whereas the affinity of Ca²⁺ for asphaltene is higher than Mg²⁺ [135, 158]. In simpler terms, different salts, depending on their nature, release different ions in the water, which give different reactions at the interface and the amount of absorption is different here. Depending on the amount and type of each particular ion, different interfacial tension values occur as a result of the dissolution of different salts. Also, in lower concentrations due to the salt-in effect, smaller IFT occurs. In the case of salt-in, organic particles tend to dissolve in water. In other words, non-organic ions break the structure of water created around organic molecules and thus reduces the solubility of organic molecules in the aqueous phase. It can be said that the effect of salt-in releases the active components in the surface from the solvent into a low salt concentration. In other words, in low salinity, the solubility of various types of hydrocarbons in crude oil increases in the aqueous bulk and ultimately the interfacial tension decreases [136, 137, 159 - 161].

When two immiscible fluids collide at the same interface, chemical and physical reactions occur between their molecules in the interface. In the presence of surfactant, there is a mechanism similar to the water-air interface. The surfactant molecules are located in the same way as the hydrophobic part in the oil phase and the hydrophilic part in the water phase. As a result, a thin film of surfactant molecules forms in the interface. This adsorption of surfactant molecules does not occur at a moment and is usually time-consuming. This time-lapse is required in IFT experiments and early data is not reliable in the short run.

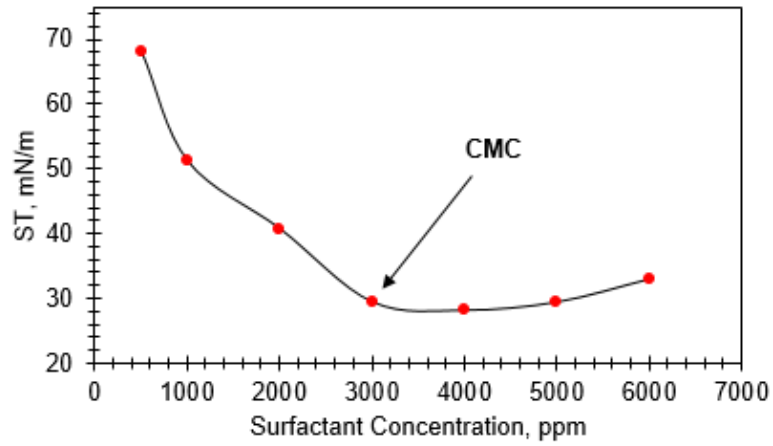


Figure 4-41: Surface tension graph at various concentrations of the surfactant and 75 °C.

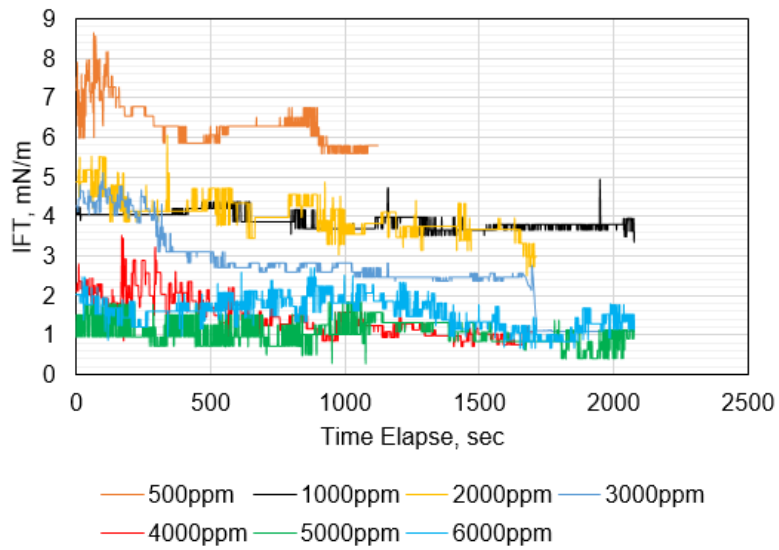


Figure 4-42: Dynamic IFT graphs for surfactant solutions at various concentrations and crude oil at 75 °C.

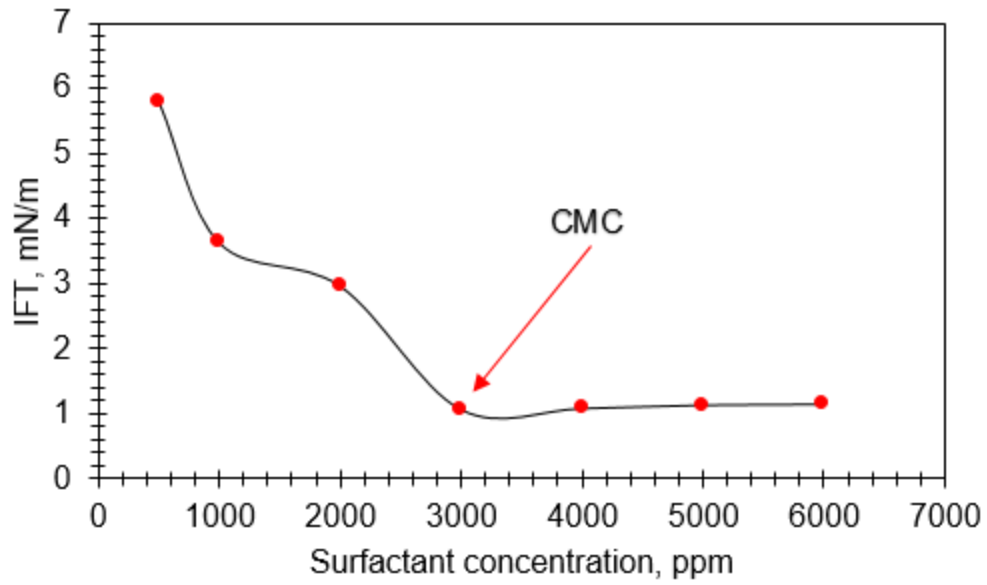
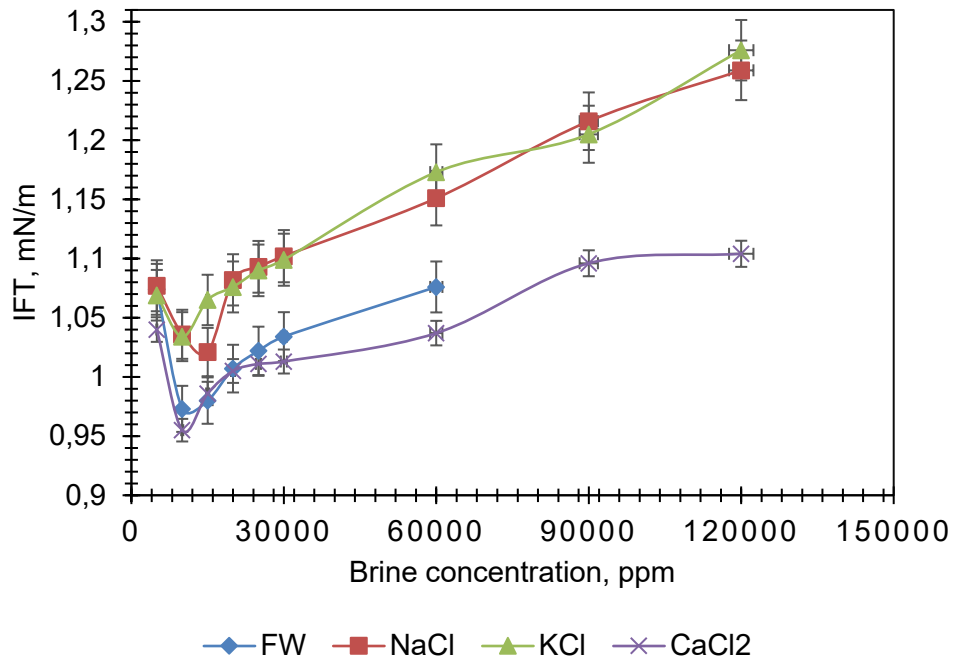


Figure 4-43: The curve of IFT of surfactant solutions at various concentrations and crude oil at 75 °C.



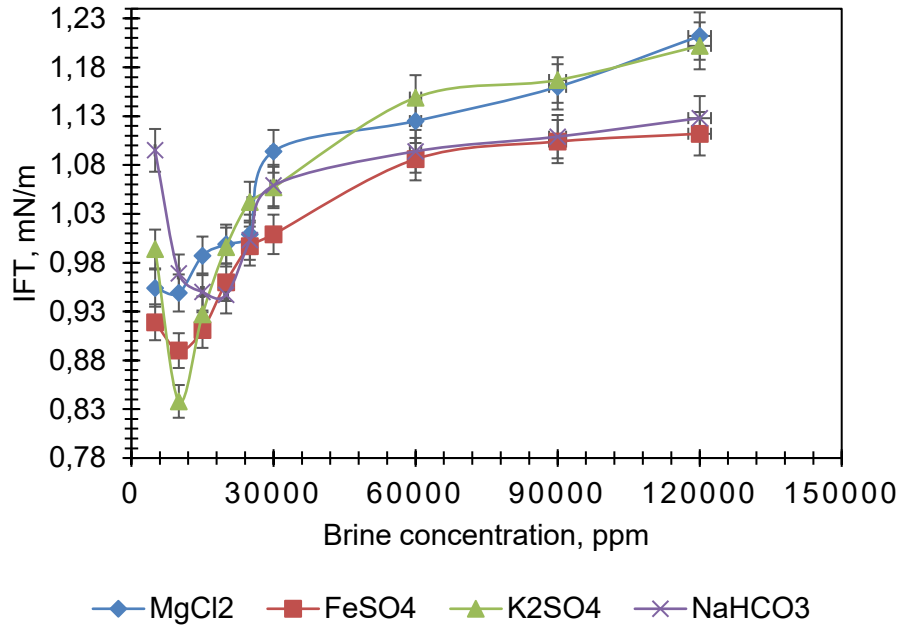


Figure 4-44: Curves of different salinity effects on IFT of surfactant solution at CMC and crude oil at 75 ° C.

4.2.3. Contact angle results

Fig. 4-45 shows the changes in the contact angle of the drop of oil on the cross-section of the rock in an aqueous solution containing surfactant at CMC and Fig. 4-46 shows the graphs of the effects of salinity on the value of the contact angle. As evident from the attached drop images in Fig. 4-45 and the numbers related to the average contact angle, the wettability tends to be hydrophilic over time. Finally, the average contact angle of 50.24 degrees was obtained which is located in a relatively hydrophilic range. Considering Fig. 4-46, we find that different salts also have a significant influence on the contact angle of the final contact angle, although, in a particular concentration of salts, this amount reaches its minimum. In this way, the average contact angles for different concentrations were obtained as follows: FW at a concentration of 10000ppm equal to 45.39°, NaCl at a concentration of 15000ppm equal to 53.12°, KCl at a concentration of 10000ppm equal to 51.92°, CaCl₂ at a concentration of 10000ppm equal to 41.3°, MgCl₂ at a concentration of 10000ppm equal to 42.54°, FeSO₄ at a concentration of 10000ppm equal to 40.22°, K₂SO₄ at a concentration of 10000ppm equal to 39.67° and NaHCO₃ at a concentration of 20000ppm equal to 43.69°. The change in the carbonate rock wettability by the nonionic surfactant of saponin has a mechanism similar to ion exchange. The adsorbed stearic acid in the aging stage adsorbs the surfactant molecules through its benzene rings. This adsorption can lead to ionic interaction in a system with significant electron density. Namely, having benzene rings in the structure of the surfactant, (as the source of the electron), can

be adsorbed by the dolomite surface with a positive charge. In this way, the Stearic acid molecule is separated from the surface of the rock. Surfactant molecules occupy active sites and stearic acid molecules are absorbed on the new layer [162, 163]. Thus, a thin film between the surface of the rock and the sessile oil drops can reduce the contact angle. When there are soluble ions in the system, there is a similar mechanism for the function of ions to change the wettability. A mechanism was developed by Zhang *et al.* They presented a model for the behavior of ions relative to the calcite surface based on the results of chromatographic experiments And evaluated properties such as the concentration of Ca^{2+} , Mg^{2+} ions, temperature and injecting fluid flow rate. They considered the reason for changing wettability to be the separation of fatty acids adsorbed from the surface of the rock. They stated that SO_4^{2-} anion reduced the positive charge of the surface and increased the ability of cations to approach the carboxylic acid adsorbed on calcite. By increasing the concentration of Mg^{2+} cation in water, the cation's ability to separate carboxylic acid, which is negatively adsorbed by rocks, increases, and causes more hydrophilicity of the rock [25]. Gomari and Hamouda found that calcite that was in contact with a sulfate solution is more inclined to adsorb water than pure calcite. They showed that the wettability of the calcite surface depends on the structure of fatty acids, water composition and pH [164]. Rezaei Doust et al. showed that sulfate is covered by hydrogen bonding in water and the reactivity of the SO_4^{2-} ion increases to the surface of the lime at high temperatures due to hydrogen defeat. As a result, at a high temperature, SO_4^{2-} is absorbed on the surface of the rock strongly which reduces the repulsive force between the positive charge of the rock surface and cations and increases the ability of cations to adsorb carboxylic groups [165]. However, as can be seen in Fig. 14, the contact angle decreased further at low salinities. The above mechanisms are most frequently mentioned for changing the wettability at high salinities. Stronger mechanisms have been developed to change the wettability at lower salinities. The salt-in effect described in the interfacial tension section also applies to wettability alteration. This means that the salt-in effect of releasing the active components of the surface from the solvent at low salt concentration makes it easier, in other words, to lower the solubility of different types of hydrocarbons adsorbed on the rock surface in water and so the surface wettability is closer to hydrophilicity. Also, reactions from equations 4-6 and 4-7 can occur in dissolved carbonate rock at low salinity, which may eventually lead to the further dissolution of carbonate rock and change its wettability to more hydrophilic [6, 47, 141]:



The reason for the further reduction of the contact angle in the presence of different salinity in the diagram of Fig. 4-46 can be explained with the above explanations.

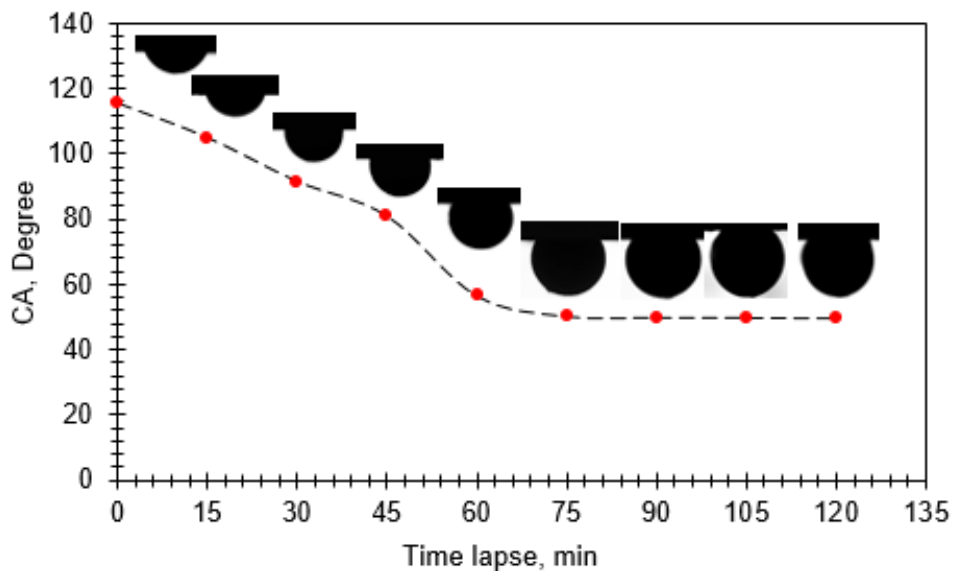


Figure 4-45: The curve of contact angle of the oil droplet on carbonate cross-section over time, in the presence of a solution of surfactant at CMC and a temperature of 75 °C.

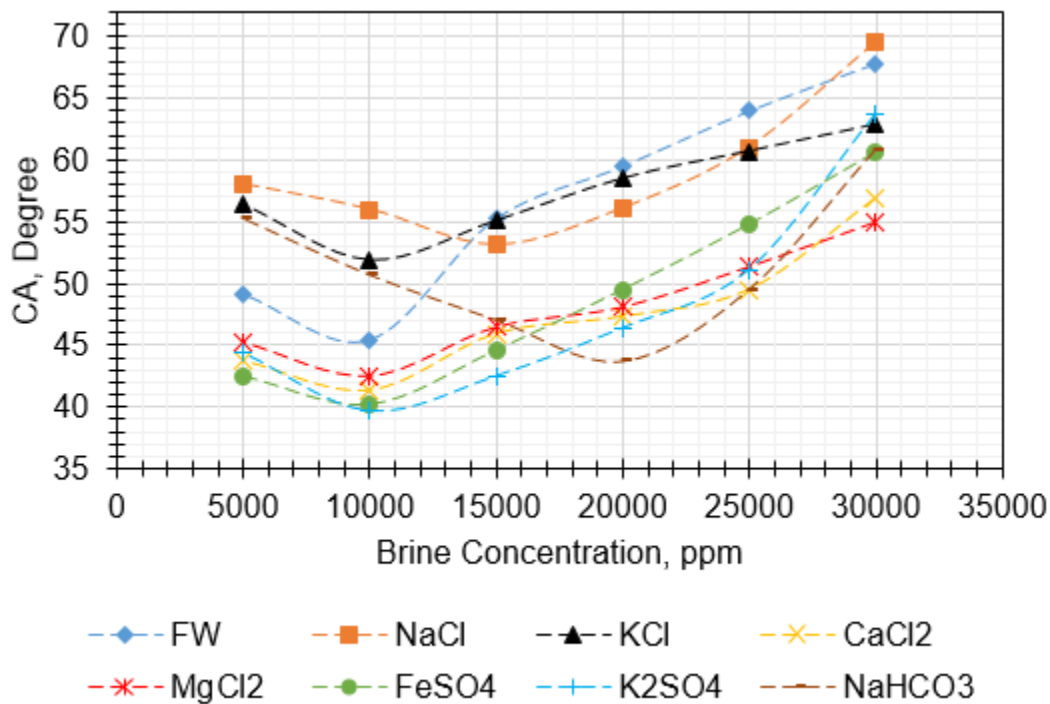


Figure 4-46: Different salinity effects on contact angle at CMC of surfactant and 75 °C.

4.2.4. Oil recovery by surfactant flooding

Fig. 4-47 shows the amount of oil production and the pressure differences corresponding to it in the flood corresponding to the injected fluid volume in the secondary flooding of brine and the tertiary surfactant injection at optimal salinity. The flooding was performed in a carbonate plug with a length of 7 cm, a diameter of 1.5 in, an effective porosity of 23.7%, an effective pore volume of 18.90 cm³, an absolute permeability of 11.5 mD, an initial water saturation of 21% and an OOIP of 15 cm³. The injection of surfactant was then continued up to a total volume of 4PV (2.5PV of surfactant) injected fluid. The final recovery factor of 66.9% was obtained by a secondary injection of brine and tertiary injection of surfactants. Based on this, recovery was achieved by injection of surfactant equivalent to 15.4%. Oil recovery in the third stage was started after injection the total volume of injected fluid equaled 1.9PV (0.4PV injection of surfactant) and ended up until the total volume of 3.3PV fluid injection (1.8 PV surfactant was injected).

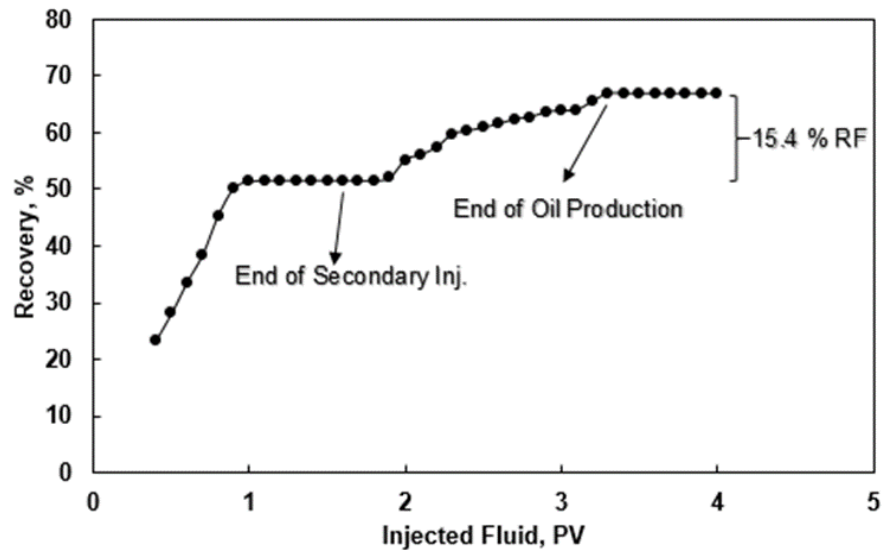


Figure 4-47: Oil recovery curve vs. injected fluid PV at CMC of the surfactant and optimum salinity of formation water.

4.2.5. CO₂-foam characterization

Figure 4-48 shows the curve of surface tension changes at 75 °C. The amount of surface tension is inversely related to the concentration of surfactant and is drastically reduced to a concentration of 3000 ppm. Surface tension at this concentration, which is equivalent to CMC, was 20.549 mN/m.

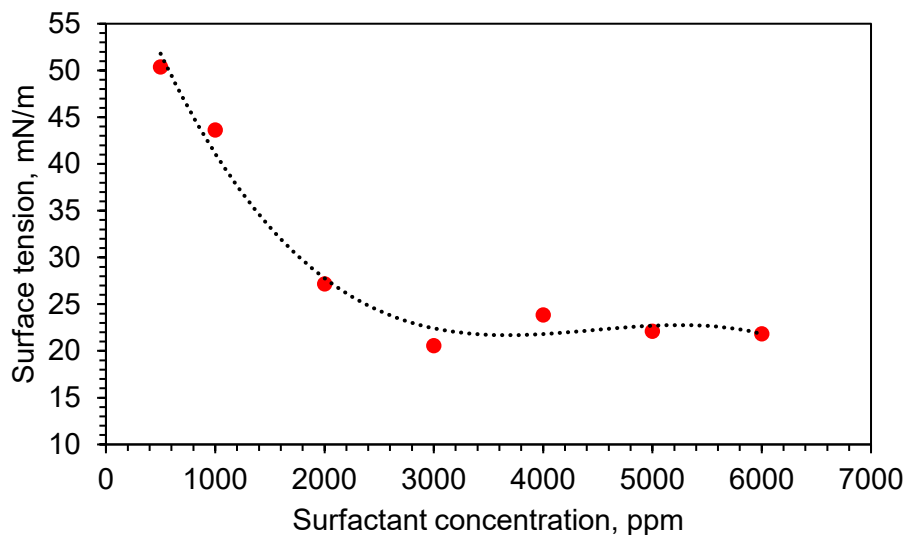


Figure 4-48: Surface tension diagram of the surfactant in a CO₂ environment at 75 °C.

Surfactants produce foam via the amphiphilic nature of the active molecules. A liquid film surrounds a bubble so that the hydrophobic tail tends to the bubble and the hydrophilic head tends to the water film. The foam is stabilized by this arrangement. The bubbles separating thin film is named “foam lamellae” [166]. Figure 4-49 shows the CO₂-foam height over time. The foam column height was measured at the moment of the column filling (when the gas valve was closed) and was based on the foam-surfactant solution joint. Based on Figure 4-49, the height of the foam is constantly decreasing over time and after 120 minutes, it completely disintegrates. During the disintegration, at a special moment, the height of the foam is reduced to half the original height. The foam half-life time, denoted by $t_{1/2}$, is defined at this time and is 40 min for surfactant in CMC, as shown in Figure 4-49. The foam initial structure affects its disintegration. The foam structure depends on some soluble impurities and gas flow rate. Figure 4-50 shows the effect of different salinities on the foam height formed in the CMC of the surfactant and 20 ml/sec gas flow rate. As it is known, the height of foam at a salinity of 10000 ppm has a longer half-life and height at any moment. For better comparison, the foam height at different salinities after 40 min is shown in Figure 4-51. Accordingly, the foam heights at salinities of 5000, 10000, 15000, 20000 and 30000 ppm, after 40 min were equal to 42, 55, 43, 38 and 25 cm, respectively. Figure 4-52 also compares the half-life time for different salinities. As Figure 4-52 shows, the half-life time for the salinities of 5000, 10000, 15000, 20000 and 30000 ppm were 33.55, 45.20, 33.91, 27.87 and 19.14 min, respectively. Solutions with lower surface tension can produce better quality foam [167 - 170]. With these interpretations, the salinity of 10000 ppm was considered as the optimal salinity for CO₂-foam flooding. The effect of salinity, time and gas flow rate on the size of bubbles was qualitatively investigated. Figure 4-53 shows the effect of salinity of 5000, 10000, 15000, 20000 and 30000 ppm on the bubble size at a 20 ml/sec gas flow rate, immediately after the

foam column filling and the gas flow is stopped. Considering the image scale and the size of the bubbles, there is no significant relationship between salinity and the size of the bubbles. But this is not true for the effect of time. Based on Figure 4-54, the size of the bubbles gets bigger with time. The liquid tendency to accumulate at the bottom of the column is increased by the effect of forces such as gravity on the water film over time. Besides, the internal force of the gas inside the bubble to the wall, which is due to both the difference between the mass of gas and liquid and the movement of gas molecules, makes the liquid film thinner. Thus, the gas phase ratio increases and some bubbles form a larger bubble with the adjacent bubble through the perforation of the liquid film. Figure 4-55 shows the gas flow rate effect on the size of the bubbles immediately after the foam column filling. The images of the bubbles in Figure 4-55 clearly show that the size of the bubbles increased with increasing gas flow rate. But larger bubbles mean an increase in the gas phase and a decrease in the liquid phase in the foam system, which in turn can alter the stability of the foam. An optimal gas flow rate should be considered to generate a stable foam for flooding. The images in Figure 4-55 confirm the lower gas flow rate in creating a uniform foam, but due to the quality of the type of inspection, the exact rate cannot be determined according to them. Therefore, considering that gas flow rates of 10 and 20 ml/sec generated more homogeneous foam compared to gas flow rates of 30 and 50 ml/sec, and some references that suggest gas flow rate between 20-30 ml/sec as the most suitable gas flow rates for generating homogeneous foam in terms of bubble size [166], here gas flow rate equal to 20 ml/sec was selected as the optimal gas flow rate for flooding. Increasing the gas flow rate following the increase in the size of the bubbles increases the volume of foam. Figure 4-56 shows the gas flow rate effect on the CO₂-foam volume over time. According to Figure 4-56, less time is required to fill the foam column or reach a certain volume with increasing the gas flow rate as for gas flow rates of 10, 20, 30 and 50 ml/sec, approximately 55, 40, 30 and 20 sec were required for the foam column filling.

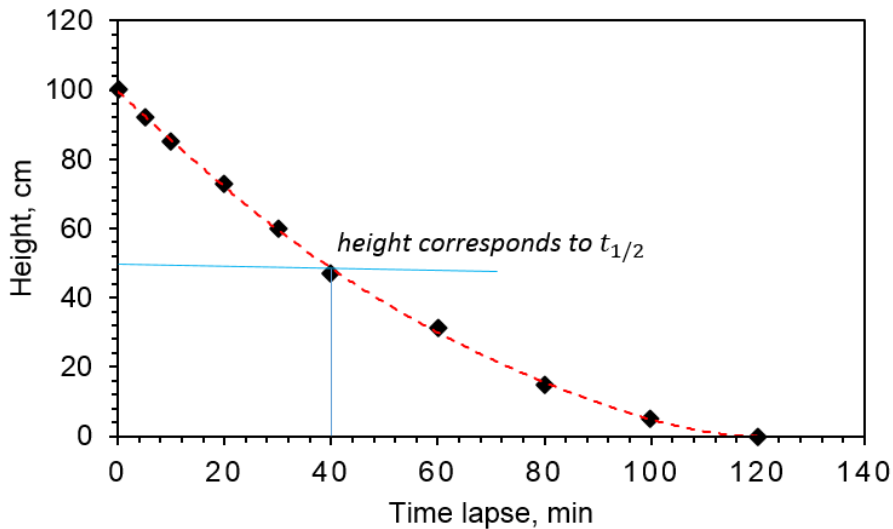


Figure 4-49: CO₂-foam height diagram formed by surfactant at CMC over time.

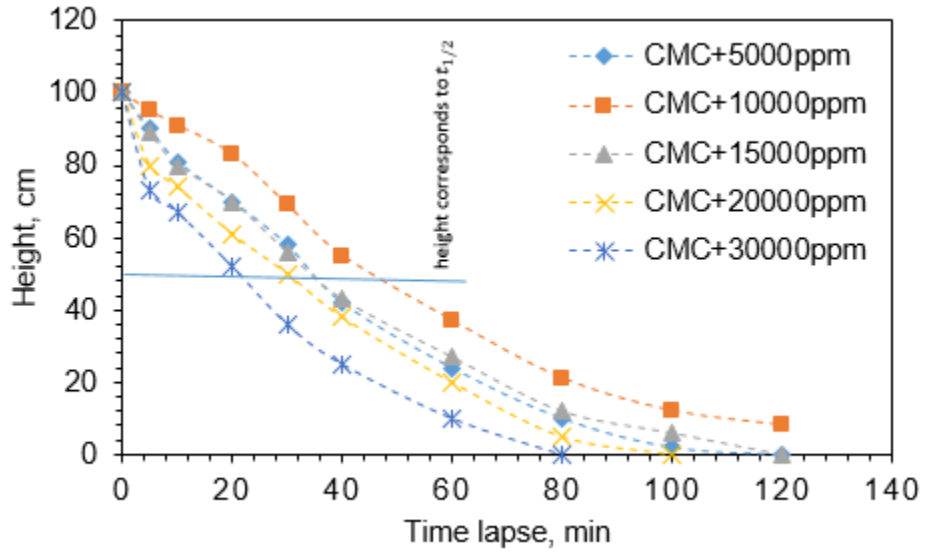


Figure 4-50: CO₂-foam height diagrams of surfactant solutions at CMC and different salinities resulting from FW dilution over time.

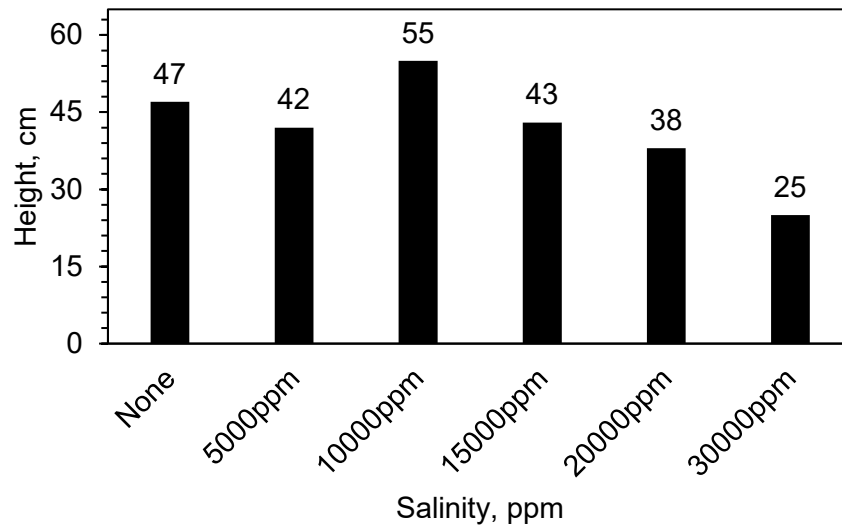


Figure 4-51: Comparison of CO₂-foam height of surfactant solutions at CMC and different salinities resulting from dilution of FW after 40 min.

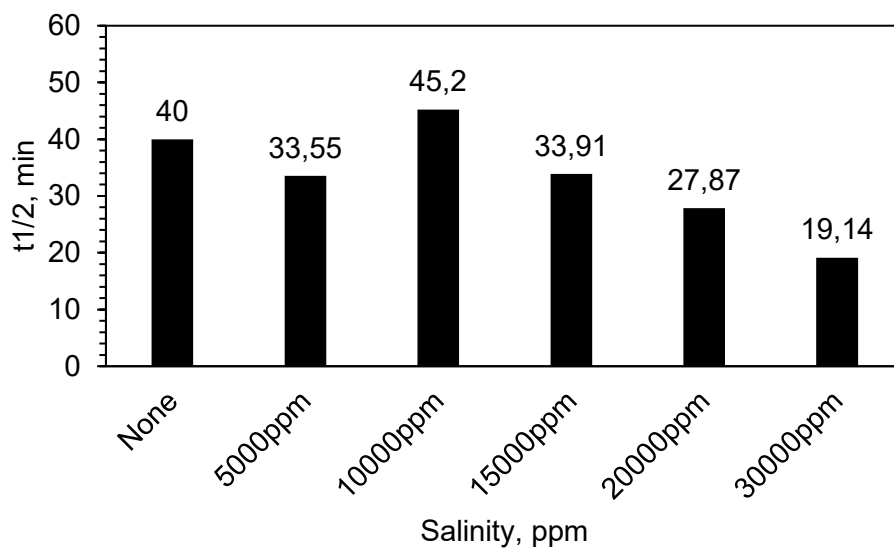


Figure 4-52: Comparison of CO₂-foam t_{1/2} formed by surfactant solutions at CMC and different salinities resulting from FW dilution.

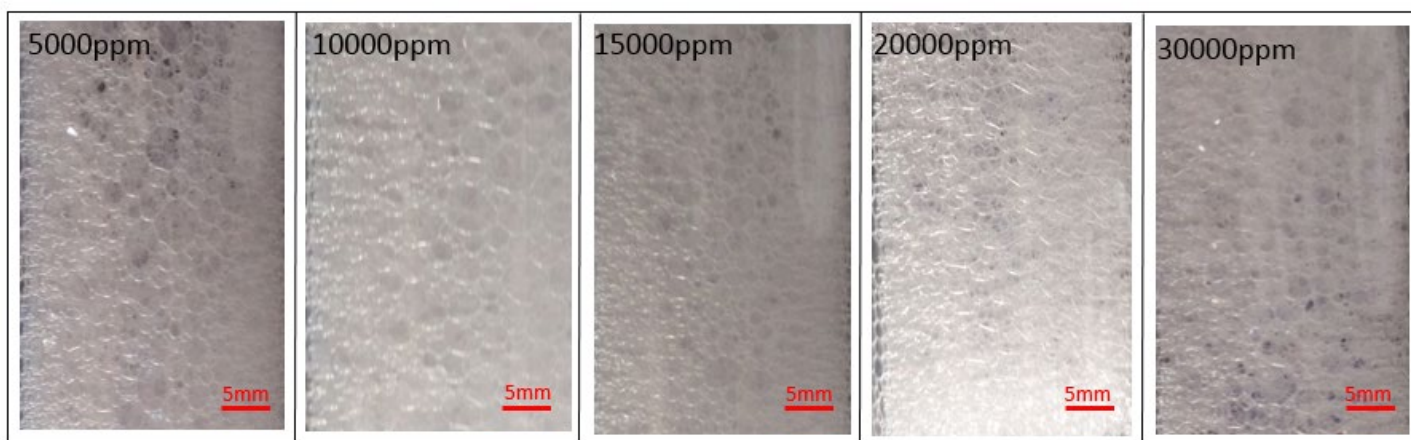


Figure 4-53: Effect of different salinities on bubble size in CO₂-foam formed by surfactant at CMC immediately after filling the CO₂-foam column at a gas flow rate equal to 20 ml/sec.

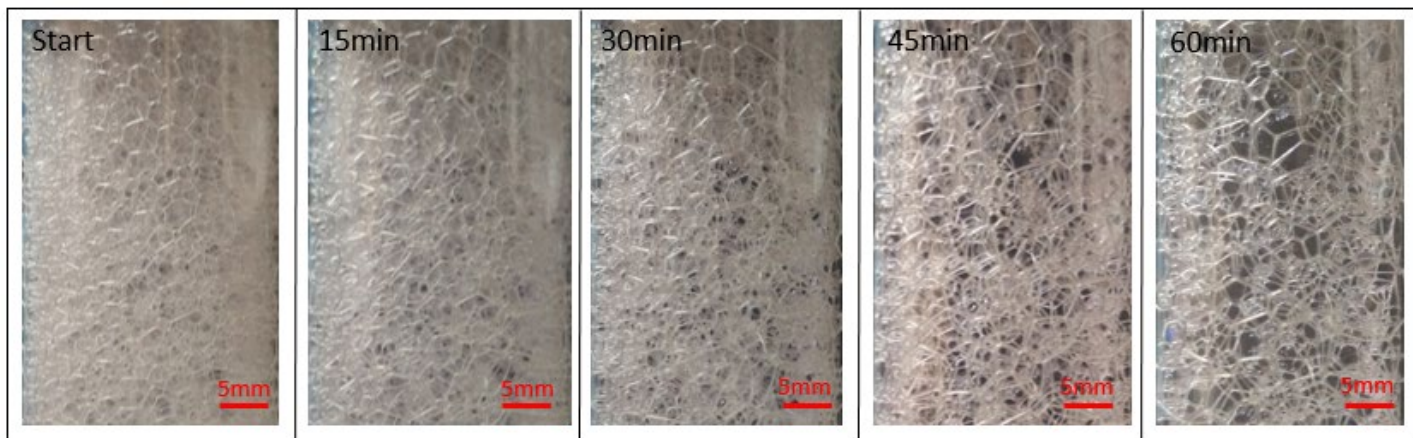


Figure 4-54: Effect of time passage on bubble size in CO₂-foam formed by surfactant at CMC, optimum salinity and gas flow rate equal to 20 ml/sec.

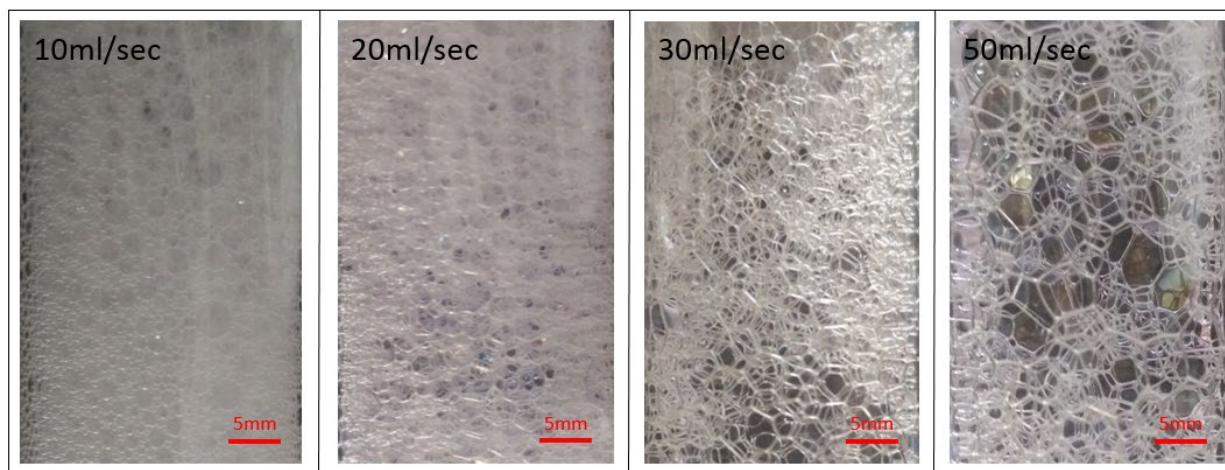


Figure 4-55: Effect of different gas flow rates on the size of bubbles in CO₂-foam formed by the surfactant at CMC immediately after filling the foam column.

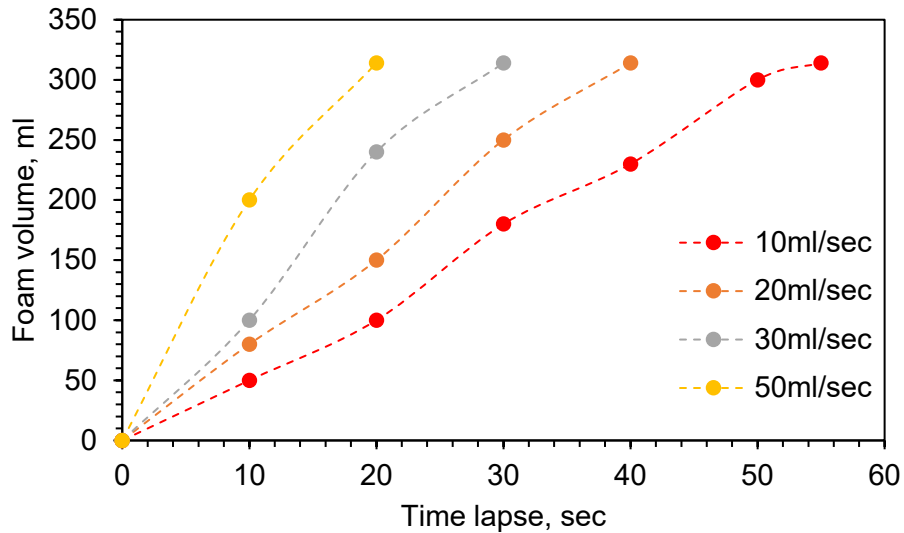


Figure 4-56: Effect of gas flow rate on the volume of CO₂-foam produced by the surfactant at CMC over time.

4.2.6. Oil recovery by secondary CO₂-foam flooding in a carbonate fractured plug

First, by measuring the weight of the dry sample and the water-saturated sample and calculating their difference and the density of the injected water, the effective pore volume was obtained equal to 20.51 cm³. Other specifications of the plug are length equivalent to 9 cm, initial water saturation equal to 4.51 cm³ and volume of primary in-situ oil equal to 16 cm³. Figure 4-57 shows the percentage of oil recovery against PV injection in secondary pre-generated CO₂-foam injection. According to Figure 4-57, oil production has stopped after injecting 2.8 PV foam into the plug. Finally, 66.79% recovery was achieved by secondary foam injection. The production mechanism in this system can be related to the deflection of the foam in the fractures and then its penetration into the matrixes. Also, during flooding and sampling of the outlet fluid, it was observed that after a while the outlet fluid comes out as a foam-emulsion. Foam-emulsion fluid leakage poses a challenge in measuring oil production. To measure the oil produced at each sampling step, as shown in Figure 4-58, the waiting time was used to remove the foam and separate the oil and aqueous phases from each other. Using methods such as adding emulsion breaker and centrifuge is another way to separate the oil and water phases from each other. In-situ emulsion breaks down large droplets of oil into smaller droplets and makes them easier to get out from pores. The formation of foam with oil may increase the viscosity and have a negative effect, although the injection fluid is also foam and the difference in viscosity is not as large as when the injection fluid is saline. On the other hand, because there is a CO₂ gas phase, it causes some CO₂ to dissolve in the oil. This dissolution of CO₂ in the oil reduces the viscosity and swells the oil, which may have offset the effect of increasing the viscosity by the formation of in-situ foam

with the oil. Figure 4-57 shows a slope difference. In such a way that the curve first has a steep slope and then decreases it. This change in the slope of the production curve may be caused by the initial emptying of the fractures and then the secondary emptying of the matrixes by the foam. Secondary flooding of saline water in the fractured reservoirs is not recommended due to its special conditions and gas injection is usually used in this type of reservoir. Flooding with saline water may change the wettability of the fractures and surround the matrix to water-wet so that the oil inside the matrix is trapped more than ever. The gas injection also has poor penetration efficiency in the matrix due to its very low viscosity. As a result, secondary injection of pre-generated foam instead of tertiary injection was recommended and used here.

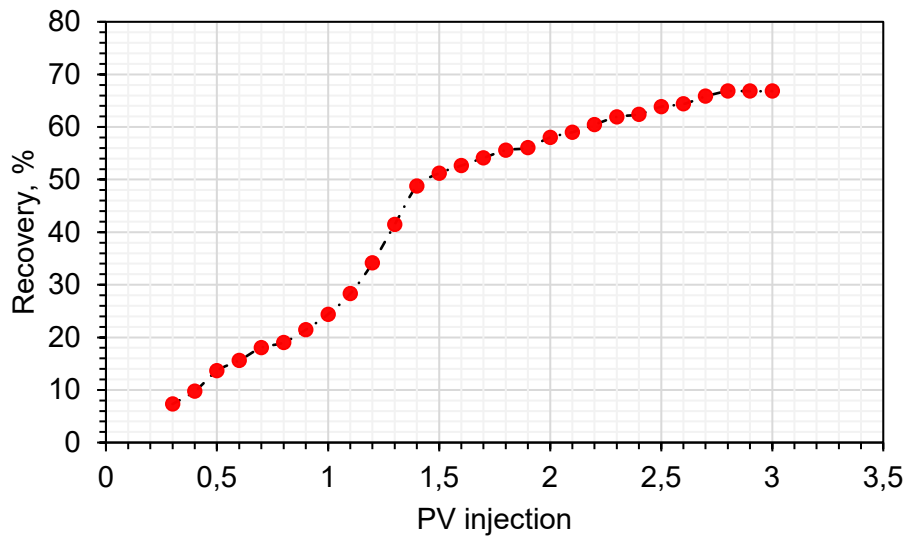


Figure 4-57: Oil recovery diagram of CO₂-foam secondary flooding.

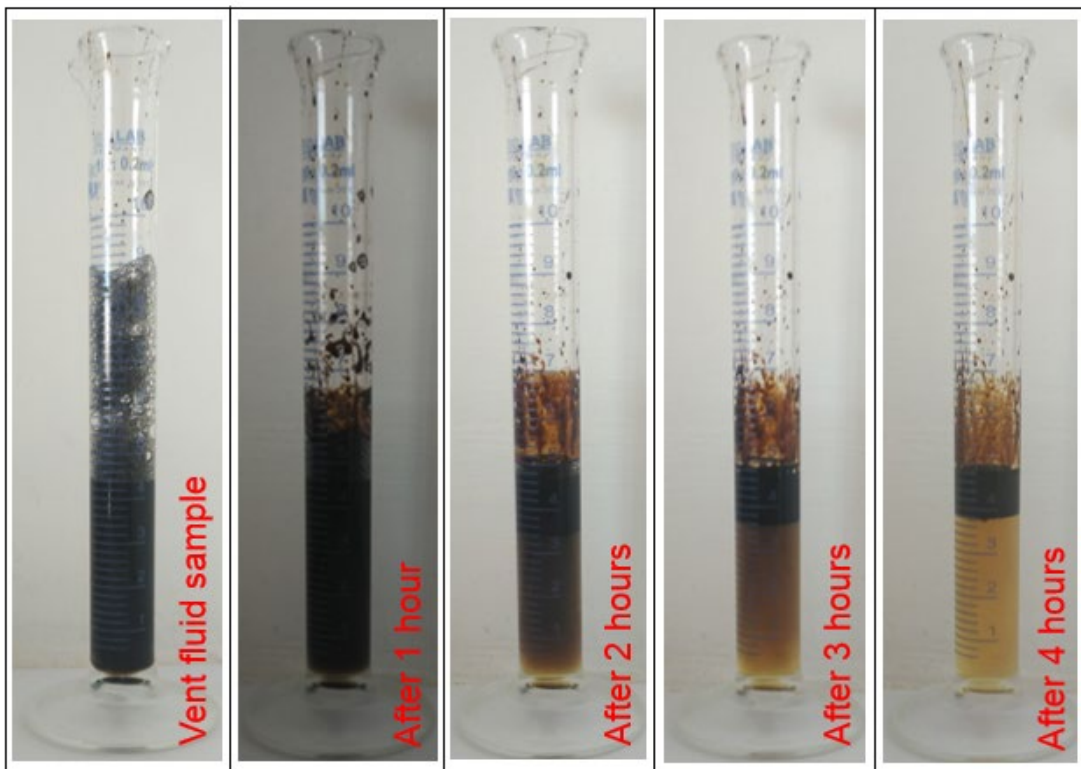


Figure 4-58: Flooding outlet fluid sample and measurement of oil production volume.

4.3. Modified saponin of *Anabasis Setifera* plant

4.3.1. FTIR, ¹H NMR and TGA analyses

According to Figure 4-59, the strong absorption between 1722 and 1657 cm^{-1} is consistent with the C=O stretching vibration band, which shows the formation of the ester bond in the improved surfactant [171].

Figure 4-60 shows the ¹H NMR analysis. Strong adsorption at 1.25 ppm related to -CH₂- was shown in Figure 4-60 [172]. As a result, the successful binding of the C12 alkyl link to the oligosaccharide portion of the extracted saponin from the *Anabasis* plant is confirmed.

The TGA analysis is shown in Figure 4-61. Based on the figure, a weight loss of about 48% occurs at 95-210 °C. Low weight loss after this temperature peak and considering the loss of sample moisture can result that the surfactant stability is suitable for the reservoir temperatures.

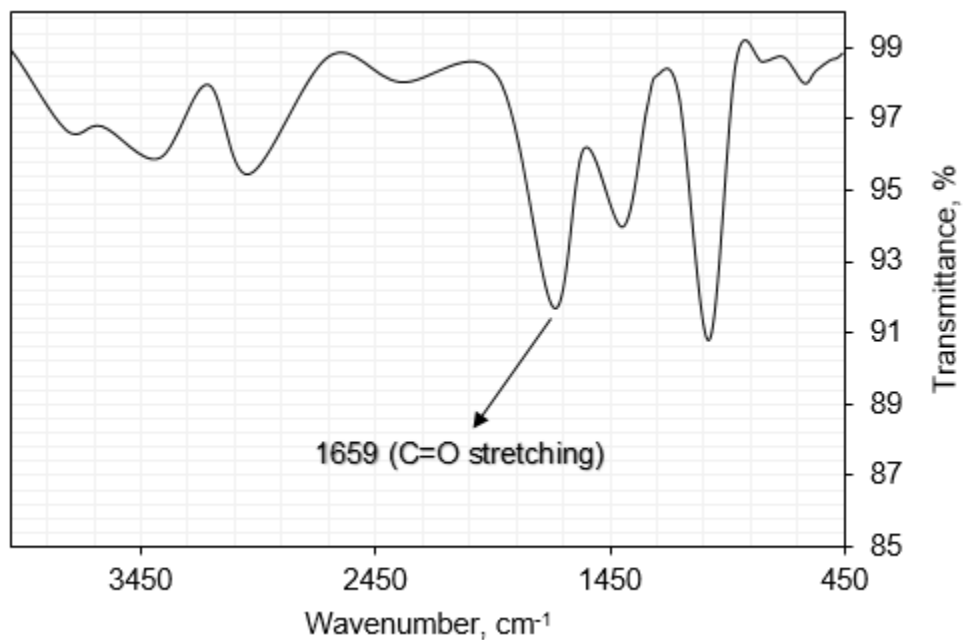


Figure 4-59: FTIR analysis of a: extracted saponin from *Anabasis Setifera* plant, b: modified surfactant.

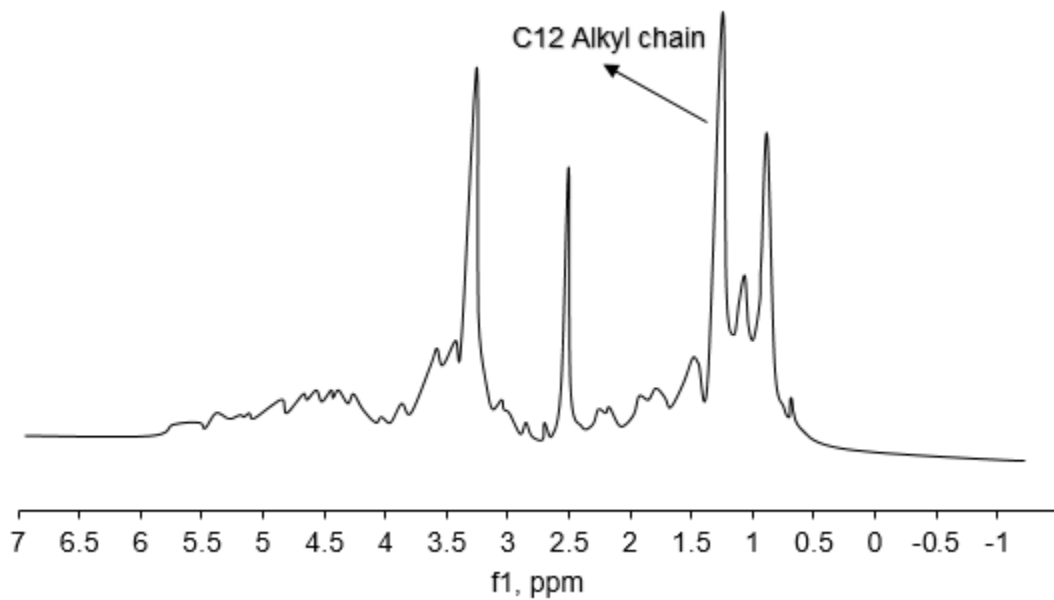


Figure 4-60: ¹H NMR analysis of modified surfactant.

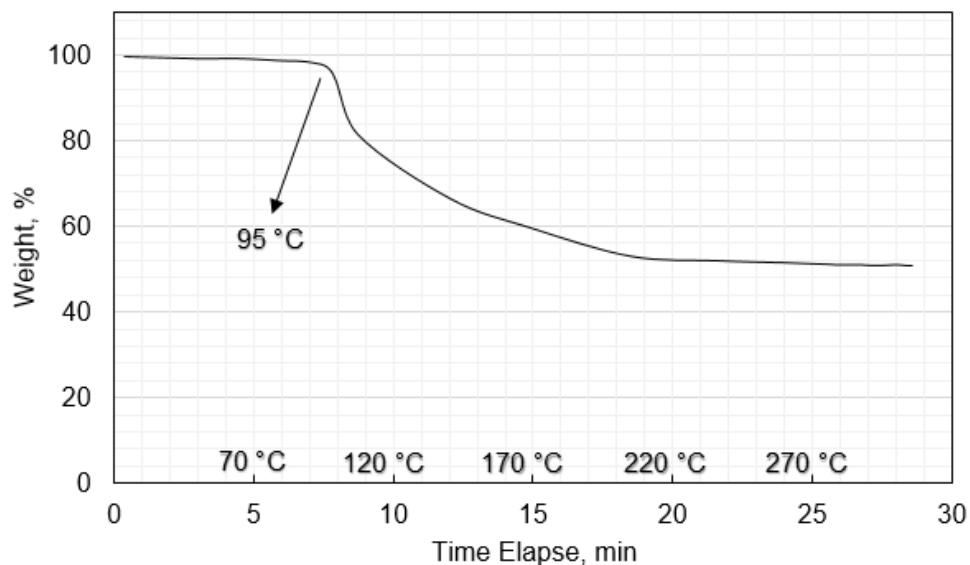


Figure 7: TGA Analysis of modified surfactant.

4.3.2. Surface tension

Figure 4-62 shows the surface tension of surfactant solutions at concentrations of 500, 1000, 2000, 3000, 4000, 5000 and 6000 ppm at temperatures of 35, 55 and 75 °C. Surface tension values decrease with increasing concentrations up to a certain concentration with steep gradients and then there is not much change in the process of decreasing or increasing surface tension. The particular concentration is defined as the critical micelle concentration (CMC). By comparing the curves for each temperature, we find that the CMC varies at different temperatures and increased with increasing temperature. As CMCs are 2000, 3000 and 4000 ppm at temperatures of 35, 55 and 75 °C, respectively. Also, the surface tensions decreased with increasing temperature. For example, surface tension values in CMC of surfactant at 35, 55 and 75 °C are 45.29, 35.12 and 29.07 mN/m, and at a specific concentration of 3000 ppm, are 44.69, 35.12 and 32.152 mN/m, respectively. This process can be justified by the breakdown of hydrogen bonds at higher temperatures that make the surfactant molecules more hydrophilic. For values above CMC, when the temperature rises, there is a small increased surface tension caused by reduced polar groups hydration. These polar groups help micellization. Also, the high temperature breaks the structure of water around the alkyl group and reduces micellization and increases surface tensions [173].

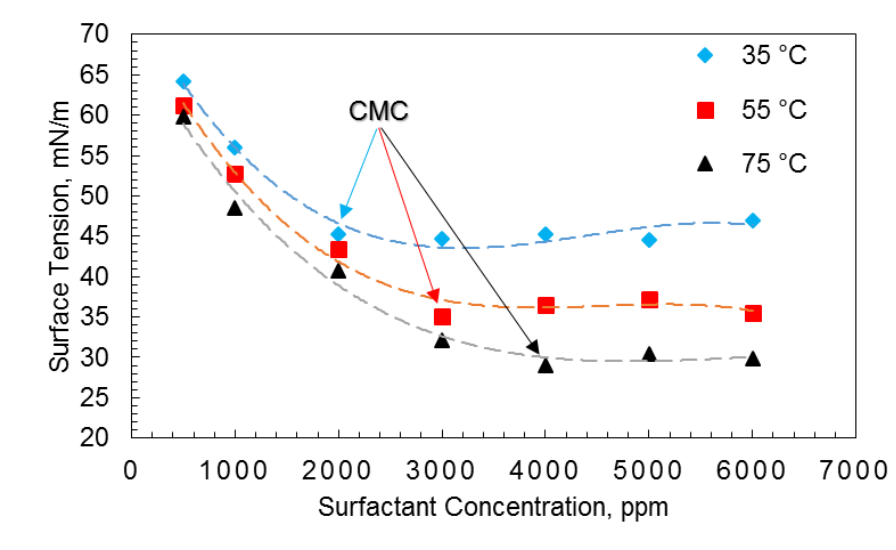


Figure 4-62: Surface tension of surfactant solutions at different concentrations and temperatures of 35, 55 and 75 °C.

4.3.3. Water-oil interfacial tension results

The IFT experiments results are plotted in Figure 4-63. Table 4-11 and Figure 4-64 show the effect of different salinity of salts and formation water. Figure 4-65 shows the effect of Na_2CO_3 alkali on IFT at the CMC. The resembling trend with Figure 4-62 is observed for the IFT results in Figure 4-63. At 75 °C, the interfacial tension decreases with increasing surfactant concentration and a fast fall of the IFT to CMC (3.6×10^{-2} mN/m) occurs. The IFTs at concentrations of 500, 1000, 2000, 3000, 4000, 5000 and 6000 ppm were obtained 2.019, 1.607, 1.178, 0.741, 0.036, 0.046 and 0.040 mN/m, respectively. The salinities also effects on IFT of oil and surfactant solution at CMC but an optimum concentration proportional to the type of salinity was obtained. According to Figure 4-64, the IFTs of surfactant solution at CMC and optimal salinities are as follows: FW, at concentration of 10000 ppm, 0.027 mN/m, NaCl, at concentration of 15000ppm, 0.032 mN/m, KCl, at concentration of 10000 ppm, 0.035 mN/m, CaCl_2 , at concentration of 15000ppm, 0.030 mN/m, MgCl_2 , at concentration of 15000 ppm, 0.034 mN/m, FeSO_4 , at concentration of 10000ppm, 0.033 mN/m, K_2SO_4 , at concentration of 15000ppm, 0.033 mN/m, NaHCO_3 , at concentration of 15000 ppm, 0.026 mN/m. When alkali is added to the surfactant, the IFT values are further reduced and we saw the highest reduction in a concentration. The IFT was found to be 0.030, 0.026, 0.024, 0.025, 0.029 and 0.033 mN/m at alkali concentrations of 1000, 1500, 2000, 2500, 3000 and 4000 ppm, respectively (Figure 4-65). In the ionic solutions, the IFT changes also depend on the ions adsorption at the water-oil interface caused by the polar compounds of crude oil such as asphaltenes. The ions released from the dissolution of the salt Show a different behavior in IFT. The behaviors depend on the type and nature of the

ion. The ions nature against the oil compounds results in different behavior in IFT. Based on the literature, the affinity of Mg^{2+} for the molecules of resin is more than Ca^{2+} , whereas the Ca^{2+} affinity for asphaltene is more than Mg^{2+} and Ca^{2+} possess more affinity towards the resin in the presence of Cl^- than SO_4^{2-} [135, 158, 174]. On the other hand, the smaller IFT occurs at lower concentrations caused by the salt-in effect. The salt-in effect is a phenomenon that at low ionic strengths increases the solubility of organic solutes in electrolyte solutions. That is, in the case of salt-in, organic particles tend to dissolve in water. In the other words, nonorganic ions break down the structure of the water created around organic molecules and thus increase the solubility of organic molecules in the aqueous phase. It can be said that the effect of salt-in releases the active components of the surface from the solvent at low salt concentration. In other words, in low salinity, the crude oil hydrocarbons solubility increases in the aqueous bulk [159, 160, 161, 121]. When surfactant molecules are present in the system, molecules are located at the water-oil interface. As a result, a thin film of the molecules is formed in the interface, resulting in less IFT than the previous one. In the presence of alkali, an electrolyte is created and salinity is increased. Adding alkali to the surfactant solution reduces the IFT more than the surfactant alone. This behavior can be related to the carboxylic acid ionization with alkali [175, 121]. Also, the reaction between the alkali and the acid compounds in the crude oil generate a kind of "natural surfactants" and this reduces the IFT [121, 176].

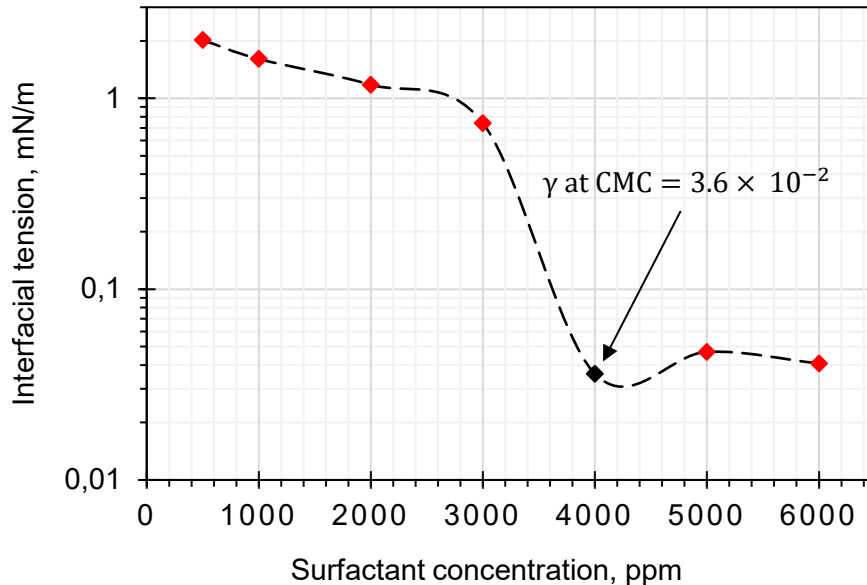


Figure 4-63: IFT values of surfactant solutions at various concentrations and crude oil at 75 °C.

Table 4-11: Effects of different salinities on interfacial tension of surfactant solution at CMC and crude oil at 75 °C.

Brine conc. [ppm]	IFT [mN/m]					
	5000	10000	15000	20000	25000	30000
FW	0.033	0.027	0.031	0.035	0.040	0.043
NaCl	0.038	0.034	0.032	0.036	0.041	0.044
KCl	0.039	0.035	0.037	0.040	0.042	0.051
CaCl ₂	0.035	0.032	0.030	0.033	0.037	0.041
MgCl ₂	0.037	0.036	0.034	0.037	0.045	0.047
FeSO ₄	0.034	0.033	0.035	0.039	0.043	0.045
K ₂ SO ₄	0.031	0.029	0.033	0.038	0.039	0.042
NaHCO ₃	0.030	0.027	0.026	0.028	0.031	0.034

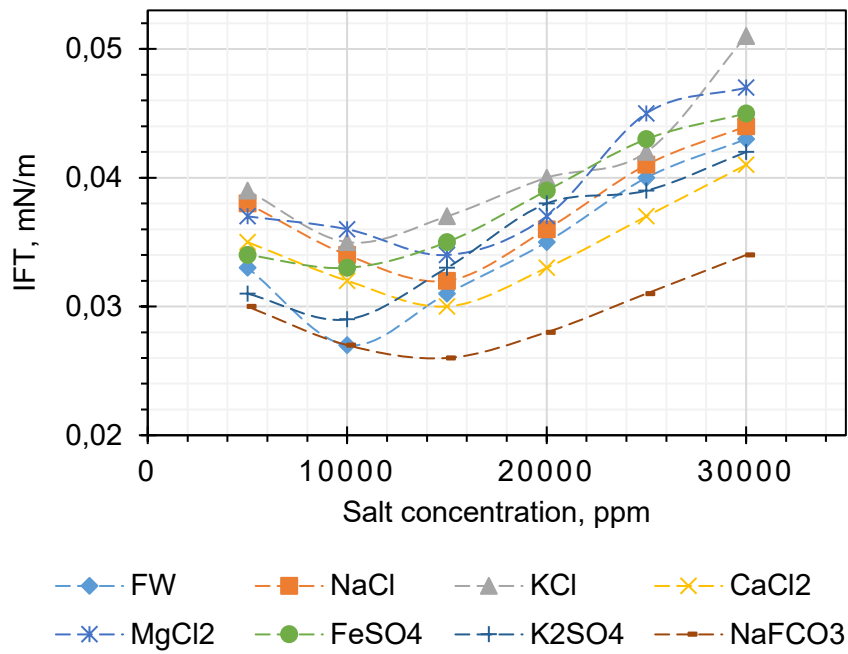


Figure 4-64: Effects of different salinity on IFT at CMC of surfactant and crude oil at 75 °C.

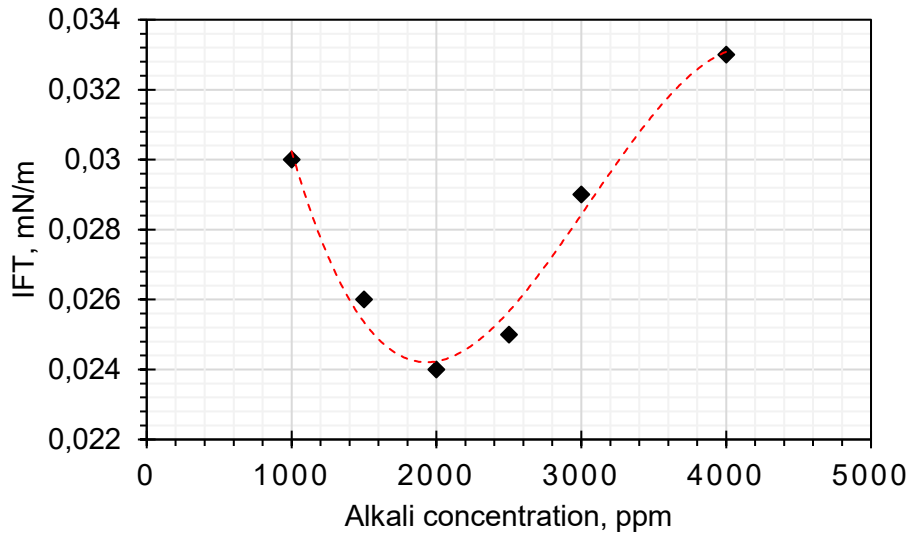


Figure 4-65: Effect of Na_2CO_3 alkali at different concentrations on IFT at CMC of surfactant and crude oil at 75 °C.

4.3.4. Contact angle experiments results

Table 4-12 and Figure 4-66 show the results of the contact angle experiments of an oil droplet on the oil-wet carbonate section in the presence of a surfactant solution at CMC relative to time and Figure 4-67 shows the effect of different salinity on the final contact angle values. Accordingly, the average angle of the oil drop and thin section at the beginning of the test was 130.8 degrees. With elapsing of time at 30, 60 and 90min, the contact angle was 103.65, 90.55, and 86.1degrees, respectively. By comparing the final and initial contact angle, we see that after 90min the wettability of the section altered to intermediate-wet. The trend of wettability alteration can be seen more clearly in Figure 4-68. As can be seen, the surface of the oil spill on the carbonate surface in the solution of surfactant at CMC decreases continuously over time. Figure 4-68, which is the result of the observational wettability test, has no numerical value and is performed merely to better represent the rock wettability change by surfactant. With the presence of various types of salinity in the system, as shown in Figure 4-67, the final contact angle reached a minimum at a salinity. The average contact angles for the optimum concentrations were as follows: FW, concentration of 10000 ppm, 80.50°, NaCl, 10000 ppm, 83.07°, KCl, 10000 ppm, 85.56°, CaCl_2 , 15000 ppm, 79.76°, MgCl_2 , 15000 ppm, 78.15°, FeSO_4 , 15000 ppm, 74.63°, K_2SO_4 , 15000 ppm, 74.63°, NaHCO_3 , 10000 ppm, 76.54°. The extra contact angle reduction in different salinities, as compared with when surfactant alone exists in the system, can be justified via the above explanation and because of the low impact of ions on the nonionic surfactant,

the surfactant and ions mechanisms each contribute more to their synergistic effect on the wettability alteration.

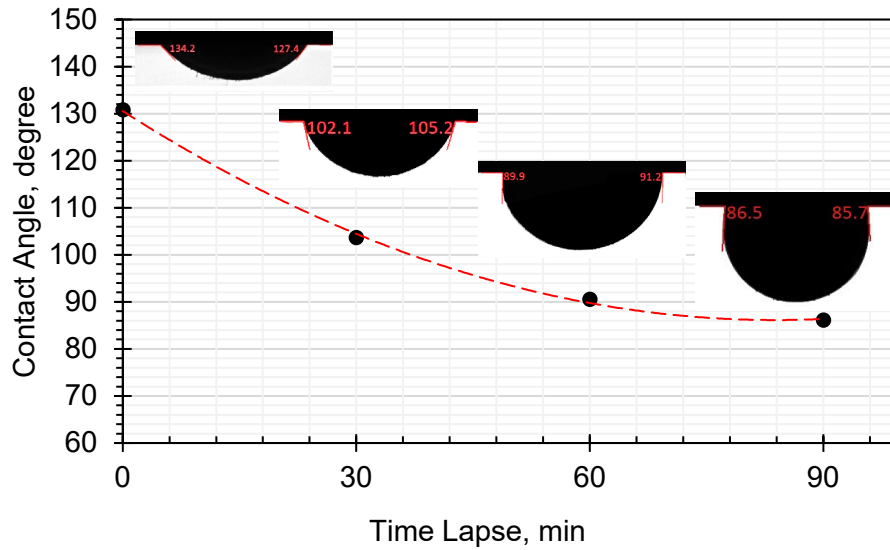


Figure 4-66: The contact angle of the oil droplet at the carbonate section against time in the presence of a surfactant solution at CMC and a temperature of 75 °C.

Table 4-12: Effects of different salinities on contact angle in the presence of the surfactant solution at CMC at 75 °C.

Brine conc. [ppm]	CA [Degree]					
	5000	10000	15000	20000	25000	30000
FW	83.27	80.50	84.64	86.56	89.95	91.07
NaCl	84.45	83.07	86.36	88.09	92.40	93.16
KCl	86.50	85.56	89.03	91.80	95.29	97.56
CaCl ₂	85.64	82.49	79.76	83.43	87.35	90.68
MgCl ₂	82.12	80.97	78.15	81.50	84.17	89.53
FeSO ₄	81.23	77.91	75.02	79.77	83.04	85.33
K ₂ SO ₄	79.19	78.22	74.63	76.69	79.81	83.17
NaHCO ₃	80.78	76.54	77.14	81.21	84.10	86.20

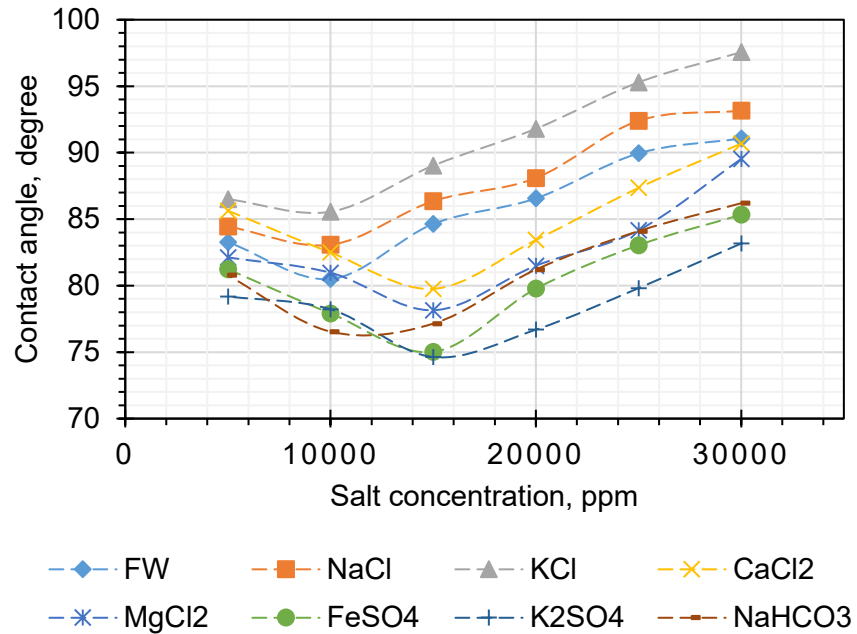


Figure 4-67: Different salinity effects on contact angle at CMC of surfactant and 75 °C.

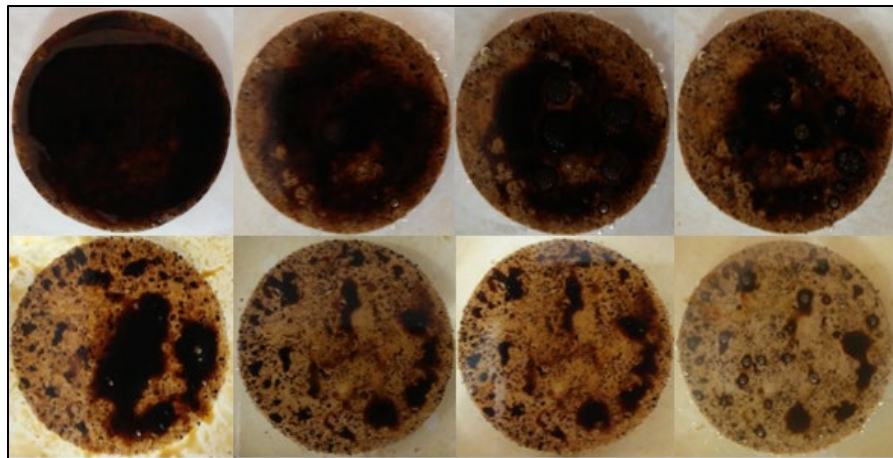


Figure 4-68: Observational wettability alteration, reduction of area of oil spill on a carbonate section in the presence of surfactant solution at CMC and optimum salinity over time.

4.3.5. Oil recovery by Surfactant-alkali injection

Figure 4-69 shows the oil recovery and pressure changes during the secondary and tertiary injections. The used carbonate plug in the flooding process had a length of 7cm, a diameter of 1.5in, a porosity of 19.6%,

a pore volume of 15.63 cm³, and a permeability of 8.71 mD. The initial water saturation and the initial OOIP were 18% and 12.8 cm³, respectively. The oil recovery was increased by 51.5% in the secondary injection of brine (1.5 PV). After 1.1 PV, the oil production was fixed. Then a 0.5PV of the surfactant-alkali slug was injected and after that brine injection was continued. Finally, a 70.9% increased oil recovery was achieved which 19.1% of that was resulted by the tertiary flooding. Oil production in the tertiary stage was started after injection of the total volume of slug and brine afterward, equaled 1.7PV, ie 0.2PV injection of surfactant-alkali injection and ended with a total volume of 3.5PV of injecting fluids. Oil recovery in secondary brine injection is a kind of sweeping mechanism. However, some of it is linked to wettability alteration by soluble ions. But in the injection of surfactant-alkali, both mechanisms of IFT reduction and wettability alteration increase the recovery after brine injection.

As indicated, the change in wettability is achieved by the surfactant to an intermediate wettability. It is generally accepted that in the surfactant injection, the change in wettability to the intermediate wettability has the highest recovery [177]. Two important mechanisms of the stability of the formed thin film and orientation of the surfactant molecules contribute to the formation of the intermediate wettability [178, 179]. With the stable thin film, the oil-like bullets spread in the central larger pores and the water extends between rock and oil. But in the presence of surfactant molecules, the thin film is unstable via their absorption on the surface of the rock. However, the instability of the thin film in the interface creates a continuous route for oil movement. This is due to the intermediate wettability of rock [177]. In other words, the continuous penetration and the surfactant molecules absorption in the system altered the rock properties, resulting in a linkage pathway for the production of oil on the rock, leading to an increase in production [177, 178, 180].

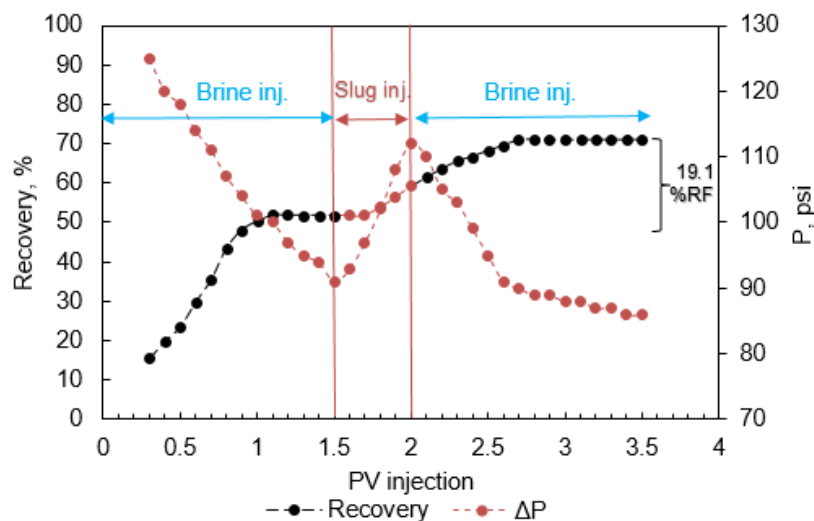


Figure 4-69: Recovery factor curve of the surfactant-alkali slug injection.

4.4. Extracted saponin from *Soapwort* plant

4.4.1. Surfactant characterization

FTIR analysis was used to define the functional groups in the molecular structure of the surfactant extracted from the *Soapwort* plant. Peaks at 3412 cm^{-1} , 2936 cm^{-1} , 1731 cm^{-1} , 1610 cm^{-1} represent the $-\text{OH}$, C-H, C=O and C=C bonds, respectively and peak at 1046 cm^{-1} indicates Oligosaccharide linkage absorptions to sapogenins. The links to the peaks shown in Figure 4-70 indicate the functional groups in the saponin structure. The general molecular structure of saponins is shown in Figure 4-71. The dual structure of the hydrophilic head and hydrophobic tail of saponin and the bond between the two are specified in this figure.

Figure 4-72 shows the ^1H NMR of the surfactant. Chemical shifts in the 2.68-5.27 ppm show mainly protons in the oligosaccharide while chemical changes at 0.70-2.34 ppm are mainly related to protons in the aglycone part of saponin [155].

The thermal properties of the surfactant were analyzed by TGA. Figure 4-73 shows this analysis for the surfactant. A weight-loss peak from the initial temperatures to $123\text{ }^\circ\text{C}$ shows only a 10% change in weight. Considering the initial moisture of the surfactant sample and its evaporation in the temperature range of the first peak, it can be concluded that the structure of the surfactant will be preserved until the end of this peak. The weight change of the surfactant at $300\text{ }^\circ\text{C}$ eventually reaches 43%, which is probably 33% due to the destruction of the molecular structure of the surfactant.

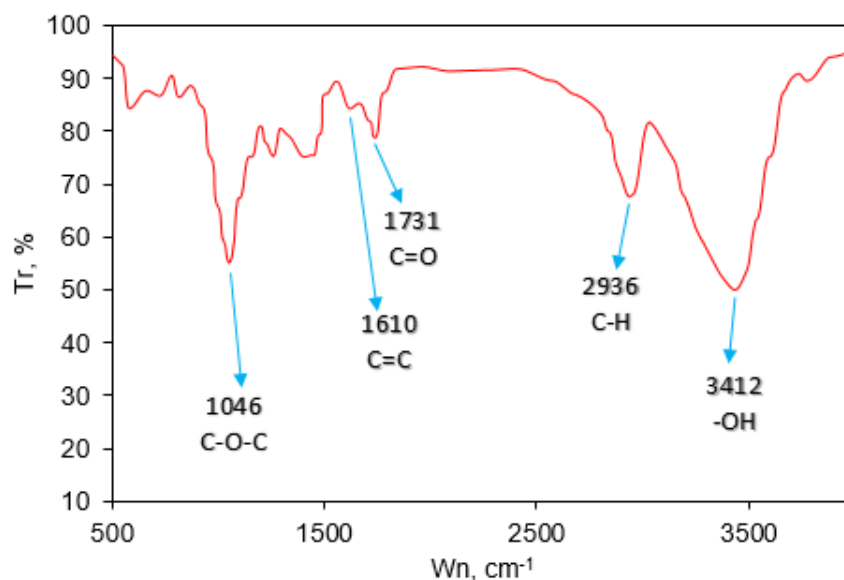


Figure 4-70: FTIR analysis of the surfactant extracted from the *Soapwort* plant extract.

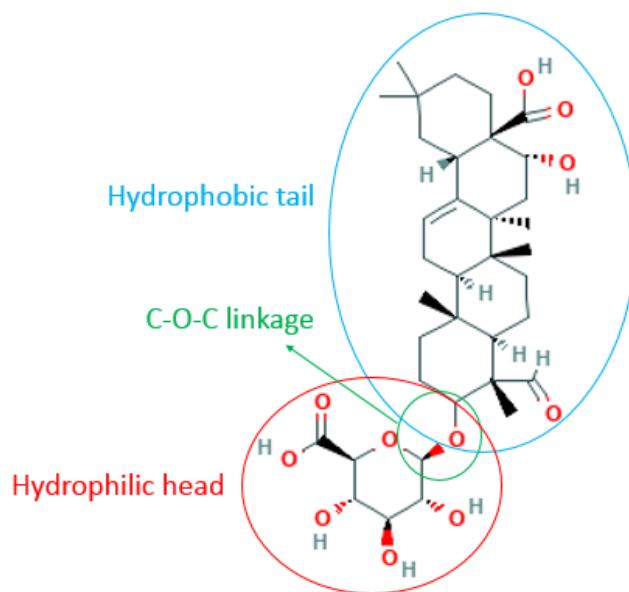


Figure 4-71: The molecular structure of saponins.

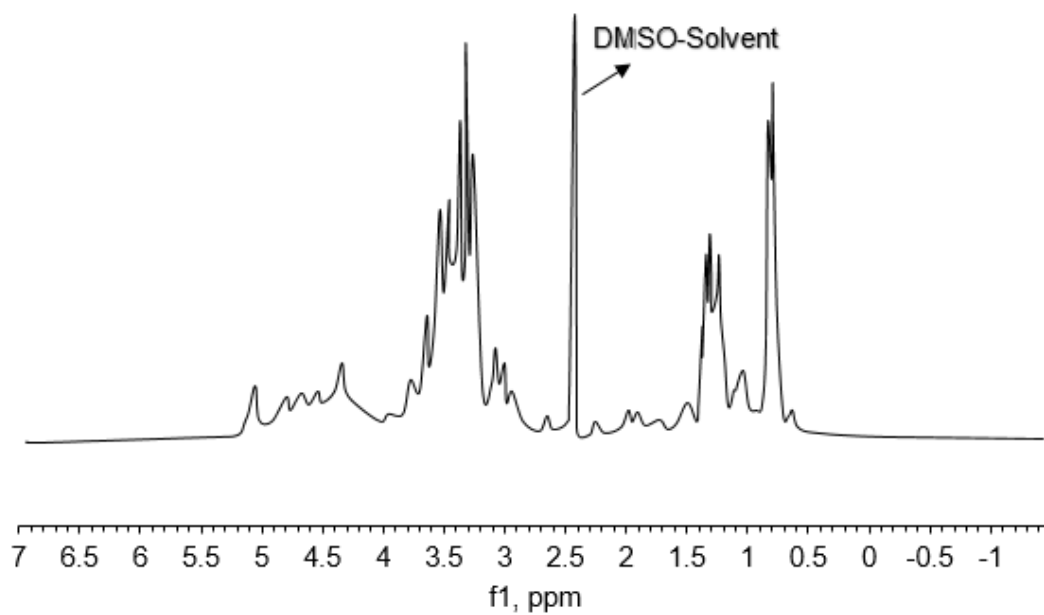


Figure 4-72. ¹H NMR analysis of the *Soapwort* saponin.

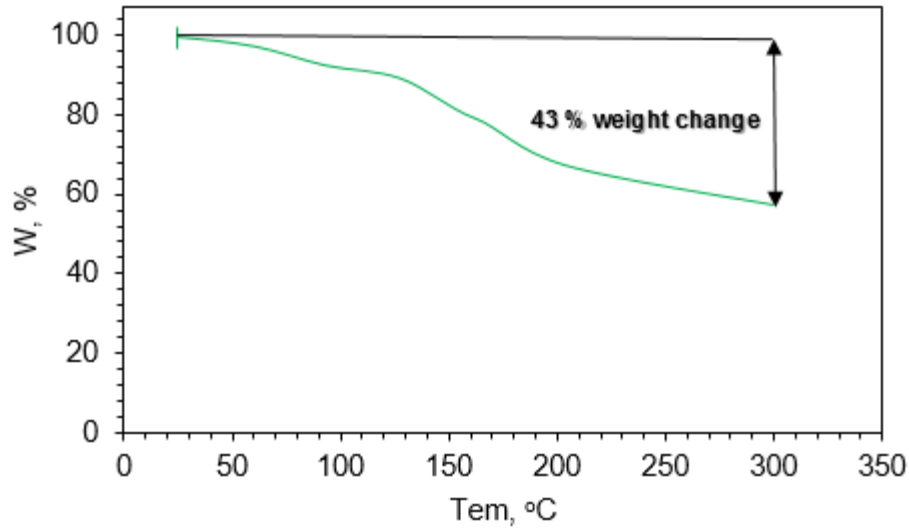


Figure 4-73: TGA analysis of the surfactant extracted from the *Soapwort* plant.

4.4.2. Surface tension and foaming behaviors of the surfactant

The pendant drop surface tension experiments are commonly used to estimate CMC. Figure 4-47 shows the surface tension values of the surfactant solutions at different concentrations and 80 °C obtained from these experiments. The curve of the surface tension values against the surfactant concentration at constant temperature decreases sharply to the CMC and then shows minor changes. Based on this, the CMC of the surfactant was 2250 ppm. The formation of micelles at low concentrations is economically important because CMC is the concentration at which the surfactant performs best in terms of surface activity, and this concentration is used for subsequent decisions in the use of surfactants in EOR. As a result, higher CMCs represent more surfactant consumption and higher costs.

To check the stability of the foam over time, the half-decay time parameter of the foam ($t_{1/2}$) is calculated. Figure 4-75 shows the results of the stability of the foam formed by the surfactant at CMC over time, and Figure 4-76 shows these results as a diagram. Based on Figure 4-76, $t_{1/2}$ equals 5.6 min. However, the entire foam disintegrated after 14 min. It should be noted that the initial level of the surfactant solution (5ml) was considered as the base level.

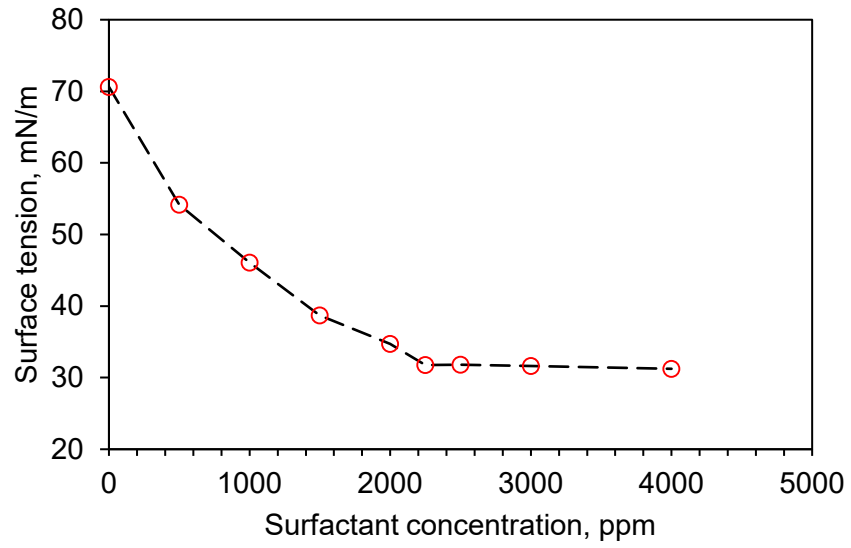


Figure 4-74: Surface tension diagram of surfactant solutions at different concentrations at 80 °C.

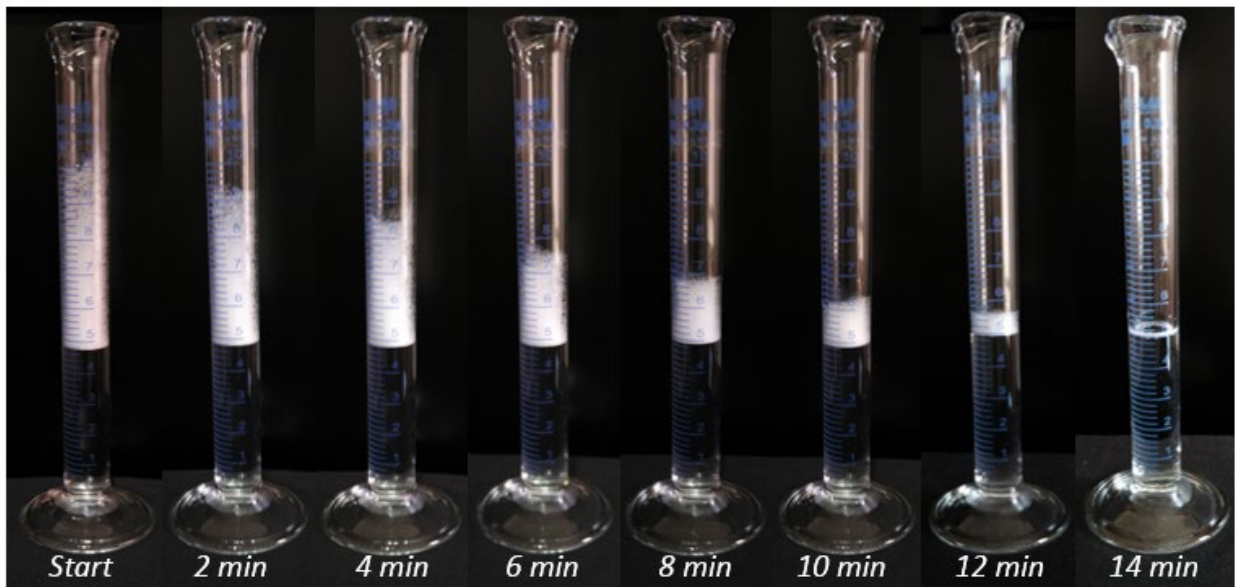


Figure 4-75: Results of the stability of the foam produced by surfactant solution at CMC over time.

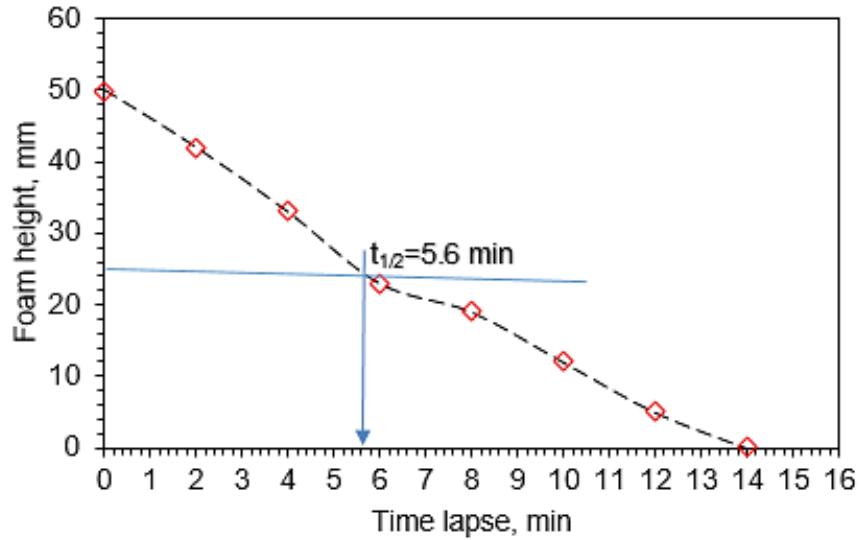


Figure 4-76: The height graph of the foam produced by the surfactant solution at CMC over time.

4.4.3. Water-oil IFT

Changing the water-oil IFT in the process of surfactant and chemical solution flooding directly affects the capillary pressure, and reducing it to appropriate values can improve oil recovery. Figure 4-77 shows the values of the water-oil IFT at different concentrations of the surfactant. The IFT values at concentrations of 750, 1250, 1750, 2250, 2750, 3250 and 3750 ppm were 10.275, 7.536, 3.947, 0.834, 0.852, 0.816 and 0.807 mN/m, respectively. As the trends of the water-oil IFT and the water-air surface tension are similar, their mechanism is the same, with the exception that the thin film composed of surfactant molecules in surface tension tests is formed in the water-air interface, but in the water-oil IFT tests this film is formed in the water-oil interface. The surfactant solution is never injected into the reservoirs with distilled water-based fluid. This means that the injection fluid must be engineered in advance. The engineering of the injectable fluid containing surfactant depends on many issues, such as water resources available for injection into the reservoir. In setting the concentration of the base fluid additives, an optimal salinity is generally considered for surfactant flooding and an optimal salinity and alkalinity for surfactant-alkali and ASP injection are considered. Therefore, it is necessary to investigate the effect of salinity and alkalinity on the IFT. By selecting CMC as the optimal concentration of the surfactant, the concentrations of salt and then alkali are considered variables. Table 4-13 shows the IFT values in the presence of different salinities and alkalis. Figure 4-78 shows the effect of different salinities resulting from the dilution of formation water and the dissolution of NaCl and MgCl₂ salts. As can be seen, the IFT was variable in the presence of different salinities. Examining the trend of the graphs shows that the IFT in the lower salinities has reached lower values. At least two other mechanisms in the presence of soluble ions are effective in reducing IFT. One of

these mechanisms is the pairing of ions with polar oil components such as asphaltene and resin at the interface [158]. The absorption of ions in the interface by oil-polar components, just like surfactants, creates a thin film. When surfactants and ions are both present in the system, the mechanism of ions strengthens the thin film in the interface [88, 157, 181]. As the surfactant molecules cover the interface, a thin film of ions is formed at a certain concentration with the full capacity of the interface. As a result, the IFT is minimized at optimal salinity. The tendency to pair with polar molecules is not the same in different ions so different salinities have different effects on the amount of the IFT [158, 135]. Another mechanism called the salting-in effect causes optimal salinity to occur at lower concentrations. The salting-in effect causes the solubility of organic components in water to increase in low salinity, thus the IFT is reduced but in high salinity, the salting-out effect, which is the opposite of salting-in, is the predominant mechanism [159, 160]. According to Figure 4-78, the IFT at the optimal salinity of the formation water was 0.541 mN/m, at the optimal salinity of $MgCl_2$ was 0.714 mN/m and the optimal salinity of $NaCl$ was 0.775 mN/m. Alkalis behave similarly to salts, both altering IFT and increasing electrolytes [175]. Alkalis reduce IFT more than when there is the only surfactant in the system. Figure 4-79 shows the effect of different alkalis on the IFT at the CMC of the surfactant. It is generally accepted that the reduction of IFT by alkalis is due to the production of in-situ petroleum soap, resulting in alkali reaction and acidic components of the oil in the interface [121]. Therefore, the optimal amount of IFT in the presence of alkali depends on the alkaline strength of the solution and the number of acidic components in crude oil. According to Figure 4-79, the amount of the IFT at the optimal $NaOH$ concentration was 0.047 mN/m, at the optimal Na_2CO_3 concentration was 0.78 mN/m and at the optimal $NaHCO_3$ concentration was 0.096 mN/m.

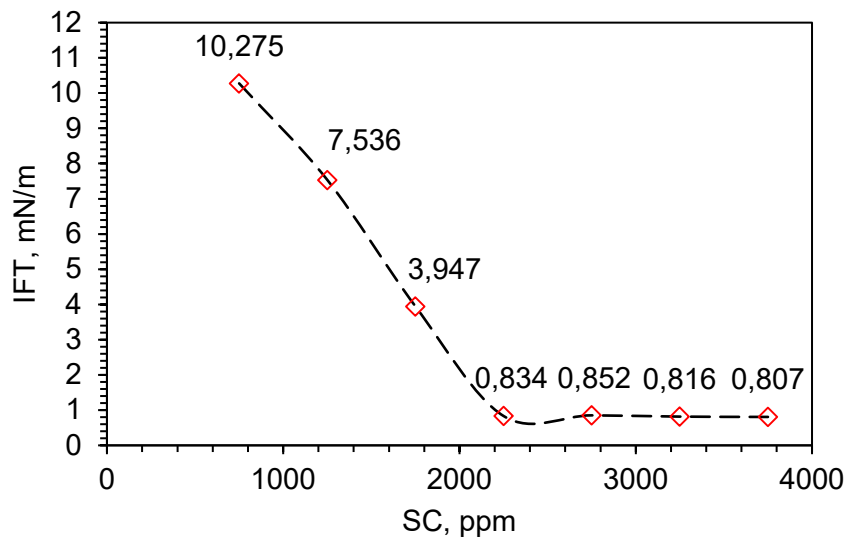


Figure 4-77: IFT diagram of the surfactant solutions at different concentrations and crude oil at 80 °C.

Table 4-13: The IFT values of the surfactant solutions at CMC in the presence of various salinities and alkalis at 80 °C.

Brine concentration, ppm	IFT, mN/m			Alkali concentration, ppm	IFT, mN/m		
	FW	NaCl	MgCl ₂		NaHCO ₃	Na ₂ CO ₃	NaOH
5000	0.726	0.829	0.806	500	0.563	0.255	0.119
10000	0.541	0.775	0.739	1500	0.359	0.142	0.047
15000	0.613	0.848	0.714	2000	0.125	0.078	0.051
20000	0.759	0.973	0.821	2500	0.096	0.084	0.072
30000	0.886	1.194	0.957	3000	0.106	0.093	0.08
40000	0.905	1.256	1.036	4000	0.268	0.175	0.095
				5000	0.418	0.392	0.194

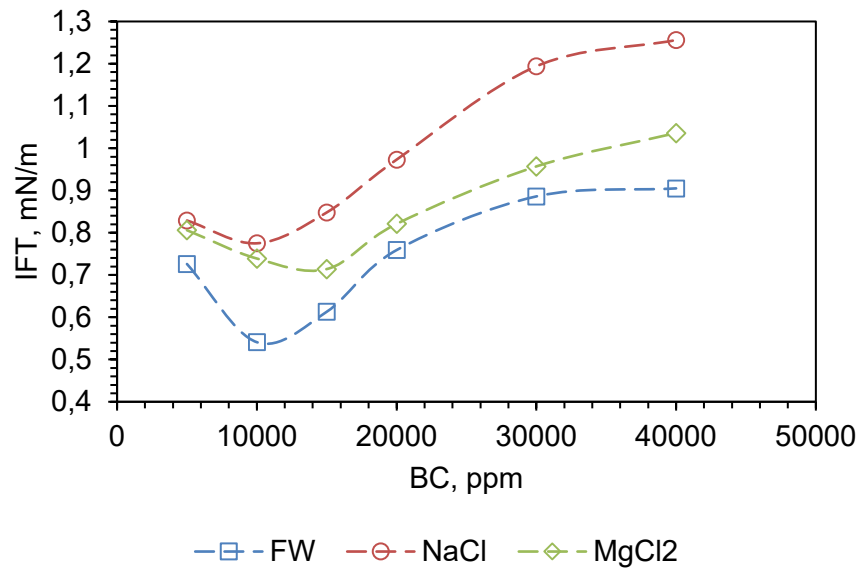


Figure 4-78: Diagram of the effect of different salinities on the IFT of the surfactant solution at CMC and crude oil at 80 °C.

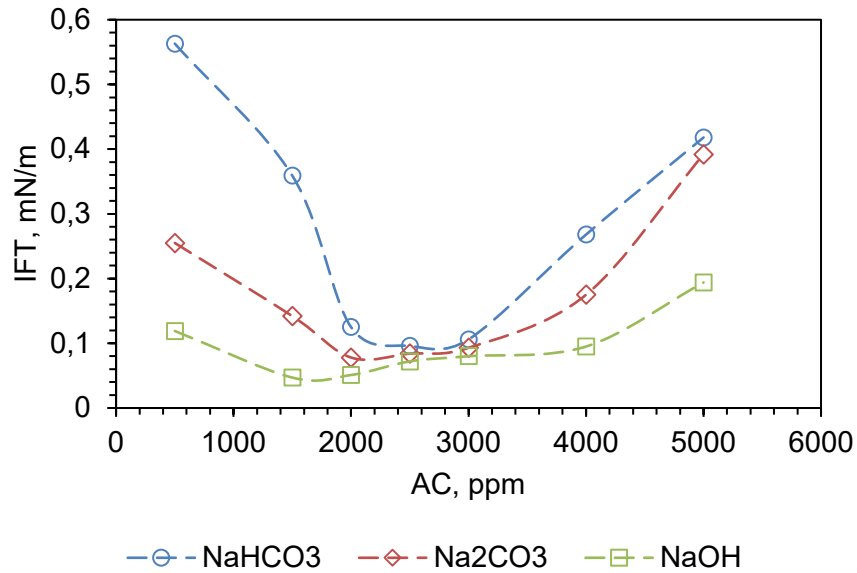


Figure 4-79: The effect of different alkalis on the IFT of the surfactant solution at CMC and crude oil at 80 °C.

4.4.4. Sandstone wettability alteration

Rock wettability is another parameter affecting the capillary pressure in the reservoir. The main mechanism of surfactants is to reduce IFT, but the alteration in the wettability from hydrophobicity to hydrophilicity is most often caused by surfactants. Contact angle tests are widely used to indicate the wettability of the rock [15, 182, 183]. Figure 4-80 shows the results of the oil droplet contact angle test in the presence of the surfactant solution at CMC over time. The contact angle is a dynamic parameter and changes over time, but after a sufficient time, it reaches equilibrium so that its changes after the equilibrium time are very small. Figure 4-80 shows that the contact angle at the start of the test was 124.42°, which is within the hydrophobicity range. Over time, after 15, 30, and 60 minutes, the contact angle reached 100.89°, 66.98°, and 44.36°, respectively, after which no significant change in its value was observed. The wettability alteration of sandstone by the surfactant depends on two factors, the absorption of surfactant and the orientation of the absorbed molecules. Adsorption of surfactants usually does not occur with the desired orientation to create a thin film with an opposite wettability with the initial status. Therefore, it cannot be said that adsorption always causes more variability. The hemi-micelle provides this orientation for altering the wettability by surfactant solution at the CMC. Hemi-micelle is the two-layer accumulation of surfactant molecules on the solid surface at a specific concentration (CMC) [184, 185]. The orientation of the molecules in the hemi-micelle arrangement is uniform. Hou et al. showed that a two-layer arrangement of non-ionic surfactants alters the sandstone wettability [186]. In addition to the mechanism of the arrangement

of surfactant molecules with the desired orientation and the creation of a thin film, Wang et al. developed a general mechanism of the washing and removing oil from the surface by the surfactants [187]. This mechanism, by removing oil components from the surface and dissolving them in the fluid containing surfactant by creating an intermediary, causes the rock wettability to alter to hydrophilic. This intermediary is created by double-structured surfactant molecules. Different salinities also affect the contact angle and wettability. Table 4-14 shows the values of contact angle in the presence of the surfactant solution at CMC and different salinities. In the case of non-ionic surfactants, the coupling of ions and the surfactant molecules are less common due to the lack of attraction force between different loads, but ions can interact with the sandstone surface. Ions are adsorbed on the sandstone surface due to the difference in the charge with the minerals of the rock surface and removing the fatty acids that cause hydrophobicity of the rock. In the multi-ion exchange mechanism in sandstone reservoirs, the presence of divalent cationic ions such as Mg^{2+} and Ca^{2+} in saltwater plays a more important role than monovalent ions such as Na^+ [188]. However, it should also be noted that the salting-in and salting-out mechanisms are very effective in altering wettability and removing petroleum components from the rock surface so that wettability is more easily altered by lower concentrations of the ions [165]. As can be seen in Figure 4-81, different salinities had different effects based on the mentioned mechanisms, which means that the salinity of formation water due to the presence of more divalent cations in its composition caused a further decrease in contact angle and then the salinity resulting $MgCl_2$ salt dissolution caused the greatest decrease in contact angle and ultimately the salinity resulting from $NaCl$ dissolution had the least effect on the contact angle. Also, the greatest reduction in contact angle occurred at low concentrations.

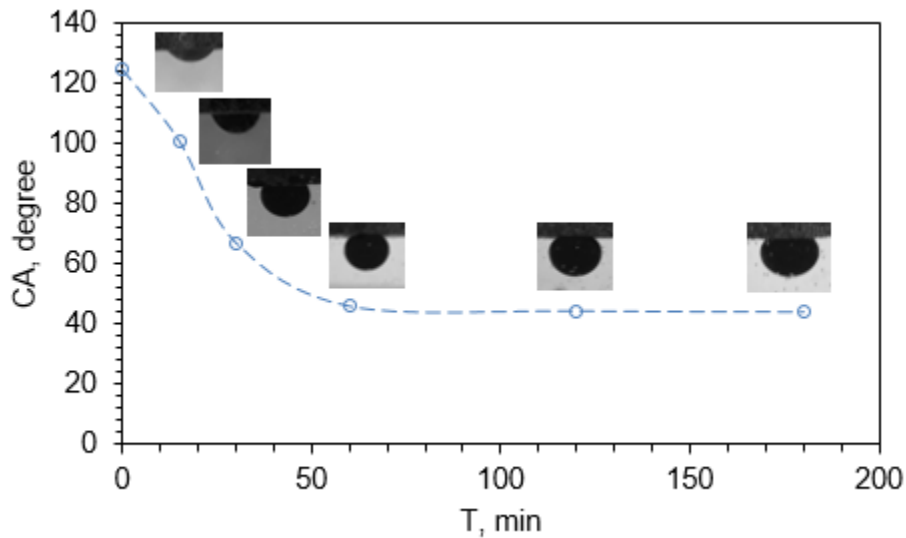


Figure 4-80: Diagram of contact angle changes in the presence of surfactant solution at CMC and 80 °C.

Table 4-14: The values of the contact angle in the presence of surfactant solution at CMC and different salinities at 80 °C.

Brine concentration, ppm	Contact angle, degree		
	FW	NaCl	MgCl ₂
5000	44.01	44.01	44.01
10000	39.53	43.62	40.19
15000	35.12	48.7	38.44
20000	41.08	51.29	44.5
30000	43.8	55.06	45.64
40000	47.32	57.21	48.3

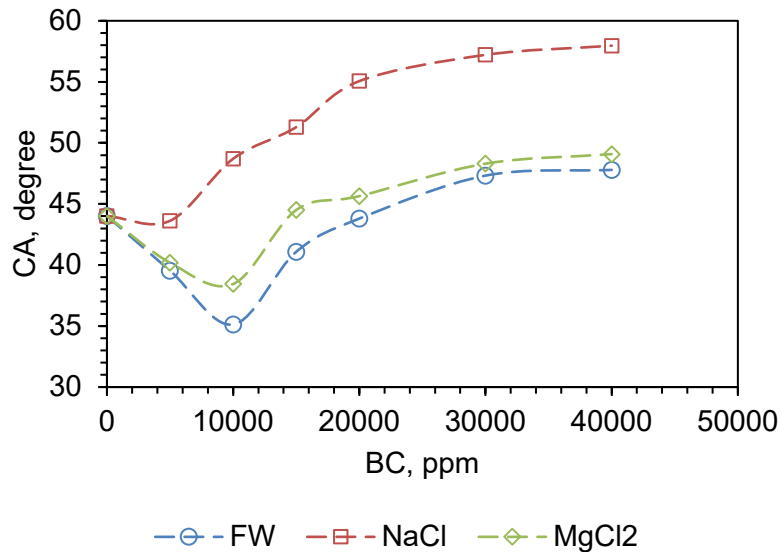


Figure 4-81: Diagram of the effect of different salinities on contact angle in the presence of the surfactant solution at CMC and crude oil at 80 °C.

4.4.5. Oil recovery

As mentioned earlier, the injection fluid in the ASP injection process requires the engineering of the additives. The ASP-slug was adjusted based on the results of the IFT tests. Based on it, the chemical solution containing surfactant at CMC, the optimal salinity of the formation water, the optimal concentration of NaOH alkali and 1000 ppm of PHPA polymer were prepared and considered as a slug for injection. The experiment was performed in a sandstone plug with a length of 7.3 cm, a diameter of 3.81 cm, a porosity

of 22.64% and permeability of 134 milli-Darcy (mD). Figure 4-82 shows the results of the percentage of oil recovery per volume of injected fluid in the Pore Volume (PV) unit. An oil recovery of 57.3 % was achieved in the flooding of brine, which was expected due to the high permeability of the sandstone. Finally, the total oil recovery of 89.4% as a result of the injection of fluids with a total volume of 4.5 PV was obtained. Accordingly, 32.1% of the oil recovery is the result of the tertiary injection. A set of parameters including the properties of the rock and the injection fluid and crude oil are effective in increasing oil recovery. The predominant mechanisms in an ASP injection are reduction of IFT due to the presence of the surfactant, optimal salinity and alkalinity and increased viscosity due to the presence of polymer. The polymer, especially in high-permeability formations, can increase the sweep efficiency and prevent the fingering and early production of injection fluid by pistonizing the injection front. According to the results of IFT tests, in the presence of alkaline, the IFT decreased more than the surfactant alone. However, the reduction of IFT by alkali requires its reaction with the acidic components of crude oil and the production of petroleum soap. To better understand alkaline performance, the FTIR analyses of the OOIP and the oil production after ASP injection were matched. Figure 4-83 shows the overlap of FTIR analyses of the OOIP and oil production. In the FTIR curve of the OOIP, the peaks at $705-1030\text{ cm}^{-1}$, 1455 cm^{-1} , $1620-1710\text{ cm}^{-1}$, $2820-3310\text{ cm}^{-1}$ and 3440 cm^{-1} represent the functional groups of $=\text{C}-\text{H}$, $\text{C}-\text{H}$, $\text{C}=\text{O}$, $\text{C}-\text{H}$ and $-\text{OH}$, respectively and in the FTIR curve of the produced oil sample, the peak at 1635 cm^{-1} shows the bond of $-\text{C}=\text{C}-$ as a result of petroleum soap production during ASP injection.

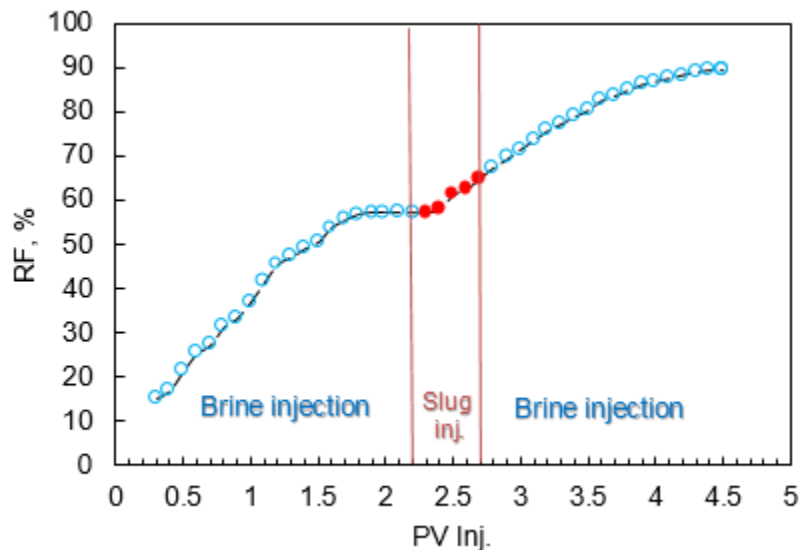


Figure 4-82: Oil recovery diagram in the ASP-slug injection process.

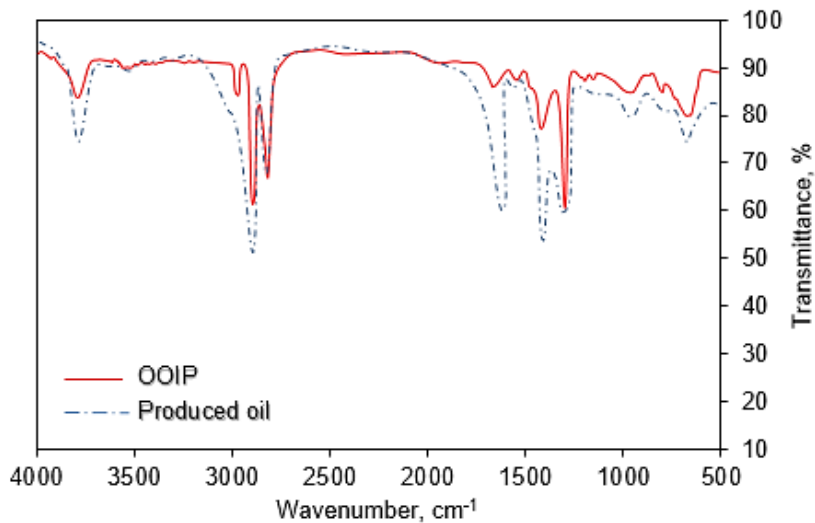


Figure 4-83: FTIR analyses for OOIP and produced oil samples.

4.5. Synthesized surfactant from *Rapeseed* oil

4.5.1. FTIR, ¹H NMR and TGA analyses

The FTIR analysis of the surfactant synthesized from *Rapeseed* oil is shown in Figure 4-84. Peaks p and n at 622 and 854 cm^{-1} are related to the S-O stretching vibrations. Peak n at 854 cm^{-1} shows the S=O bond in the sulfonate group. These peaks are related to the Sulphonation process. Some other peaks and their related functional groups in FTIR are shown in Table 4-15.

The surfactant structure is confirmed by ¹H NMR analysis shown in Figure 4-85. The resonance signal (δ) at 1.93 corresponds to allylic protons (-CH=CH-CH₂-CH=CH-) in the surfactant structure. **Table 4-16** shows the relationship between chemical shifts and the surfactant structure in ¹H NMR analysis.

The thermal properties of the surfactant are shown by the TGA analysis in **Figure 4-86**. There are two weight loss peaks in the TGA curve. The first peak starts at 25 °C and ends at 110 °C. The surfactant weight loss at this peak is equal to 5%. This amount of weight loss appears to be due to the evaporation of moisture from the sample. In other words, the surfactant structure in the first peak range is protected from heat degradation. The second peak of higher temperature is more intense and shows greater weight loss. This peak can be related to the temperature degradation of the surfactant structure.

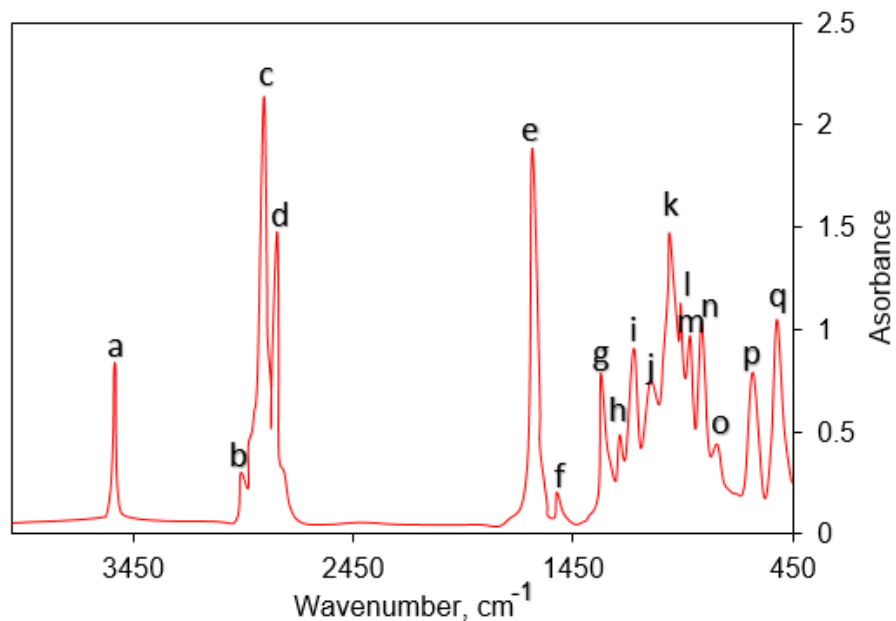


Figure 4-84: FTIR analysis of the surfactant.

Table 4-15: Relationships of peaks with functional groups in FTIR spectra of *Rapeseed* oil surfactant.

Peak	Wavenumber, cm^{-1}	Functional group	Vibration mode
a	3480	-OH	Stretching
b	3015	=C-H (<i>cis</i> -)	Stretching
c	2930	-C-H (CH_2)	Asymmetrical stretching
d	2865	-C-H (CH_2)	Symmetrical stretching
e	1752	-C=O (<i>ester</i>)	Stretching
f	1659	-C=C- (<i>cis</i> -)	Stretching
g	1473	-C-H (CH_2)	Bending
h	1426	=C-H (<i>cis</i> -)	Bending
i	1381	-C-H (CH_3)	Symmetrical bending
j	1245	-C-O	Stretching
k	1160	-C-O	Stretching
l	1124	S=O	Stretching
m	1110	-C-O	Stretching
n	854	S-O	Stretching
o	725	-CH ₂ -	Rocking
p	622	S-O	Stretching
q	610	-HC=CH- (<i>cis</i> -)	Bending

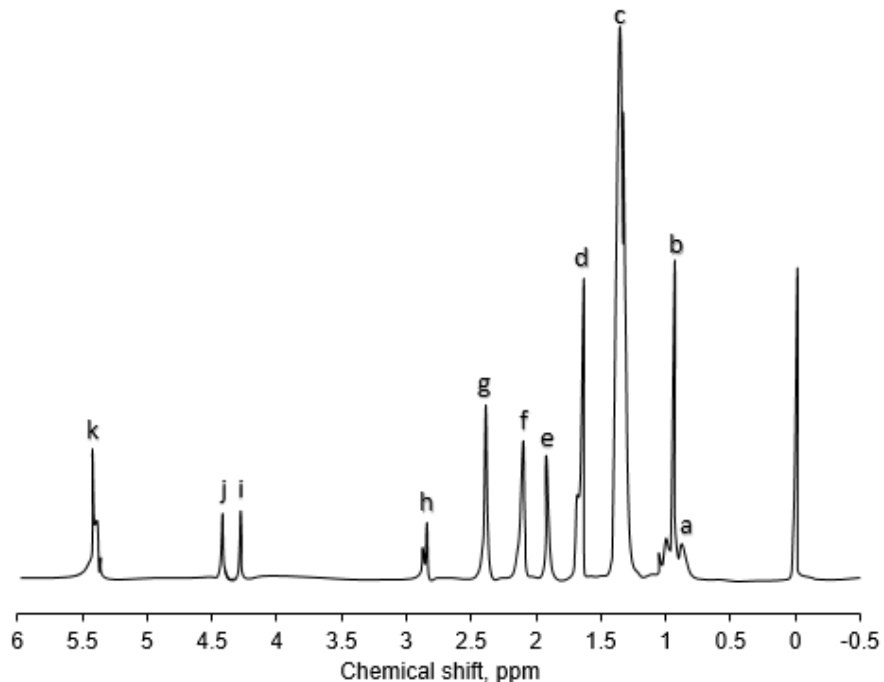


Figure 4-85: ^1H NMR analysis of the surfactant.

Table 4-16: Chemical shifts and peak assignment of ^1H NMR spectra of the *Rapeseed* oil surfactant.

Signal	δ , ppm	Proton	Compound
a	0.83	$-\text{CH}_2-\text{CH}_2-\text{CH}_2-\text{CH}_3$	all acids except linolenic acid
b	0.96	$-\text{CH}=\text{CH}-\text{CH}_2-\text{CH}_3$	linolenic acid
c	1.29	$-(\text{CH}_2)_n-$	all fatty acids
d	1.6	$-\text{CH}_2-\text{CH}_2-\text{OCO}-$	all fatty acid, β -methylene protons
e	1.93	$-\text{CH}=\text{CH}-\text{CH}_2-\text{CH}=\text{CH}-$	allylic protons
f	2.1	$-\text{CH}_2-\text{CH}=\text{CH}-$	all unsaturated fatty acid
g	2.4	$-\text{CH}_2-\text{OCO}-$	all fatty acid, α -methylene protons
h	3.8	$-\text{CH}=\text{CH}-\text{CH}_2-\text{CH}=\text{CH}-$	linoleic acid & linolenic acid
i	4.3	$-\text{CH}_2-\text{OCOR}$	all fatty acids
j	4.9	$-\text{CH}-\text{COOR}$	all unsaturated fatty acid
k	5.4	$-\text{CH}=\text{CH}-$	all unsaturated fatty acid

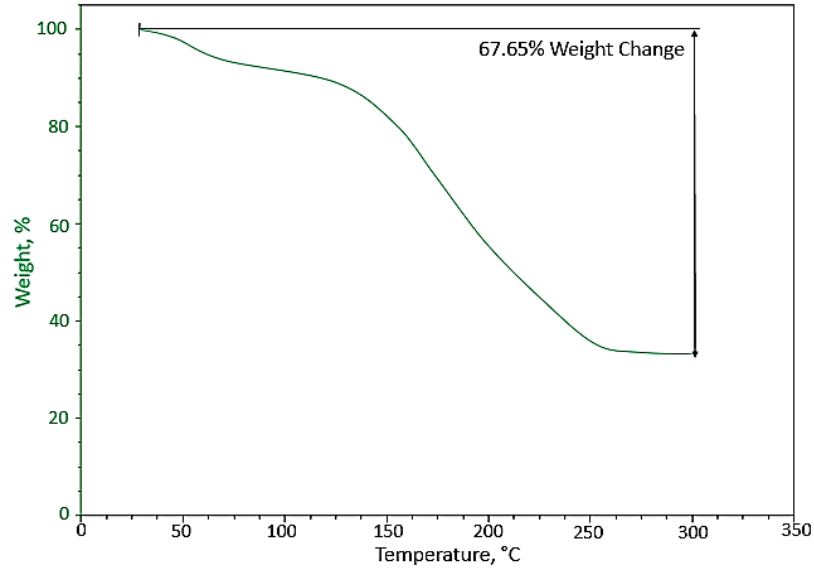


Figure 4-86: Analysis of TGA for the surfactant.

4.5.2. Surface tension and water-oil interfacial tension

Figure 4-87 shows the results of surface tension experiments. The experiments were performed for surfactant solutions at surfactant concentrations of 500, 1000, 2000, 3000, 4000, 4250, 4500, 4750, 5000 and 6000 ppm in distilled water. According to Figure 4-87, the surface tension values at surfactant concentrations of 500, 1000, 2000, 3000, 4000, 4250, 4500, 4750, 5000 and 6000 ppm were equal to 65.367, 59.846, 47.672, 41.961, 36.873, 35.229, 33.161, 33.540 and 33.714 mN/m, respectively. The curve decreases sharply to a concentration of 4500 ppm equal to CMC.

Figure 4-88 shows the IFT values and Figure 4-89 and Figure 4-90 show the effect of the presence of NaCl and NaOH on IFT in CMC, respectively. IFT reduction has a great effect on reducing capillary pressure [183, 189]. The values of IFT are inversely related to the surfactant concentration, and rapid IFT decay occurs up to a CMC of 3.4×10^{-2} mN/m. IFTs were obtained for the surfactant concentrations of 1500, 2500, 3500, 4500, 5500 and 6500 ppm equal to 3.157, 2.514, 1.089, 0.034, 0.071 and 0.095 mN/m, respectively. According to Figure 4-89, the IFT values of the surfactant solution in CMC and crude oil at salinities of 5000, 10000, 15000, 20000 and 30000 ppm were equal to 0.032, 0.030, 0.045, 0.051 and 0.076 mN/m, respectively. IFTs were obtained at alkaline concentrations of 500, 1000, 1500, 2000, 2500 and 3000 ppm equal to 0.033, 0.032, 0.030, 0.028, 0.031 and 0.034 mN/m, respectively (Figure 4-90).

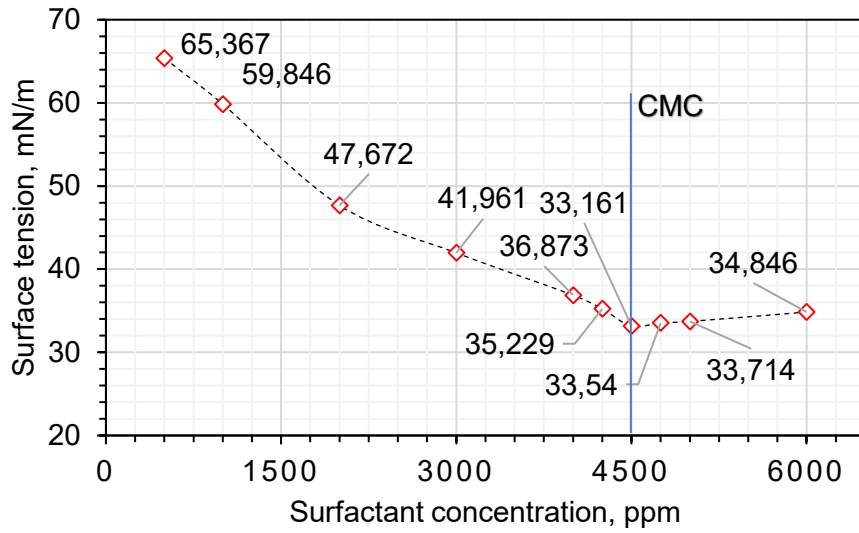


Figure 4-87: Surface tension diagram of surfactant solutions at 80 °C.

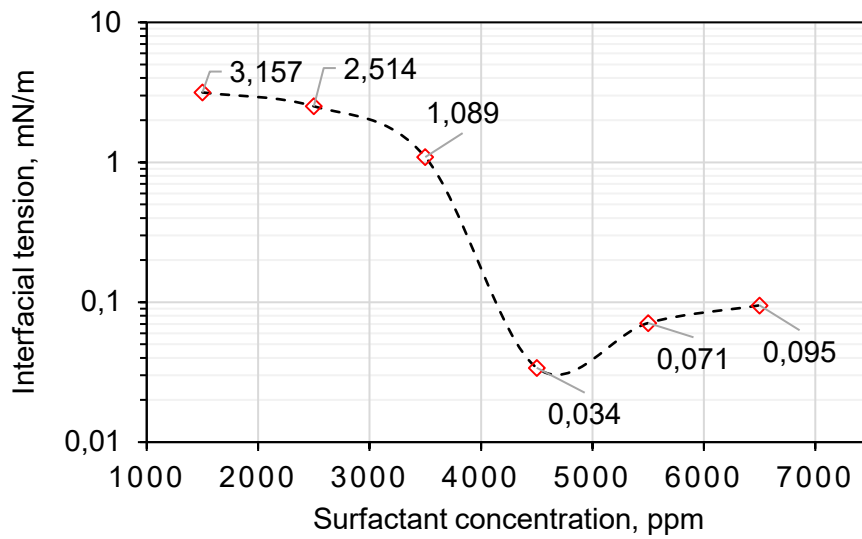


Figure 4-88: Interfacial tension diagram of surfactant solutions and crude oil at 80 °C.

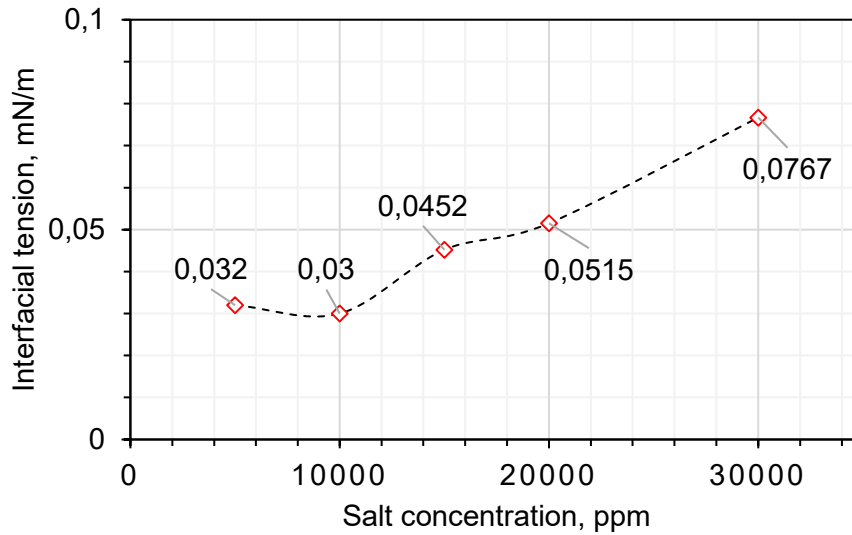


Figure 4-89: Effect of salinity on the interfacial tension in CMC at 80 °C.

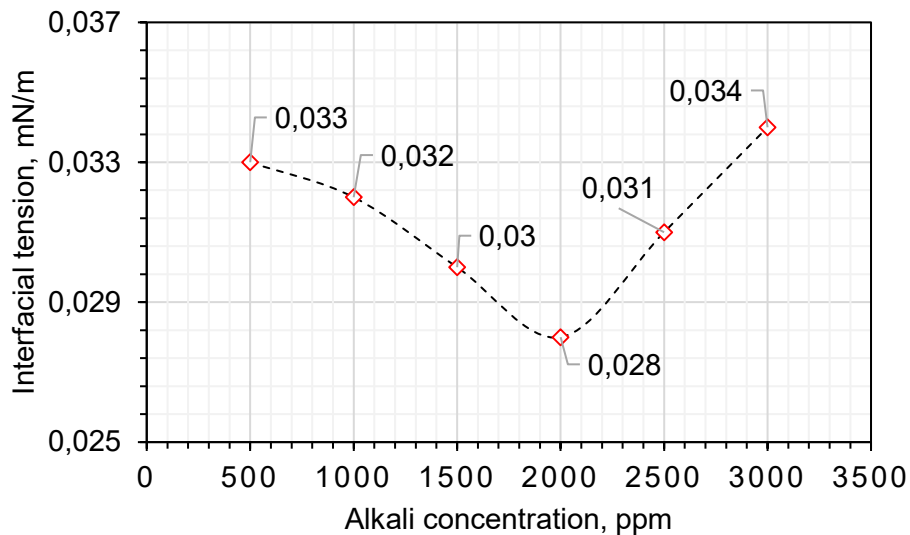


Figure 4-90: Effect of NaOH on the interfacial tension in CMC at 80 °C.

4.5.3. Contact angle

Figure 4-91 (top row) shows an oil drop image adhering to an oil-wet section in the presence of the surfactant solution in CMC over time. The average angle of the oil drop and rock section at the beginning of the experiment was 141.14°. The mean contact angles of 125.42°, 105.53°, 70.21° and 40.62° were obtained after 15, 30, 45 and 60 min, respectively. Changes in the contact angle after 60 minutes indicate the wettability alteration to hydrophilic. The contact angle test was stopped after 60 minutes because after that the contact angle changes were very small and the system reached equilibrium. The wettability

alteration can be seen more clearly in Figure 4-91 (bottom row). As can be seen, the level of oil spot on the section in the surfactant solution in CMC decreases continuously over time. These images, which are the result of an observational wettability test, have no numerical value and were taken solely to better show the alteration of rock wettability by the surfactant. The alteration of rock wettability by surfactants depends on the adsorption with the desired orientation. However, the monolayer adsorption of surfactants does not follow a regular pattern [184]. In CMC, surfactants alter rock wettability by forming hemi-micelles, which are bilayers of surfactant molecules on the surface.

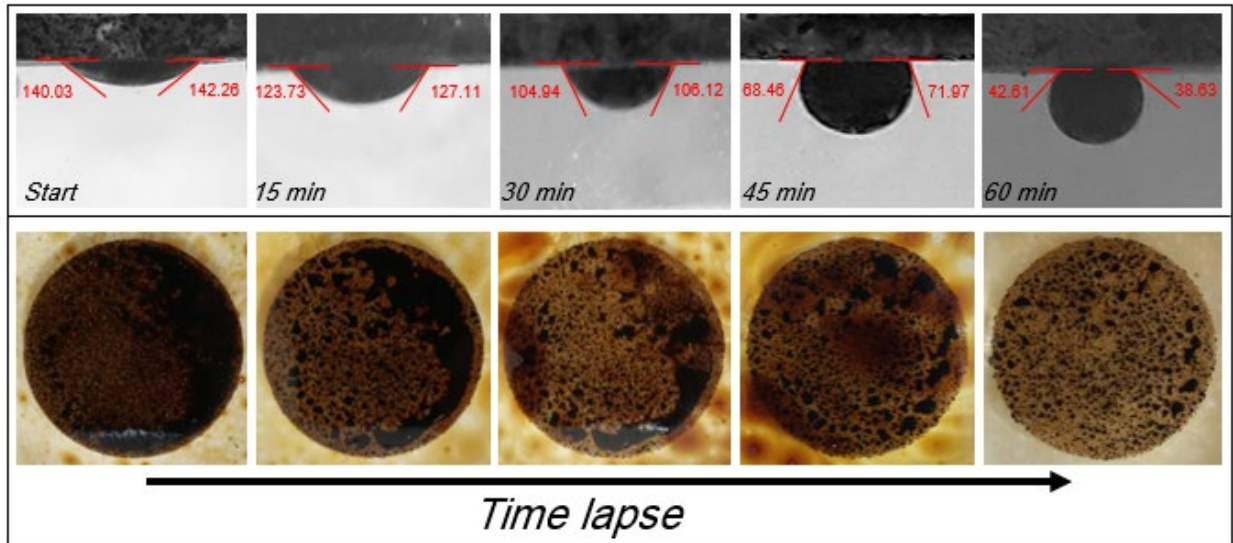


Figure 4-91: Results of contact angle experiments (top row) and observational wettability alteration: decrease in oil spot surface (bottom row) for surfactant solution in CMC over time.

4.5.4. Foamability

Here, simple experiments were performed to show the surfactant foamability. Figure 4-92 shows the foamability of the surfactant solutions at the beginning of the experiment and Figure 4-93 shows the decrease in foam volume over time. According to Figure 4-93, the volume of foam increases with increasing surfactant concentration. The volume of foam formed by 5 mL of surfactant solution at concentrations of 1500, 2500, 3500, 4500, 5500 and 6500 ppm at the beginning of the experiment is equal to 0.8, 1, 1.5, 2, 3.2 and 4.1 mL, respectively. The time of complete disintegration of the foam also depends on the surfactant concentration. The duration of the foam disintegration shows its stability.

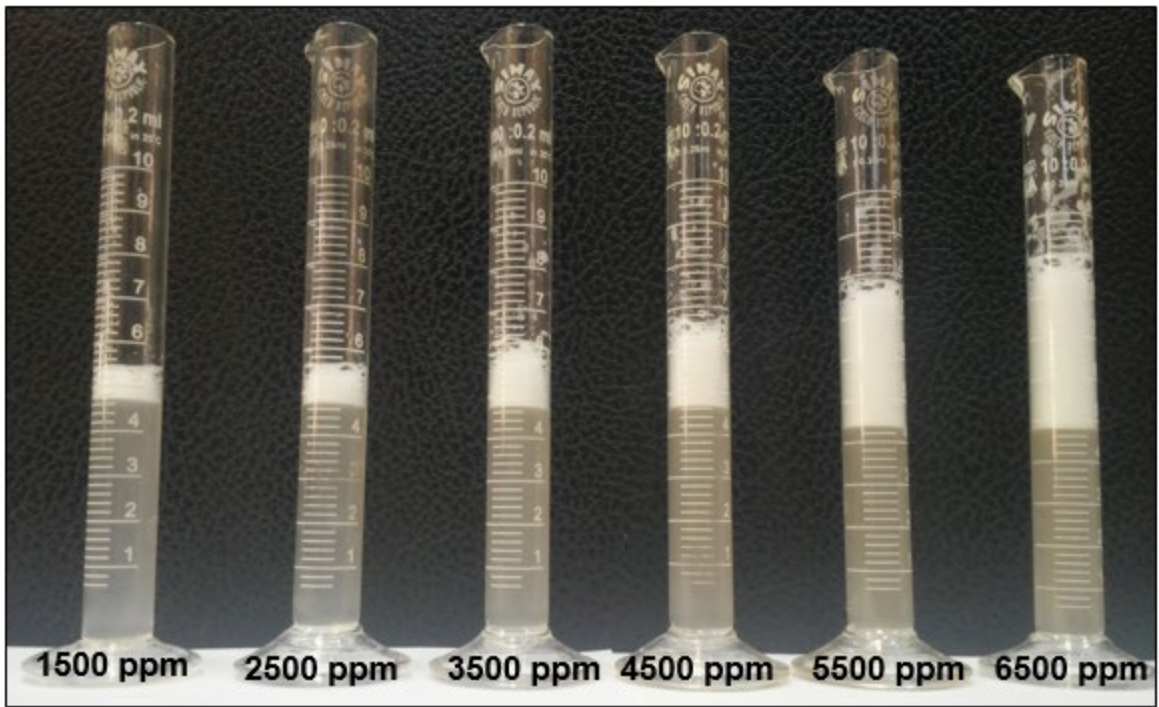


Figure 4-91: Foamability of surfactant solutions at different concentrations (at the beginning of the experiment).

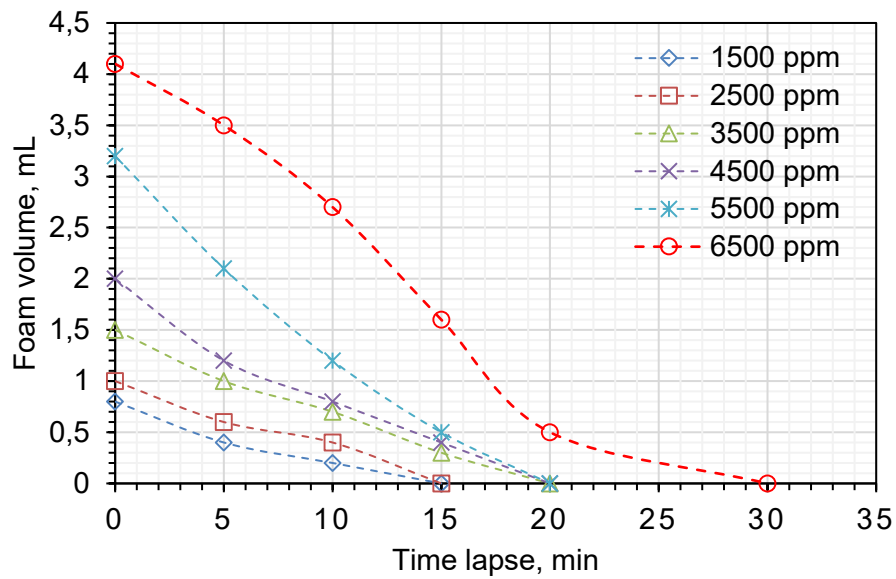


Figure 4-93: Graph of volume reduction of foam formed at different concentrations of surfactant over time.

4.5.5. Emulsion stability

The results of emulsion stability and phase separation over time are shown in Figure 4-94. Initial separation was observed after 5 days. As the volume of water and oil increases, the volume of the emulsion decreases. Acceptable emulsion stability is confirmed when, after 30 days, the volume of the aqueous phase is still less than half of the volume of the total emulsion and has not reached the initial volume of the aqueous phase. Formation and stability of oil-injection phase emulsion will lead to more oil production. The emulsion splits the large trapped droplets into smaller droplets. Small droplets of oil flow easily into pores and narrow channels. Also, the emulsion further reduces IFT. As the oil droplets break at the interface, the water-oil contact surface increases. As the interface space increases, more surfactant molecules are adsorbed and consequently, IFT is reduced [190, 191].

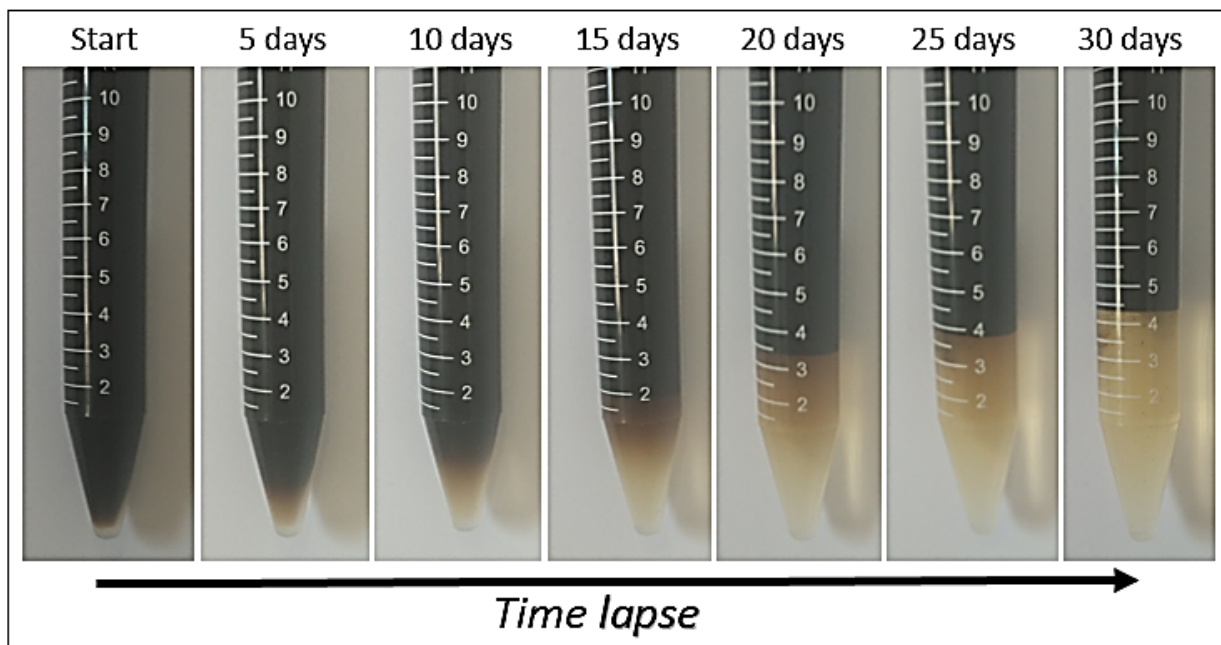


Figure 4-94: Stability of emulsion of surfactant solution in CMC and crude oil against time.

4.5.6. Surfactant adsorption

The conductivity values of the surfactant solutions are shown in Figure 4-95. It was used as a conductivity calibration curve to find the unknown concentration of the surfactant solution after flooding. In this way, the conductivity of the output solution was measured and the corresponding concentration was calculated from this curve. Based on Figure 4-95, the conductivity increases with increasing concentration, and at one point failure is seen in the diagram so that the trend-lines crossed for the points follow two separate equations before and after the breakpoint. This breakpoint shows the CMC value in the conductivity versus

the concentration curve [192]. Figure 4-96 shows the amount of adsorption of the surfactant in the CSC plug. The adsorption curve first climbs with a steep slope and then has a much smaller slope and eventually, becomes almost horizontal. The adsorption values for 0.25, 0.5, 0.75, 1, 1.25, 1.5, 1.75 and 2 PV of the injected fluid were 40, 80, 120, 150, 165, 170, 175 and 180 ppm, respectively. At the beginning of the flood, the surface of the rock is not occupied by any surfactant molecules. As the flood continues, the occupation of the rock surface area increases rapidly, resulting in an increase in the ratio of the occupied area to the unoccupied area, and eventually, it becomes saturated. As the unoccupied area decreases, the ratio of the amount of adsorption to the injected PV is reduced, resulting in a lower slope at the end of the curve. The main mechanisms of EOR in surfactant solution injection methods such as IFT reduction, foam and emulsion formation are related to the interface and liquid-liquid interactions. Adsorption of surfactant on the rock causes it to leave the oil phase-injecting phase system and somehow it is wasted. This contradicts the economic objectives of the EOR process considering surfactants as expensive materials. In surfactant flooding operations, it seems reasonable to calculate the amount of surfactant adsorption before injecting the optimum fluid and add it so as not to damage the liquid-liquid system mechanisms through adsorption. The amount of surfactant loss is illustrated more clearly with a simple general example. By saturating the surface of the rock with surfactant molecules, a layer is formed on the rock. Suppose a surfactant solution injection operation is performed for one acre (4047 m^2) to a depth of 3 m. This area of the reservoir (porous media) can have a surface equivalent to $1.06 \times 10^{10} \text{ m}^2$. By adsorption of the surfactant onto the layer, a density of 1 molecule per 0.5 nm^2 of the existing surface is reached (usually for ionic surfactant), so approximately 3.5×10^4 mole of the surfactant is adsorbed onto the solid. Assuming a molecular weight of 500 g/mol for surfactant, the amount of surfactant adsorption reaches $1.76 \times 10^4 \text{ kg}$ [127]. The salinity, pH, temperature, type of surfactant and rock are effective parameters on the adsorption [156]. It is accepted that the adsorption of the ionic surfactant onto the rock is controlled by electrostatic attraction [185, 193]. The similarity of anionic surfactant charges and sandstone reservoirs makes the use of these surfactants more preferred than cationic and non-ionic types in this type of reservoir. With these interpretations in this particular example, CSC rock, the tendency to adsorb *Rapeseed* oil-derived anionic surfactant onto the carbonate content of the rock surface is higher due to the difference between the charges of the rock surface (positively) and the surfactant head (negatively).

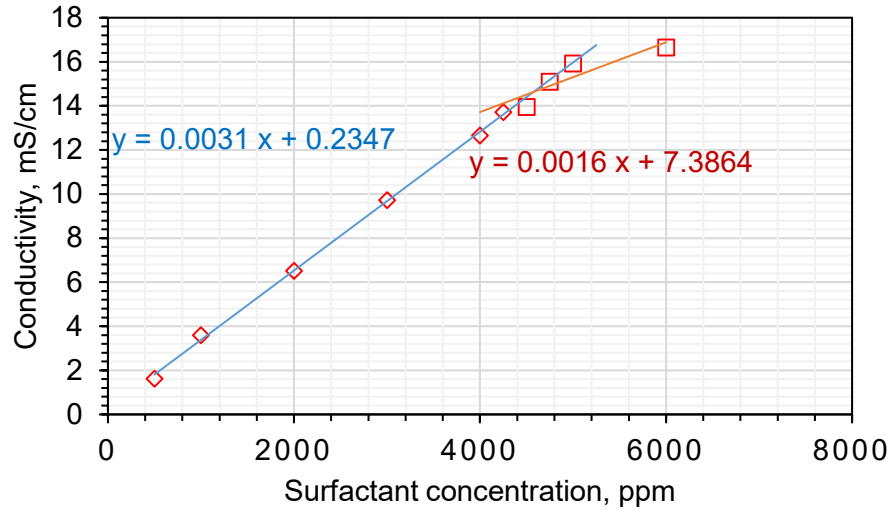


Figure 4-95: Conductivity diagram of surfactant solutions at different concentrations.

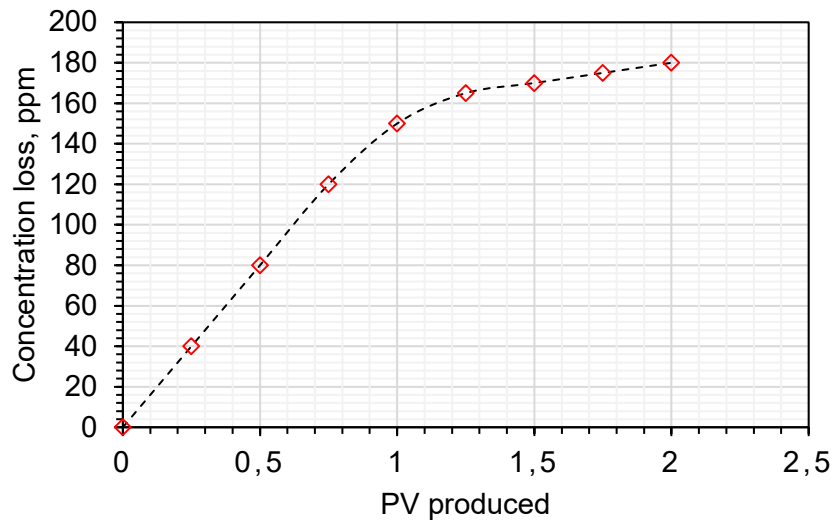


Figure 4-96: Reduction of surfactant concentration in CMC due to adsorption in the porous medium.

4.5.7. Oil recover by ASP injection

Table 4-17 shows the specifications of the plugs used in flooding experiments and Figure 4-97 shows the results of chemical injection experiments in different scenarios. In integrated flooding of surfactant in CMC (plug #C1), oil recovery due to secondary saline injection was 44.8%. Oil production was resumed after the injection of 0.3 PV of surfactant solution. The oil recovery of 61.3% was obtained after the injection of 2 PV of saline and surfactant. In the injection of SA slug with a volume of 0.5 PV (plug #C2), the secondary oil recovery due to the injection of saline water was 44.7%. Tertiary oil production resumed after injection of 0.2 PV of SA solution at optimal salinity and final oil recovery of 59.3% was achieved. Secondary

recovery was achieved in the injection of 0.5 PV of SP slug (plug #C3), equivalent to 44.8%. Oil production at this stage started after injection of 0.3 PV from the slug and the final oil recovery was equal to 64.7%. In the injection of 0.25 PV of ASP slug (plug #C4), the secondary oil production of 44.7% finally reached 66.7%. In the injection of 0.25 PV of ASP slug, the secondary oil production of 44.7% finally reached 66.7%. This is while oil production at this stage had started after 0.2 PV injection. Finally, the oil recovery factor of 44.9% obtained in the secondary injection of saline water reached 70.6% by injection of 0.5 PV of ASP slug (plug #C5). Early production of saline water for all plugs occurred in the secondary stage. This could be due to the high permeability of the plugs and the presence of channels in the rock and the phenomenon of fingering. By chemical injection in different scenarios, the increase in oil recycling was not achieved equality and the final value is proportional to the type and size of the slug. Figure 4-98 compares the increased rates of oil recycling in different scenarios. Based on this, the oil recovery values in different scenarios of surfactant flooding in CMC with optimal salinity, SA slug with 0.5 PV volume containing the surfactant in CMC, optimal salinity and alkalinity, SP slug with 0.5 PV volume containing the surfactant in CMC and optimal salinity and 1000 ppm of polymer and finally ASP slug in the sizes of 0.25 and 0.5 PV containing the surfactant in CMC, optimum salinity and alkalinity and 1000 ppm of polymer were equal to 16.5, 14.6, 19.9, 20.5 and 25.7%, respectively. This indicates that injecting ASP at a larger size will produce more output. Of course, choosing the size of the slug in the field, in addition to increasing oil recycling, requires a general summary of costs. Also, this study makes no claims about ASP slugs larger than 0.5 PV. The amount of oil production indicates that the use of polymer along with the surfactant is essential. The first reason is the cessation of oil production and early production of water, which indicates the phenomenon of fingering, and the second reason is the comparison of the amount of oil production when the polymer is in the system with when it is not present. Comparison of integrated flooding of surfactant and SA slug studies, although not correct in terms of chemical volume, shows that reducing the volume of surfactant to a slug of 0.5 PV and instead of adding alkali at the optimal concentration only reduces the oil recovery by 1.9%. This kind of comparison can be interesting for experts in the field who are interested in reducing costs. Also, in adding polymer to the injection fluid with the same interpretation, it is clear that by reducing the volume of surfactant to 0.5 PV slug and adding a small amount of polymer, the oil recovery has increased by 3.4%. It should be noted that the volume of chemical solution in the integrated injection of surfactant is much larger than the injection of SA slug. The absence of polymer in the system causes the phenomenon of fingering on the injection front. The low volume of slug means that no chemical front is provided in the process more than the slug, while in the integrated injection of surfactant from the beginning to the end of the process, the surfactant solution and the in-situ oil interact with each other. The AS flooding recovers less percentage of oil as compared to ASP, SP and surfactant flooding. This can also be justified by the presence of polymer and pistonizing the injection front and

prevent the phenomenon of fingering. The polymer may also increase the capillary imbibition rate and viscosity which also aids in oil recovery [194].

Table 4-17: Specifications of the plugs used in flooding tests.

Plug No.	K, mD	Porosity, %	L, cm	Plug PV, cm ³	S _{wi} , %	OOIP, cm ³	Inj. fluid
#C1	76.52	22.16	7.0	17.58	16.41	14.70	Integrated injection of the surfactant solution at CMC and optimal salinity
#C2	80.94	25.60	7.2	20.89	15.19	17.71	0.50 PV of the surfactant solution at CMC and optimal salinity and NaOH alkalinity (SA)
#C3	73.67	21.46	7.4	18.00	18.44	14.68	0.50 PV of the surfactant solution at CMC and optimal salinity and 1000 ppm of PHPA polymer (SP)
#C4	75.25	22.07	7.1	17.76	20.67	14.08	0.25 PV of the surfactant solution at CMC and optimal salinity and NaOH alkalinity and 1000 ppm of PHPA polymer (ASP)
#C5	78.40	23.59	7.3	19.52	19.28	15.75	0.50 PV of the surfactant solution at CMC and optimal salinity and NaOH alkalinity and 1000 ppm of PHPA polymer (ASP)

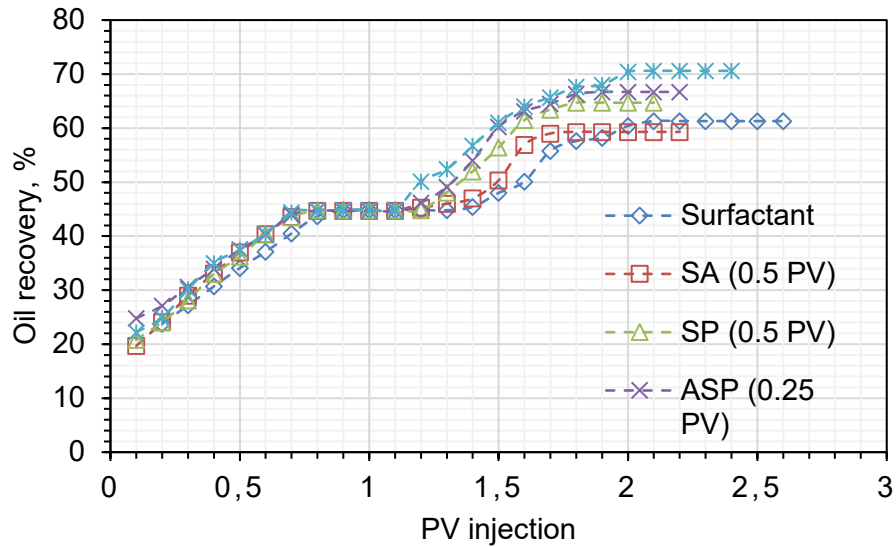


Figure 4-97: Oil recovery diagram versus injected PV in different chemical injection scenarios.

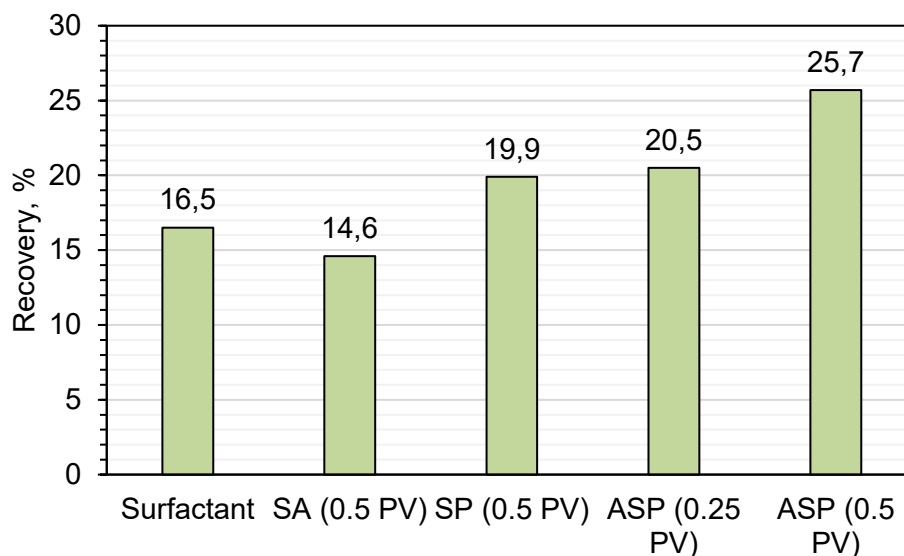


Figure 4-98: Comparison of oil recovery enhancement in different chemical injection scenarios.

4.6. Synergic effect of dissolved carbon dioxide and the *Rapeseed* oil surfactant

Table 4-18 reports the densities of carbonated solutions, the results of IFT and contact angle experiments and changes in the drop volume and oil swelling. The densities of carbonated solutions decrease with increasing pressure. As the pressure increases, the solubility of the dissolved carbon dioxide as a lighter component in the water increases, which reduces the density. The temperature has the opposite effect of pressure on the solubility of carbon dioxide in water and density. With the addition of surfactant to the system, the density increases according to its concentration. However, the values of density are very close to each other in all cases. Figure 4-99 shows the IFT values listed in Table 4-18 as curves in 1000 and 2000 psi. As shown in Figure 4-99, IFT decreases with increasing surfactant concentration even at higher concentrations than CMC (5500 ppm) with a steep slope. IFT values of surfactant-free carbonated water also give smaller numbers than initial water/oil IFT of 25.692 mN/m. The decrease in IFT by dissolved carbon dioxide is related to the reactions of carbonic acid and nitrogenous bases in the crude oil composition. Carbon dioxide dissolves in water to produce carbonic acid. Carbonic acid combines with alkali compounds in the interface and produces in-situ soap [61, 195]. The severity of these reactions depends on the composition of the oil. In other words, IFT is less reduced in more acidic oils. When a surfactant is added to the solution, the surfactant molecules form a thin film by their surface activity that reduces IFT. The interface in CMC is saturated with surfactant molecules and micelles are formed in the solution [156, 89, 99]. After CMC, IFT experiences a slight decrease, and in some cases a slight increase due to thermodynamic reasons [173]. However, this common trend is not seen in Figure 4-99. This means that IFT is reduced even at concentrations higher than CMC in line with the IFT reduction rate in CMC and

lower concentration than CMC. The reason for the continuous decline in higher concentration than CMC could be the increase in systemic irregularities caused by the dissolution of carbon dioxide. This disorder may have prevented the formation of micelles in the solution to some extent and increased CMC. In this case, more surfactant molecules are adsorbed into the interface and strengthen the thin layer. The increase in irregularity and the prevention of the micelle formation also occur with increasing temperature. As shown in Figure 4-99, the IFT is further reduced by increasing the temperature from 30 °C to 80 °C. The increase in temperature reduces the solubility of carbon dioxide in water and thus the production of carbonic acid and soap in-place is reduced but according to the trends in Figure 4-99, the effect of surfactant on IFT is much greater than the effect of dissolved carbon dioxide on it. This means that the effect of reducing the solubility of carbon dioxide in water as a result of increasing the temperature on IFT in the presence of the surfactant is not enough to neutralize the effect of surfactant on IFT. But when surfactants are not present in the system, this effect increases IFT. In other words, the IFT of surfactant-free carbonated water and oil decreases with increasing temperature. IFT values in Table 4-18 and Figure 4-99 show that at 30 °C and 1000 psi IFT of the carbonated solutions at the surfactant concentrations of 0, 3500, 4500 and 5500 ppm were 9.340, 6.458, 4.024 and 2.194 mN/m, respectively. At a temperature of 80 °C and a pressure of 1000 psi, IFT of the carbonated solutions at the surfactant concentrations of 0, 3500, 4500 and 5500 ppm were 13.759, 5.212, 3.703 and 1.863 mN/m, respectively. At 30 °C and 2000 psi, IFT of the carbonated solutions at the surfactant concentrations of 0, 3500, 4500 and 5500 ppm were 8.612, 5.326, 5.112 and 2.431 mN/m, respectively. At temperatures of 80 °C and a pressure of 2000 psi, IFT of carbonated solutions at the surfactant concentrations of 0, 3500, 4500, and 5500 ppm were 10.927, 4.948, 3.596, and 1.503 mN/m, respectively (Figure 4-99).

Table 4-18: Densities of carbonated solutions and the results of IFT, contact angle and crude oil swelling tests at temperatures of 30 and 80 °C and pressures of 1000 and 2000 psi.

Surfactant concentration, ppm	P, psi (0.5% full scale)	T, °C	Density, g/cm ³	IFT, mN/m	CA, degree	DV ₁ , mm ³	DV ₂ , mm ³	$\frac{ \Delta DV }{DV_1}$	Oil swelling, %
0	1000	30	0.9967	9.340	83.14	25.46	26.53	0.04202671	4.20
		80	0.9914	13.759	75.93	24.71	26.38	0.06758397	6.75
	2000	30	0.9925	8.612	78.62	25.54	27.47	0.07556774	7.55
		80	0.9903	10.927	71.41	25.93	28.56	0.10142692	10.14
3500	1000	30	1.0021	6.458	94.73	20.15	22.32	0.10769231	10.76
		80	1.006	5.212	89.69	21.41	23.98	0.12003737	12.00
	2000	30	1.009	5.326	83.20	21.74	24.76	0.13891444	13.89
		80	0.998	4.948	80.52	19.92	22.99	0.15411647	15.41
4500	1000	30	1.0037	4.024	62.19	13.15	14.60	0.11026616	11.02
		80	1.0026	3.703	65.28	13.07	14.75	0.12853864	12.85
	2000	30	1.0044	5.112	61.96	13.12	15.07	0.14862805	14.86
		80	1.0032	3.596	60.44	14.34	16.58	0.15620642	15.62
5500	1000	30	1.0050	2.194	61.82	10.56	11.63	0.10132576	10.13
		80	1.0039	1.863	58.34	7.23	8.06	0.11479945	11.47
	2000	30	1.0043	2.431	61.03	7.19	8.17	0.13630042	13.63
		80	1.0026	1.503	55.18	6.06	6.94	0.14521452	14.52

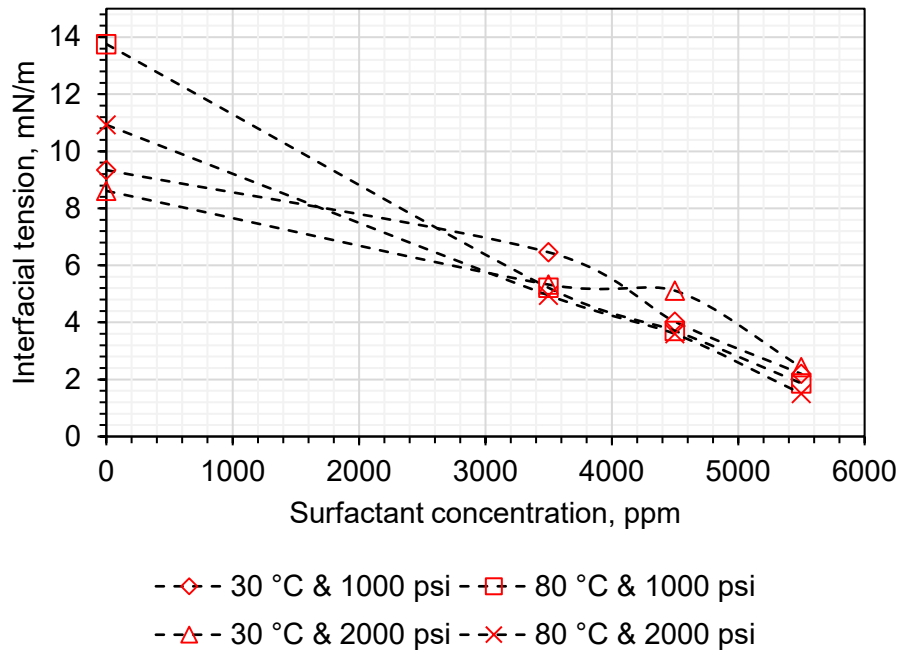


Figure 4-99: Curves of IFT values of carbonated solutions containing the surfactant at different concentrations and crude oil at temperatures of 30 and 80 °C and pressures of 1000 and 2000 psi.

Measurement of carbonate rock wettability was demonstrated using contact angle experiments. Wettability can control the amount of oil production during EOR [152]. Table 4-18 shows the results of the contact angle tests and Figure 4-100 shows these results as curves at 1000 and 2000 psi, respectively. The surface wettability of the reservoir rock depends on its physical and chemical properties, mineralogy, surface load and adsorbed materials [196, 197]. It is generally accepted that carbonate rock wettability alteration by carbonated water is caused by the mechanism of dissolution of the surface minerals of the rock, including dolomite and calcite, and the removal of oil-wetting elements from the surface through it [5, 15].

Based on the results, surfactant-free carbonated water reduced the contact angle to the range of 71.41° - 83.14° . That is, it created a relatively hydrophilic wettability. Increasing the temperature further reduced the contact angle so that at 1000 psi the contact angle values at 30 and 80 °C were 83.14° and 75.93° , respectively, and at 2000 psi these values were reduced to 78.93° and 71.41° , respectively. Increasing the temperature reduces the solubility of carbon dioxide in the water and subsequently reduces the amount of carbonic acid produced, but it should be noted that the dissolution at higher temperatures is more common. Besides, the dissolution of surface minerals, especially calcium carbonate, occurs more frequently in the water at high-temperatures, even without dissolved carbon dioxide. Reducing the contact angle at higher pressure, in addition to increasing the dissolution of surface minerals in carbonated water, is justified by strengthening the mechanism of dissolution at higher pressure. It is expected that in the presence of the surfactant, in addition to the carbonated water mechanism in wettability alteration, the surfactant mechanism and its interaction with dissolved carbon dioxide will be added. Given the curves in Figure 4-100, there seems to be no regular trend for the contact angle versus the surfactant concentration. The contact angle increased at a lower concentration than CMC. At CMC, the contact angle was greatly reduced and at a concentration higher than CMC, the contact angle often showed a milder decrease. With the addition of a surfactant as a soluble solid to the system, the solubility of carbon dioxide decreases. Whiston and Brulé stated that for every 100000 ppm of water-soluble solids, the solubility of carbon dioxide decreases by 30%. This theory is independent of the type of solids and is moderately expressed [149]. In other words, in the presence of surfactant, the solubility of carbon dioxide is reduced and as a result, less carbonic acid is produced. This can weaken the mechanism of carbonated water in altering the wettability, i.e. dissolving the surface minerals of carbonate rock. Therefore, at a concentration lower than CMC, as shown in Figure 4-100, the contact angle is increased. However, the contact angle at CMC and above CMC is reduced, while reducing the solubility of carbon dioxide in water decreases with increasing surfactant concentration, this argument cannot be generalized to them. In CMC and above CMC, there is another mechanism that affects surface wetting that is related to the presence of the surfactant. The wettability alteration by surfactants depends on the adsorption and orientation of the surfactant molecules on the solid surface. Surfactants in CMC form a layer of regular orientation on the surface called hemi-micelle [184, 185]. With the formation

of this layer, the surface wettability alters. This layer does not form at concentrations below CMC and the adsorbed molecules do not have a regular orientation at the surface. Therefore, in CMC, the contact angle is greatly reduced due to the formation of hemi-micelle. If the dissolution of surface minerals in water increases, more molecules of surfactant will leave the system and join the layer formed on the surface. Therefore, the interaction of dissolved carbon dioxide and surfactant strengthens the surface layer. This synergistic effect only increases the contact angle when the adsorption of surfactant molecules on the surface lacks the desired orientation (i.e., a concentration lower than CMC). It is also present in higher concentrations than CMC but has the greatest effect on the contact angle reduction in CMC due to hemi-micelle formation and then increasing the surfactant concentration only strengthens the formed layer. Experiments indicate that the values of contact angle at 1000 psi and 30 °C and the surfactant concentrations of 0, 3500, 4500 and 5500 ppm were 83.14°, 94.73°, 62.19° and 61.82°, respectively. At 80 °C and 1000 psi, the contact angles at the surfactant concentrations of 0, 3500, 4500 and 5500 ppm were 75.93°, 89.69°, 65.28° and 58.34°, respectively. At 30 °C and 2000 psi, the contact angles at the surfactant concentrations of 0, 3500, 4500 and 5500 ppm were 78.62°, 83.20°, 61.96° and 61.03°, respectively. At 80 °C and 2000 psi, the contact angles at the surfactant concentrations of 0, 3500, 4500 and 5500 ppm were 71.41°, 80.52°, 60.44° and 55.18°, respectively (Figure 4-100).

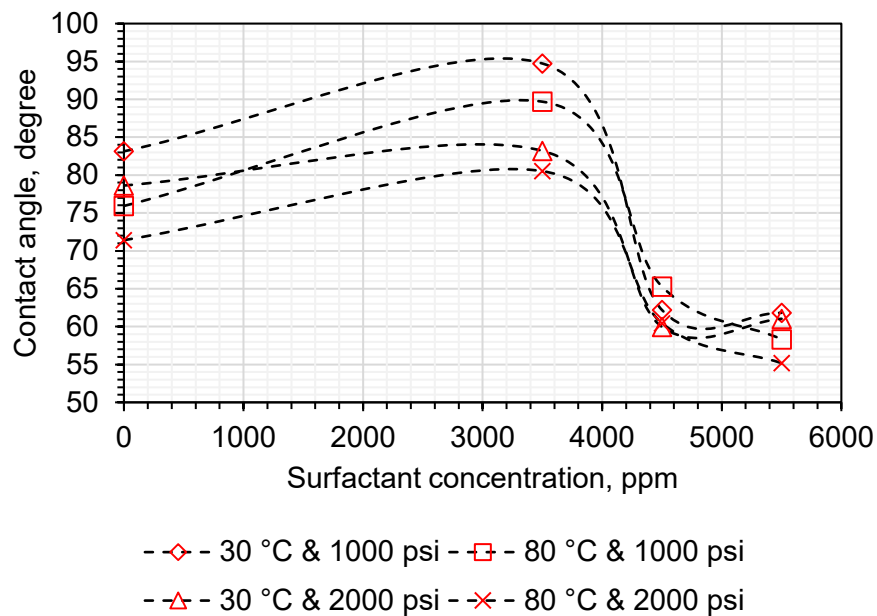


Figure 4-100: Curves of the oil droplet contact angle on the carbonate sections in the presence of carbonated solution containing the surfactant at different concentrations at temperatures of 30 and 80 °C and pressures of 1000 and 2000 psi.

Oil swelling is another important mechanism in carbonated water injection. The percentages of oil swelling are listed in Table 4-18 and the curves are shown in Figure 4-101 according to the surfactant concentration. Oil swelling is caused by the mass transfer of carbon dioxide from the water into the oil. The solubility of carbon dioxide in oil is greater than its solubility in water. This is one of the causes of carbon dioxide transfer. According to trends in changes in oil swelling in contrast to surfactant-free carbonated water, oil swelling rose as the temperature rose. Carbon dioxide mass transfer in oil is caused by solution, diffusion and dispersion mechanisms [195, 71]. As the temperature increases, the solubility of the gas in oil decreases with solution, while its diffusion increases. Therefore, increasing the mass transfer of carbon dioxide by increasing the temperature makes sense. With the addition of surfactant to the system, it is observed that in all three concentrations lower than CMC, CMC and above CMC, oil swelling is higher than zero surfactant concentration. However, at a concentration higher than CMC, the rate of oil swelling decreases as the highest amount of oil swelling is achieved in CMC. Surfactants in aqueous solutions increase the mass transfer under the influence of Marangoni instability in the interface [198, 199]. The phase behavior in the carbonated water-oil system is one-sided, unlike the carbon dioxide-oil system. This means that carbon dioxide is gradually transferred from the water into the oil in the carbonated water injection, causing it to swell [147, 148]. With these interpretations, oil swelling increases with increasing surfactant concentration, but as shown in the curves in Figure 4-101, oil swelling at a concentration higher than CMC is lower than oil swelling at CMC. The reason may be found in the mechanism of carbon dioxide absorption. Surfactant molecules can absorb carbon dioxide. In this case, the carbon dioxide molecules absorbed by the surfactants are harder to transport into the oil phase. At concentrations lower than CMC and CMC, surfactant molecules are arranged in the interface, which means that the mass of carbon dioxide absorbed can be transferred. But at concentrations higher than CMC, surfactant molecules in the solution form aggregates that have no connection with the interface and the oil phase. As a result, the carbon dioxide molecules absorbed by surfactants are trapped in a trap formed by micelles and are not easily transferred into the oil phase. In the quantitative study, increased oil swelling values at a pressure of 1000 psi, a temperature of 30 °C and the surfactant concentrations of 0, 3500, 4500 and 5500 ppm were 4.20%, 10.76%, 11.02% and 10.13%, respectively. At 80 °C and 1000 psi, increased oil swelling values at the surfactant concentrations of 0, 3500, 4500 and 5500 ppm were 6.75%, 12.00%, 12.85% and 11.47%, respectively. At 30 °C and 2000 psi, increased oil swelling values at the surfactant concentrations of 0, 3500, 4500 and 5500 ppm were 7.55%, 13.89%, 14.86% and 13.63%, respectively. At 80 °C and 2000 psi, increased oil swelling values at the surfactant concentrations of 0, 3500, 4500 and 5500 ppm were 10.10%, 15.41%, 15.62% and 14.52%, respectively. Salinity along with temperature and pressure has a significant effect on the solubility of carbon dioxide [189]. The salinity of the base fluid affects all three parameters of interfacial tension, oil swelling and rock wettability. Table 4-19 shows the results of the density, interfacial tension, oil swelling and rock

wettability experiments for carbonated solutions containing the surfactant in CMC and different salinities at 80 °C and 2000 psi. Figure 4-102 shows the interfacial tension values of carbonated fluids containing the surfactant in CMC and various salinities and crude oil at 80 °C and 2000 psi. The interfacial tension values at salinities of 0, 5000, 10000, 20000, 40000, 80000 and 120000 ppm were 3.596, 3.025, 2.437, 2.618, 3.765, 4.504 and 5.873 mN/m, respectively. The trend of the diagram shows that there is an optimal salinity at 10000 ppm where the interfacial tension is at its lowest. The reduction of interfacial tension by water-soluble ions is related to the salt-in effect and adsorption of ions onto the polar compounds of the oil at the interface [200].

Table 4-19: Densities of carbonated solutions containing the surfactant in CMC and different salinities and the results of IFT, contact angle and crude oil swelling tests at 80 °C and 2000 psi.

NaCl concentration, ppm	Density, g/cm ³	IFT, mN/m	CA, degree	DV ₁ , mm ³	DV ₂ , mm ³	$\frac{ \Delta DV }{DV_1}$	OS, %
0	1.0032	3.596	60.44	14.34	16.58	0.15620642	15.62
5000	1.0071	3.025	56.02	14.12	16.36	0.15864023	15.86
10000	1.0136	2.437	61.75	13.41	15.60	0.16331096	16.33
20000	1.0224	2.618	65.15	14.19	16.81	0.18463707	18.46
40000	1.0431	3.765	68.39	14.70	17.52	0.19183673	19.18
80000	1.0822	4.504	69.02	14.51	17.32	0.19365955	19.36
120000	1.1030	5.873	69.57	13.93	16.63	0.19382627	19.38

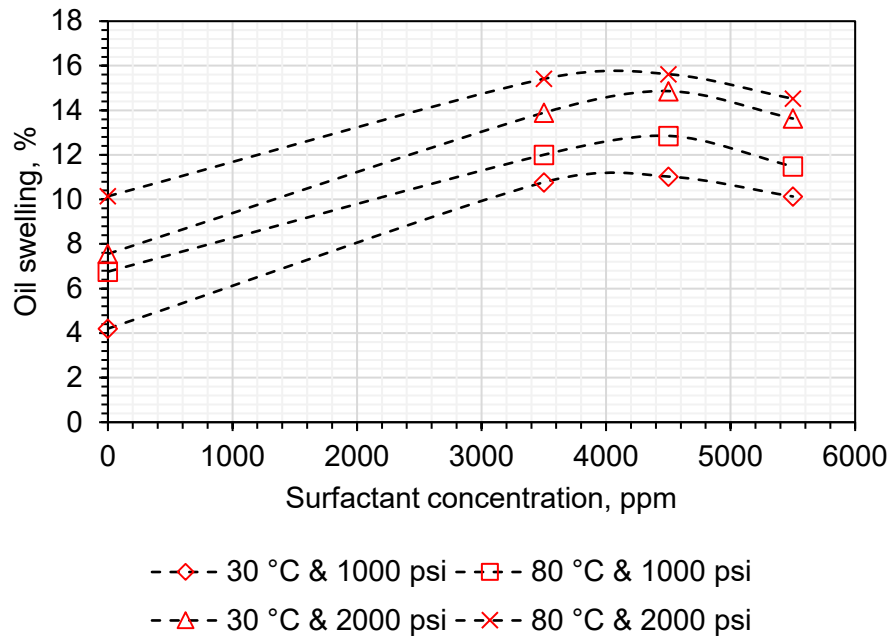


Figure 4-101: Curves of oil swelling percentage in the presence of carbonated solution containing the surfactant at different concentrations at temperatures of 30 and 80 °C and pressures of 1000 and 2000 psi.

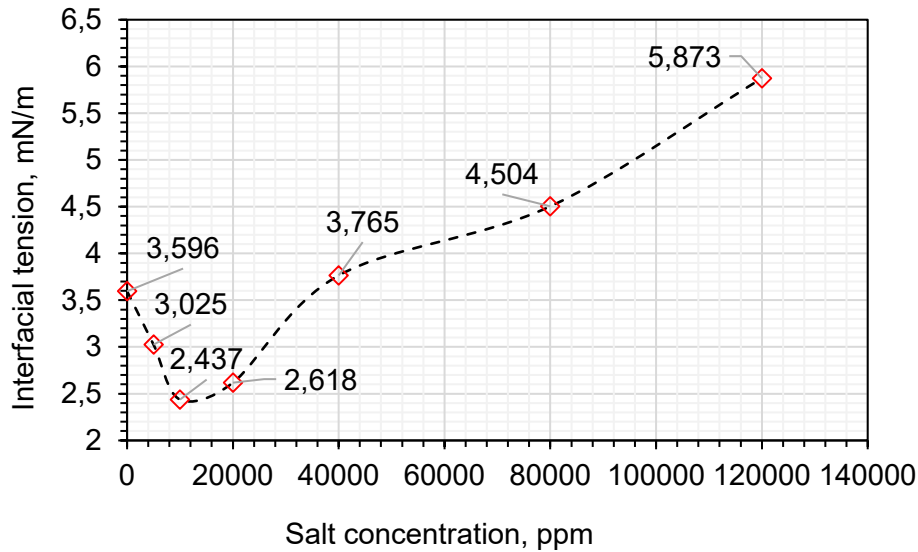


Figure 4-102: Curve of interfacial tension of carbonated solution containing the surfactant in CMC and different salinities and crude oil at 80 °C and 2000 psi.

Figure 4-103 shows the diagram of the contact angle changes at different salinities. According to Figure 4-103, the contact angle values at salinities of 0, 5000, 10000, 20000, 40000, 80000 and 120000 ppm were equal to 60.44°, 56.02°, 61.75°, 65.15°, 68.39°, 69.02° and 69.57°, respectively. There are two mechanisms of ion exchange and dissolution of rock and organic compounds in the alteration of wettability by saline water [150, 201, 202]. The mechanism of rock organic compounds dissolution is enhanced at lower salinities. When the salinity, surfactant and carbon dioxide are present in the solution simultaneously, their interactions with the reservoir rock change. The mechanism of dissolution of rock by carbonic acid is weakened by reducing the solubility of carbon dioxide, but the pairing of ions and surfactant molecules thickens the layer formed by the surfactant on the rock surface. In carbonate rocks, the surface dissolution mechanism in carbonated water plays a more effective role, so weakening this mechanism leads to hydrophobic wettability. Higher contact angle values at high salinities could be due to this. However, at low salinities, the effect of salinity on this mechanism is less. Also, the mechanism of dissolution of calcite in water is active, especially at high temperatures. The trend for oil swelling increases in the presence of various salinities. Figure 4-104 shows these changes. According to this graph, oil swelling values at salinities of 0, 5000, 10000, 20000, 40000, 80000 and 120000 ppm were equal to 15.62 %, 15.86 %, 16.33 %, 18.46 %, 19.18 %, 19.36 % and 19.38 %, respectively. The increasing trend of the oil swelling graph can be justified by reducing the dissolution of carbon dioxide in the aqueous phase and its further transfer into the oil phase. However, this trend eventually reaches equilibrium with increasing salinity, and the oil swelling graph eventually becomes horizontal. It should be noted that the time parameter also affects interfacial tension, contact angle and oil swelling. When fluids and rocks are in the same system,

interactions between them occur at the interfaces. These interactions may be chemical or physical. Adsorption, the coupling of molecules and chemical bonds, and mass transfer of additives, especially dissolved carbon dioxide, are completed over time [203].

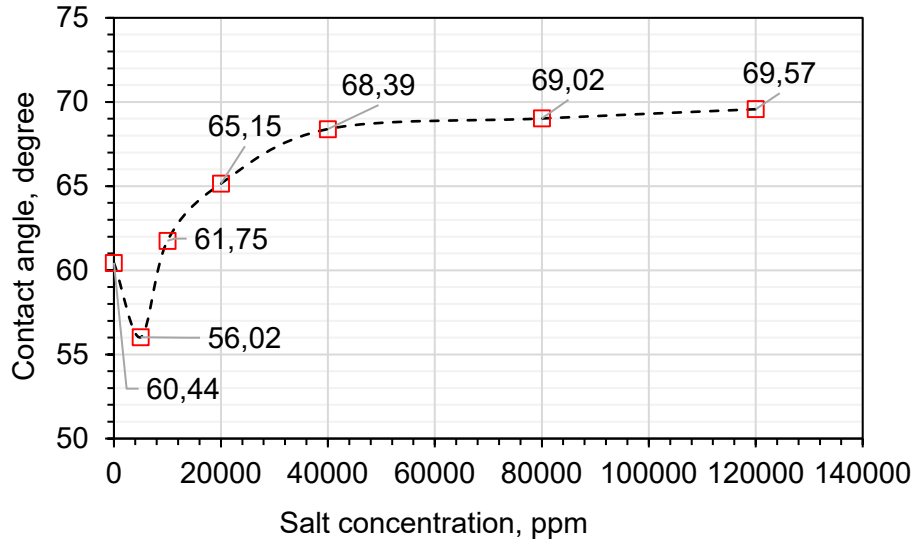


Figure 4-103: Curve of contact angle of an oil droplet in the presence of carbonated solution containing the surfactant in CMC and different salinities and crude oil at 80 °C and 2000 psi.

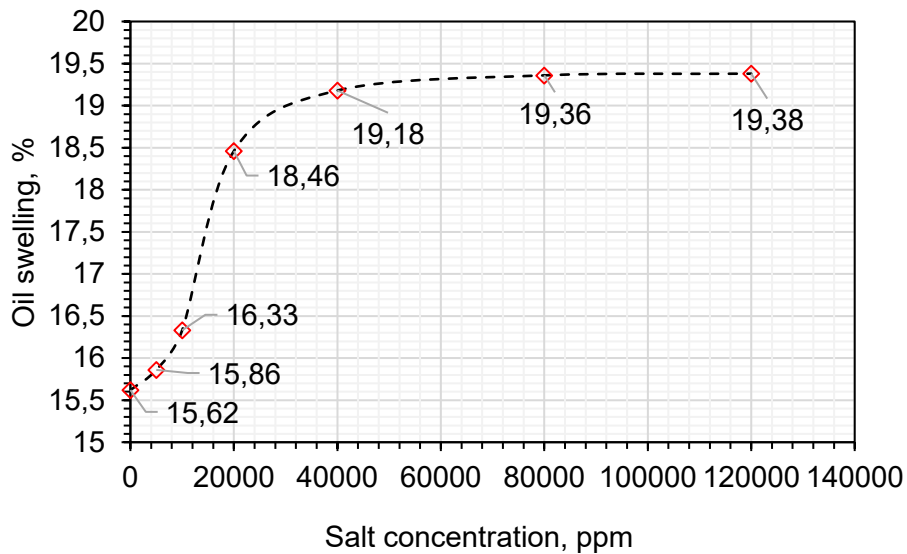


Figure 4-104: Curve of oil swelling in the presence of carbonated solution containing the surfactant in CMC and different salinities and crude oil at 80 °C and 2000 psi.

4.7. Synthesized surfactant from waste chicken fat

4.7.1. FTIR and TGA analyses

The FTIR analysis is shown in Fig. 4-105. The sulphonation fat is confirmed by peaks (a) at 622, (d) at 857 and (g) at 1161 cm^{-1} , indicating the stretching vibrations of the S=O, S-O and S-O bonds in the sulfonate group, respectively. The overall correlation of peaks with functional groups derived from FTIR analysis is presented in Table 4-20. The temperature stability of the surfactant is also confirmed according to the TGA analysis shown in Fig. 4-106. A temperature peak starts at 25 °C and continues at about 140 °C. Weight loss after this peak reaches 15%. Considering the evaporation of the sample moisture at this temperature peak, the composition of the surfactant at reservoir temperatures is protected from degradation.

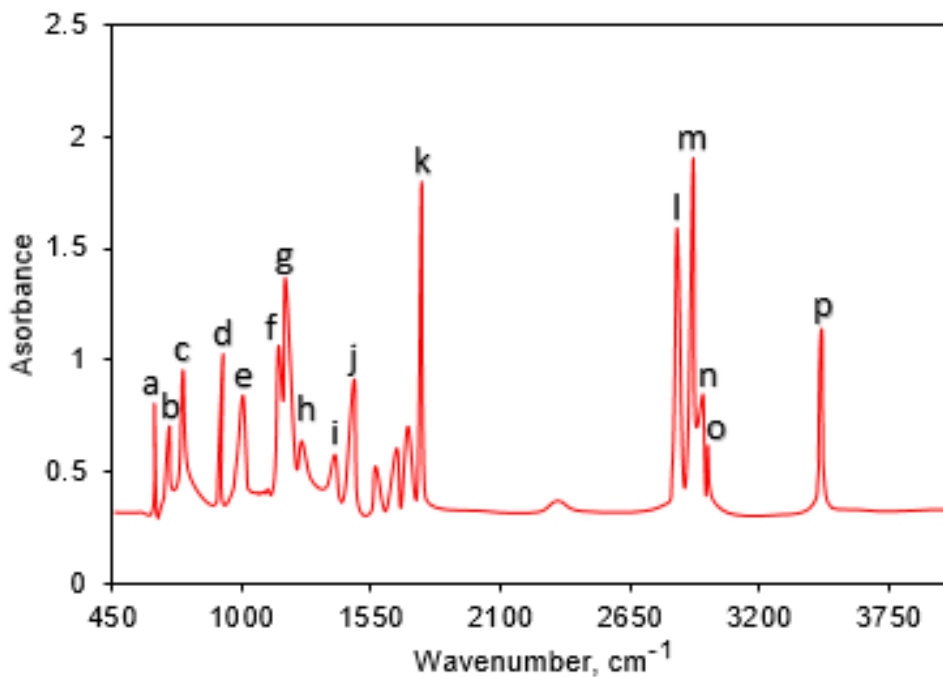


Figure 4-105: FTIR analysis of the surfactant.

Table 4-20: Peak communication with functional groups in FTIR spectra of chicken skin fat surfactant.

Peak	Wavenumber, cm^{-1}	Functional group	Vibration mode
a	622	S-O	Stretching
b	710	-CH=CH	bending
c	715	-CH=CH	bending
d	857	S-O	Stretching
e	963	CH-CH	bending
f	1234	-CH	bending
g	1161	S=O	stretching
h	1234	C-H (CH_2)	bending
i	1371	C-H (CH_3)	bending
j	1451	C-H (CH_2)	bending
k	1736	C=O	stretching
l	2851	C-H ($-\text{CH}_2$)	stretching vibration
m	2924	C-H ($-\text{CH}_2$)	stretching vibration
n	2955	C-H (CH_3)	stretching vibration
o	3006	C=H	stretching
p	3477	-OH	stretching

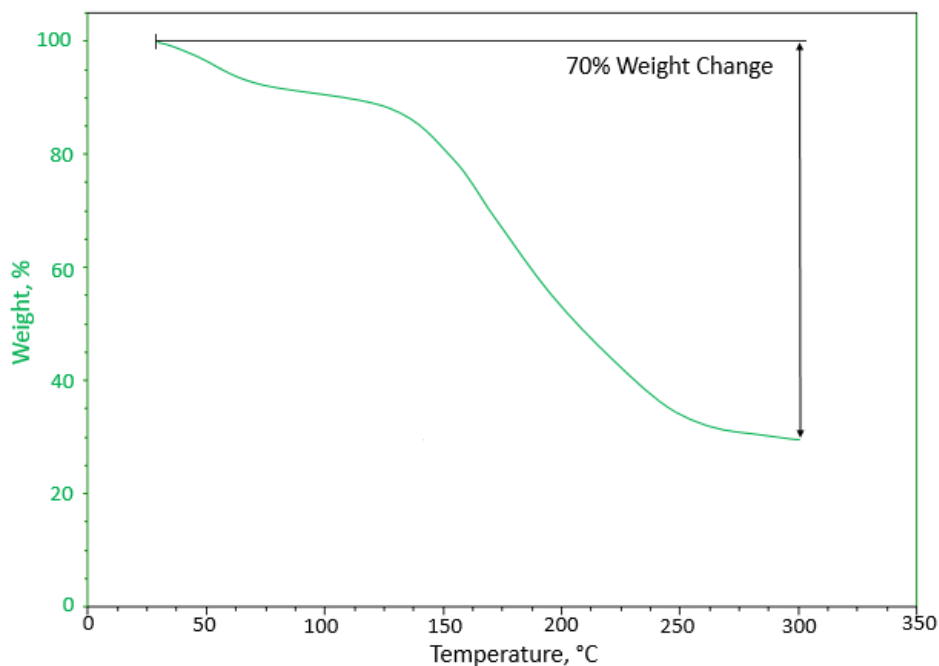


Figure 4-106: TGA analysis of the surfactant.

4.7.2. Surface tension and water-oil interfacial tension

Fig. 4-107 shows the results of the surface tension experiments. Surface tension decreases with a steep slope by increasing the concentration to a CMC of 5500 ppm and then there is not much change in the decreasing or increasing trends of surface tension. Fig. 4-108 shows the IFT values of surfactant solutions and crude oil, and Fig. 4-109 shows the effect of salinity from NaCl salt. Fig. 4-110 shows the effect of NaOH alkali on IFT at CMC. A similar trend with surface tension variations is observed in Fig. 4-108 for surfactant solutions and crude oil IFT. At 75 °C, the IFT value of the surfactant concentration has an inverse relationship, and the rapid drop out of the IFT occurs to a specific concentration of CMC (4.3×10^{-2} mN/m). Thus, IFT values at concentrations of 1500, 2500, 3500, 4500, 5500, 6500 and 7500 ppm were obtained 10.421, 7.813, 3.578, 0.974, 0.043, 0.063 and 0.060 mN/m, respectively. Different amounts of salinity also affect the IFT of surfactant solution at CMC and crude oil but there is an optimal concentration. According to Fig. 4-109, the values of IFT of surfactant at CMC and at salinity of 5000, 10000, 15000, 20000, 30000 and 40000 ppm were achieved to 0.046, 0.044, 0.038, 0.042, 0.069 and 0.091 mN/m, respectively. By adding alkali, the IFT values are further reduced. The IFT values at concentrations of 500, 1000, 1500, 2000, 2500, 3000, 4000 and 5000 ppm alkali, were obtained 0.042, 0.040, 0.037, 0.030, 0.034, 0.041 and 0.045 mN/m, respectively (Fig. 4-110).

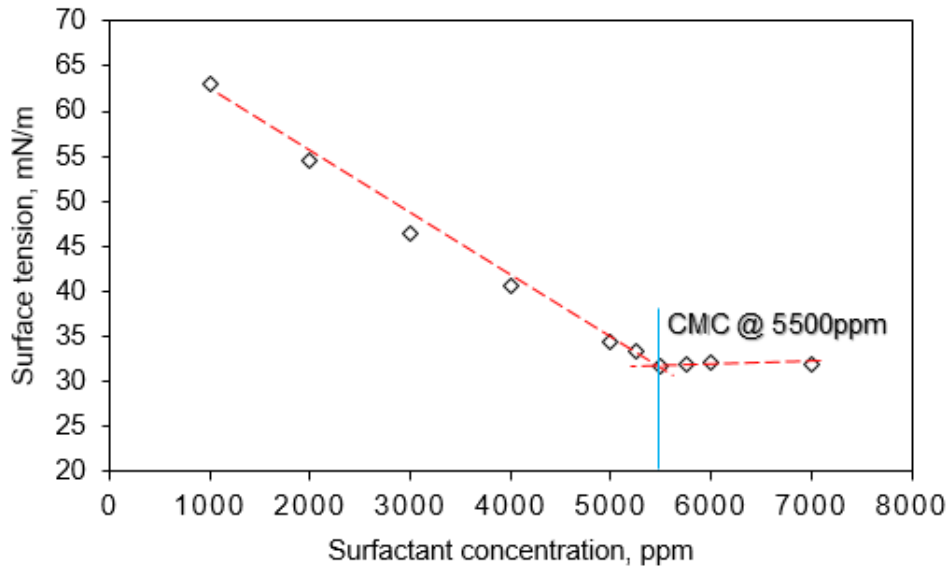


Figure 4-107: Surface tension graph of the surfactant solutions at 75 °C.

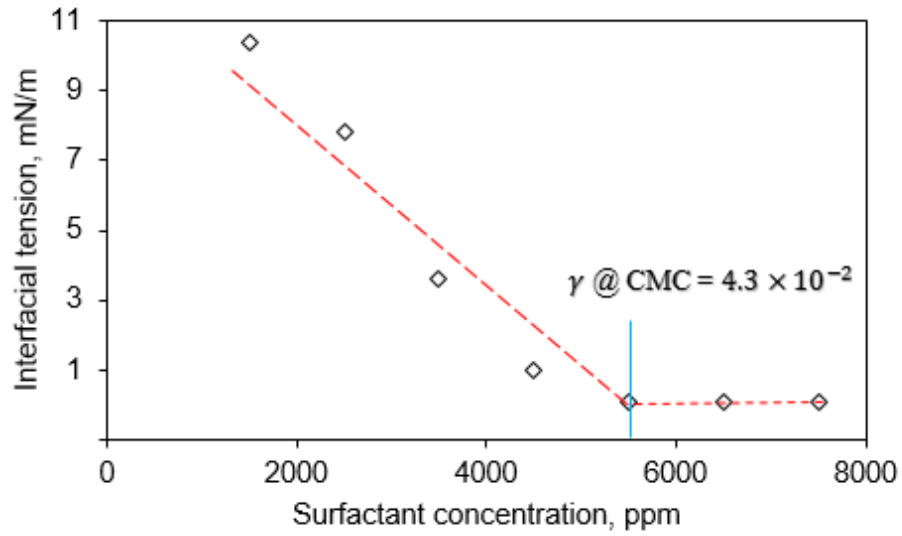


Figure 4-108: IFT curve of the surfactant solutions and crude oil at 75 °C.

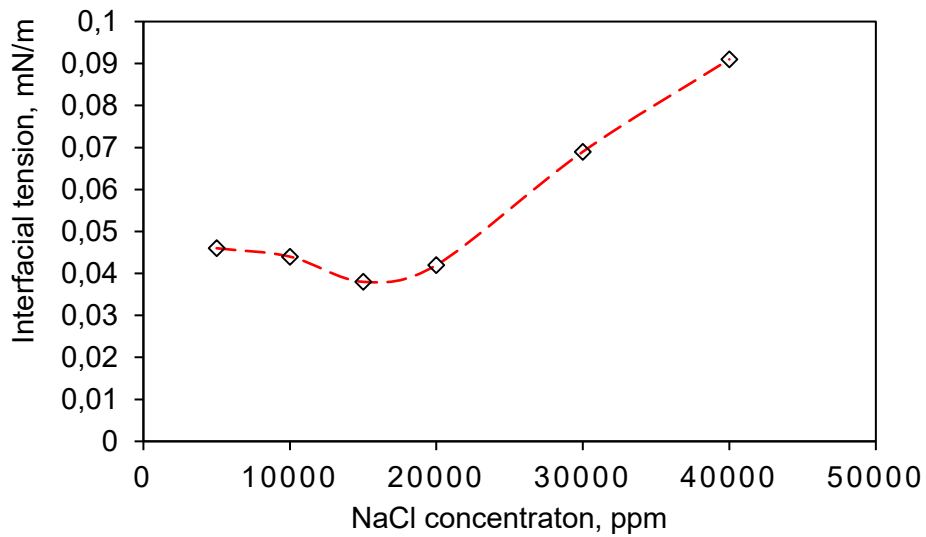


Figure 4-109: Effect of salinity on the IFT of the surfactant solution at CMC and 75 °C.

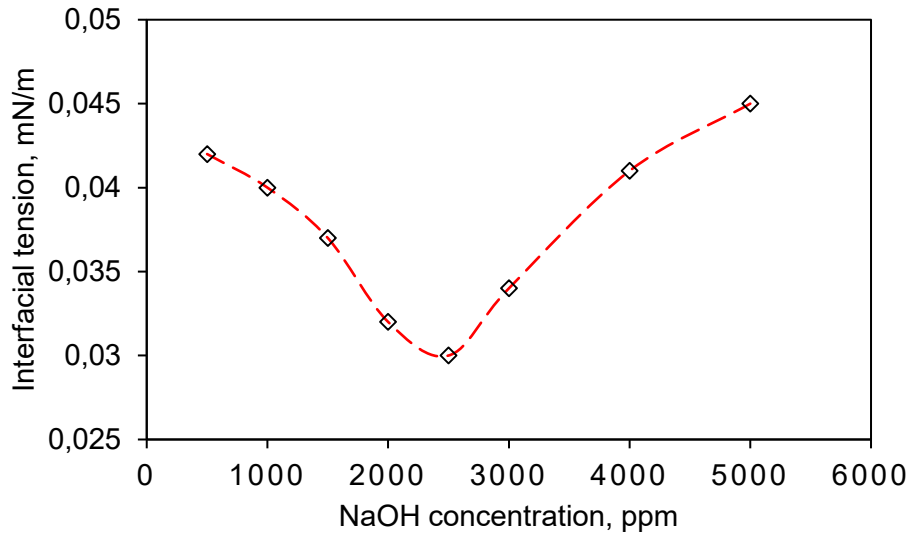


Figure 4-110: Effect of NaOH alkali on the IFT of the surfactant solution at CMC and 75 °C.

4.7.3. Contact angle

Fig. 4-111 shows the average contact angle values as a graph. Accordingly, the contact angle of the oil droplet and the cross-section over time in the surfactant solution at 15, 30, 45, 60 and 120 min were obtained 139.21, 101.65, 73.15, 43.16 and 43.11 degrees, respectively. By comparing the magnitude of the contact angle and the initial angle, after 60 min, the wettability has altered from hydrophobic to hydrophilic. Also, the diagram of contact angle changes over time shows that after 60 min there is little change in the contact angle so that only 3° of change is observed after 120 min. Therefore, 60 min can be considered as the equilibrium time. Contact angle variations over time are due to the time-varying mechanisms of the wettability alteration and interactions of surfactant molecules and the surface of the rock.

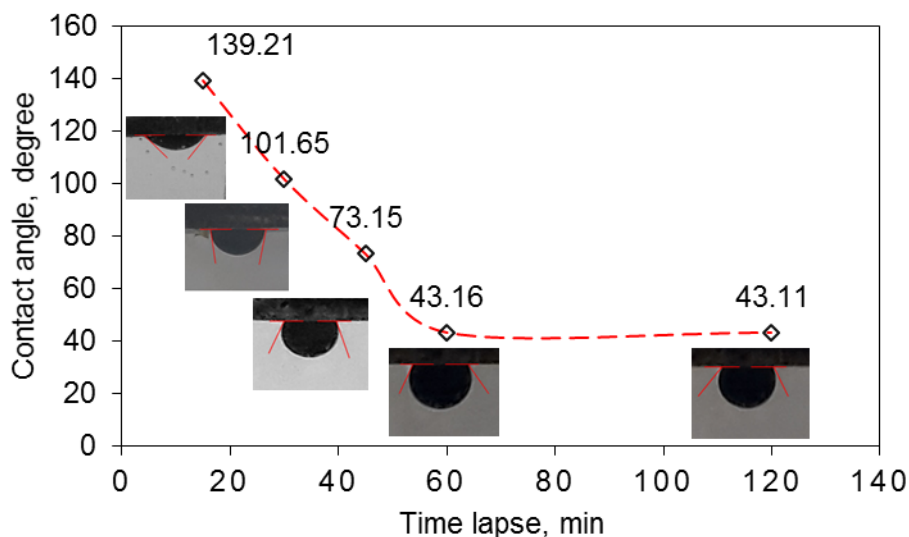


Figure 4-111: The curve of contact angle of an oil droplet on the cross-section changes in the presence of a solution of surfactant at CMC over time.

4.7.4. Nitrogen-foam characterization

Fig. 4-112 shows the height chart of N_2 -foam at different times. The height of the foam column was measured when the foam column was filled (at this moment the gas flow was cut off) and it was based on the interface of the surfactant-foam solution. Based on Fig. 4-112, the height of the foam decreases over time and reaches zero after 35 min. This time is known as half-life time foam, which is shown with $t_{1/2}$ and as shown in Fig. 4-112 for the surfactant at CMC is equal to 13 min. Foam decay depends on the initial structure of the foam. The foam structure is determined by some parameters, such as gas flow rate and soluble impurities such as salts. The effects of gas flow rate and time on bubble size were evaluated qualitatively. Given the scale of the images and the size of the bubbles, as shown in Fig. 4-113, the size of the bubbles increases over time. Over time, the effects of the forces involved in the aqueous film, such as gravity, increase the tendency of the fluid to collapse at the bottom of the foam column. On the other hand, the internal force of the gas inside the bubble to the wall, due to both the difference in the mass of gas and liquid and the movement of gas molecules, makes the film of the thinner. As a result, the gas phase ratio increases so that some bubbles with an adjacent bubble through the percolation of a liquid film form a larger bubble. Fig. 4-114 shows the effect of different gas flow rates on the size of the bubbles in the N_2 -foam formed by the surfactant at CMC immediately after filling the column of foam. The bubble images in Fig. 4-114 clearly show that with increasing gas flow rate the size of the bubbles increases. However, bubble enlargement means increasing the gas phase and decreasing the liquid phase in the foam system, which can change the foam stability. The images of Fig. 4-114 confirm the lower gas flow rate for a homogeneous-

foam creation. However, due to the qualitative nature of the survey, it is not possible to determine the exact rate according to them. Some references suggest the Gas flow rate between 20-30 ml/sec as the most suitable Gas flow rate for homogeneous foam in terms of bubble size [166]. Increasing the gas flow rate with increasing bubble size also increases foam volume. Fig. 4-115 shows the effect of gas flow rate on the volume of N₂-foam produced by the surfactant at CMC over time. Based on Fig. 4-115, as gas flow rate increases, less time is needed to fill foam columns or to reach a constant volume. For gas flow rates of 10, 20, 30 and 50 ml/sec, approximately 55, 40, 30 and 20 seconds are needed to fill foam columns, respectively.

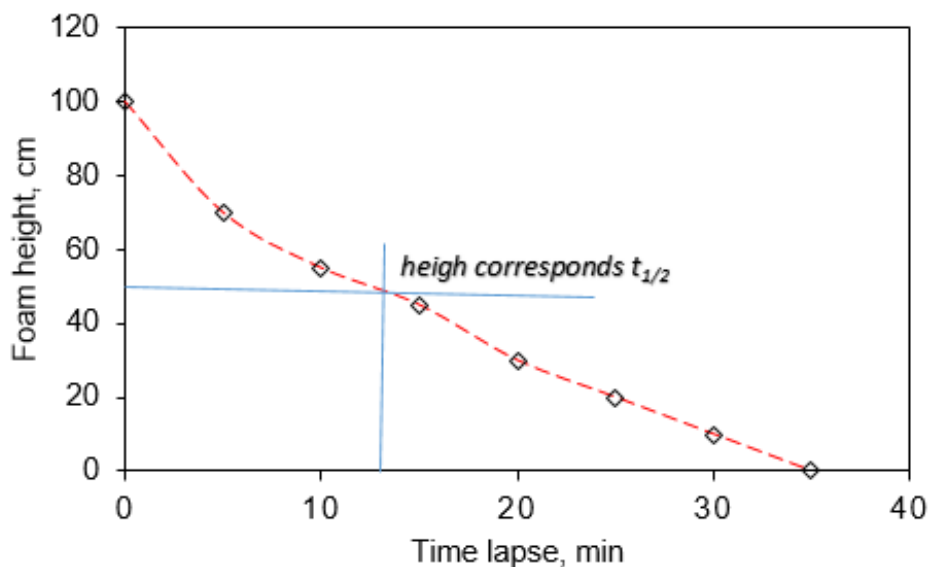


Figure 4-112: The curve of N₂-foam height formed by surfactant at CMC over time.

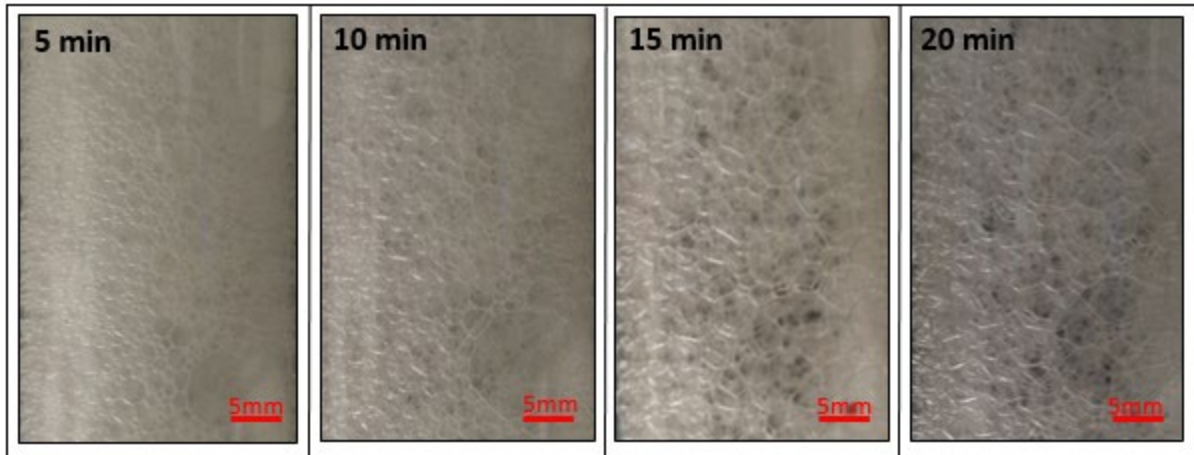


Figure 4-113: Time-effect on bubble size of N_2 -foam generated by the surfactant at CMC and optimum salinity and gas flow rate equal to 10ml/sec.

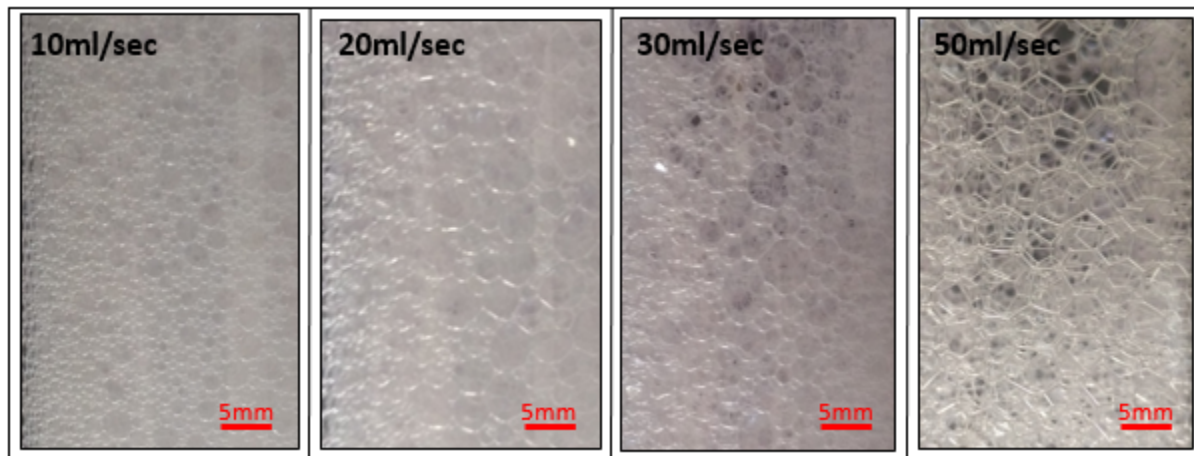


Figure 4-114: Effect of different gas flow rates on the size of the bubbles in the N_2 -foam generated by the surfactant at CMC immediately after filling the column of foam.

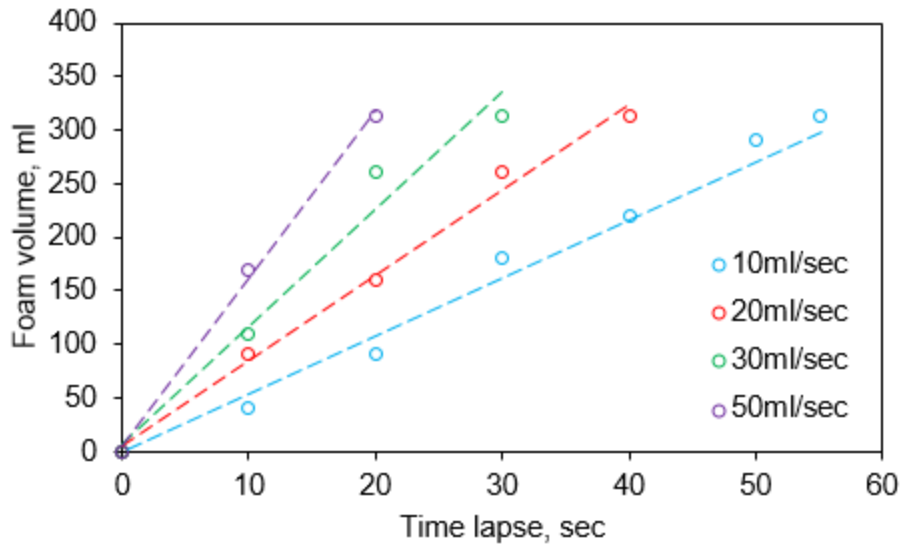


Figure 4-115: Gas flow rate effect on the volume of N₂-foam generated by surfactant at CMC over time.

4.7.5. Compatibility and emulsion stability

Fig. 4-116 shows the results of experiments of compatibility with formation water and saline water at different NaCl concentrations. Based on the results, after 2 weeks of mixing the solution of surfactant with saline samples at 75 °C, the surfactant compatibility with formation water is confirmed because the sediment is not seen in the solution. With increasing salinity of 20,000, 30,000, 50000, 70000 and 100,000 ppm, the solution remains consistent. The sediment was observed for solutions of 130,000 and 160000 ppm, at 0.1417 and 0.2376 g, respectively. This means that the surfactant for reservoirs with a salinity of less than 130000 ppm is applicable and after this critical salinity, the formation of sediment occurs and pore plugging may occur in the reservoir.

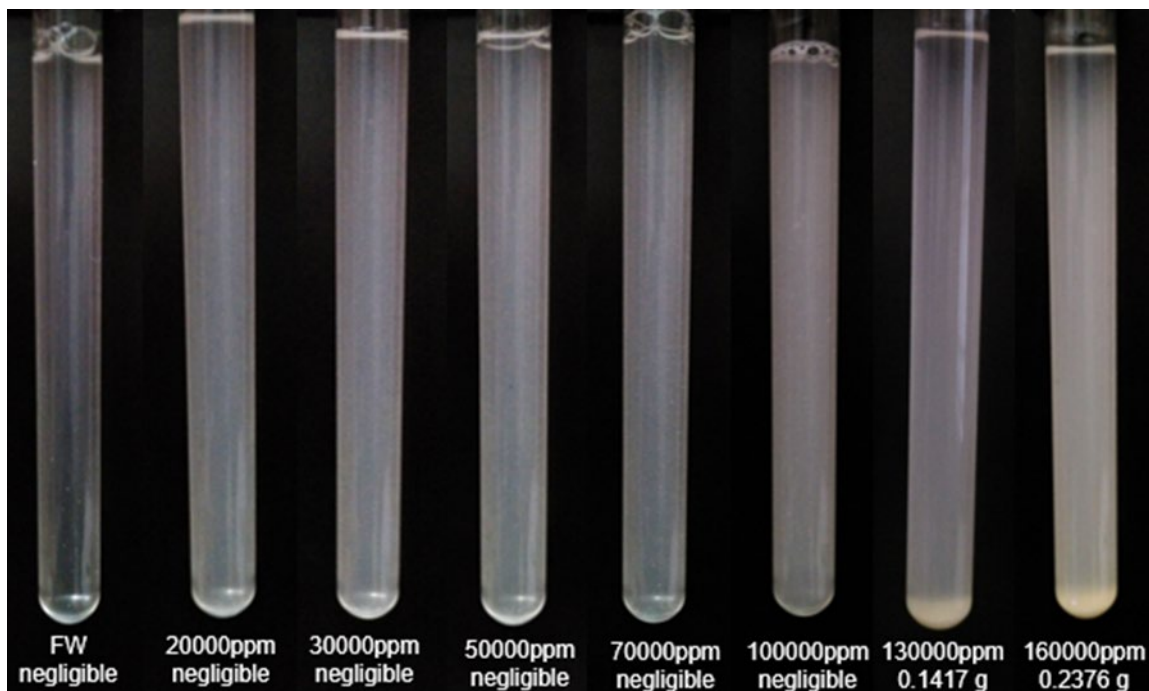


Figure 4-116: Compatibility of a solution of the surfactant at CMC with different salinity at 75 °C.

Fig. 4-117 shows the stability of the emulsion formed by the surfactant solution at CMC and crude oil over time. The first phase separation and exit from the monophasic mode occurred after 5 days. After that, the three phases of oil, water, and the middle are in the system. As time goes on, the volume of the oil and water phase increases and the volume of the middle phase decreases accordingly. In these experiments, the exact amount of phases cannot be determined, but the separation of the three phases can be distinguished from one another. The acceptable stability of the emulsion is confirmed after 25 days of complete phase separation.

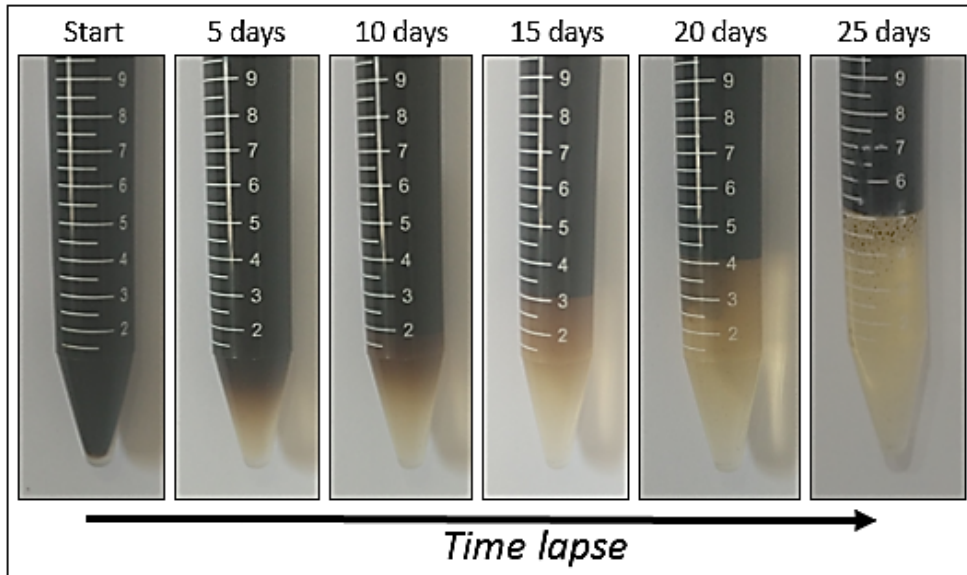


Figure 4-117: Emulsion stability of a surfactant solution at CMC and crude oil over time.

4.7.6. Oil recovery by ASP injection

Fig. 4-118 shows the oil recovery and the pressure drop in the flood versus injected fluid volume. The injection test was done in a carbonate plug with a length of 7 cm, a diameter of 1.5in, an effective porosity of 18.4%, an effective pore volume of 14.67 cm³, an absolute permeability of 5.39 md, initial water saturation of 16%, and an original oil in place of 12.2 cm³. Secondary brine injection increased oil recovery by 44.7%. An ASP injection of 0.5 PV was continued and the brine was injected again. A final recovery factor of 62.5% was obtained which is 17.8% belongs to the tertiary injection.

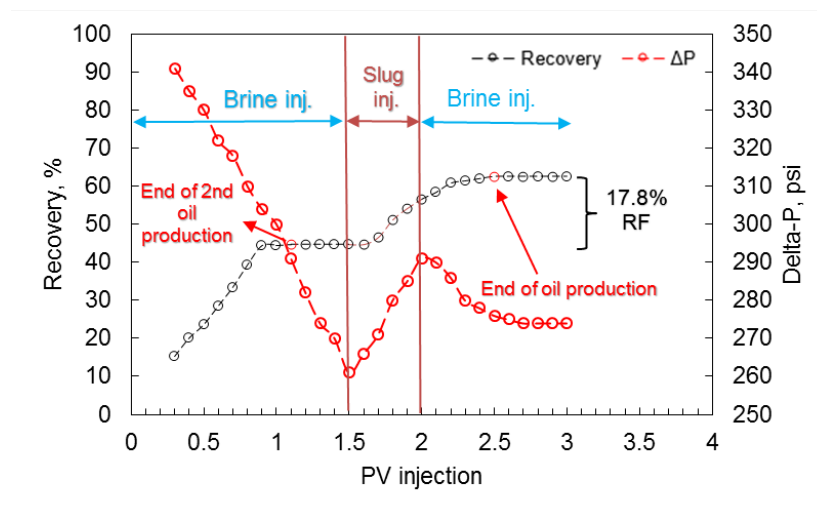


Figure 4-118: Oil recovery curve for injectable PV in the chemical ASP slug injection.

4.8. Synthesized fluorinated surfactant

4.8.1. FTIR and TGA analyses

Fig. 4-119 shows the FTIR analysis of the synthesized surfactant. Peak (a) at 746.30 cm^{-1} shows the flexural vibration stretching of C–F. Peaks (c) at 1015.83 cm^{-1} and (d) at 1056.41 cm^{-1} are stretching peaks of S–O. Peaks (b) at 983.70 cm^{-1} , (e) at 1202.61 cm^{-1} , (f) at 1193.19 cm^{-1} , and (g) at 1251.08 cm^{-1} represent the stretching of C–F bonds. Peak (h) at 1512.07 cm^{-1} represents the stretching bond C=C in the benzene ring. Peak (i) at 1602.39 cm^{-1} is related to the stretching of the C=C bond in perfluorononene.

Fig. 4-120 shows the TGA analysis of the surfactant. F-surfactants normally have high-temperature stability. As shown in Fig. 4-120, the total weight loss at $300\text{ }^{\circ}\text{C}$ reaches only 28% of the initial weight. A temperature peak starts at $25\text{ }^{\circ}\text{C}$ and continues up to about $150\text{ }^{\circ}\text{C}$, with the weight loss of this temperature peak reaching about 8%. Weight loss at this stage is justified by the evaporation of the sample moisture. According to these interpretations, the surfactant is suitable for use at temperatures of condensate gas reservoirs in terms of temperature stability.

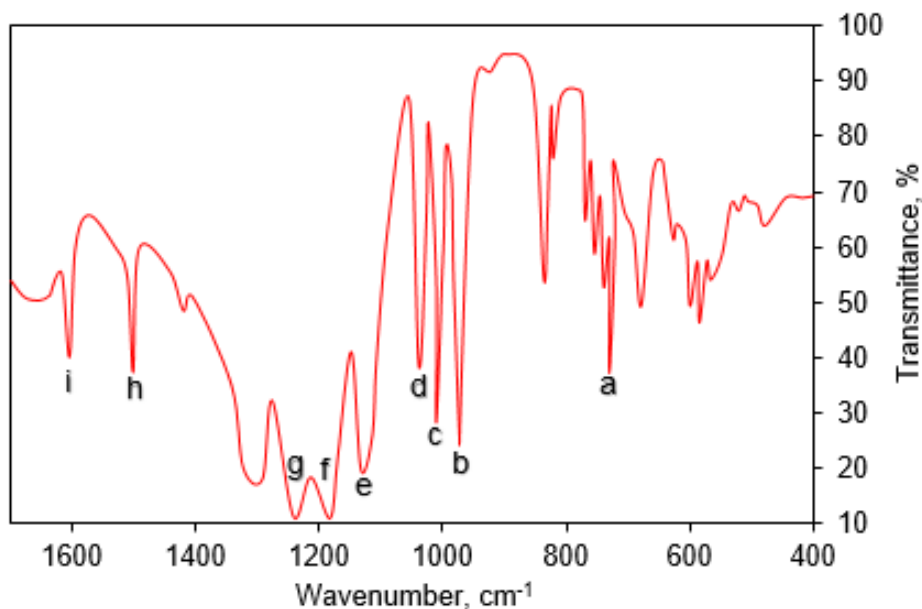


Figure 4-119: FTIR analysis of the F-surfactant.

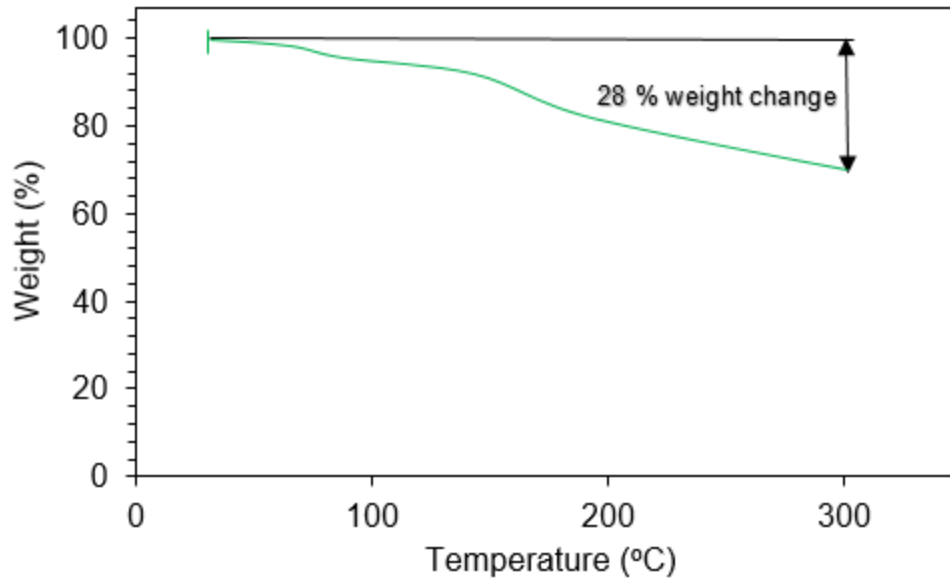


Figure 4-120: TGA analysis of the F-surfactant.

4.8.2. Surface tension and contact angle results

The results of surface tension experiments are plotted in Fig. 4-121. The steep slope decreases with increasing surfactant concentration in the surface tension graph up to a concentration of 3500 ppm. The curve is then almost horizontal and the surface tension variations are negligible. This is a common trend in surface tension versus concentration curves.

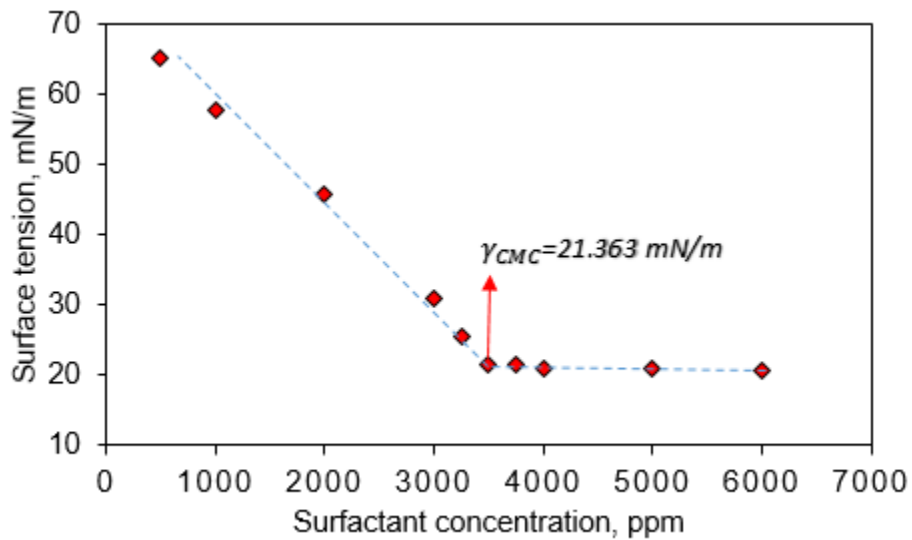


Figure 4-121: Surface tension curve of surfactant solutions at ambient pressure and temperature.

Table 4-21 shows the values obtained from the contact angle experiments. Parameters of temperature, treatment time and surfactant concentration were considered in these experiments. Figs 4-122 to 4-124 show the data in this table as graphs at temperatures of 313, 343 and 373 K, respectively. Based on the results, there is a clear relationship between the parameters and the contact angle. Thus, the contact angle decreases with increasing temperature and increases with increasing surfactant concentration and treatment time. That is to say, strongly gas-wetting was achieved by increasing surfactant concentration and treatment time and by decreasing temperature. However, the change in contact angle after CMC and the specific duration for each concentration is less. In the statistical evaluation, Table 4-21 and Fig. 4-122 show that at 313 K, the final values of contact angle, i.e. 240 min after treatment, for concentrations of 500, 1500, 2500, 3500, 4500, 5500 and 6500 ppm, equivalent to 94.08, 105.56, 112.70, 121.97, 122.17, 124.61 and 124.72, respectively. Given the constant concentration at CMC, contact angles at treatment times of 30, 60, 120 and 240 min were obtained as 101.83, 108.04, 114.86 and 121.97 degrees, respectively. Similarly, according to the data in Table 4-21 and Fig. 4-123 at 343 K, the final values of contact angle, for concentrations of 500, 1500, 2500, 3500, 4500, 5500 and 6500 ppm, equal to 88.22, 100.79, 108.71, 111.72, 113.85, 115.77 and 116.79 degrees were obtained, respectively. At CMC the contact angles at treatment times of 30, 60, 120 and 240 min equal to 91.70, 100.39, 106.80 and 111.72 degrees were obtained, respectively. Also, according to Table 4-21 and Fig. 4-124 at 373 K, the final contact angle values for concentrations of 500, 1500, 2500, 3500, 4500, 5500 and 6500 ppm were obtained 77.08, 94.58, 100.11, 106.03, 112.72, 114.91 and 115.48 degrees, respectively. At the constant concentration of CMC the contact angles at treatment times of 30, 60, 120 and 240 min were obtained 87.94, 93.50, 99.79 and 106.03 degrees, respectively. With these interpretations, the obtained angles are in the range of intermediate to almost strong gas-wetting proportional to the variables investigated and the said dependencies. For a better understanding of the subject, images of the contact angle of the final treatment time of 240 min at different surfactant concentrations and temperatures are given in Fig. 4-125.

Table 4: Liquid droplet contact angle values on treated carbonate sections in surfactant solutions with different concentrations at temperatures of 313, 343 and 373 K.

T [K]	Treatment time [min]	Contact angle [Degree]						
		Surfactant concentration [ppm]						
		500	1500	2500	3500	4500	5500	6500
313	30	75.28	87.29	92.94	101.83	101.94	102.85	103.22
	60	81.67	92.72	98.61	108.04	110.48	111.06	112.76
	120	88.45	100.03	105.39	114.86	115.27	115.97	116.21
	240	94.08	105.56	112.70	121.97	122.17	124.61	124.72
343	30	69.41	81.07	86.05	91.70	91.80	92.45	92.76
	60	72.36	86.65	90.94	100.39	102.14	102.70	103.69
	120	79.01	93.40	101.96	106.80	106.95	107.06	107.77
	240	88.22	100.79	108.71	111.72	113.85	115.77	116.79
373	30	61.14	75.09	86.19	87.94	88.25	88.91	89.20
	60	69.43	81.60	91.32	93.12	93.50	93.81	95.07
	120	73.22	89.15	96.60	99.79	101.39	102.17	102.29
	240	77.08	94.58	100.11	106.03	112.72	114.91	115.48

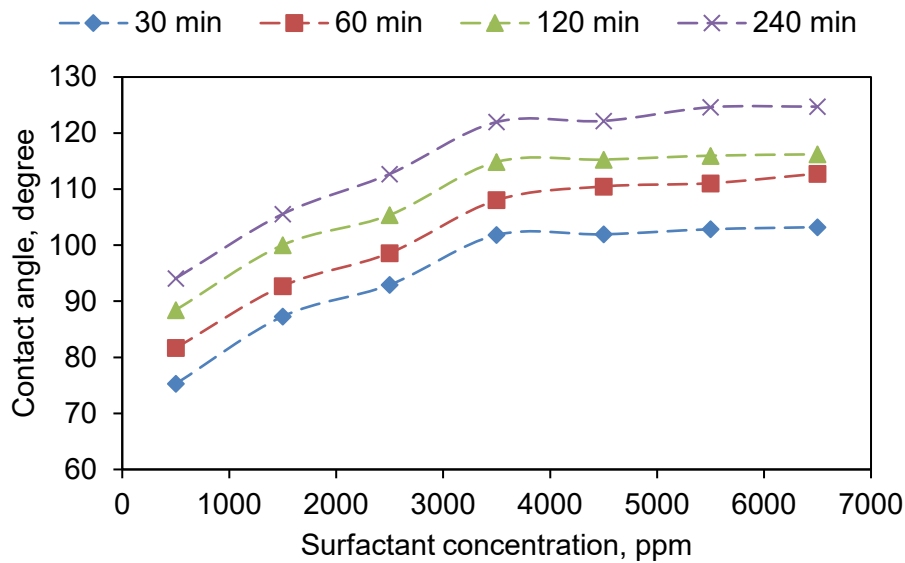


Figure 4-122: Diagram of contact angle values of liquid droplets on treated cross-sections in surfactant solutions at different concentrations at 333 K.

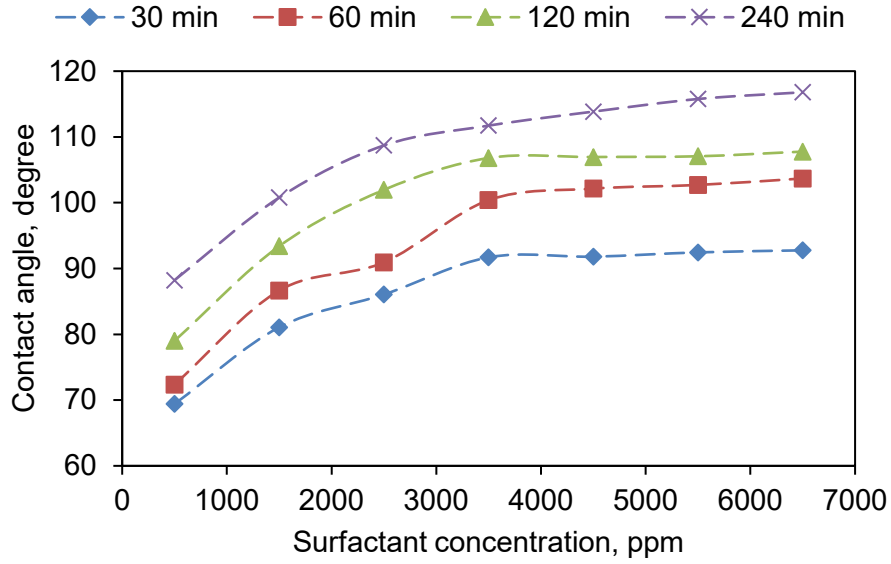


Figure 4-123: Diagram of contact angle values of liquid droplets on treated cross-sections in surfactant solutions at different concentrations at 343 K.

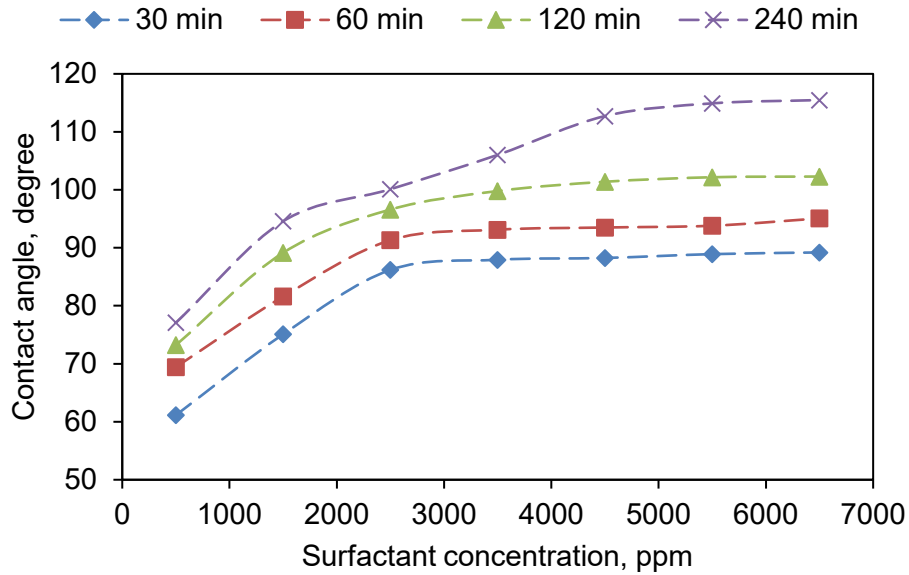


Figure 4-124: Diagram of contact angle values of liquid droplets on treated cross-sections in surfactant solutions at different concentrations at 373 K.

T [K]	Surfactant concentration [ppm]						
	500	1500	2500	3500	4500	5500	6500
313							
343							
373							

Figure 4-125: Liquid droplet images on the treated sections in surfactant solutions at different concentrations and at temperatures of 313, 343 and 373 K and treatment time equal to 240 min.

4.8.3. Surfactant adsorption in carbonate porous media

Fig. 4-126 shows diagrams of the conductivity values of surfactant solutions at different concentrations and temperatures of 313, 343 and 373 K. This graph was used as the calibration graph to estimate the unknown concentration in the adsorption experiments. According to the figure, the conductivity of surfactant solutions is directly related to concentration and temperature. Breakpoint in the chart shows the CMC value. The trend-lines for the points before and after the breakpoint follow two distinct equations. The sudden change of slope due to micelle binding and the formation of agglomerates and less micelle mobility compared to the surfactant monomers is justified [192]. As temperatures increase, the molecules move faster and have more freedom, so micelles are expected to become more difficult to form at lower temperatures, increasing CMC. Fig. 4-127 shows the adsorption values in the porous media during the flooding of the surfactant solution at CMC and temperatures of 313, 343 and 373 K. There is a clear trend for absorption values with the increasing amount of injection fluid. It can be said that the cumulative adsorption increases with increasing injection fluid, but the adsorption is lower in each step than before. In other words, as the flooding continues, the surface of the rock is rapidly occupied by the adsorption of surfactant molecules onto the surface, thereby increasing the ratio of the occupied surface to the unoccupied surface and eventually achieves to saturation. As the unoccupied surface decreases, the adsorption-to-PV injection ratio decreases, resulting in a lower slope at the ends of the graph. The layer formed by the adsorption of the surfactant on the rock surface creates a coating that is opposite to the initial wettability.

Table 4-22: Characteristics of carbonate plugs used in surfactant adsorption in porous media measurements.

Plug No.	K [mD]	Porosity [%]	L [cm]	Effective PV [cm ³]	Injection Tem. [K]
#1	9.68	22.46	7	17.91	313
#2	9.50	22.75	7	18.14	343
#3	9.23	22.61	7	18.03	373

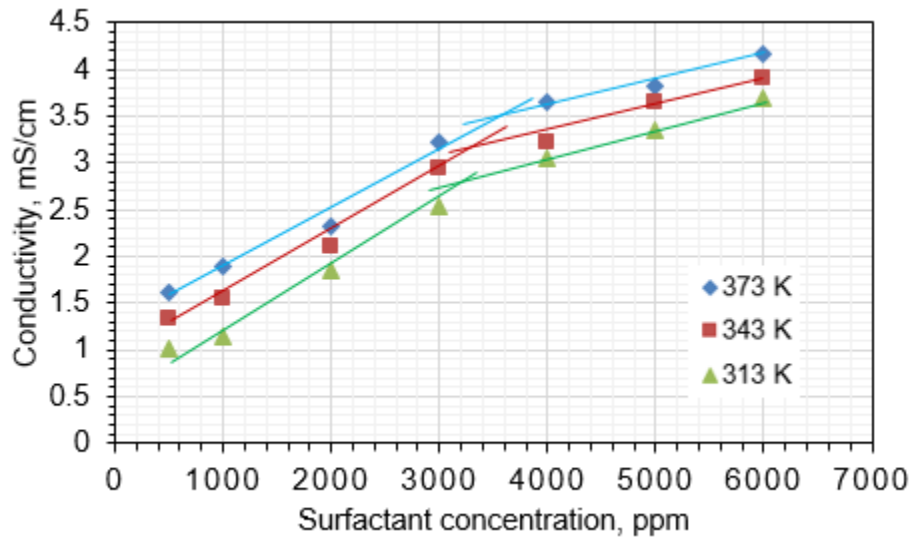


Figure 4-126: Conductivity diagram of surfactant solutions at different concentrations.

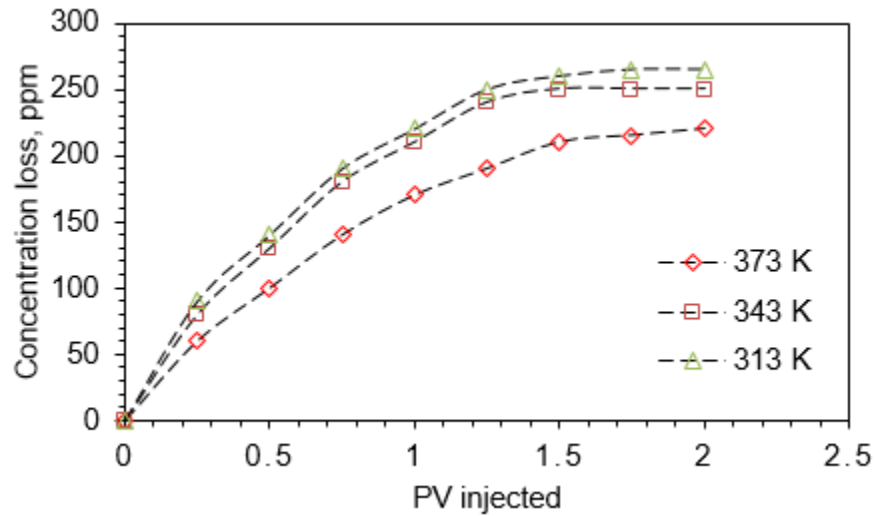


Figure 4-127: Decrease of surfactant concentration at CMC due to adsorption in porous media.

4.8.4. Foam stability

Fig. 4-128 shows the foam height diagram after filling the 100 cm foam column over time. The formation of stable foam by F-surfactants is due to their dual gasphilic-hydrophilic structure. According to Fig. 4-128, the foam height decreases over time and reaches zero after 60 min. During the decay of foam height at one point, the foam height reaches half the initial height. This time is known as the half-life time of the foam, denoted by $t_{1/2}$, and as shown in Fig. 4-128 for the surfactant at CMC equals 13 min.

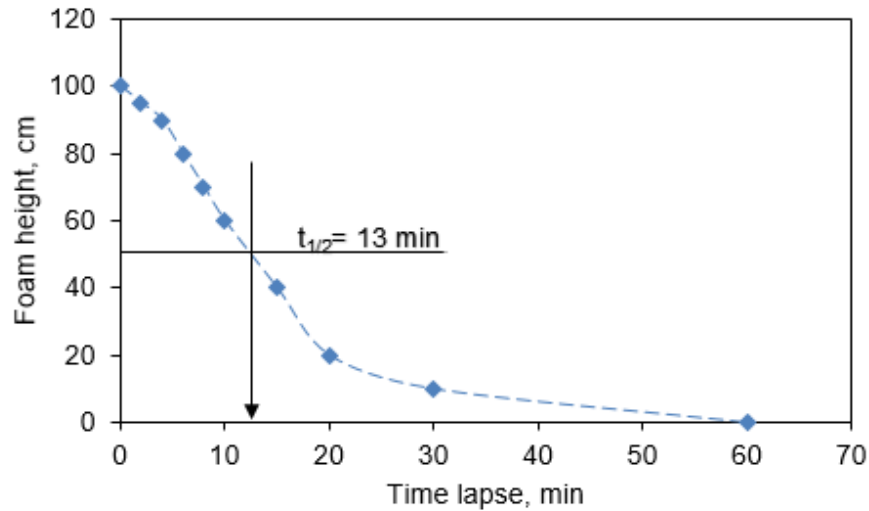


Figure 4-128: Foam height diagram over time.

4.8.5. Imbibition tests results

Fig. 4-129 shows the diagrams of imbibition in treated and untreated plugs over time. The curve of imbibition in untreated 7 cm length, 18.21% effective porosity and 7.3 mD permeability plug show that the liquid imbibition at the very beginning of the test. The curve has a very steep upward slope in the early minutes. Over time, the intensity of the slope decreases so that after 480 min, approximately 91% of the effective plug space volume is saturated with the liquid, leaving a small amount of it empty. The initial wettability of water-wetting and the difference in liquid and gas density justify this process. But it is completely different for the treated plug with a length of 7 cm, effective porosity of 18.53% and the permeability of 7.1 mD and initial wettability. The treated plug after 60 min the start of the experiment has almost no effective filling with liquid. The imbibition was stopped 300 min after the start of the experiment, with only 2% of the effective plug space being saturated with liquid. Wettability alteration to gas-wetting

has caused the non-wetting to no longer enter the plug and, the imbibition, which is caused by liquid wetting, cannot be carried out.

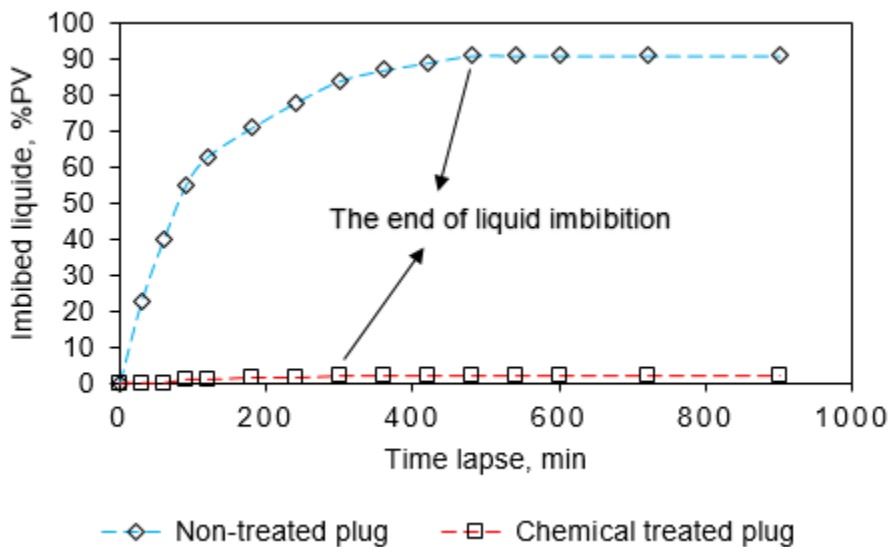


Figure 4-129: the results of gas-liquid imbibition in non-treated and chemical treated plugs.

3.1. Extracted mucilage from Hollyhocks plant as a natural polymer

3.1.1. Characterization

As mentioned earlier, FTIR was used to define the functional groups in the natural polymer composition. Figure 4-130 shows the FTIR analysis. The hydroxyl functional group, -OH bond, is represented by a peak at 3430 cm^{-1} [204]. The peak at 2925 cm^{-1} is related to the stretching vibrations of C-H [205]. The peaks at 1643 cm^{-1} and 1540 cm^{-1} indicate the asymmetric vibrations of carboxylic acid [206]. Also, the peak at 1643 cm^{-1} is related to N-H stretching and bending motions [207]. The peak, which appears at 1442 cm^{-1} , is related to C-O stretching and O-H deformation vibrations [204]. C-N stretching modes are defined by the peak at 1392 cm^{-1} [208]. C-O stretching and O-H deformation vibrations are shown with the peak at 1285 cm^{-1} [204]. The peak at 1055 cm^{-1} is related to the presence of monosaccharides such as mannose and glucose in pyranose ring conformations [209]. The peak at 895 cm^{-1} indicates β -dglucose and finally, the peak at 643 cm^{-1} is related to O-H out-of-plane vibrations [206].

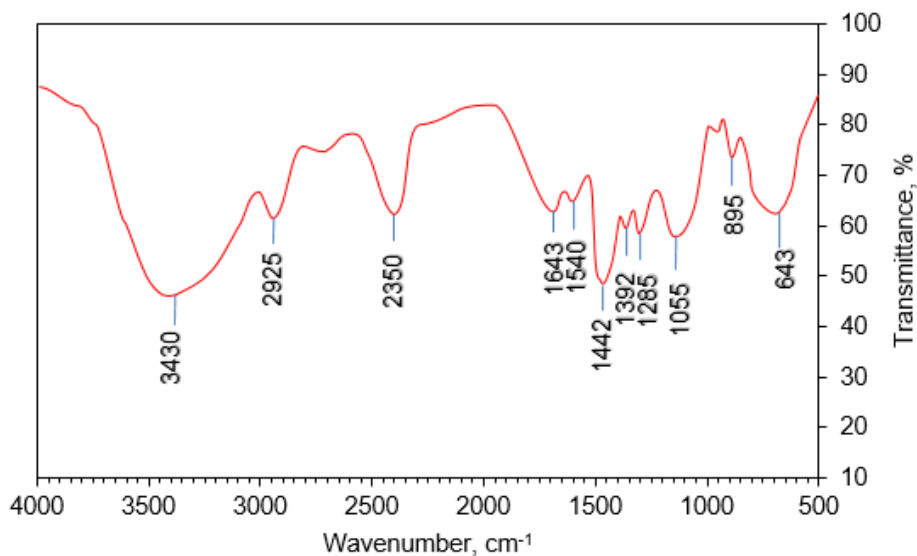


Figure 4-130: FTIR analysis of the natural polymer.

Figure 4-131 shows the weight change curve of the polymer sample against the increase in temperature associated with TGA. The five temperature peaks of 20-129, 130-224, 225-341, 341-417 and 418-600 °C are seen in Figure 4-131. Considering the weight loss of 9% in the peak temperature of 20-129 °C, it can be attributed to the evaporation of polymer sample moisture. This moisture is due to the adsorption of water from the atmosphere by the saccharide structure [210, 211]. With this interpretation, and considering the temperature range of the oil reservoirs, the temperature stability of the polymer is confirmed. Subsequent peaks are related to the destruction of the molecular structure of short-chain monomers and then to long-chain polysaccharides and their conversion into lighter components. The final peaks are related to the polymer oxidation and decomposition [212, 213]. To study the application of a polymer in EOR, initial temperature peaks and polymer weight changes in these peaks are more important than the final peaks related to high temperatures, because the temperature of most reservoirs is within the range of primary peaks.

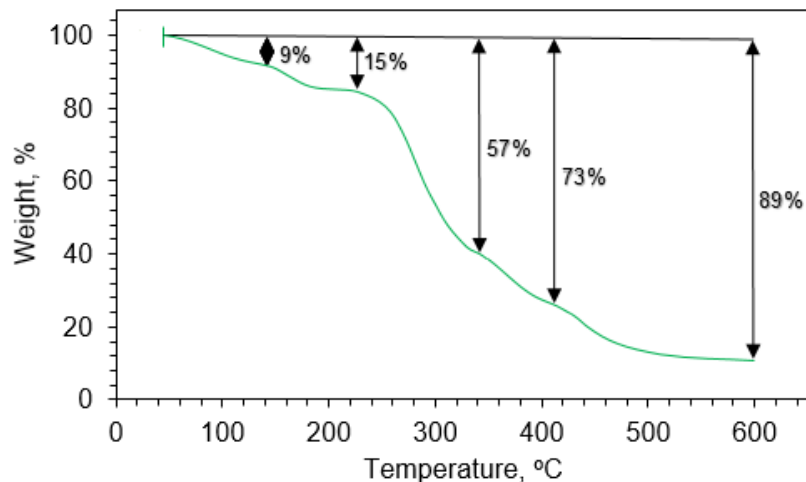


Figure 4-131: TGA of the natural polymer.

3.1.2. Viscous behavior

As mentioned earlier, the viscosity of the injection phase plays a very important role in increasing the sweep efficiency and preventing early water production. In the preparation of polymeric solutions containing mucilage, hydration time is an effective factor in increasing the viscosity because the process of water absorption by the polymer is time-consuming. Table 4-23 shows the viscosity values of the polymeric solutions at hydration times of 6, 12, and 24 h at a constant temperature of 30 °C. Figures 4-132 – 4-134 show the data in this table in the log-log charts. Changes in the parameters of hydration time, polymer concentration and shear rate were included in these experiments. The results show that the viscosity increases significantly with increasing hydration time. Besides, the viscosity of the solutions increases with increasing polymer concentration. The viscosity values of immature solutions, i.e. solutions with a hydration time of 6 and 12 hours, regardless of the amount, are not important for EOR operations. Because of the use of these active solutions and by changing (increasing) the viscosity, problems such as blockage of pipes and equipment can be caused if the solutions become mature during operation by absorbing water and reach their maximum viscosity. Therefore, it is necessary to estimate the final time of maturity to prevent this problem. Polymeric solutions did not have significant viscosity changes after 24 h, and accordingly, 24 h was sufficient as the final time of hydration. However, the viscosity values after 6 h at concentrations of 500, 1000, 2000 and 3000 ppm and the lowest shear rate were obtained 20.51, 31.17, 80.46 and 103.28 mPa.s, respectively. These values after 12 h were 47.14, 70.29, 125.21 and 216.79 mPa.s, respectively. Finally, after 24 h, the viscosity values for polymeric solutions with concentrations of 500, 1000, 2000 and 3000 ppm and at the lowest shear rate were 63.07, 86.82, 137.90 and 232.46 mPa.s, respectively. The mechanism for increasing the viscosity of aqueous solutions by mucilage is related to its complex molecular structure. Mucilage is a combination of polar glycoproteins, polysaccharides, pectin and sometimes mineral elements such as calcium, potassium and nitrogen. There are two soluble and insoluble parts in the mucilage structure. The insoluble part swells with water absorption and forms hydrocolloid [214]. Hydrocolloids are defined as colloidal systems in which the colloidal particles are hydrophilic polymers or hydrophilic scattered in water. This mucilage structure can increase the water viscosity from low to infinite (depending on the structure). However, the soluble part of mucilage does not

have much effect on viscosity. With this interpretation, the solubility of mucilage in water determines its ability to form hydrocolloids and increase viscosity. Temperature is a very effective parameter on the solubility of mucilage in water so that these compounds become more swollen at low temperatures and form a jelly material while dissolved in hot water, they form lower viscosity colloidal solutions that re-jelly if the temperature drops.

Table 4-23: Viscosity values of the polymeric solutions at different hydration times and 30 °C.

		Viscosity, mPa.s							
Shear rate, s ⁻¹		2	5	10	20	40	80	160	320
Time, h	Conc., ppm								
6	500	20.51	19.93	19.04	18.56	18.10	17.34	16.55	15.16
	1000	31.17	28.75	27.12	26.50	25.26	22.80	20.14	18.37
	2000	80.46	76.14	73.19	70.35	65.57	61.30	55.76	51.69
	3000	103.28	100.49	96.33	90.61	84.20	78.62	71.75	66.15
12	500	47.14	43.61	40.59	38.27	32.34	27.68	22.56	18.91
	1000	70.29	67.18	62.50	57.93	51.75	46.37	40.68	33.17
	2000	125.21	116.31	110.14	102.29	95.94	88.13	81.22	74.05
	3000	216.79	209.74	200.15	191.67	182.05	173.94	161.83	150.11
24	500	63.07	61.38	57.54	52.49	47.06	41.10	36.13	30.95
	1000	86.82	81.05	76.56	71.93	66.51	59.19	51.27	42.66
	2000	137.90	130.73	121.21	110.52	98.44	85.25	77.30	70.39
	3000	232.46	222.38	214.62	201.19	189.72	175.84	162.67	151.81

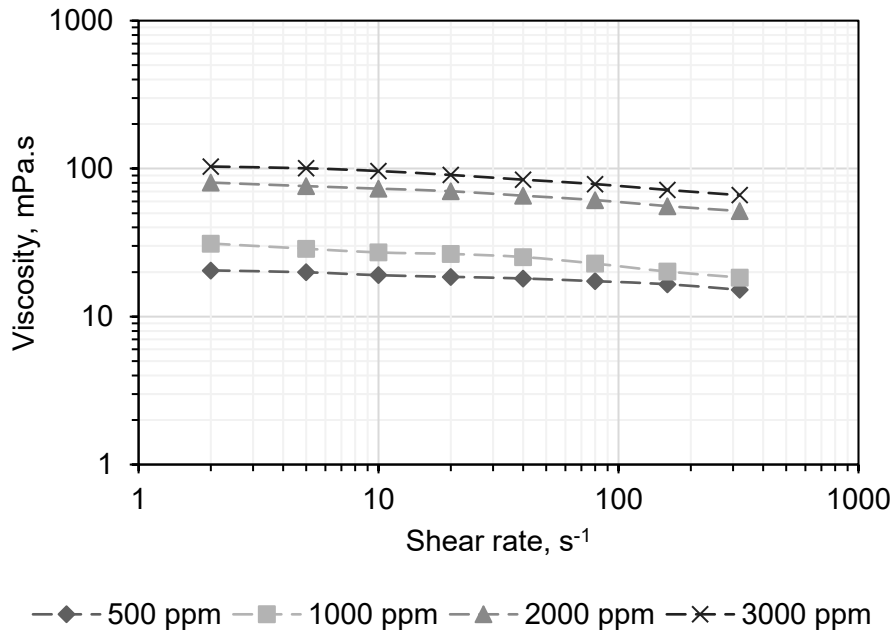


Figure 4-132: Viscosity changes curves of the polymeric solutions in different concentrations against shear rate changes at hydration time equal to 6 h and 30 °C.

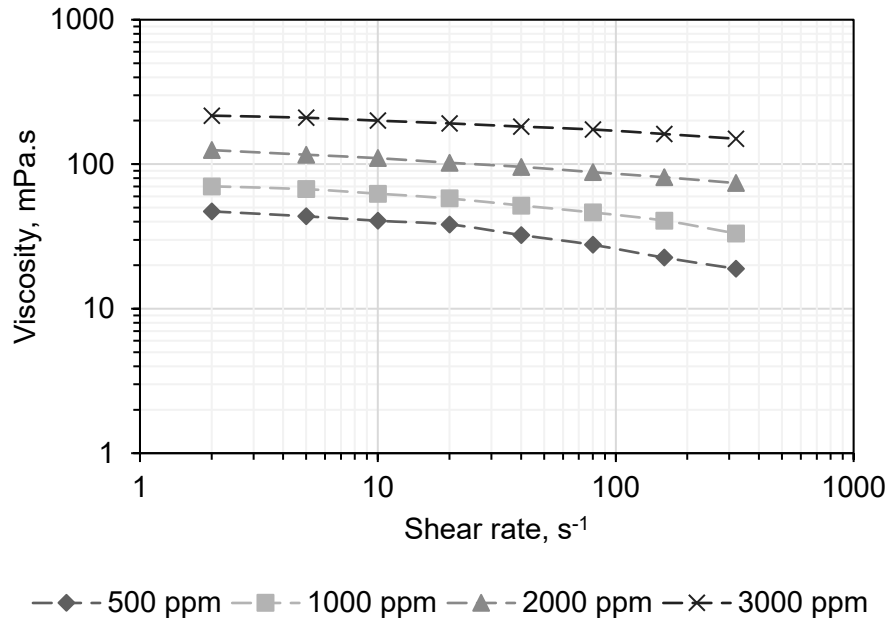


Figure 4-133: Viscosity changes curves of the polymeric solutions in different concentrations against shear rate changes at hydration time equal to 12 h and 30 °C.

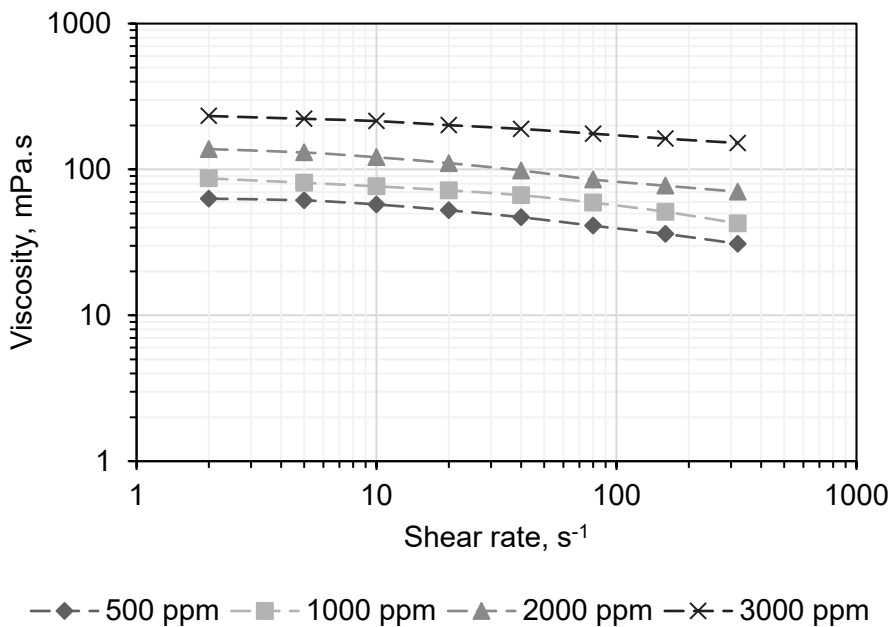


Figure 4-134: Viscosity changes curves of the polymeric solutions in different concentrations against shear rate changes at hydration time equal to 24 h and 30 °C.

Table 4-24 and Figures 4-135 and 4-136 show the effect of temperature on the polymeric solutions. Due to the appropriate time for maturity and complete hydration in previous experiments, the hydration time in

these experiments was considered to be 24 h. As can be seen, the viscosity of the solutions decreases with increasing temperature, and the process is following the mechanism of solubility of mucilage with increasing temperature. Despite the significant decrease in viscosity against temperature, the values obtained even at 80 °C are several tens of times higher than the water and surfactant solutions viscosity. This confirms the effectiveness of mucilage at reservoir temperatures. Although mucilage is a plant compound, it exhibits good temperature stability and has a relatively high viscosity at high temperatures. The reason for this could be the presence of high molecular weight polysaccharides in their composition. High molecular weight allows polysaccharides to form a thick stabilizing layer and protect jelly-coated particles from heat shock [215]. Numerical studies of Table 4-24 and Figures 4-135 and 4-136 show that at the lowest shear rate and 50 °C, the viscosity values of the solutions at the polymer concentrations of 500, 1000, 2000 and 3000 ppm were 55.13, 80.61, 123.66 and 208.79 mPa.s, respectively. As temperatures rose to 80 °C, these values reached 43.80, 67.05, 105.12, and 194.83 mPa.s, respectively. The salinity effect is another parameter studied on the efficiency of the natural polymer in increasing the viscosity of the injection phase. The salinity effect on polymer performance in ASP-slug injection is important in two ways. The first case is the adjusted salinity of the slug based on the optimal salinity of the surfactant and the second case is the salinity of the FW.

Table 4-24: The viscosity values of the polymeric solutions at hydration time of 24h and different temperatures.

		Viscosity, mPa.s							
Shear rate, s ⁻¹		2	5	10	20	40	80	160	320
Tem, °C	Conc., ppm								
30	500	63.07	61.38	57.54	52.49	47.06	41.10	36.13	30.95
	1000	86.82	81.05	76.56	71.93	66.51	59.19	51.27	42.66
	2000	137.90	120.73	121.21	110.52	98.44	85.25	77.30	70.39
	3000	232.46	222.38	214.62	201.19	189.72	175.84	162.67	151.81
50	500	55.13	54.49	52.60	50.71	44.62	39.37	32.18	24.94
	1000	80.61	76.54	72.70	68.85	63.28	55.92	44.35	38.16
	2000	123.66	116.12	108.54	100.61	91.32	80.25	69.90	63.47
	3000	208.79	201.28	194.15	185.95	174.33	162.50	149.10	135.98
80	500	43.80	41.95	39.60	37.41	33.53	29.12	23.42	18.78
	1000	67.05	64.52	60.19	55.47	49.58	41.32	38.77	31.15
	2000	105.12	101.53	94.37	88.19	81.60	72.46	61.92	53.48
	3000	194.83	190.62	184.73	173.59	163.80	153.67	138.60	129.36

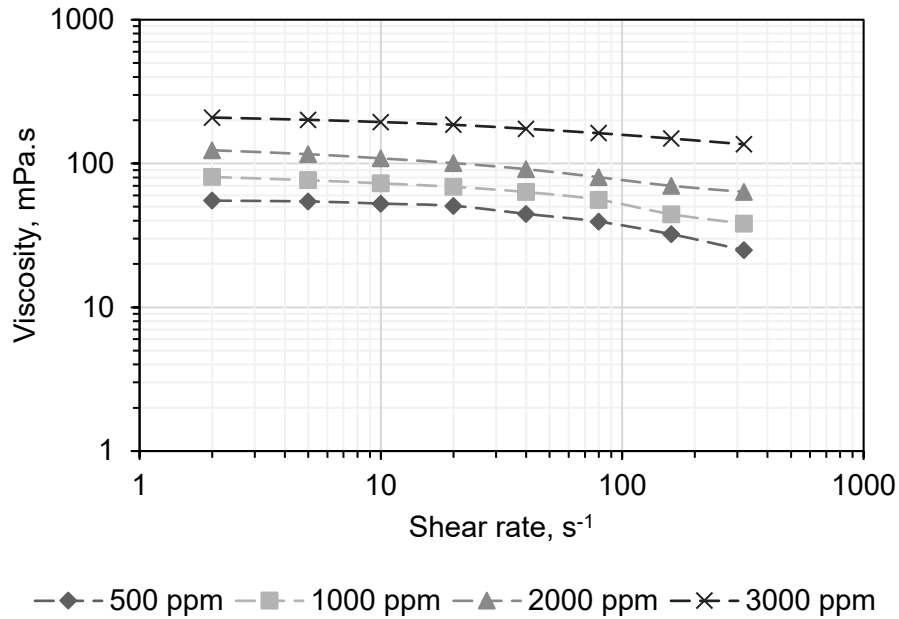


Figure 4-135: Viscosity changes curves of the polymeric solutions at different concentrations against shear rate changes at hydration time of 24 h and 50 °C.

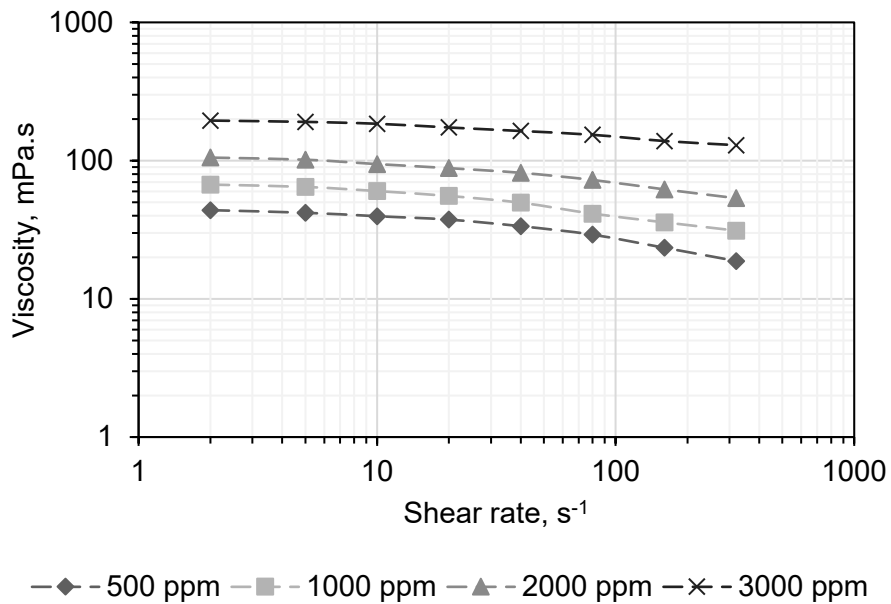


Figure 4-136: Viscosity changes curves of the polymeric solutions at different concentrations against shear rate changes at hydration time of 24 h and 80 °C.

Table 4-25 and Figures 4-137 – 4-139 show the effects of different salinities of FW at the initial concentration and diluted samples. Based on the results, with increasing salinity, the viscosity of the

polymeric solutions decreases. However, the viscosity values are still much higher than the saline water viscosity. Taking into account the shear rate at the lowest value and temperature of 80 °C, the viscosity values of the polymeric solutions at concentrations of 500, 1000, 2000 and 3000 ppm and the salinity of the FW were 28.50, 52.68, 90.91 and 167.10 mPa.s, respectively. By reducing the salinity to 5-times diluted, the viscosity values at the lowest shear rate and 80 °C and at concentrations of 500, 1000, 2000 and 3000ppm were obtained 34.15, 61.42, 93.94 and 178.91 mPa.s, respectively. These values at the salinity of 10-times diluted FW were 41.81, 63.04, 99.71 and 183.78 mPa.s, respectively. The curves in Figure 4-140 are plotted for a constant polymer concentration of 2000 ppm to clearly show the effect of salinity on the viscosity of the polymer solution at different shear rates. Similar behaviors were reported for many polysaccharide gums such as pectin and gum Arabic [216, 217]. The structure of uronic acid makes the gum pregnant, and in pure water, the amount of charge is greater due to the release of H⁺ from COOH groups. The repulsion between these charges causes a wider structure and ultimately higher viscosity. Salinity neutralizes these charges. As a result, repulsion is reduced and the polysaccharide structure becomes a flexible chain and viscosity decreases [218, 219]. Viscosity changes against shear rate changes are also observed at lower concentrations, although the intensity is higher at higher concentrations. Reducing the viscosity against shear rate changes confirms the non-Newtonian behavior of polymeric solutions even at the lowest concentrations. This is an important feature of these solutions for use in ASP-slug injections. Non-Newtonian behavior of polymeric solutions is often very important when injectivity is a critical factor [220].

Table 4-25: Viscosity values of the polymeric solutions at hydration time of 24h and 80 °C and different salinities.

		Viscosity, mPa.s							
Shear rate, s ⁻¹		2	5	10	20	40	80	160	320
Brine	Conc., ppm								
FW	500	28.50	27.67	25.31	21.17	18.35	15.17	11.90	8.48
	1000	52.68	51.28	48.44	43.35	36.12	29.04	21.27	14.75
	2000	90.91	85.64	81.75	75.68	67.92	59.10	50.87	42.94
	3000	167.10	162.44	154.39	149.20	140.96	127.19	118.42	109.30
5-times diluted	500	34.15	33.47	32.28	30.89	27.65	23.03	18.15	13.65
	1000	61.42	57.20	51.23	46.85	39.28	30.12	23.98	17.37
FW	2000	93.94	87.25	82.16	77.76	69.32	61.59	52.38	44.90
	3000	178.91	169.85	160.25	151.38	142.64	130.82	122.61	113.45
10-times diluted	500	41.81	40.95	38.01	35.58	31.77	26.13	20.92	16.40
	1000	63.04	60.22	56.72	50.66	43.29	37.87	30.73	22.01
FW	2000	99.71	95.01	91.07	85.82	76.27	64.24	55.59	47.34
	3000	183.78	172.83	166.15	158.91	145.14	137.50	128.62	119.18

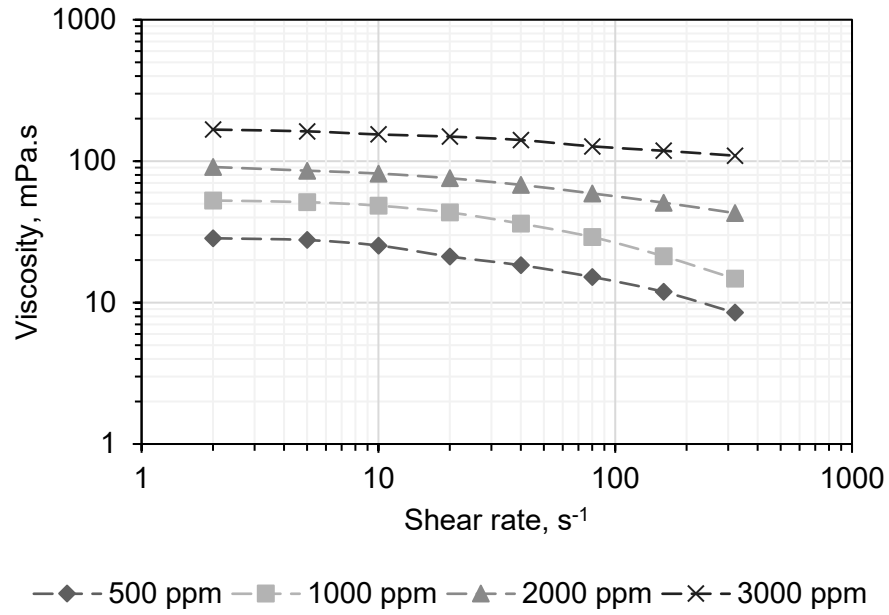


Figure 4-137: Viscosity changes curves of the polymeric solutions at different concentrations against shear rate changes at hydration time of 24 h and 80 °C and FW salinity.

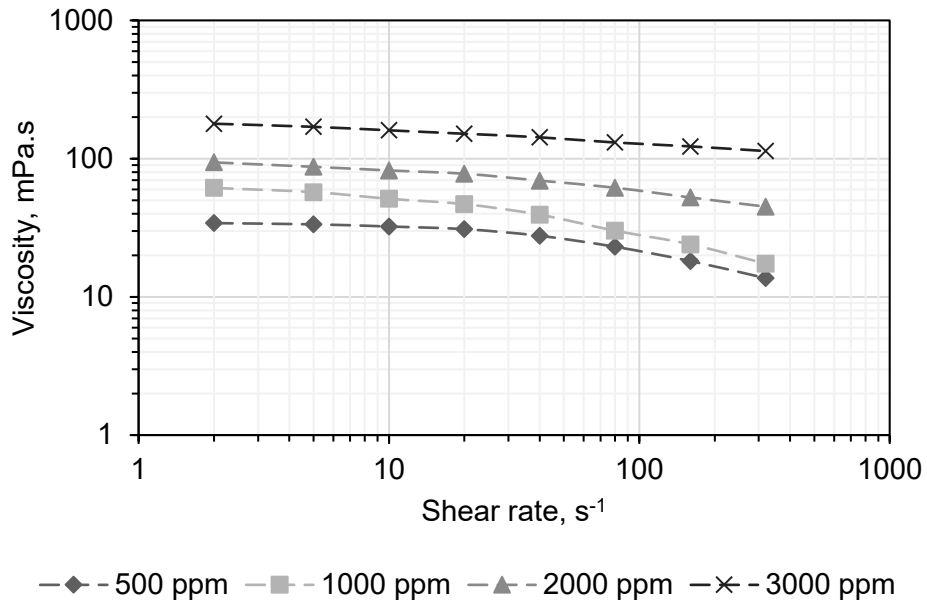


Figure 4-138: Viscosity changes curves of the polymeric solutions at different concentrations against shear rate changes at hydration time of 24 h and 80 °C and 5-times diluted FW salinity.

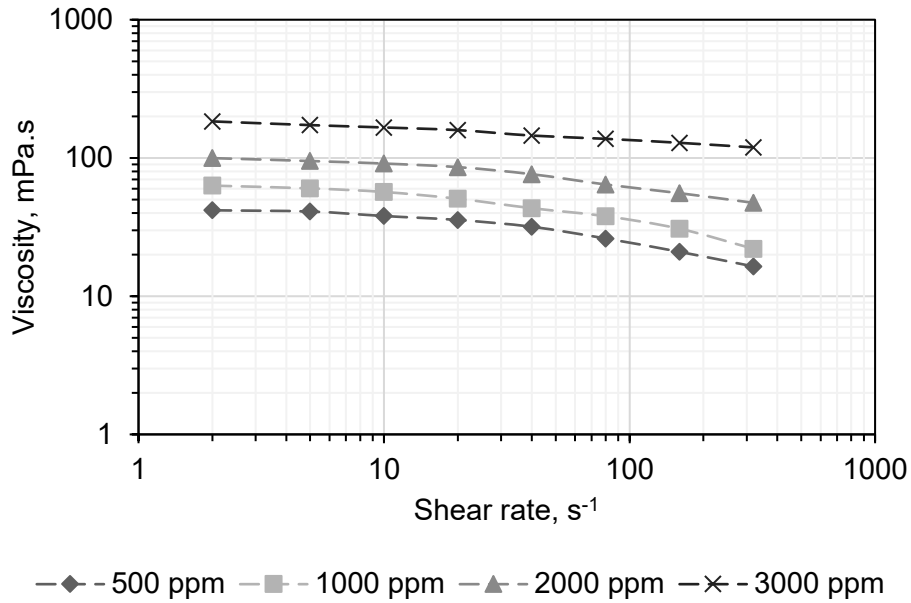


Figure 4-139: Viscosity changes curves of the polymeric solutions at different concentrations against shear rate changes at hydration time of 24 h and 80 °C and 10-times diluted FW salinity.

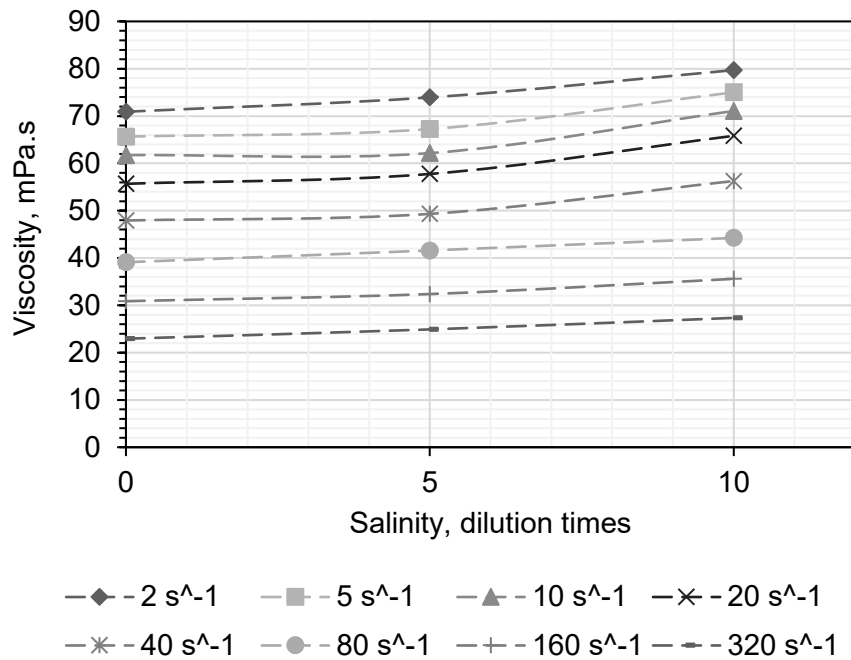


Figure 4-140: Viscosity changes curves of the polymeric solutions at different shear rates against salinity of the base fluid at a constant polymer concentration of 2000ppm.

3.1.3. Oil recovery

Adjustment of additive concentrations in ASP-slug was performed based on the performance of the additives, i.e. the anionic surfactant synthesized from waste chicken fat, NaOH alkali and the polymer extracted from the *Hollyhocks* plant. Accordingly, the surfactant was considered at 5500 ppm (CMC), NaOH at 2500 ppm and the polymer at 2000 ppm. ASP-slug injection was performed into a sandstone plug with a length of 7.5 cm, a diameter of 3.81 cm, a porosity of 27 % and a permeability of 163.89 mD. The sandstone plug had a pore volume (PV) of 23.07 cm³, which reached 83% of the initial oil saturation. Figure 4-141 shows the values of the oil recovery factor against injectable PV. The oil recovery factor of 53.2% was achieved by secondary brine flooding. The 0.5 PV ASP slug was injected after 2.1 PV brine injection (98% water cut). The increase in oil production resumed in the beginning. Finally, the total oil recovery was 81.1 %, resulting in a total injection of fluids with a total volume of 4.4 PV (99 % water cut). Accordingly, 27.9 % of oil recovery is the result of the tertiary injection. The predominant mechanisms in the ASP injection are reduction of interfacial tension due to the presence of surfactant, optimal alkalinity and increased viscosity due to the presence of polymer.

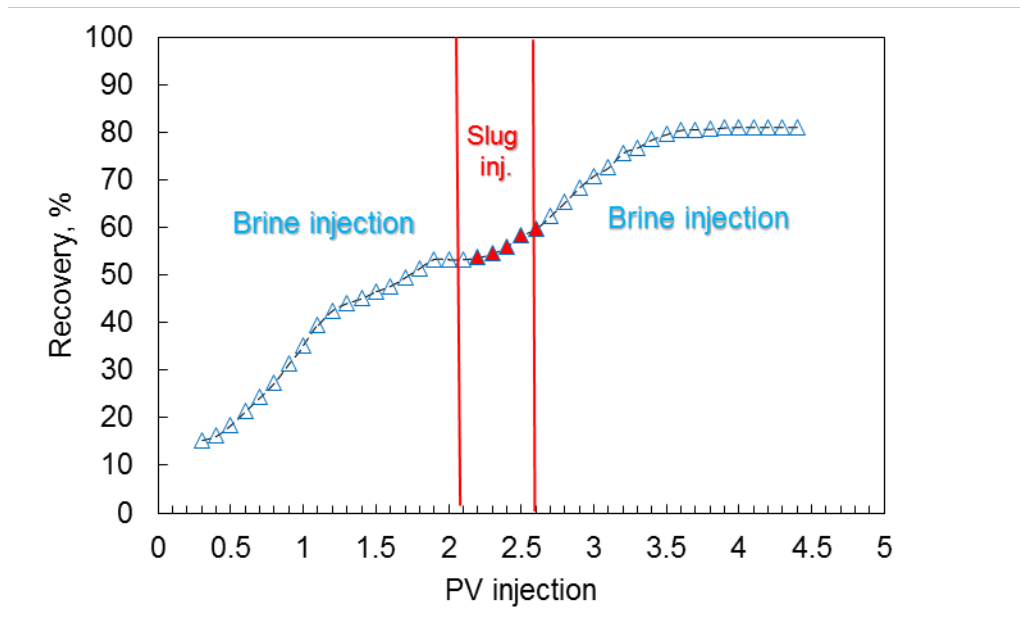


Figure 4-141: Oil recovery curve versus injectable PV in the ASP-slug injection process.

Chapter 5: Conclusion and recommendations

In this chapter, the general results of each section of the project are described based on the classification of additives and the methods of chemical water injection.

5.1. Effects of mutual solvents on smart carbonated water

5.1.1. Interfacial tension

In this part of the study, the effects of methanol and acetone solvents on the performance of carbonated smart water in reducing the interfacial tension of water and oil were investigated separately by performing pendant drop experiments. Based on this, the following results were obtained:

- IFT decreases via increasing the concentration of methanol and acetone in smart water.
- The IFT values for binary solutions of smart water-methanol and smart water-acetone and oil are roughly the same, but more reduction was recorded for acetone-containing solutions.
- Diluted samples of seawater, as seen in the previous studies, have less IFT than primary seawater.
- The addition of CO₂ to the smart water-solvent system leads to a further reduction in IFT. Thus, the lowest IFT for these solutions in the presence of dissolved CO₂ at 75 °C and 10.342 MPa, and a dilution of seawater at a concentration of 11000 ppm were obtained 3.315 and 2.037 mN/m, respectively.
- IFT reduction for smart water-solvent- CO₂ and crude oil systems at a constant temperature of 75 °C, has a direct proportion to the applied pressure to CO₂ and the volume ratio of the solvent and an opposed proportion to smart water salinity.

For further studies, to better understand the mechanisms of solvents in dealing with oil, flooding tests can be done in a glass micro-model.

5.1.2. Wettability and imbibition

Contact angle experiments to investigate the effect of methanol and acetone on the carbonate rock wettability alteration by carbonated water and imbibition tests to measure oil production in the hybrid method of carbonated water with mutual solvents were carried out. The following results are the most prominent findings of this part of the study:

- The wettability alteration to hydrophilic in the use of methanol and acetone solvents with the samples with different seawater salinities in the presence of dissolved CO₂ is confirmed by the

contact angle results. In the presence of dissolved CO₂, the contact angle values are smaller than those without dissolved CO₂.

- The size of the contact angle depends on the volume of solvent, the amount of base fluid salinity and the system pressure. In the absence of CO₂, the contact angle decreases with the increasing percentage of solvent, salinity and pressure, but with dissolved CO₂, the magnitude of contact angle increases with increasing salinity. For carbonated fluids, however, the contact angle depends on the volume of solvent and pressure, such as in the absence of dissolved CO₂.
- Acetone yields a smaller contact angle at all volume ratios than methanol, which could be due to more solubility of CO₂ in a binary mixture of water + acetone than the binary mixture of water + methanol and also greater solubility of oil in acetone relative to methanol.
- Final oil production of 66.29%, 28.44%, 85.42% and 91.38% for imbibition of carbonated water containing 15 %Vol of methanol and final oil production of 70.32%, 32.10%, 90.60% and 94.09% for imbibition of carbonated water containing 15 %Vol of acetone were obtained, respectively that were performed as one-dimensional COCSI, one-dimensional COUCSI, multi-dimensional COUCSI and imbibition in the fractured plug, respectively. The final oil production is in line with the results of the contact angle tests so that the injection fluid with the lowest contact angle yields more oil production.

It is recommended that the composition of other solvents, such as dimethyl ether, as well as other alcoholic and ketone solvents with carbonated water, be considered.

5.1.3. Oil swelling

The effects of the combination of carbonated water and acetone as a mutual solvent in a new formulation based on these two methods on the dynamic and equilibrium crude oil swelling with the pendant drop experiments and the drop volume calculations were investigated. The effects of time, the acetone fraction in carbonated water, the salinity of the base fluid and the pressure on the oil swelling were considered. The most prominent results of this research are as follows:

- Combining the two methods of carbonated water and mutual solvents is an effective way to strengthen the mechanism of oil swelling in these methods. The presence of acetone can increase oil swelling by 13.64%, taking into account its ratio.
- The effect of acetone and salinity on the trends obtained in dynamic and equilibrium oil swelling curves is following their effect on the solubility of CO₂ and the rate of transfer of CO₂ and the mutual solvent.

- Oil swelling is highly dependent on time so that crude oil swelling in the early times and the presence of acetone is less than oil swelling in the presence of acetone-free carbonated water, while in times of equilibrium, its final rate is higher than oil swelling in the presence of acetone-free carbonated water.
- Increasing pressure increases mass transfer and subsequent oil swelling.
- Equilibrium time decreases with increasing pressure and salinity and increases with increasing the acetone component in carbonated water.

It is suggested to use the mutual solvents with unique properties to enhance other EOR methods such as injection of surfactants, polymers and nanofluids in different volume percentages. In addition to acetone, other solvents, such as alcoholic solvents, are also suggested for combination with over EOR methods.

5.2. Extracted saponin from *Anabasis Setifera* plant

Anabasis Setifera plant was introduced as a new source for surfactant extraction and the extracted saponin was used in the EOR experiments. Based on the results:

- Saponin extracted from the *Anabasis Setifera* plant can be considered as a natural surfactant with acceptable performance by the EOR companies, because saponin is an environmentally friendly surfactant and its extraction is very low cost.
- According to TGA analysis, the surfactant is suitable for operation at reservoir temperatures.
- The achieved values of the IFT is in the low-IFT range. Saponin extracted from the *Anabasis Setifera* plant has not reduced IFT to ultra-low values but the comparison between the initial water-oil IFT (25.608 mN/m) and the interfacial tension at CMC shows more than 95% reduction in, a significant reduction compared to other plant surfactants.
- The surfactant has an appropriate function in different salinity of injection water and, in lower salinity, creates a smaller IFT. Although IFT increased at higher salinities, the values remained low. Also, IFT values at high salinities appear to be very close to each other.
- The performance of the surfactant in the contact angle reduction indicates the change in the wettability of the carbonate rock to the hydrophilic, and this is one of the main mechanisms in EOR.
- The oil recovery in the tertiary injection of the surfactant was obtained by 15.4%, which is a significant amount in the surfactant flooding without polymer and alkali.

5.2.1. CO₂-foam characterization

Saponin extracted from the *Anabasis Setifera* plant was used to prepare CO₂-foam and inject it into the fractured carbonate plug. Based on results and observations:

- The foam formed by the surfactant extracted from *Anabasis Setifera* and CO₂ has a good quality for injection because its half-life time and height of the foam is in the appropriate range.
- The various salinities resulting from the FW dilution enhance the performance of the foam up to a salinity of 15000ppm and then weaken it, while the half-life time and height of the foam reach a maximum at an optimum salinity of 10,000 ppm.
- The qualitative study of the CO₂-foam shows that the use of foam at CMC alone does not guarantee the optimal quality of the foam and factors such as salinity, gas flow rate, and of course, time affect the quality of the foam. As the gas flow rate and the time increase, the bubbles become larger. However, the size of the bubbles was not significantly related to the change in the salinity of the surfactant solution. Increasing the gas flow rate, in addition to enlarging the bubbles, also increases the height and volume of the foam in less time.
- Secondary flooding of pre-generated CO₂-foam is very effective in carbonate plug so that a 63% recovery factor was achieved after 3 PV injection due to the diversion of the injection fluid into the fractures and then into the matrixes and the formation of foam-emulsion with oil-in-place.

It is common to use some additives to increase the stability and quality of the foam along with the surfactant. Nano-materials and polymers can increase foam stability. Although the foam formed by the surfactant extracted from *Anabasis Setifera* is of good quality, it is suggested that these additives be used in future studies to improve it.

5.3. Modified saponin of *Anabasis Setifera* plant

The extracted surfactant from the *Anabasis Setifera* plant as a new source was modified through esterification and its application in EOR was investigated. Accordingly:

- FTIR and ¹H NMR analyses confirm the formation of the desired chains in the modified surfactant compared to the extracted saponin from *Anabasis Setifera*, and the TGA analysis confirms its temperature stability at the reservoir temperature range.
- Low-IFT at CMC of surfactant and optimum salinity alkali in the range of 10⁻² mN/m was obtained, which is very suitable for EOR processes.

- The results of the contact angle tests indicate that the carbonate rock wettability is shifted to intermediate wettability by the surfactant solution at CMC, which, in optimum salinity, reduces the contact angle by adding the soluble ions mechanism.
- 19.1 % increase in recovery was achieved only with 0.5 PV of surfactant-alkali slug injection. However, the total recovery factor at the end of the process of secondary and tertiary injection was about 70 %.
- The accepted performance of the plant-based surfactant in EOR along with affordable and available sources can meet many of the challenges in chemical methods and provide preconditions for industrial production and application in the field.

5.4. Extracted saponin from *Soapwort* plant

A non-ionic surfactant was extracted from the *Soapwort* plant as a renewable resource. The use of the surfactant in EOR was investigated by various experiments after characterization. The main results of this study are as follows:

- The CMC was obtained at 2250 ppm by surface tension experiments using the pendant drop method. Due to the low CMC of the surfactant, it can also be considered economically viable.
- The water-oil IFT at CMC decreased by 0.832 mN/m. However, this value was reduced to 0.541 and 0.047 mN/m at the optimal salinity of formation water and optimal concentration of NaOH alkali, respectively.
- According to the contact angle test, the wettability of the sandstone was altered from hydrophobicity to hydrophilicity by the surfactant solution at CMC.
- Eventually, the oil recovery increased by more than 32% with the tertiary injection of alkali-surfactant-polymer slug containing the surfactant at CMC, optimal salinity of formation water, optimal NaOH alkali concentration and 1000 ppm of partially hydrolyzed polyacrylamide.

Saponins are known as surfactants with stable foam formation. A comprehensive study of foam for this surfactant is suggested for further studies. Besides, it is suggested that other plant resources be studied to provide surfactants and measure their application in EOR.

5.5. Synthesized surfactant from *Rapeseed* oil

The capabilities of an anionic surfactant synthesized from *Rapeseed* oil in the EOR process were investigated by performing related experiments. Results show that:

- The CMC of the surfactant was equal to 4500 ppm and the value of IFT in this concentration was in the range of 3.4×10^{-2} mN/m, which shows lower values in optimal salinity and alkalinity.
- CSC rock wettability by surfactant in CMC altered from hydrophobic to hydrophilic with a final contact angle of 40.62° .
- The surfactant adsorption test in the porous medium of CSC rock shows that the amount of adsorption decreases with increasing PV injection, but as the injection continues, the adsorption tends to a constant value.
- The volume of foam is proportional to the concentration of surfactant. The emulsion formed in CMC surfactant with crude oil has significant stability so that after 5 days the single-phase state of the emulsion began to separate and after one month it did not reach complete separation.
- Oil production in various chemical injection scenarios increased by about 14.6% -25.7%, depending on the type and amount of injection fluids.

5.6. Synergic effect of dissolved carbon dioxide and the *Rapeseed* oil surfactant

The effects of combining carbonated water and surfactant solution injection methods on EOR parameters including IFT, reservoir rock wettability and crude oil swelling were investigated using pendant drop and contact angle experiments. The followings are the main results of this study:

- The surfactant enhances the performance of carbonated water in regulating the mechanisms of IFT reduction, wettability alteration and oil swelling, but improving the performance of this combined method is not the same at different concentrations of the surfactant, temperature and pressure.
- IFT of carbonated water and oil in all the surfactant concentrations decreases sharply so that its value ranges from a maximum of 13.759 mN/m at zero surfactant concentration, a temperature of 80°C and a pressure of 1000 psi reaches a minimum of 1.503 mN/m at a concentration of 5500 ppm of the surfactant, a temperature 80°C and a pressure of 2000 psi.
- IFT of the free-surfactant carbonated solutions increases with increasing temperature, while IFT decreases with increasing temperature in the presence of the surfactant.
- The contact angle of the oil droplet on the carbonate rock at the concentration below CMC of the surfactant increases compared to the contact angle in the presence of surfactant-free carbonated water but decreases at the CMC and above the CMC. However, at a higher concentration than CMC, its severity decreases.
- The presence of the surfactant increases oil swelling compared to surfactant-free carbonated water. However, the rate of increase in oil swelling at a concentration higher than CMC decreases so that the highest rate of oil swelling is achieved in CMC.

5.7. Synthesized surfactant from waste chicken fat

An anionic surfactant from waste chicken fat as a renewable source was synthesized and its application in EOR was investigated. Based on the tests and analyses, the following results were obtained:

- The TGA analysis of the surfactant confirms its temperature stability at the reservoir temperature.
- A low-IFT of 4.3×10^{-2} mN/m was achieved at CMC while this amount also decreased at optimum salinity and alkali. The values obtained for the IFT confirm that this surfactant is suitable for EOR operations to reduce IFT.
- The wettability alteration from hydrophobic to hydrophilic with an average contact angle of 43.16° was obtained.
- The surfactant foam behavior at CMC showed that after 13 min the foam height to half. Also, the size of the bubbles has a direct relation to the gas flow rate and the passage of time.
- The emulsion stability test showed that complete separation of phases occurs after 25 days, and this confirms the proper stability for the emulsion formed with the surfactant solution at CMC.
- Compatibility tests showed that the surfactant in formation water still does not produce sediment. However, this compatibility is up to a critical 130000 ppm salinity. As a result of these experiments, it is permissible to use this surfactant for reservoirs with lower salinity levels than this critical salinity.
- Eventually, an increase in oil recovery of 17.8% was achieved by chemical ASP slug injection into the carbonate plug.

The use of fats and oils extracted from waste plant and animal tissues produced in various industries can be considered as a very cheap source for the preparation of various surfactants. Based on this, it is suggested that other sources in this category be evaluated for the preparation of surfactants and their use in EOR investigations.

5.8. Synthesized fluorinated surfactant

An anionic F-surfactant was synthesized and characterized by FTIR and TGA analyses and surface tension experiments. Contact angle and liquid-gas imbibition experiments were performed to demonstrate the ability of the surfactant in wettability alteration of carbonate rock to gas-wetting. The adsorption of

surfactant on carbonate porous media during flooding and the foam stability of the surfactant solution at CMC were calculated. Based on the results:

- TGA analysis confirms the temperature stability of the synthesized surfactant at the gas condensate reservoir temperatures.
- The surfactant CMC was obtained according to the results of surface tension tests equal to 3500 ppm.
- The contact angle is proportional to the surfactant concentration, treatment time and temperature. As the treatment time increases, the contact angle increases and gas-wetting becomes more, but in the final times due to the system moving toward equilibrium, there are no significant changes in the contact angle. As the temperature increases, gas-wetting decreases, which may be due to the decrease in surfactant absorption with increasing temperature.
- Surfactant adsorption in the porous media of the carbonate plug is proportional to the amount of solution injected and the temperature. As the amount of injected solution increases, the adsorption increases, while this increase does not have the same slope until the final stages of injection. That is, the incremental slope decreases in the late stages, which may be due to the saturation of the effective surface area of the porous medium by the molecules adsorbed in the previous steps.
- Half-life time of foam decay at CMC was obtained to 13 min. This foam stability is due to the nature of the F-surfactants, i.e. the hydrophilic-gasphilic dual structure.
- Imbibition tests show the wettability alteration via the chemical treatment by surfactant as such, the liquid imbibition in the treated carbonate plug is negligible compared to the non-treated plug with an initial (wettability) state.

5.9. Extracted mucilage from *Hollyhocks* plant as a natural polymer

The polymer extracted from the *Hollyhocks* plant was characterized and preliminary studies were performed to investigate the possibility of its use in EOR by the ASP-slug injection method. The most prominent results of the experiments are as follows:

- FIIR analysis of the mucilage shows the O–H, C–H, and –COO as carbohydrate polymer bonds.
- TGA analysis in the initial peak shows only 9% weight loss, which, due to the evaporation of moisture adsorbed by polymer bonds from the atmosphere, shows its structure retention up to 129 °C. While most oil reservoirs have a lower temperature than this peak, the use of the polymer is confirmed in terms of temperature stability.

- The viscosity of polymeric solutions containing mucilage increases sharply even at low concentrations. The polymeric solutions show non-Newtonian behavior due to reduced viscosity versus an increasing shear rate.
- The viscosity of the solutions containing mucilage increases significantly with increasing concentration and at the lowest shear rate and temperature of 30 °C is in the range of 232-60 mPa.s and proportional to the concentration. This viscosity was obtained for mature solutions after 24 h hydration and distilled water base.
- The viscosity of the polymeric solutions decreases with increasing temperature and salinity, but the final values, i.e., the salinity of the FW, and the temperature of 80 °C are several tens of times higher than the viscosity of the water and the surfactant solutions.
- The injection of ASP-slug containing surfactant at CMC equal to 5500 ppm, NaOH at 2500 ppm and the polymer at 2000 ppm in a sandstone plug increases oil recovery by 27.9%.

Due to the characteristics of mucilage extracted from plants, it is recommended to examine its ability to increase the stability of foam and emulsion in future studies. Besides, other high-efficiency plant sources for polymer extraction can be identified and the use of plant polymers in EOR can be investigated.

References

- [1] Roehl, P.O. and Choquette, P.W. eds., 2012. Carbonate petroleum reservoirs. Springer Science & Business Media.
- [2] Ali, S.M. and Thomas, S., 1996. The promise and problems of enhanced oil recovery methods. *Journal of Canadian Petroleum Technology*, 35(07). PETSOC-96-07-07.
- [3] Mai, A. and Kantzas, A., 2009. Heavy oil waterflooding: effects of flow rate and oil viscosity. *Journal of Canadian Petroleum Technology*, 48(03), pp.42-51.
- [4] Sheng, J., 2010. Modern chemical enhanced oil recovery: theory and practice. Gulf Professional Publishing.
- [5] Manshad, A.K., Nowrouzi, I. and Mohammadi, A.H., 2017. Effects of water soluble ions on wettability alteration and contact angle in smart and carbonated smart water injection process in oil reservoirs. *Journal of Molecular Liquids*, 244, pp.440-452.
- [6] Nowrouzi, I., Manshad, A.K. and Mohammadi, A.H., 2019. Effects of ions and dissolved carbon dioxide in brine on wettability alteration, contact angle and oil production in smart water and carbonated smart water injection processes in carbonate oil reservoirs. *Fuel*, 235, pp.1039-1051.
- [7] Tang, G.Q. and Morrow, N.R., 1999. Influence of brine composition and fines migration on crude oil/brine/rock interactions and oil recovery. *Journal of Petroleum Science and Engineering*, 24(2-4), pp.99-111.
- [8] McGuire, P.L., Chatham, J.R., Paskvan, F.K., Sommer, D.M. and Carini, F.H., 2005, January. Low salinity oil recovery: An exciting new EOR opportunity for Alaska's North Slope. In SPE western regional meeting. Society of Petroleum Engineers. SPE-93903-MS.
- [9] Lager, A., Webb, K.J., Black, C.J.J., Singleton, M. and Sorbie, K.S., 2008. Low salinity oil recovery-an experimental investigation. *Petrophysics*, 49(01).
- [10] Ligthelm, D.J., Gronsveld, J., Hofman, J., Brussee, N., Marcelis, F. and van der Linde, H., 2009, January. Novel Waterflooding Strategy by Manipulation of Injection Brine Composition. In EUROPEC/EAGE conference and exhibition. Society of Petroleum Engineers. SPE-119835-MS.
- [11] Buckley, J.S. and Morrow, N.R., 2010, September. Improved oil recovery by low salinity waterflooding: a mechanistic review. In 11th international symposium on evaluation of wettability and its effect on oil recovery, Calgary (pp. 6-9).

- [12] A. A. Yousef, S. Al-Saleh, A. Al-Kaabi, and M. Al-Jawfi. , Laboratory investigation of novel oil recovery method for carbonate reservoirs, in Proceedings of the SPE Canadian Unconventional Resources and International Petroleum Conference, pp. 1825– 1859, Alberta, Canada, October 2010, SPE-137634-MS.
- [13] Zhang, P. and Austad, T., 2006. Wettability and oil recovery from carbonates: Effects of temperature and potential determining ions. *Colloids and Surfaces A: Physicochemical and Engineering Aspects*, 279(1-3), pp.179-187.
- [14] Zhang, P., Tweheyo, M.T. and Austad, T., 2006. Wettability alteration and improved oil recovery in chalk: The effect of calcium in the presence of sulfate. *Energy & fuels*, 20(5), pp.2056-2062.
- [15] Nowrouzi, I., Manshad, A.K. and Mohammadi, A.H., 2020. The mutual effects of injected fluid and rock during imbibition in the process of low and high salinity carbonated water injection into carbonate oil reservoirs. *Journal of Molecular Liquids*, p.112432.
- [16] Ahmed, A.A., Mohd Saaid, I. and Mohd Shafian, S.R., 2020. Novel Relative Permeability Modifier using Polymer Grafted Nanoclay. *Energy & Fuels*, 34(3), pp.2703-2709.
- [17] Kakati, A., Kumar, G. and Sangwai, J.S., 2020. Low Salinity Polymer Flooding: Effect on Polymer Rheology, Injectivity, Retention and Oil Recovery Efficiency. *Energy & Fuels*. In Press.
- [18] Ma, S., Muriel, H., Valencia, L., James, L.A. and Azmy, K., 2020. Pore Network Changes due to Polymer Flooding: Hebron Field Case. *Energy & Fuels*. In Press.
- [19] Wei, P., Guo, K., Pu, W., Xie, Y., Huang, X. and Zhang, J., 2020. Aqueous Foam Stabilized by an in Situ Hydrophobic Polymer via Interaction with Alkyl Polyglycoside for Enhancing Oil Recovery. *Energy & Fuels*, 34(2), pp.1639-1652.
- [20] Sharma, T., Kumar, G.S. and Sangwai, J.S., 2015. Viscoelastic properties of oil-in-water (o/w) Pickering emulsion stabilized by surfactant–polymer and nanoparticle–surfactant–polymer systems. *Industrial & Engineering Chemistry Research*, 54(5), pp.1576-1584.
- [21] Ramos, G.A., Akanji, L.T. and Afzal, W., 2020. A Novel Surfactant–Polymer/Alkaline–Surfactant–Polymer Formulation for Enhanced Oil Recovery (EOR) Processes. *Energy & Fuels*, 34(2), pp.1230-1239.
- [22] Yousef, A.A., Liu, J., Blanchard, G., Al-Saleh, S., Al-Zahrani, T., Al-Tammar, H. and Al-Mulhim, N., 2012. SmartWater Flooding: Industry’s First Field Test in Carbonate Reservoirs, SPE-159526 presented at the SPE Annual Technical Conference and Exhibition held in San Antonio, Texas, USA, 8–10 October.

- [23] Smith, K.W., 1942, November. Brines as flooding liquids. In 7th Annual Technical Meeting, Min. Ind. Exper. Sta., Pennsylvania State College.
- [24] G. Q. Tang and N. R. Morrow, "Salinity, temperature, oil composition, and oil recovery by waterflooding," SPE Reservoir Engineering, vol. 12, pp. 269–276, SPE-36680-PA, 1997.
- [25] Zhang P, Tweheyo MT, Austad T. Wettability alteration and improved oil recovery by spontaneous imbibition of seawater into chalk: impact of the potential determining ions Ca^{2+} , Mg^{2+} , and SO_4^{2-} . Colloids Surf A Physicochem Eng Asp 2007; 301:199–208.
- [26] K.J. Webb, C.J.J. Black, G. Tjetland, A laboratory study investigating methods for improving oil recovery in carbonates, in: IPTC10506, Paper Presented at the International Petroleum Technology Conference, Doha, Qatar, November 21–23, 2005.
- [27] A.Y. Ali, A.-S. Salah Hamad, A.-K. Abdulaziz, A.-J. Mohammed Saleh, Laboratory Investigation of the Impact of Injection-Water Salinity and Ionic Content on Oil Recovery From Carbonate Reservoirs, SPE Reservoir Evaluation & Engineering (2011).
- [28] Aghaeifar, Z., Strand, S., Puntervold, T., Austad, T. and Sajjad, F.M., 2018. Smart Water injection strategies for optimized EOR in a high temperature offshore oil reservoir. Journal of Petroleum Science and Engineering, 165, pp.743-751.
- [29] Shabaninejad, M., Middleton, J. and Fogden, A., 2018. Systematic pore-scale study of low salinity recovery from Berea sandstone analyzed by micro-CT. Journal of Petroleum Science and Engineering, 163, pp.283-294.
- [30] Sharma, H. and Mohanty, K.K., 2018. An experimental and modeling study to investigate brine-rock interactions during low salinity water flooding in carbonates. Journal of Petroleum Science and Engineering, 165, pp.1021-1039.
- [31] Xie, Q., Brady, P.V., Pooryousefy, E., Zhou, D., Liu, Y. and Saeedi, A., 2017. The low salinity effect at high temperatures. Fuel, 200, pp.419-426.
- [32] Wang, X. and Alvarado, V., 2017. Effects of low-salinity waterflooding on capillary pressure hysteresis. Fuel, 207, pp.336-343.
- [33] Amirian, T., Haghghi, M. and Mostaghimi, P., 2017. Pore Scale Visualization of Low Salinity Water Flooding as an Enhanced Oil Recovery Method. Energy & Fuels, 31 (12), pp. 13133–13143.

- [34] Ameri, A., Esmaeilzadeh, F. and Mowla, D., 2018. Effect of low-salinity water on asphaltene precipitation. *Journal of Dispersion Science and Technology*, 39 (7), pp.1031-1039.
- [35] Ashtari Larki, S., Banashoostari, H., Shokrollahzadeh Behbahani, H. and Najafi-Marghmaleki, A., 2018. Effect of acid number of crude oil on oil recovery of smart water coupled with silica nanoparticles. *Petroleum Science and Technology*, 36 (5), pp.343-349.
- [36] Kakati, A., Jha, N.K., Kumar, G. and Sangwai, J.S., 2017. Application of Low Salinity Water Flooding for Light Paraffinic Crude Oil Reservoir. In *SPE Symposium: Production Enhancement and Cost Optimisation*. Society of Petroleum Engineers. Optimisation, 7-8 November, Kuala Lumpur, Malaysia, SPE-189249-MS.
- [37] Kakati, A. and Sangwai, J.S., 2017. Effect of monovalent and divalent salts on the interfacial tension of pure hydrocarbon-brine systems relevant for low salinity water flooding. *Journal of Petroleum Science and Engineering*, 157, pp.1106-1114.
- [38] Lashkarbolooki, M. and Ayatollahi, S., 2018. Evaluation of effect of temperature and pressure on the dynamic interfacial tension of crude oil/aqueous solutions containing chloride anion through experimental and modelling approaches. *The Canadian Journal of Chemical Engineering*, 96(6), pp.1396-1402.
- [39] Moustafa, E.A.A. and Shedid, S.A., 2017. Effects of magnesium and potassium sulfates on oil recovery by water flooding. *Egyptian Journal of Petroleum*, In Press, Corrected Proof.
- [40] Mahzari, P., Sohrabi, M., Cooke, A.J. and Carnegie, A., 2018. Direct pore-scale visualization of interactions between different crude oils and low salinity brine. *Journal of Petroleum Science and Engineering*, 166, pp.73-84.
- [41] Manshad, A.K., Olad, M., Taghipour, S.A., Nowrouzi, I. and Mohammadi, A.H., 2016. Effects of water soluble ions on interfacial tension (IFT) between oil and brine in smart and carbonated smart water injection process in oil reservoirs. *Journal of Molecular Liquids*, 223, pp.987-993.
- [42] Nowrouzi, I., Manshad, A.K. and Mohammadi, A.H., 2018. Effects of dissolved binary ionic compounds and different densities of brine on interfacial tension (IFT), wettability alteration, and contact angle in smart water and carbonated smart water injection processes in carbonate oil reservoirs. *Journal of Molecular Liquids*, 254, pp.83-92.
- [43] AlHammadi, M., Mahzari, P. and Sohrabi, M., 2018. Fundamental investigation of underlying mechanisms behind improved oil recovery by low salinity water injection in carbonate rocks. *Fuel*, 220, pp.345-357.

- [44] Alhuraishawy, A.K., Bai, B., Wei, M., Geng, J. and Pu, J., 2018. Mineral dissolution and fine migration effect on oil recovery factor by low-salinity water flooding in low-permeability sandstone reservoir. *Fuel*, 220, pp.898-907.
- [45] Chen, S.Y., Kaufman, Y., Kristiansen, K., Seo, D., Schrader, A.M., Alotaibi, M.B., Dobbs, H.A., Cadirov, N.A., Boles, J.R., Ayirala, S.C. and Israelachvili, J.N., 2017. Effects of salinity on oil recovery (the “Dilution Effect”): Experimental and theoretical studies of crude oil/brine/carbonate surface restructuring and associated physicochemical interactions. *Energy & Fuels*, 31(9), pp.8925-8941.
- [46] Chen, Y., Xie, Q., Sari, A., Brady, P.V. and Saeedi, A., 2018. Oil/water/rock wettability: Influencing factors and implications for low salinity water flooding in carbonate reservoirs. *Fuel*, 215, pp.171-177.
- [47] Lashkarbolooki, M., Ayatollahi, S. and Riazi, M., 2017. Mechanistical study of effect of ions in smart water injection into carbonate oil reservoir. *Process Safety and Environmental Protection*, 105, pp.361-372.
- [48] Mahani, H., Menezes, R., Berg, S., Fadili, A., Nasralla, R., Voskov, D. and Joekar-Niasar, V., 2017. Insights into the impact of temperature on the wettability alteration by low salinity in carbonate rocks. *Energy & Fuels*, 31(8), pp.7839-7853.
- [49] Pooryousefy, E., Xie, Q., Chen, Y., Sari, A. and Saeedi, A., 2018. Drivers of low salinity effect in sandstone reservoirs. *Journal of Molecular Liquids*, 250, pp.396-403.
- [50] Johnson, W.E., Macfarlane, R.M., Breston, J.N. and Neil, D.C., 1952. Laboratory experiments with carbonated water and liquid carbon dioxide as oil recovery agents. *Prod. Monthly*, 17.
- [51] Hickok, C.W., Christensen, R.J. and Ramsay Jr, H.J., 1960. Progress review of the K&S carbonated waterflood project. *Journal of petroleum technology*, 12(12), pp.20-24.
- [52] Esene, C., Rezaei, N., Aborig, A. and Zendehboudi, S., 2019. Comprehensive review of carbonated water injection for enhanced oil recovery. *Fuel*, 237, pp.1086-1107.
- [53] Ahmadi, M.A., zeinali Hasanvand, M., Behbahani, S.S., Nourmohammad, A., Vahidi, A., Amiri, M. and Ahmadi, G., 2016. Effect of operational parameters on the performance of carbonated water injection: experimental and numerical modeling study. *The Journal of Supercritical Fluids*, 107, pp.542-548.
- [54] Esene, C., Zendehboudi, S., Shiri, H. and Aborig, A., 2020. Systematic sensitivity analysis to investigate performance of carbonated water injection based on computational dynamic modeling. *Fuel*, p.117318.

- [55] Esene, C., Zendejboudi, S., Shiri, H. and Aborig, A., 2020. Deterministic tools to predict recovery performance of carbonated water injection. *Journal of Molecular Liquids*, 301, p.111911.
- [56] Esene, C., Zendejboudi, S., Aborig, A. and Shiri, H., 2019. A modeling strategy to investigate carbonated water injection for EOR and CO₂ sequestration. *Fuel*, 252, pp.710-721.
- [57] Mahzari, P., Jones, A.P. and Oelkers, E.H., 2019. An integrated evaluation of enhanced oil recovery and geochemical processes for carbonated water injection in carbonate rocks. *Journal of Petroleum Science and Engineering*, 181, p.106188.
- [58] Hamouda, A.A. and Bagalkot, N., 2019. Effect of salts on interfacial tension and CO₂ mass transfer in carbonated water injection. *Energies*, 12(4), p.748.
- [59] Lashkarbolooki, M., Hezave, A.Z. and Ayatollahi, S., 2019. The role of CO₂ and ion type in the dynamic interfacial tension of acidic crude oil/carbonated brine. *Petroleum Science*, 16(4), pp.850-858.
- [60] Lashkarbolooki, M., Hezave, A.Z. and Ayatollahi, S., 2019. Swelling behavior of heavy crude oil during injection of carbonated brine containing chloride anion. *Journal of Molecular Liquids*, 276, pp.7-14.
- [61] Lashkarbolooki, M., Riazi, M. and Ayatollahi, S., 2017. Effect of CO₂ and natural surfactant of crude oil on the dynamic interfacial tensions during carbonated water flooding: experimental and modeling investigation. *Journal of Petroleum Science and Engineering*, 159, pp.58-67.
- [62] Chaturvedi, K.R., Trivedi, J. and Sharma, T., 2019. Evaluation of Polymer-Assisted Carbonated Water Injection in Sandstone Reservoir: Absorption Kinetics, Rheology, and Oil Recovery Results. *Energy & Fuels*, 33(6), pp.5438-5451.
- [63] Bagalkot, N., Hamouda, A.A. and Isdahl, O.M., 2019. Influence of Silica Nanofluid on CO₂ Mass Transfer and Hydrocarbon Property Alteration in a Carbonated Water-Hydrocarbon System. In *Defect and Diffusion Forum* (Vol. 390, pp. 99-111). Trans Tech Publications.
- [64] Ruidiaz, E.M., Winter, A. and Trevisan, O.V., 2018. Oil recovery and wettability alteration in carbonates due to carbonate water injection. *Journal of Petroleum Exploration and Production Technology*, 8(1), pp.249-258.
- [65] Seyyedi, M., Sohrabi, M. and Farzaneh, A., 2015. Investigation of rock wettability alteration by carbonated water through contact angle measurements. *Energy & Fuels*, 29(9), pp.5544-5553.

- [66] Seyyedi, M., Mahzari, P. and Sohrabi, M., 2018. A comparative study of oil compositional variations during CO₂ and carbonated water injection scenarios for EOR. *Journal of Petroleum Science and Engineering*, 164, pp.685-695.
- [67] Seyyedi, M., Sohrabi, M., Sisson, A. and Ireland, S., 2018. Quantification of oil recovery efficiency, CO₂ storage potential, and fluid-rock interactions by CWI in heterogeneous sandstone oil reservoirs. *Journal of Molecular Liquids*, 249, pp.779-788.
- [68] Zaker, S., Parvizi, R., Hosseini, S. and Ghaseminejad, E., 2020. Crude oil behavior during injection of solutions containing MgSO₄ in the presence and absence of CO₂. *Energy Sources, Part A: Recovery, Utilization, and Environmental Effects*, pp.1-18.
- [69] Foroozesh, J. and Jamiolahmady, M., 2018. The physics of CO₂ transfer during carbonated water injection into oil reservoirs: From non-equilibrium core-scale physics to field-scale implication. *Journal of Petroleum Science and Engineering*, 166, pp.798-805.
- [70] Riazi, M. and Golkari, A., 2016. The influence of spreading coefficient on carbonated water alternating gas injection in a heavy crude oil. *Fuel*, 178, pp.1-9.
- [71] Bakhshi, P., Kharrat, R., Hashemi, A. and Zallaghi, M., 2018. Experimental evaluation of carbonated waterflooding: A practical process for enhanced oil recovery and geological CO₂ storage. *Greenhouse Gases: Science and Technology*, 8(2), pp.238-256.
- [72] Adiputra, E., Mucharam, L. and Rahmawati, S.D., 2018. Experimental Evaluation of Carbonated Water Injection to Increase Oil Recovery Using Spontaneous Imbibition. In *Selected Topics on Improved Oil Recovery* (pp. 33-44). Springer, Singapore.
- [73] Honarvar, B., Azdarpour, A., Karimi, M., Rahimi, A., Afkhami Karaei, M., Hamidi, H., Ing, J. and Mohammadian, E., 2017. Experimental Investigation of Interfacial Tension Measurement and Oil Recovery by Carbonated Water Injection: A Case Study Using Core Samples from an Iranian Carbonate Oil Reservoir. *Energy & Fuels*, 31(3), pp.2740-2748.
- [74] Mahzari, P., Tsolis, P., Sohrabi, M., Enezi, S., Yousef, A.A. and Eidan, A.A., 2018. Carbonated water injection under reservoir conditions; in-situ WAG-type EOR. *Fuel*, 217, pp.285-296.
- [75] Lashkarbolooki, M., Riazi, M. and Ayatollahi, S., 2018. Experimental investigation of dynamic swelling and Bond number of crude oil during carbonated water flooding; Effect of temperature and pressure. *Fuel*, 214, pp.135-143.

- [76] Lashkarbolooki, M., Riazi, M. and Ayatollahi, S., 2018. Effect of CO₂ and crude oil type on the dynamic interfacial tension of crude oil/carbonated water at different operational conditions. *Journal of Petroleum Science and Engineering*, 170, pp. 576-581.
- [77] Hamouda A. A. and Bagalkot N., 2018. Experimental Investigation of Temperature on Interfacial Tension and its Relation to Alterations of Hydrocarbon Properties in a Carbonated Water/ Hydrocarbon System. *International Journal of Chemical Engineering and Applications*, 9 (2), pp. 58-63.
- [78] Holm, L.W. and Csaszar, A.K., 1962. Oil recovery by solvents mutually soluble in oil and water. *Society of Petroleum Engineers Journal*, 2(02), pp.129-144.
- [79] Dehaghani, A.H.S. and Badizad, M.H., 2016. Experimental study of Iranian heavy crude oil viscosity reduction by diluting with heptane, methanol, toluene, gas condensate and naphtha. *Petroleum*, 2(4), pp.415-424.
- [80] Chernetsky, A., Masalmeh, S., Eikmans, D., Boerrigter, P.M., Fadili, A., Parsons, C.A., Parker, A., Boersma, D.M., Cui, J., Dindoruk, B. and Te Riele, P.M., 2015, November. A novel enhanced oil recovery technique: experimental results and modelling workflow of the DME enhanced waterflood technology. In Abu Dhabi International Petroleum Exhibition and Conference. Society of Petroleum Engineers. SPE-177919-MS.
- [81] Parsons, C., Chernetsky, A., Eikmans, D., Te Riele, P., Boersma, D., Sersic, I. and Broos, R., 2017, April. Introducing a novel enhanced oil recovery technology. In IOR 2017-19th European Symposium on Improved Oil Recovery. SPE-179560-MS.
- [82] Chahardowli, M., Farajzadeh, R. and Bruining, H., 2016, March. Experimental investigation of dimethyl ether/polymer hybrid as an enhanced oil recovery method. In SPE EOR Conference at Oil and Gas West Asia. Society of Petroleum Engineers. SPE-179850-MS.
- [83] Ratnakar, R.R., Dindoruk, B. and Wilson, L., 2016. Experimental investigation of DME–water–crude oil phase behavior and PVT modeling for the application of DME-enhanced waterflooding. *Fuel*, 182, pp.188-197.
- [84] Ratnakar, R.R., Dindoruk, B. and Wilson, L.C., 2017. Phase behavior experiments and PVT modeling of DME-brine-crude oil mixtures based on Huron-Vidal mixing rules for EOR applications. *Fluid Phase Equilibria*, 434, pp.49-62.
- [85] Ratnakar, R.R., Dindoruk, B. and Wilson, L., 2016, September. Use of DME as an EOR Agent: Experimental and Modeling Study to Capture Interactions of DME, Brine and Crudes at Reservoir

Conditions. In SPE Annual Technical Conference and Exhibition. Society of Petroleum Engineers. SPE-181515-MS.

[86] Mahdizadeh, M., Eftekhari, A.A. and Nick, H.M., 2019. Numerical modeling of water-soluble solvents for enhancing oil recovery in heterogeneous chalk reservoirs. *Journal of Petroleum Science and Engineering*, 175, pp.681-692.

[87] AlZayer, A., Sanaei, A., Mohanty, K. and Sepehrnoori, K., 2019. Experimental and numerical investigation of mutual solvents for EOR applications. *Journal of Petroleum Science and Engineering*, 177, pp. 224-235.

[88] Lu, Y., Najafabadi, N.F. and Firoozabadi, A., 2019. Effect of Low-Concentration of 1-Pentanol on the Wettability of Petroleum Fluid–Brine–Rock Systems. *Langmuir*, 35(12), pp.4263-4269.

[89] Saxena, N., Saxena, A. and Mandal, A., 2019. Synthesis, characterization and enhanced oil recovery potential analysis through simulation of a natural anionic surfactant. *Journal of Molecular Liquids*, 282, pp.545-556.

[90] Saxena, N., Goswami, A., Dhodapkar, P.K., Nihalani, M.C. and Mandal, A., 2019. Bio-based surfactant for enhanced oil recovery: Interfacial properties, emulsification and rock-fluid interactions. *Journal of Petroleum Science and Engineering*, 176, pp.299-311.

[91] Kiani, S., Rogers, S.E., Sagisaka, M., Alexander, S. and Barron, A.R., 2019. A New Class of Low Surface Energy Anionic Surfactant for Enhanced Oil Recovery (EOR). *Energy & Fuels*.

[92] Tay, A., Mouret, A. and Mascle, M., 2019, April. Internal Ketone Sulfonate: A New Bio-Sourced Surfactant for Chemical EOR in Sea Water. In *Offshore Technology Conference*. Offshore Technology Conference. OTC-29575-MS.

[93] Ganie, K., Manan, M.A., Ibrahim, A. and Idris, A.K., 2019. An Experimental Approach to Formulate Lignin-Based Surfactant for Enhanced Oil Recovery. *International Journal of Chemical Engineering*, 2019, 6 Pages.

[94] Najimi, S., Nowrouzi, I., Manshad, A.K., Farsangi, M.H., Hezave, A.Z., Ali, J.A., Keshavarz, A. and Mohammadi, A.H., Investigating the effect of [C 8 Py][Cl] and [C 18 Py][Cl] ionic liquids on the water/oil interfacial tension by considering Taguchi method. *Journal of Petroleum Exploration and Production Technology*, pp.1-9.

- [95] Manshad, A.K., Rezaei, M., Moradi, S., Nowrouzi, I. and Mohammadi, A.H., 2017. Wettability alteration and interfacial tension (IFT) reduction in enhanced oil recovery (EOR) process by ionic liquid flooding. *Journal of Molecular Liquids*, 248, pp.153-162.
- [96] Kumar, A. and Mandal, A., 2018. Characterization of rock-fluid and fluid-fluid interactions in presence of a family of synthesized zwitterionic surfactants for application in enhanced oil recovery. *Colloids and Surfaces A: Physicochemical and Engineering Aspects*, 549, pp.1-12.
- [97] Madani, M., Zargar, G., Takassi, M.A., Daryasafar, A., Wood, D.A. and Zhang, Z., 2019. Fundamental investigation of an environmentally-friendly surfactant agent for chemical enhanced oil recovery. *Fuel*, 238, pp.186-197.
- [98] Pal, N., Kumar, N., Verma, A., Ojha, K. and Mandal, A., 2018. Performance evaluation of novel sunflower oil-based gemini surfactant (s) with different spacer lengths: application in enhanced oil recovery. *Energy & Fuels*, 32(11), pp.11344-11361.
- [99] Pal, N., Saxena, N., Laxmi, K.D. and Mandal, A., 2018. Interfacial behaviour, wettability alteration and emulsification characteristics of a novel surfactant: Implications for enhanced oil recovery. *Chemical Engineering Science*, 187, pp.200-212.
- [100] Pal, N., Saxena, N. and Mandal, A., 2018. Studies on the physicochemical properties of synthesized tailor-made gemini surfactants for application in enhanced oil recovery. *Journal of Molecular Liquids*, 258, pp.211-224.
- [101] Pillai, P., Kumar, A. and Mandal, A., 2018. Mechanistic studies of enhanced oil recovery by imidazolium-based ionic liquids as novel surfactants. *Journal of industrial and engineering chemistry*, 63, pp.262-274.
- [102] Rostami, A., Hashemi, A., Takassi, M.A. and Zadehnazari, A., 2017. Experimental assessment of a lysine derivative surfactant for enhanced oil recovery in carbonate rocks: Mechanistic and core displacement analysis. *Journal of Molecular Liquids*, 232, pp.310-318.
- [103] Yan, L., Ma, J., Cui, Z., Jiang, J., Song, B. and Pei, X., 2019. A New Series of Double-Chain Single-Head Sulfobetaine Surfactants Derived from 1, 3-Dialkyl Glyceryl Ether for Reducing Crude Oil/Water Interfacial Tension. *Journal of Surfactants and Detergents*, 22(1), pp.47-60.
- [104] Hussain, S.M., Kamal, M.S. and Murtaza, M., 2019. Synthesis of Novel Ethoxylated Quaternary Ammonium Gemini Surfactants for Enhanced Oil Recovery Application. *Energies*, 12(9), p.1731.

- [105] Chhetri, A.B., Watts, K.C., Rahman, M.S. and Islam, M.R., 2009. Soapnut extract as a natural surfactant for enhanced oil recovery. *Energy Sources, Part A: Recovery, Utilization, and Environmental Effects*, 31(20), pp.1893-1903.
- [106] Deymeh, H., Shadizadeh, S.R. and Motafakkerfard, R., 2012. Experimental investigation of *Seidlitzia rosmarinus* effect on oil–water interfacial tension: usable for chemical enhanced oil recovery. *Scientia Iranica*, 19(6), pp.1661-1664.
- [107] Pordel Shahri, M., Shadizadeh, S.R. and Jamialahmadi, M., 2012. A new type of surfactant for enhanced oil recovery. *Petroleum Science and Technology*, 30(6), pp.585-593.
- [108] Zendehboudi, S., Ahmadi, M.A., Rajabzadeh, A.R., Mahinpey, N. and Chatzis, I., 2013. Experimental study on adsorption of a new surfactant onto carbonate reservoir samples—application to EOR. *The Canadian Journal of Chemical Engineering*, 91(8), pp.1439-1449.
- [109] Ahmadi, M.A., Arabsahebi, Y., Shadizadeh, S.R. and Behbahani, S.S., 2014. Preliminary evaluation of mulberry leaf-derived surfactant on interfacial tension in an oil-aqueous system: EOR application. *Fuel*, 117, pp.749-755.
- [110] Mehdi, R., Milad, M., Reza, S. and Amin, D., 2015. Effect of Natural Leaf-derived Surfactants on Wettability Alteration and Interfacial Tension Reduction in Water-oil System: EOR Application. *Journal of the Japan Petroleum Institute*, 58(4), pp.245-251.
- [111] Ghahfarokhi, A.K., Dadashi, A., Daryasafar, A. and Moghadasi, J., 2015. Feasibility study of new natural leaf-derived surfactants on the IFT in an oil–aqueous system: experimental investigation. *Journal of Petroleum Exploration and Production Technology*, 5(4), pp.375-382.
- [112] Shadizadeh, S. and Kharrat, R., 2015. Experimental Investigation of *Matricaria chamomilla* Extract Effect on Oil-Water Interfacial Tension: Usable for Chemical Enhanced Oil Recovery. *Petroleum Science and Technology*, 33(8), pp.901-907.
- [113] Barati-Harooni, A., Najafi-Marghmaleki, A., Tatar, A. and Mohammadi, A.H., 2016. Experimental and modeling studies on adsorption of a nonionic surfactant on sandstone minerals in enhanced oil recovery process with surfactant flooding. *Journal of Molecular Liquids*, 220, pp.1022-1032.
- [114] Babu, K., Pal, N., Bera, A., Saxena, V.K. and Mandal, A., 2015. Studies on interfacial tension and contact angle of synthesized surfactant and polymeric from castor oil for enhanced oil recovery. *Applied Surface Science*, 353, pp.1126-1136.

- [115] Zhong, C., Luo, P., Ye, Z. and Chen, H., 2009. Characterization and solution properties of a novel water-soluble terpolymer for enhanced oil recovery. *Polymer Bulletin*, 62(1), pp.79-89.
- [116] Fakher, S., Ahdaya, M. and Imqam, A., 2020. Hydrolyzed polyacrylamide–Fly ash reinforced polymer for chemical enhanced oil recovery: Part 1–Injectivity experiments. *Fuel*, 260, p.116310.
- [117] Qi, L., Wanfen, P., Yabo, W. and Tianhong, Z., 2013, June. Synthesis and assessment of a novel AM-co-AMPS polymer for enhanced oil recovery (EOR). In 2013 International Conference on Computational and Information Sciences (pp. 997-1000). IEEE.
- [118] Sarsenbekuly, B., Kang, W., Yang, H., Zhao, B., Aidarova, S., Yu, B. and Issakhov, M., 2017. Evaluation of rheological properties of a novel thermo-viscosifying functional polymer for enhanced oil recovery. *Colloids and Surfaces A: Physicochemical and Engineering Aspects*, 532, pp.405-410.
- [119] Wang, Y., Lu, Z.Y., Han, Y.G., Feng, Y.J. and Tang, C.L., 2011. A novel thermoviscosifying water-soluble polymer for enhancing oil recovery from high-temperature and high-salinity oil reservoirs. In *Advanced materials research* (Vol. 306, pp. 654-657). Trans Tech Publications Ltd.
- [120] Wang, R., Pu, W., Dang, S., Jiang, F. and Zhao, S., 2020. Synthesis and characterization of a graft-modified copolymer for enhanced oil recovery. *Journal of Petroleum Science and Engineering*, 184, p.106473.
- [121] Nowrouzi, I., Manshad, A.K. and Mohammadi, A.H., 2020. Effects of Tragacanth Gum as a natural polymeric surfactant and soluble ions on chemical smart water injection into oil reservoirs. *Journal of Molecular Structure*, 1200, p.127078.
- [122] https://species.wikimedia.org/wiki/Anabasis_setifera
- [123] Azwanida, N.N., 2015. A review on the extraction methods use in medicinal plants, principle, strength and limitation. *Med Aromat Plants*, 4(196), pp.2167-0412.
- [124] Massiot, G., Lavaud, C., Benkhaled, M. and Le Men-Olivier, L., 1992. Soyasaponin VI, a new maltol conjugate from alfalfa and soybean. *Journal of natural products*, 55(9), pp.1339-1342.
- [125] Yang, L., Yang, Z., 2012. *Chinese Oil and Gas Industry Standards: Analytical method of alkali-surfactant-polymer flooding system (SY/T 6424-2000)*, Petroleum Industry Press, Beijing.
- [126] Rabiei, K., Bekhradnia, S., Nabavi, S.M., Nabavi, S.F. and Ebrahimzadeh, M.A., 2012. Antioxidant activity of polyphenol and ultrasonic extracts from fruits of *Crataegus pentagyna* subsp. *elburensis*. *Natural product research*, 26(24), pp.2353-2357.

- [127] İbanoğlu, E. and İbanoğlu, Ş., 2000. Foaming behaviour of liquorice (*Glycyrrhiza glabra*) extract. *Food chemistry*, 70(3), pp.333-336.
- [128] Chen, L., Shi, H., Wu, H. and Xiang, J., 2011. Synthesis and combined properties of novel fluorinated anionic surfactant. *Colloids and Surfaces A: Physicochemical and Engineering Aspects*, 384(1-3), pp.331-336.
- [129] Tsochatzidis, N.A., Guiraud, P., Wilhelm, A.M. and Delmas, H., 2001. Determination of velocity, size and concentration of ultrasonic cavitation bubbles by the phase-Doppler technique. *Chemical engineering science*, 56(5), pp.1831-1840.
- [130] Fabre, J.F., Lacroux, E., Valentin, R. and Mouloungui, Z., 2015. Ultrasonication as a highly efficient method of flaxseed mucilage extraction. *Industrial Crops and Products*, 65, pp.354-360.
- [131] Zana, R., 1995. Aqueous surfactant-alcohol systems: a review. *Advances in Colloid and Interface Science*, 57, pp.1-64.
- [132] Biscay, F., Ghoufi, A. and Malfreyt, P., 2011. Surface tension of water–alcohol mixtures from Monte Carlo simulations. *The Journal of Chemical Physics*, 134(4), p.044709.
- [133] Russo, N., Anastassopoulou, J. and Barone, G. eds., 2012. *Properties and Chemistry of Biomolecular Systems: Proceedings of the Second Joint Greek-Italian Meeting on Chemistry and Biological Systems and Molecular Chemical Engineering*, Cetraro, Italy, October 1992 (Vol. 11). Springer Science & Business Media.
- [134] Lu, Y., Najafabadi, N.F. and Firoozabadi, A., 2019. Effect of Low-concentration of 1-Pentanol on Wettability of Petroleum Fluid-Brine-Rock Systems. *Langmuir*.
- [135] Nowrouzi, I., Manshad, A.K. and Mohammadi, A.H., 2019. Effects of dissolved carbon dioxide and ions in water on the dynamic interfacial tension of water and oil in the process of carbonated smart water injection into oil reservoirs. *Fuel*, 243, pp.569-578.
- [136] Nowrouzi, I., Manshad, A.K. and Mohammadi, A.H., 2019. Effects of concentration and size of TiO₂ nano-particles on the performance of smart water in wettability alteration and oil production under spontaneous imbibition. *Journal of Petroleum Science and Engineering*, 183, p.106357.
- [137] Nowrouzi, I., Manshad, A.K. and Mohammadi, A.H., 2019. Effects of TiO₂, MgO, and γ -Al₂O₃ nano-particles in carbonated water on water-oil interfacial tension (IFT) reduction in chemical enhanced oil recovery (CEOR) process. *Journal of Molecular Liquids*, 292, p.111348.

- [138] Urukova, I., Vorholz, J. and Maurer, G., 2006. Solubility of carbon dioxide in aqueous solutions of methanol. Predictions by molecular simulation and comparison with experimental data. *The Journal of Physical Chemistry B*, 110(30), pp.14943-14949.
- [139] Jödecke, M., Pérez-Salado Kamps, Á. and Maurer, G., 2007. Experimental investigation of the solubility of CO₂ in (acetone+water). *Journal of Chemical & Engineering Data*, 52(3), pp.1003-1009.
- [140] Schüler, N., Hecht, K., Kraut, M. and Dittmeyer, R., 2012. On the solubility of carbon dioxide in binary water–methanol mixtures. *Journal of Chemical & Engineering Data*, 57(8), pp.2304-2308.
- [141] Lashkarbolooki, M., Riazi, M., Hajibagheri, F. and Ayatollahi, S., 2016. Low salinity injection into asphaltenic-carbonate oil reservoir, mechanistical study. *Journal of Molecular Liquids*, 216, pp.377-386.
- [142] Nowrouzi, I., Manshad, A.K. and Mohammadi, A.H., 2020. Evaluation of interfacial tension (IFT), oil swelling and oil production under imbibition of carbonated water in carbonate oil reservoirs. *Journal of Molecular Liquids*, 312, p.113455.
- [143] Bathurst, R.G., *Carbonate sediments and their diagenesis*. Vol. 12. 1972: Elsevier.
- [144] Sayegh, S.G., Krause, F.F., Girard, M. and DeBree, C., 1990. Rock/fluid interactions of carbonated brines in a sandstone reservoir: Pembina Cardium, Alberta, Canada. *SPE formation evaluation*, 5(04), pp.399-405. SPE-19392-PA.
- [145] Standnes, D.C., 2004. Experimental study of the impact of boundary conditions on oil recovery by co-current and counter-current spontaneous imbibition. *Energy & fuels*, 18(1), pp.271-282.
- [146] Harimi, B., Masihi, M., Mirzaei-Paiaman, A. and Hamidpour, E., 2019. Experimental study of dynamic imbibition during water flooding of naturally fractured reservoirs. *Journal of Petroleum Science and Engineering*, 174, pp.1-13.
- [147] Seyyedi, M., Mahzari, P. and Sohrabi, M., 2017. An integrated study of the dominant mechanism leading to improved oil recovery by carbonated water injection. *Journal of Industrial and Engineering Chemistry*, 45, pp.22-32.
- [148] Shu, G., Dong, M., Chen, S. and Hassanzadeh, H., 2016. Mass transfer of CO₂ in a carbonated water–oil system at high pressures. *Industrial & Engineering Chemistry Research*, 56(1), pp.404-416.
- [149] Whitson, C.H. and Brulé, M.R., 2000. *Phase behavior* (Vol. 20). Richardson, TX: Henry L. Doherty Memorial Fund of AIME, Society of Petroleum Engineers.

- [150] Honarvar, B., Rahimi, A., Safari, M., Khajehahmadi, S. and Karimi, M., 2020. Smart water effects on a crude oil-brine-carbonate rock (CBR) system: Further suggestions on mechanisms and conditions. *Journal of Molecular Liquids*, 299, p.112173.
- [151] Safari, M., Rahimi, A., Lah, R.M., Gholami, R. and Khur, W.S., 2020. Sustaining sulfate ions throughout smart water flooding by nanoparticle based scale inhibitors. *Journal of Molecular Liquids*, p.113250.
- [152] Safari, M., 2014. Variations in wettability caused by nanoparticles. *Petroleum science and technology*, 32(12), pp.1505-1511.
- [153] Gilbert, K., Bennett, P.C., Wolfe, W., Zhang, T. and Romanak, K.D., 2016. CO₂ solubility in aqueous solutions containing Na⁺, Ca²⁺, Cl⁻, SO₄²⁻ and HCO₃⁻: The effects of electrostricted water and ion hydration thermodynamics. *Applied Geochemistry*, 67, pp.59-67.
- [154] Wang, C., Chao, Z., Sun, W., Wu, X. and Ito, Y., 2014. Isolation of five glycosides from the barks of *Ilex rotunda* by high-speed counter-current chromatography. *Journal of liquid chromatography & related technologies*, 37(16), pp.2363-2376.
- [155] Xiong, H., Ding, X., Yang, X. Z., Yang, G. Z., & Mei, Z. N. (2014). Triterpene saponins from the stems of *Entada phaseoloides*. *Planta Medica*, 80(8–9), 710–718.
- [156] Schramm, L.L. ed., 2000. *Surfactants: fundamentals and applications in the petroleum industry*. Cambridge University Press.
- [157] Najimi, S., Nowrouzi, I., Manshad, A.K. and Mohammadi, A.H., 2019. Experimental study of the performances of commercial surfactants in reducing interfacial tension and wettability alteration in the process of chemical water injection into carbonate reservoirs. *Journal of Petroleum Exploration and Production Technology*, pp.1-13.
- [158] Lashkarbolooki, M., Ayatollahi, S. and Riazi, M., 2014. The impacts of aqueous ions on interfacial tension and wettability of an asphaltenic–acidic crude oil reservoir during smart water injection. *Journal of Chemical & Engineering Data*, 59(11), pp.3624-3634.
- [159] Yi, C., Xie, S. and Qiu, X., 2014. Salting-out effect of dipotassium hydrogen phosphate on the recovery of acetone, butanol, and ethanol from a prefractionator. *Journal of Chemical & Engineering Data*, 59(5), pp.1507-1514.
- [160] Armenante, P.M. and Karlsson, H.T., 1982. Salting-out parameters for organic acids. *Journal of Chemical and Engineering Data*, 27(2), pp.155-156.

- [161] Standal, S.H., Blokhus, A.M., Haavik, J., Skauge, A. and Barth, T., 1999. Partition coefficients and interfacial activity for polar components in oil/water model systems. *Journal of colloid and interface science*, 212(1), pp.33-41.
- [162] M.J. Rosen, *Surfactants and Interfacial Phenomena*, John Wiley and Sons, New York, 1979, p. 39.
- [163] Jarrahian, K., Seiedi, O., Sheykhani, M., Sefti, M.V. and Ayatollahi, S., 2012. Wettability alteration of carbonate rocks by surfactants: a mechanistic study. *Colloids and Surfaces A: Physicochemical and Engineering Aspects*, 410, pp.1-10.
- [164] Gomari, K.R. and Hamouda, A.A., 2006. Effect of fatty acids, water composition and pH on the wettability alteration of calcite surface. *Journal of petroleum science and engineering*, 50(2), pp.140-150.
- [165] RezaeiDoust, A., Puntervold, T., Strand, S. and Austad, T., 2009. Smart water as wettability modifier in carbonate and sandstone: A discussion of similarities/differences in the chemical mechanisms. *Energy & fuels*, 23(9), pp.4479-4485.
- [166] Kumar, S. and Mandal, A. Investigation on stabilization of CO₂ foam by ionic and nonionic surfactants in presence of different additives for application in enhanced oil recovery. *Applied Surface Science* 2017, 420, 9-20.
- [167] Angarska, J.K., Ivanova, D.S. and Manev, E.D. Drainage of foam films stabilized by nonionic, ionic surfactants and their mixtures. *Colloids and Surfaces A: Physicochemical and Engineering Aspects* 2015, 481, 87-99.
- [168] Carey, E. and Stubenrauch, C. Free drainage of aqueous foams stabilized by mixtures of a non-ionic (C12DMPO) and an ionic (C12TAB) surfactant. *Colloids and Surfaces A: Physicochemical and Engineering Aspects* 2013, 419, 7-14.
- [169] Arabadzhieva, D., Tchoukov, P., Soklev, B. and Mileva, E. Interfacial layer properties and foam film drainage kinetics of aqueous solutions of hexadecyltrimethylammonium chloride. *Colloids and Surfaces A: Physicochemical and Engineering Aspects* 2014, 460, 28-37.
- [170] Simjoo, M., Rezaei, T., Andrianov, A. and Zitha, P.L.J. Foam stability in the presence of oil: effect of surfactant concentration and oil type. *Colloids and Surfaces A: Physicochemical and Engineering Aspects* 2013, 438, 148-158.
- [171] Elbandy, M., Rho, J.R. and Afifi, R., 2014. Analysis of saponins as bioactive zoochemicals from the marine functional food sea cucumber *Bohadschia cousteaui*. *European Food Research and Technology*, 238(6), pp.937-955.

- [172] Li, Q.J., Zhu, Z., Yang, X.S. and Hao, X.J., 2014. Four New 13, 28-Epoxyoleanane Saponins from *Lysimachia lobelioides*. *Helvetica Chimica Acta*, 97(6), pp.839-846.
- [173] Chen, L.J., Lin, S.Y., Huang, C.C. and Chen, E.M., 1998. Temperature dependence of critical micelle concentration of polyoxyethylenated non-ionic surfactants. *Colloids and Surfaces A: Physicochemical and Engineering Aspects*, 135(1-3), pp.175-181.
- [174] Hamidian, R., Lashkarbolooki, M. and Amani, H., 2019. Evaluation of surface activity of asphaltene and resin fractions of crude oil in the presence of different electrolytes through dynamic interfacial tension measurement. *Journal of Molecular Liquids*, p.112297.
- [175] Martin, F.D. and Oxley, J.C., 1985, January. Effect of various alkaline chemicals on phase behavior of surfactant/brine/oil mixtures. In *SPE Oilfield and Geothermal Chemistry Symposium*. Society of Petroleum Engineers. SPE-13575-MS.
- [176] Sheng J.J., 2015. Status of Alkaline-surfactant Flooding. *Polym Sci.* 1(1), pp. 1-6.
- [177] Ayirala, S. C.; Vijapurapu, C. S.; Rao, D. N., Beneficial effects of wettability altering surfactants in oil-wet fractured reservoirs. *Journal of petroleum science and engineering* 2006, 52, (1), 261-274.
- [178] Salathiel, R.A., 1973. Oil recovery by surface film drainage in mixed-wettability rocks. *Journal of Petroleum Technology*, 25(10), pp.1-216.
- [179] Spinler, E.A., Zornes, D.R., Tobola, D.P. and Moradi-Araghi, A., 2000, January. Enhancement of oil recovery using a low concentration of surfactant to improve spontaneous and forced imbibition in chalk. In *SPE/DOE Improved Oil Recovery Symposium*. Society of Petroleum Engineers. SPE-59290-MS.
- [180] Jadhunandan, P.P. and Morrow, N.R., 1995. Effect of wettability on waterflood recovery for crude-oil/brine/rock systems. *SPE reservoir engineering*, 10(01), pp.40-46. SPE-22597-PA.
- [181] Emadi, S., Shadizadeh, S.R., Manshad, A.K., Rahimi, A.M., Nowrouzi, I. and Mohammadi, A.H., 2019. Effect of using *Zyziphus spina christi* or Cedar Extract (CE) as a natural surfactant on oil mobility control by foam flooding. *Journal of Molecular Liquids*, 293, p.111573.
- [182] Nowrouzi, I., Manshad, A.K. and Mohammadi, A.H., 2020. Effects of TiO₂, MgO and γ -Al₂O₃ nano-particles on wettability alteration and oil production under carbonated nano-fluid imbibition in carbonate oil reservoirs. *Fuel*, 259, p.116110.

- [183] Bahraminejad, H., Khaksar Manshad, A., Riazi, M., Ali, J.A., Sajadi, S.M. and Keshavarz, A., 2019. CuO/TiO₂/PAM as a novel introduced hybrid agent for water—Oil interfacial tension and wettability optimization in chemical enhanced oil recovery. *Energy & Fuels*, 33(11), pp.10547-10560.
- [184] Tadros, T., 2013. *Encyclopedia of Colloid and Interface Science*. Springer.
- [185] Bera, Achinta, et al. "Adsorption of surfactants on sand surface in enhanced oil recovery: Isotherms, kinetics and thermodynamic studies." *Applied Surface Science* 284 (2013): 87-99.
- [186] Hou, B.F., Wang, Y.F. and Huang, Y., 2015. Mechanistic study of wettability alteration of oil-wet sandstone surface using different surfactants. *Applied Surface Science*, 330, pp.56-64.
- [187] Wang, S., Li, Z., Liu, B., Zhang, X. and Yang, Q., 2015. Molecular mechanisms for surfactant-aided oil removal from a solid surface. *Applied Surface Science*, 359, pp.98-105.
- [188] Lager, A., Webb, K.J., Black, C.J.J., Singleton, M. and Sorbie, K.S., 2008. Low salinity oil recovery—an experimental investigation. *Petrophysics*, 49 (1), 28–35.
- [189] Al-Anssari, S., Arain, Z.U.A., Barifcani, A., Keshavarz, A., Ali, M. and Iglauer, S. Influence of pressure and temperature on CO₂-nanofluid interfacial tension: Implication for enhanced oil recovery and carbon geosequestration. In *Abu Dhabi International Petroleum Exhibition & Conference 2018*. Society of Petroleum Engineers.
- [190] Yang, J., Jovancevic, V. and Ramachandran, S. Foam for gas well deliquification. *Colloids and Surfaces A: Physicochemical and Engineering Aspects* 2007, 309(1-3), 177-181.
- [191] Kundu, P., Agrawal, A., Mateen, H. and Mishra, I.M. Stability of oil-in-water macro-emulsion with anionic surfactant: Effect of electrolytes and temperature. *Chemical Engineering Science* 2013, 102, 176-185.
- [192] Williams, R.J., Phillips, J.N. and Mysels, K.J. The critical micelle concentration of sodium lauryl sulphate at 25 C. *Transactions of the Faraday Society* 1955, 51, 728-737.
- [193] Saxena, N., Kumar, A. and Mandal, A. Adsorption analysis of natural anionic surfactant for enhanced oil recovery: The role of mineralogy, salinity, alkalinity and nanoparticles. *Journal of Petroleum Science and Engineering* 2019, 173, 1264-1283.
- [194] Babadagli, T. Dynamics of capillary imbibition when surfactant, polymer, and hot water are used as aqueous phase for oil recovery. *Journal of colloid and interface science* 2002, 246(1), 203-213.

- [195] Rojas, G.A. and Ali, S.M., 1988. Dynamics of subcritical CO₂/brine floods for heavy-oil recovery. SPE Reservoir Engineering, 3(01), pp.35-44. SPE-13598-PA.
- [196] Abramov, A., Keshavarz, A. and Iglauer, S., 2019. Wettability of Fully Hydroxylated and Alkylated (001) α -Quartz Surface in Carbon Dioxide Atmosphere. The Journal of Physical Chemistry C, 123(14), pp.9027-9040.
- [197] Nowrouzi, I., Manshad, A.K. and Mohammadi, A.H., 2020. Wettability alteration and enhanced gas condensate recovery by treatment of carbonate reservoir rock using supercritical R134A and R404A gases. Journal of Petroleum Exploration and Production Technology, 10(8), pp.3751-3766.
- [198] Burnett Jr, J.C. and Himmelblau, D.M., 1970. The effect of surface active agents on interphase mass transfer. AIChE Journal, 16(2), pp.185-193.
- [199] Gomez-Diaz, D., Navaza, J.M. and Sanjurjo, B., 2009. Mass-transfer enhancement or reduction by surfactant presence at a gas– liquid interface. Industrial & engineering chemistry research, 48(5), pp.2671-2677.
- [200] Rahimi, A., Honarvar, B. and Safari, M., 2020. The role of salinity and aging time on carbonate reservoir in low salinity seawater and smart seawater flooding. Journal of Petroleum Science and Engineering, 187, p.106739.
- [201] Honarvar, B., Rahimi, A., Safari, M., Rezaee, S. and Karimi, M., 2020. Favorable attributes of low salinity water aided alkaline on crude oil-brine-carbonate rock system. Colloids and Surfaces A: Physicochemical and Engineering Aspects, 585, p.124144.
- [202] Safari, M., Rahimi, A., Gholami, R., Permana, A. and Siaw Khur, W., 2020. Underlying mechanisms of shale wettability alteration by low salinity water injection (LSWI). Journal of Dispersion Science and Technology, pp.1-9.
- [203] Rahimi, A., Safari, M., Honarvar, B., Chabook, H. and Gholami, R., 2020. On time dependency of interfacial tension through low salinity carbonated water injection. Fuel, 280, p.118492.
- [204] Han, Y.L., Gao, J., Yin, Y.Y., Jin, Z.Y., Xu, X.M. and Chen, H.Q., 2016. Extraction optimization by response surface methodology of mucilage polysaccharide from the peel of *Opuntia dillenii* haw. Fruits and their physicochemical properties. Carbohydrate polymers, 151, pp.381-391.
- [205] Contreras-Padilla, M., Rodríguez-García, M.E., Gutiérrez-Cortez, E., del Carmen Valderrama-Bravo, M., Rojas-Molina, J.I. and Rivera-Muñoz, E.M., 2016. Physicochemical and rheological characterization

of *Opuntia ficus mucilage* at three different maturity stages of cladode. *European Polymer Journal*, 78, pp.226-234.

[206] Zhao, M., Yang, N., Yang, B., Jiang, Y. and Zhang, G., 2007. Structural characterization of water-soluble polysaccharides from *Opuntia monacantha* cladodes in relation to their anti-glycated activities. *Food chemistry*, 105(4), pp.1480-1486.

[207] Monrroy, M., García, E., Ríos, K. and García, J.R., 2017. Extraction and physicochemical characterization of mucilage from *Opuntia cochenillifera* (L.) Miller. *Journal of Chemistry*, 2017.

[208] Smith, B.C., 1998. *Infrared spectral interpretation: a systematic approach*. CRC press LLC, Boca Raton, Fla, USA.

[209] Nejatizadeh-Barandozi, F. and Enferadi, S.T., 2012. FT-IR study of the polysaccharides isolated from the skin juice, gel juice, and flower of *Aloe vera* tissues affected by fertilizer treatment. *Organic and medicinal chemistry letters*, 2(1), p.33.

[210] Kittur, F.S., Prashanth, K.H., Sankar, K.U. and Tharanathan, R.N., 2002. Characterization of chitin, chitosan and their carboxymethyl derivatives by differential scanning calorimetry. *Carbohydrate polymers*, 49(2), pp.185-193.

[211] Vendruscolo, C.W., Ferrero, C., Pineda, E.A., Silveira, J.L., Freitas, R.A., Jiménez-Castellanos, M.R. and Bresolin, T.M., 2009. Physicochemical and mechanical characterization of galactomannan from *Mimosa scabrella*: Effect of drying method. *Carbohydrate Polymers*, 76(1), pp.86-93.

[212] Zohuriaan, M.J. and Shokrolahi, F., 2004. Thermal studies on natural and modified gums. *Polymer Testing*, 23(5), pp.575-579.

[213] Varma, A.J., Kokane, S.P., Pathak, G. and Pradhan, S.D., 1997. Thermal behavior of galactomannan guar gum and its periodate oxidation products. *Carbohydrate polymers*, 32(2), pp.111-114.

[214] Sepúlveda, E., Sáenz, C., Aliaga, E. and Aceituno, C., 2007. Extraction and characterization of mucilage in *Opuntia* spp. *Journal of Arid Environments*, 68(4), pp.534-545.

[215] Chanamai, R.A.D.J.M. and McClements, D.J., 2002. Comparison of gum arabic, modified starch, and whey protein isolate as emulsifiers: influence of pH, CaCl₂ and temperature. *Journal of Food Science*, 67(1), pp.120-125.

[216] Lefebvre J, Doublier JI. *Rheological behavior of polysaccharides aqueous systems*. New York: Marko Decker 2005.

- [217] Marcotte, M., Taherian, A.R., Trigui, M. and Ramaswamy, H.S., 2001. Evaluation of rheological properties of selected salt enriched food hydrocolloids. *Journal of Food Engineering*, 48(2), pp.157-167.
- [218] Mohammadifar, M.A., Musavi, S.M., Kiumarsi, A. and Williams, P.A., 2006. Solution properties of targacanthin (water-soluble part of gum tragacanth exudate from *Astragalus gossypinus*). *International Journal of Biological Macromolecules*, 38(1), pp.31-39.
- [219] Vinod, V.T.P., Sashidhar, R.B., Sarma, V.U.M. and Vijaya Saradhi, U.V.R., 2008. Compositional analysis and rheological properties of gum kondagogu (*Cochlospermum gossypium*): a tree gum from India. *Journal of Agricultural and Food Chemistry*, 56(6), pp.2199-2207.
- [220] Speight, J.G., 2013. *Enhanced recovery methods for heavy oil and tar sands*. Elsevier